QATAR UNIVERSITY

COLLEGE OF ENGINEERING

DEVELOPMENT OF POLYMER BASED AND RECOVERABLE FE-MNP DEMULSIFIERS TO ENHANCE THE OIL RECOVERY PROCESS FROM OIL IN WATER EMULSION

BY

WAMDA FAISAL ELHAJ

A Dissertation Submitted to

The College of Engineering

In Partial Fulfilment of the Requirements for the Degree of

Doctorate of Philosophy in Chemical Engineering

January 2022

COMMITTEE PAGE

The members of the Committee approve the Dissertation of

Wamda Faisal Elhaj defended on 05/12/2021.

_____

Prof. Fares Almomani

Thesis/Dissertation Supervisor

_____

Dr. Fadwa Eljack

Committee Member

_____

Prof. Bassim Hameed

Committee Member

_____

Dr. Evans Chirwa

Committee Member

Approved:

_____

Khalid Kamal Naji, Dean, College of Engineering

ABSTRACT

ELHAJ, WAMDA, FAISAL, Doctorate: January : 2022,

Doctorate of Philosophy in Chemical Engineering

Title: Development of Polymer Based And Recoverable FE-MNP Demulsifiers To Enhance The Oil Recovery Process From Oil In Water Emulsion

Supervisor of Dissertation: Prof. Fares, Abedalwally, Almomani.

The demulsification process has grown in significance due to the rapid development of oil and gas industries, which generate high amounts of oil, and the formation of different complicated emulsion types, a big challenge in the petroleum industry. Stable emulsions are commonly faced in oil generation and lead to a sequence of environmental and operational problems. Chemical demulsification was extensively applied to remove oil from water or vice versa (water from oil). The chemicals utilized in the demulsification method are very attractive to the oil/water (O/W) interface and could develop the demulsification mechanisms of oil in water (O/W) emulsions.

This work proposes different demulsifiers for the Enhanced Oil Recovery (EOR) process from the O/W emulsion systems. First, this research aimed to study the efficiency of high and low molecular weight hyperbranched polyglycerol (HPG) polymers for oil recovery process. Results showed prepared polymers are environmentally friendly, biodegradable, and can recover up to 90.30% of oil from O/W emulsion. Second, the efficiency of Fe_3O_4 magnetic nanoparticles (Fe-MNP), the effects of different process parameters, the re-usability of the synthesized Fe-MNP, and kinetic studies on the $\%\eta_{dem}$ are studied. Results showed the synthesized Fe-MNP achieved a $\%\eta_{dem} \geq 95\%$, recovered up to 55.6% using a lower D_{MNP} of 5 mg/L, and exhibited an excellent adsorption capacity of 51 mg/g. Third, an innovative magnetic demulsifier (MD) was prepared by grafting a

silica layer onto the surface of the Fe_3O_4 MNPs. The MD showed an excellent $\%\eta_{dem}$ in the range of 93% to 94.3%. Fourth, a detailed evaluation of Fe_3O_4-SiO_2 (Fe-Si-MNP) prepared with differing silica layer thicknesses (5 nm, 8 nm, 10 nm, and 15 nm) were tested for the $\%S_{oil}$. The Results showed that the Fe_3O_4-SiO_2 (Fe-Si-MNPs) exhibited excellent $\%S_{oil}$, reliable stability, high magnetization values ranging between 46.1 to 80.2 emu/g, achieved oil separation efficiency of ~ 96.3%. Fifth, the functionalized Fe-Si-MNPs were coated with the HPG polymer to produce the PSiMNPs demulsifiers and tested for the $\%\eta_{dem}$. Results illustrated that PSiMNPs dose ($D_{PSiMNPs}$) of 100 mg/L achieved $\%\eta_{dem}$ of 99.4%, the PSiMNPs can be reused up to 15 cycles at a successful steady $\%\eta_{dem}$ of 89.1% with high q_{max} of 192.8 g/mg. Sixth, the effect of Fe_3O_4@SiO_2 NPs as a novel nanocomposite on EOR from reservoirs is studied utilizing a two-dimensional glass micromodel. The results showed that the NPs achieved an oil recovery rate ($\%R_{oil}$) of 90.2%, while other nanofluids (seawater, Fe_3O_4, and SiO_2) achieved lower values of 76.5%, 70.8%, and 55.3%, respectively. Seventh, the efficiency of three ILs, two halogenide ionic liquids (HIL-1, HIL-2) and one non-halogenide ionic liquid (Non-HIL) in the oil recovery process was assessed. The demulsification mechanism is based on ion exchange among ILs anions and the oil-surfactant. The efficiency was tested using tube and bottle tests. Bottle tests demonstrated that HILs-1, HILs-2, and Non-HILs achieved a D% of 97.7%, 88.2%, and 90% in 20 min, respectively. However, the efficiency of the Non-HILs was less than the HILs (~85.2%) using a low V_{sur} of 0.05 g/L.

DEDICATION

I dedicate this work to my Supervisor, Prof. Fares Almomani, my mother, and my father, who with love and effort have accompanied me in this process, without hesitating at any moment of seeing my dreams come true, which are also their dreams. To my sisters Saba and Maab, who have been my support in the difficulties in this journey. To my husband, to my aunties, to my friends, to my country, my motherland- beloved "Sudan."

ACKNOWLEDGMENTS

"I want to thank my supervisor Prof. Fares Almomani for his consistent support and always providing guidance and feedback throughout this research; his exceptional supervision and encouragement made this journey possible. I also greatly appreciate and acknowledge the support and valuable assistance received from the central laboratory unit (CLU), gas processing center (GPC), and center of advanced material (CAM). Moreover, I extend my sincere thanks to Dr. Musaab Magzoub, Dr. Ahmed Elkhatat, Dr. Ahmed Awadallah, and Dr. Ahmed Abdelsalam for their respected time and for sharing their valuable knowledge. Special thanks to all my colleagues and friends, Hesan, Fatima, Reem, Afnan, Abubaker, Roba, Asmaa, Shereen, Haneen, Malak, and Hania, who contributed to my progress.

I would also like to express my deepest gratitude to my family, with a special mention to my dear sisters “Saba and Maab” and aunties, “Howaida-Nesreen-Azahir-Hanadi- and Eitidal,” for always supporting and encouraging me. I can never thank my beloved mother and father enough for their endless efforts, support, prayers, and for always being on my side in every hard time, and to my cousin Dr. Mohamed Abdelhameed for his continued support and encouragement. I also need to thank my husband “Ahmed,” for his always assistance. Without him, I would not be who I am today. Last but not least, I would like to extend my gratitude to all the CHE department members, especially Mr. Khalid Aljamal, Mr. Saied, and Mr. Siva. Thank you all".

TABLE OF CONTENTS

LIST OF TABLES

LIST OF FIGURES

CHAPTER 1: INTRODUCTION

1.1 Introduction

In general, crude oil is found combined with gas and saline formation water. As the reservoir grows to be drained, water is cogenerated with oil, and the several wells generating water along with crude oil are gradually rising [1]. These unmixable fluids are emulsified easily by the simultaneous shear and pressure reduction action at the head of the well, clogs, and controller valves [2]. When at least two immiscible phases are present in a system, they are called emulsions. The production of an emulsion mixture involves a dispersed phase and a continuous phase [3]. The emulsion is a system that contains two phases consisting of two liquids not producing homogenous when mixed. One called the dispersed phase continuously distributed as drops in another stage called the continuous phase [4]. The emulsion is generated during the oil production (oil recovery) process. The main cause for enhancing the emulsion formation is applying surface-active materials called surfactants to reduce the interfacial tension between the two phases and thus stabilize the emulsion mixture and consider other parameters such as and pH of the water phase [5]. The stability of the O/W emulsions has earned interest in several studies about petroleum oil to create various efficient and related methods for oil separation.

The treatment of oil-in-water emulsions includes using a thermal, electrical, chemical method or their integrations. The application of a thermal method or heat treatment in the emulsion separation process generally relies on the overall economic prospects of the treatment resource. Additional heat is not ancillary when it is further commercial to insert chemical or set up electrostatic heat. Temperatures are not sufficient to substantially increase the solubility of a particular crude oil in the water.

High temperatures do not produce significant volumes of asphaltenes that become unsolvable in the crude oil and make an interface film that affects the process efficiency [6]. Electrical techniques interrupt the surface tension of every oil droplet, possibly by creating polar particles to reorient themselves [7]. This redirection reduces the film over every droplet since the polar particles are no longer strong at the surface of oil droplets. This technique does not usually treat the emulsions totally, while it is effective when adding chemicals or heat. The technology mentioned above has not treated the emulsions systems with high efficiency, and these techniques' oil removal percentages were minimal. Also, these types have not fully met operation goals from the economic perspective.

Chemical methods are the prevalent approach of emulsion treatment oil and gas field. The application of chemicals improves the impacts of emulsifying agents (surfactants). In addition, it has a high ability to efficiently separate an interfacial film between the oil and water phases, with no additional processes or alterations of the present system. Therefore, many researchers were interested in using the chemical demulsification method by applying different types of demulsifiers, including the magnetic nanoparticles (MNPs) (separately or coated) [8], hyperbranched polymers (HP) [9], ionic liquids (ILs) [10], etc. for oil recovery from oil-in-water emulsions.

1.2 Motivation

The rapid development of oil and gas industries which generates high amounts of oil [2] and emulsion formation, is a complicated challenge in the petroleum industry. It is essential to have powerful and effective demulsifiers to apply in the oil recovery process. The demulsification process has grown in significance due to the rapid development of the oil and gas industries. The strengthening of upcoming requirements

for the most significant and highest oil recovery needs remarkable and influential enhancement works regarding developing the demulsification mechanisms of O/W emulsions [11]. Researchers have been trying to find an alternative method to improve the oil recovery process to remove the highest amounts of oil from emulsions systems. Experts in the oil and gas industry agreed that proper demulsifier types and the functionalization of the MNPs demulsifiers with other demulsifier types such as polymers and different types achieved higher demulsification efficiency and enhanced the oil recovery from oil-in-water emulsions and improved the treatment of petroleum produced water. Researchers examined numerous kinds of metal oxide, including NiO, Fe_2O_3, CuO, and SiO_2, separately and coated them with other NPs in the demulsification of O/W emulsions [12]. The outcome for applying these nanoparticles alone was not so favourable because it could just achieve a maximum oil recovery of not more than 57%. In comparison, the coated nanoparticles might attain more than 85%. Nevertheless, others have demonstrated that iron oxide nanoparticles could enhance oil recovery efficiency by more than 24% (extra) when dispersed in water [13]. The mechanism of magnetic recovery works by applying an external magnet to the oil in water emulsions and driving the NPs toward the magnet to assemble the highest amount of oil. Moreover, researchers found that hyperbranched polymer demulsifiers are highly beneficial in oily wastewater treatment due to their branched and 3D expanded structure, additional branch bonds, more significant interfacial action, better dispersion, and a more considerable amount of end groups. [14]. The application of hyperbranched polyglycerol polymers (HPG) in enhanced oil recovery methods shows an essential part in covering the present energy need and can be regenerate up to 20% extra oil from oil content [15]. The HPG polymers present a biodegradable and green demulsifier (i.e., environmentally friendly), in which employing them in the oil

recovery method is viable and reduce the usage of toxic compounds [16, 17]. Ionic liquids (ILs) demulsifiers are also applied by researchers and found to be an effective type used in enhanced oil recovery (EOR) methods and generate high oil recovery rates. It can stay steady even at extreme temperatures (300◦C and above). Still, the challenge is that other traditional surfactants applied to the emulsion might decompose at those temperatures, reducing their application and efficiency [18].

1.3 Research Objectives

This research aims to develop different demulsifier systems with certain properties for oil recovery from oil in water emulsions to improve the demulsification process under different conditions and eliminate the oil traces from water for produced water treatment. The detailed objectives of this study are as follows:

- To examine the efficiency of synthesized hyperbranched polyglycerol (HPG) polymers with high and low molecular weight in oil recovery from oil/water emulsion under different process parameters.
- To investigate the efficiency of produced Fe_3O_4 magnetic nanoparticles (Fe-MNP), the effects of various process parameters on the demulsification efficiency ($\%\eta_{dem}$), the re-usability, and the kinetic studies of the as-synthesized Fe-MNP.
- To test the ability of an innovative magnetic demulsifier (Fe-Si MD) developed by grafting a silica layer onto the surface of the Fe-MNPs in oil recovery, test the reusability of the Fe-MNPs demulsifier and the kinetics of the oil removal process.

- To test the efficiency of the Fe-Si-MNP prepared with different silica layer thicknesses tested for the percentage of oil separation ($\%S_{oil}$) under different process parameters, the demulsifiers were also tested for their recyclability.
- To evaluate the efficiency of the developed functionalized Fe-Si-MNPs coated with HPG polymer (PSiMNPs) in oil recovery from oil in water (O/W) emulsions below various process factors, test the recyclability of the demulsifier, and the isotherms and kinetics of oil adsorption on the PSiMNPs demulsifier.
- To investigate the effect of Fe-Si MNPs as a novel nanocomposite on enhanced oil recovery from the real formation of the reservoir rock utilizing a two-dimensional glass micromodel.
- To assess the efficiency of three ionic liquids (ILs), two halogenide ILs (HILs-1, HILs-2), and one non-halogenide Non-HILs in the oil recovery process, using bottle and tube test.

1.4 Outline of the Dissertation

This dissertation consists of eight main chapters. The details of each chapter are as following:

- Chapter 1 introduces the present context and motivation of the research.
- Chapter 2 surveys the literature on the chemical demulsification process and applying different demulsifier types in the oil recovery process.
- Chapter 3 presents a detailed investigation of the efficiency of high and low molecular weight hyperbranched polyglycerol (HPG) polymers in the oil recovery process applying different process parameters.

- Chapter 4 provides a detailed examination of the efficiency of produced Fe-MNP and the effects of several process parameters on the efficiency of the demulsification process, demulsifier re-usability, and the kinetic studies of the as-synthesized Fe-MNP.
- Chapter 5 introduces an innovative magnetic demulsifier (Fe-Si MD), evaluates its efficiency in the oil recovery process, and tests its reusability and the kinetics of the Fe-Si MD in the oil removal process.
- Chapter 6 gives a comprehensive assessment of the efficiency of Fe-Si-MNP prepared with different silica layer thicknesses in the oil separation process and tests all the developed demulsifiers for their recyclability.
- Chapter 7 provides a detailed evaluation of the PSiMNPs demulsifier developed from the grafting of iron-silica MNPs with HPG polymer in the demulsification process, tests its recyclability, and the kinetics studies of the PSiMNPs demulsifier in the demulsification process.
- Chapter 8 introduces a detailed investigation of the effect of Fe-Si MNPs as a novel nanocomposite on enhanced oil recovery from the real formation of the reservoir rock utilizing a two-dimensional glass micromodel.
- Chapter 9 presents an assessment of the efficiency of three ionic liquids (ILs), two halogenide ILs (HILs-1, HILs-2) and one non-halogenide Non-HILs (ILs-3) in the oil recovery process using bottle test and tube test
- Chapter 10 presents the overall current research work conclusion and recommends future work for improving the efficiency of the demulsification process using all demulsifier scenarios.

1.5 List of Publications

1. Wamda Faisal Elmobarak, Fares Almomani., 2021. A critical review of the development and demulsification processes applied for oil recovery from oil in water emulsions. Chemosphere (October 2021).
2. Wamda Faisal Elmobarak, Fares Almomani., 2019. Laboratory Evaluation of fractional distillation products of Sudanese crude oils. IOSR, Volume 12, Issue 10.
3. Wamda Faisal Elmobarak, Fares Almomani., 2020. Utilizing environmentally friendly hyperbranched polyglycerol polymers to separate gasoline from deionized water. GHG, 10:759–770.
4. Wamda Faisal Elmobarak, Fares Almomani., 2021. Application of magnetic nanoparticles for the removal of oil from oil-in-water emulsion: Regeneration/reuse of spent particles. JPSE, 203, 108591.
5. Wamda Faisal Elmobarak, Fares Almomani., 2021. Application of Fe_3O_4 magnetite nanoparticles grafted in silica (SiO_2) for oil recovery from oil in water emulsions. Chemosphere, Volume 265, 129054.
6. Wamda Faisal Elmobarak, Fares Almomani., 2021. Functionalization of silica-coated magnetic nanoparticles as powerful demulsifier to recover oil from oil-in-water emulsion. Chemosphere, Volume 279, 130360.
7. Wamda Faisal Elmobarak, Fares Almomani., 2021. Enhanced oil recovery using hyperbranched polyglycerol polymer-coated silica nanoparticles. Chemosphere, Volume 285, 131295.
8. Wamda Faisal Elmobarak, Fares Almomani., 2021. A new insight into the separation of oil from oil/water emulsion by Fe_3O_4-SiO_2 nanoparticles using a glass micromodel. Environmental Research, Volume 202, 111645.

9. Wamda Faisal Elmobarak, Fares Almomani., 2021. Experimental Investigation of Fe_3O_4-SiO_2 magnetic nanoparticles performance in the demulsification of oil/water emulsions using glass micro model ”12th International Exergy, Energy and Environment (IEEE) Symposium”.
10. Wamda Faisal Elmobarak, Fares Almomani., 2021. Investigational study for the efficiency of Fe_3O_4-SiO_2 nanoparticles in the oil recovery process using glass micro model ” Annual Research Forum, Qatar University”.
11. Wamda Faisal Elmobarak, Fares Almomani., 2021. Evaluation of the efficiency of the ionic liquids in the demulsification of oil-in-water emulsions. Environmental Technology & Innovation, 102003.

CHAPTER 2: LITERATURE REVIEW

In natural systems, crude oil is found combined with gas and saline formation water. As the reservoir grows to be drained, water is cogenerated with oil, and the several wells generating water along with crude oil are gradually rising [1]. These unmixable fluids are easily emulsified by the simultaneous shear and pressure reduction action at the head of the well, clogs, and controller valves [2]. When at least two immiscible phases are present in a system, they are called emulsions. The production of an emulsion mixture involves a dispersed phase and a continuous phase [3]. The emulsion is a system containing two phases consisting of two liquids not producing homogenous when mixed. One called the dispersed phase continuously distributed as drops in another phase called the continuous phase [4]. The emulsion was generated during the oil production (oil recovery) process. The main cause for enhancing the emulsion formation is applying surface-active materials called surfactants to reduce the interfacial tension between the two phases and thus stabilize the emulsion mixture and consider other parameters such as the pH of the water phase [5]. The stability of the O/W emulsions has earned interest in several studies about petroleum oil to create various efficient and related methods for oil separation.

Several problems occur in the transportation and treatment of crude oil due to the presence of the emulsion [19]. These obstacles involve rising transportation costs, equipment, corrosion of pipelines, contaminating downstream refinery catalysts [20]. Thus, the O/W emulsion separation is crucial before transportation and treatment [21]. The popular demulsification techniques contain thermal, biological, electrical, chemical, and mechanical [22, 23]. Between the techniques mentioned above, chemical demulsification is the highly commonly used method. It uses the demulsifiers to improve the film-thinning rate and reduces the stability of the emulsion. Thus, it leads

to the O/W separation in the subsequent approaches: demulsifiers with great interfacial activity permeate into the interfacial film steadied by the surfactants [24, 25], and the demulsifiers substitute the surfactants to break the interfacial film the emulsion viscosity, increase the film drainage and hence enhance the oil recovery rates [26]. The demulsification process has grown in significance due to the rapid development of oil and gas industries that generate high amounts of oil [2]. The formation of emulsion is a complicated challenge in the petroleum industry.

Several chemical demulsifiers, such as polymeric surfactants, ionic liquids, and nanoparticle-based demulsifiers, have been designed for the O/W separation [27]. For example, silicon polyether [28], ethylene oxide-propylene oxide (EO-PO) block copolymers [29], biodegradable polymeric surfactants [30], ionic liquids [31, 32], and nanoparticle-based demulsifiers (magnetic nanoparticles (MNPs) [33] and non-magnetic nanoparticles (E.g., silicon oxide [34], titanium oxide [35], and carbon-based demulsifier [36]) have drawn significant interests in industrial fields. The highly popular demulsifiers are amphiphilic materials with both hydrophilic and hydrophobic components. For example, in our previous work, hyperbranched polymers [37, 38], Fe_3O_4 nanoparticles [39], functionalized Fe_3O_4-SiO_2 nanoparticles [40, 41] were synthesized to treat the O/W emulsions. However, these demulsifiers showed high oil recovery rates, and great demulsification efficiency reached up to 95%.

The strengthening of upcoming requirements for the most significant and highest oil recovery needs remarkable and influential enhancement works regarding developing the demulsification mechanisms of O/W emulsions. As stated by [42], the oil is hardly ever generated alone. It is generally formed with water, which produces numerous problems throughout its formation. Also, regarding water production, the water can be created through two methods. The water can be generated as free water, which will

settle out instantly, or the existence of water can result in emulsion production. The demulsification process is affected by numerous parameters; below is some of these factors [19, 43]:

- The addition of emulsifying agents (surfactant) at the O/W interfaces
- The addition of different demulsifier materials to the emulsion mixture.
- The mixing time and mixing rate (long time and high rate enhance the demulsification efficiency) will affect the performance of the demulsification process.
- The dispersion and mixing of these chemical demulsifiers in the emulsion solution
- The dispersion and mixing of oil inside the emulsion will also influence the process.

This chapter introduced an overview of the emulsion formation, types of emulsion, emulsion stabilization, the oil recovery process from oil in water emulsion, and the oil recovery mechanism utilizing the demulsification method. The application of the chemical demulsification method using different demulsifiers, including magnetic nanoparticles (separately or coated), hyperbranched polymers (our focus hyperbranched polyglycerol polymers HPGs), and ionic liquids for oil recovery from O/W emulsion mixtures, have been discussed and have demonstrated favourable results in the research. The studies showed that the surface coating with nanoparticles enhances the oil recovery process and achieves high demulsification rates. The factors that impact the application of NPs in the oil recovery process, such as nanoparticle size, NPs concentrations, the salinity of the emulsion, wettability, etc., were also reviewed. Moreover, this chapter identified and provided the scientific literature on knowledge gaps and future research ways of chemical demulsification method using these

demulsifiers to assess the effects of these technologies in the treatment of oil recovery from O/W emulsions and thus the treatment petroleum produced water.

2.1 Emulsions

2.1.1 Emulsion Production

The emulsion is formed when two or extra non-mixable liquids mix strongly together, producing two phases (continuous and dispersed) [44, 45]. The lesser amount of phase is generally known as the dispersed phase, and the greater one is the continuous phase. If the two phases are similar, other parameters could be deemed to understand the continuous and dispersed phases [3, 42]. According to the Bancroft theory, a continuous phase is a phase when the emulsifying agents are more solvable [46]. Generally examined emulsions have an oil phase and a water phase. Small particles and crude oils surface-active composites, for example, SARA (saturates, asphaltenes, resins, and aromatics), can perform as natural surfactants (emulsifying agents)[47, 48]. Below potent mix, natural emulsifying agents can adsorb at the interface of oil/water, forming a solid interfacial thin layer over the dissolved drops and obstructing the coalescence of the droplets [49]. The great tension among oil and water phases is known as interfacial tension (IFT), and the greater IFT leads to high steady emulsion [50].

2.1.2 Emulsion Types

Following the dispersed phase nature, emulsions are classified into oil in water (O/W), water in oil (W/O), and multiple emulsions (water in oil in water (W/O/W) or oil in water in oil (O/W/O) (Figure 1). Oil in water emulsions occurs when oil drops are the dispersed phase (internal phase) in the continuous water phase (external phase), also known as reversal emulsion. The production of W/O emulsions occurs when the drops of the water are the dispersed phase in the oil phase (continuous phase). Multiple types

are a combination of oil in water and water in oil emulsions. When oil drops are the dispersed phase in water particles that are dispersed in the continuous oil phase, the oil in water in oil emulsions are created, whereas water in oil in water emulsions are created vice versa. Various emulsions are further widespread in the food, wastewater treatment, cosmetics, and pharmaceutics industries [51, 52]. It would be observed that these emulsions are kinetically stable but thermodynamically not steady since they are generated from a mix of two or further unmixable liquids, which be separated later. Nevertheless, the emulsion's kinetic stability implies that emulsions are steady for long (days to weeks) due to solid film's creation over them via emulsifiers [19].

Reliant on the time that one phase can remain dissolved in the other phase, the emulsions mentioned above can be classified into stable, mesostable, entrained water, and unstable [48, 53]. Generally, steady water in oil emulsions can take the majority of the water in the oil phase for further than 5 days [54]. Mesostable emulsions are stable in just 1-3 days, while entrained water and changeable W/O emulsions are not considered as steady emulsions since both could just stay water in oil for fewer than one day [45, 53]. The emulsion type is an essential parameter in choosing demulsifiers solvable in the continuous phase and can reach the interface (oil/water interface) [51]. The type of emulsion relies on the attraction of surfactants to the water or oil phase. If the surfactant has an affinity to the oil phase (i.e., hydrophobic surfactants), water/oil emulsions could be produced, whereas the hydrophilic surfactants would generate oil/water emulsions.

On the other hand, the same tendency of natural surfactants to the two phases (oil and water) would create unstable emulsions. The parameters defining the surfactant's attraction contain relative solubility number (RSN), hydrophilic-lipophilic deviation (HLD), hydrophilic-lipophilic balance (HLB), and recovery (R_{oil}) ratio [55, 56]. Very

well, the affinity of surfactants to a hydrophilic or a lipophilic phase results in fewer steady emulsions since the surfactants are likely to remain in the emulsion instead of transferring to the interface of oil and water [57].

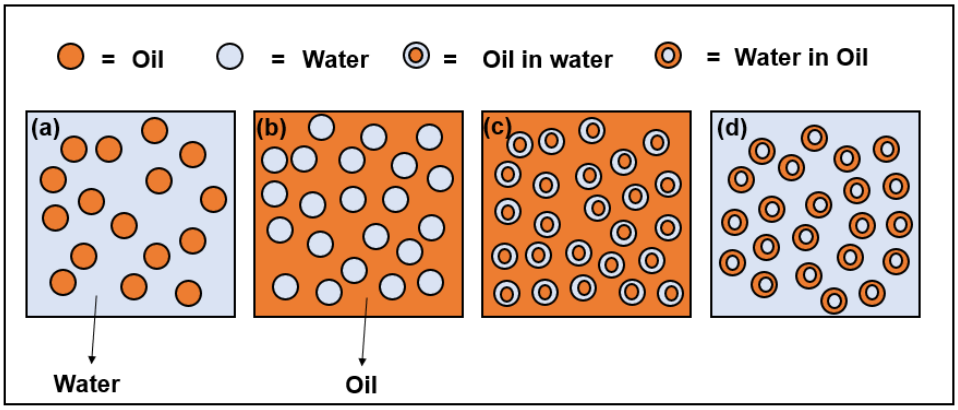

Figure 1. Emulsion types (a) oil in water (O/W), (b) water in oil (W/O), (c) multiple emulsion oil in water in oil (O/W/O) (d) multiple emulsion water in oil in water (W/O/W).

2.1.3 Emulsion Stability

The stability of the emulsion is linked to the type and volume of surfactants. These surfactants encourage the stability of the emulsion by creating films over the water droplets in O/W interfaces. The production of films enhances the emulsion stability by raising the interfacial viscosity and reducing interfacial tension (IFT) [58]. However, it has been observed that some factors, for example, oil concentration and mixing rate, can alter the stability of the emulsion [59]. By inserting energy into the system, the particles will break into lesser sizes, and at last, the emulsion turns out to be more stable, which will not be simple to handle. These parameters can affect the physical feature of O/W interfacial films, and the emulsion stability can be affected by surfactant solubility in the oil and water phase [60]. Moreover, emulsions are thermodynamically unstable, and the characteristics of emulsions vary in a specific time. Thus, it is crucial to examine

its thermodynamic and kinetic stabilities in terms of a good understanding of the emulsion stability mechanism.

2.2 Interfacial Film

As stated earlier, generated oilfield emulsions are steadied with films that create over the water droplets at the O/W interface [19]. These films are considered the consequence of the high-molecular-weight polar particles adsorption that is interfacially active (i.e., present surfactant-like performance). These films improve the emulsion stability by (a) decreasing IFT and (b) raising the interfacial viscosity. On the other hand, highly viscous interfacial films hinder the oil/film discharge rate through the coagulation of the water particles by giving a mechanical barrier to coalescence, reducing the rate of emulsion separation [50].

The properties of interfacial films are a function of the type of crude oil, the composition of oil, and water pH, the degree to which the adsorbed film is driven, contact or aging time, and volume of polar particles in the crude oil [61, 62]. A better correlation occurs between the rate of incompressible interfacial film and emulsion stability. These films are classed into two types according to their movements.

2.3 Surfactants

The term surfactant is an acronym of the expression surface-active agents having two-fold hydrophilicity and hydrophobicity characteristics. It indicates the surface-active nature of these types of composites and their propensity to adsorb at interfaces. The polar part shows a powerful attraction for polar solvents, and it is often known as the hydrophilic part or hydrophile. On the other hand, the polar part is so-called hydrophobic or lipophile, attracting oil [63] (Figure 2).

For preparing kinetically stable emulsions, an emulsifier (i.e., surfactant) is required to save the freshly produced droplets versus the various destabilization methods. The surfactant generates a protecting interfacial film when it adsorbs to the surface of the droplets, inhibiting the particles from combining all. On the other hand, the surfactant tends to keep the physical and chemical condition of an emulsion mostly by acting as a thickening factor, improving the viscosity of the water phase, and subsequently reducing the droplet encounters and the precipitation rate [64].

Demulsifier hydrophilic-lipophilic balance (HLB) is the extremely crucial factor that indicates its comparative concurrent attractiveness to the oil and/or water phase. Generally, a range of 0-20 is utilized to describe the surfactant nature. HLB values greater than 10 (high HLB value) reveal that the surfactant is hydrophilic and greatly appeals to the water phase that produces O/W emulsion. HLB value smaller than 10 (low HLB value) implies that the surfactant has further attractiveness to the oil phase and manages to create W/O emulsion. When the HLB value equals 10, oil and water-affectionate groups are perfectly stable [65]. Surfactants can be categorized into four wide types: anionic [66], cationic [67], non-ionic [68], and amphoteric [69] (Figure 3 [70]). Some information about these types of surfactants used for stabilizing oil in water emulsions is presented in Table 1.

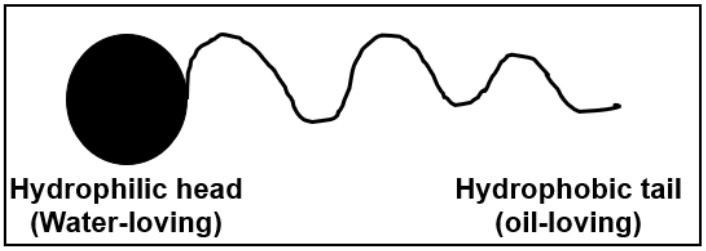

Figure 2. Structure of surfactant molecule.

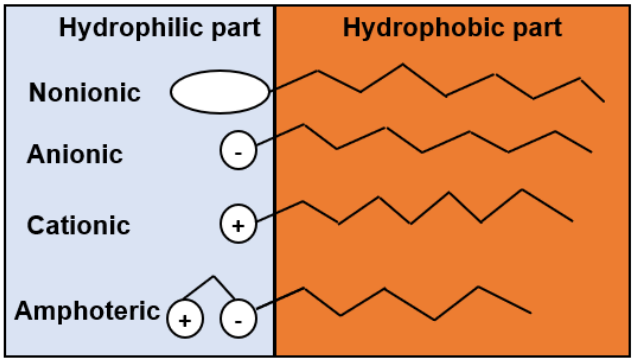

Figure 3. Surfactant classification.

Table 1. Some information and examples of the four types of surfactants.

Surfactant Types	Definition	Examples	Charge Carrier	Ref
Anionic	Surfactants that are dissociated in water into an amphiphilic anion and a cation, usually alkaline metal (Na+, K+) or quaternary ammonium	Phosphate esters, Sarcosine, Stearine/Stearic fatty acids. Sodium lauryl sulfate Sodium dodecylbenzene sulphonate (SDBS) Sodium lauroyl sarcosinate (INCI)	Negative	[66]
Cationic	Surfactants are dissociated in water into an amphiphilic cation and anion, most frequently halogen type.	Benzalkonium, Benzethonium, Methyl benzethonium, Cetylpyridinium, Alkyl-dimethyl Dichlorobenzene Ammonium, Dequalinium, Phenamylinium, Chlorides, Cetrimonium, Cethexonium bromides	Positive	[67]
Nonionic	Surfactants that have multiple polar groups in their hydrophilic end are typically not as effective as ionic surfactants and are frequently used in combination with ionic surfactants	Polyglycerol alkyl ethers, Glucosyl dialkyl ethers, Crown ethers, Ester-linked surfactants, Polyoxyethylene alkyl ethers, Spans (sorbitan esters) and Tweens (Polysorbates).	No electrical charge	[68]

Surfactant types	Definition	Examples	Charge carrier	Ref
Amphoteric (Zwitterionic)	Surfactant molecules display both anionic and cationic dissociations.	Phospholipids Alkyl betaines, alkyl dimethyl imidazoline derivatives such as alkyl amphoacetates	Positive and negative charges (dependent on emulsion pH)	[69]

2.4 Surface Wettability

Wettability, one of the highly significant surface properties, impacts the properties and the use of the material, particularly its use in fields of enhanced oil recovery (EOR) [71, 72]. It's well known that the contact angle created with the liquid on its surface was usually used for describing the wettability; however, various measurement techniques have been observed and used for additional determination of the wetting characteristic of the material surface [73]. Commonly, two wettability types, hydrophobicity, and hydrophilicity have been categorized by the wettability index, such as contact angle; furthermore, super hydrophobicity and super hydrophilicity can be classified more classified when the contact angle is $< 10°$ or $> 150°$, respectively [74, 75]. The study introduced by [76, 77] evaluated the wettability of O/W emulsions using ionic surfactants as demulsifiers for oil removal. When the ionic surfactants are presented into the O/W surface, the wetting region of the surface might turn to water/wet because of the desorption of adsorbed oil. Still, when the surfactants are placed in the undefiled charged surface, the hydrophobic phase is created onto the surface via interactions, causing the lyophobic wettability [78]. Furthermore, wettability also differs with an increase in temperature. And the high-wetting surface is usually produced by rolling and coating techniques [79]. Depending on these varying approaches, several wettability alterations, for example, hydrophobic alteration and hydrophilic alteration,

can be applied, which perform various functions in produced water treatment and oil generation.

The hydrophilic surface alteration, which can be achieved by the inorganic ions and certain surfactants with hydrophilic head groups, is highly significant in enhancing oil recovery [4,20]. After primary and secondary oil generation, the remaining oil creates a hydrophobic surface on the rock, which disrupts the oil separation; thus, the wettability alteration that encourages the separation of remaining oil from the reservoir surface can play a role as the main process mechanism in the oil recovery technique [80]. Numerous oil replacement techniques, for example, surfactant flooding (SF), molecule deposition (MD), low salinity water flooding (LSWF), filming flooding (FF), and nanoparticle fluid flooding (NFF) that alter the wettability to further hydrophilic by inserting replacement liquids have been suggested and discovered to be operative for improving the recovery [81, 82]. Purswani et al. [83] have examined the mechanism of LSWF in oil/wet carbonate rocks, and they implied that the rise of water/wet causes the increase of oil generation. Surfactant flooding (SF) has been tested over the previous years, and further green agents have been designed. Deljooei et al. [84] have prepared a new green surfactant for the oil recovery process, revealing significant wettability alteration and oil recovery abilities. The other oil displacement methods, including filming flooding (FF), has been suggested by [85], which shows their high ability to alter the wettability and consequently increase the recovery.

For the surface hydrophobic alteration, it is always favorable to treat organic pollutants in the produced water. Issaoui et al. [86] have prepared a type of organic clay that demonstrates the high adsorption capacity for bisphenol-A. Wang et al. [87] have examined gemini, and monomer surfactant modified nanoparticle's demulsification efficiencies; results showed that the oil adsorption increases with the modifier's

hydrophobicity. Through a reaction of ion exchange or electrostatic interaction among the surfactant and the demulsifier, the surface has occurred, the surfactant is inserted into the clay, causing more hydrophobic adsorbent surface, which gives a good condition of adsorption [88, 89] and aiding the oil adsorption by the interactions between the demulsifier functional group and the oil [90, 91]. According to these findings, the surface with unique wetting characteristics is usually dedicated to O/W removal. Beshkar et al. [92] have produced a hydrophobic/super oleophilic fabric filter for O/W removal, which reveals high removal efficiency. The methods and implementations of wettability alteration on the O/W removal deserve more explanation, which gives the most critical impact for its upcoming development.

2.5 Oil Recovery Process

Chemically enhanced oil recovery (EOR) methods are anticipated to perform the main part in worldwide crude oil production [93]. Nevertheless, the separation of generated O/W emulsions for the oil recovery process is crucial for method achievement. These emulsions can be highly steady, and the emulsion stability was accomplished by adding the surface-active materials (surfactant) to the emulsion. As an example, for the chemical enhanced oil recovery process, Hjartnes et al. [94] stated that emulsions might have continuous aqueous phases, including a mixture of an anionic surfactant and materials with high molecular weights (demulsifiers), for example, hydrolyzed polyacrylamide (HPAM) polymers. They presented that after adding the demulsifier to the emulsion mixture and applying surfactant concentrations differ throughout the method in the range from under 0.1 to possibly 0.5% by mass, the oil recovery rate was improved reliant upon specific parameters, for example, the concentration of the demulsifier, the concentration of the surfactant, and other process design parameters such as pH, salinity, oil concentration, etc. The employed polymer amount is more than

around 0.1% by weight. Other chemicals, such as nanoparticles, ionic liquids, and functionalized materials, may also be present in the enhanced oil recovery chemical mixture as demulsifiers for recovering the oil from O/W emulsions [95]. The surfactant must be favourably solvable in the water phase for these conditions and dissolve specific oil in the oil separation method. Therefore, the water phase is an oil-in-water emulsion. A standard method necessity is to create cost-effective removal of the emulsion, giving an oil phase including no further than 0.3-0.5 (volume%) water and a water phase including no further than 200 ppm oil, if possible 100 ppm [96].

2.5 Mechanisms of Oil Recovery

The oil recovery mechanism focuses on the electrostatic attraction forces among the oil and the demulsifier applied. Overall, the oil particles negatively charged from the oil in water emulsion can graft to the functional groups with positively charged on the demulsifier surface via electrostatic attractiveness force of the hydrophobic bond [97]. Most of the oil removal techniques involve the dispersion of the demulsifier into the emulsion mixture. Subsequently, the focus on materials, ion, functional groups surface is adsorbed onto the surface of the demulsifier. A magnetic field is introduced when using magnetic nanoparticles demulsifiers separately or grafted with other demulsifiers (polymers, different magnetic nanoparticle types such as silica nanoparticles). Finally, the NPs with the adsorbed substance are removed from the emulsion mixture [98].

Furthermore, oil separation from O/W emulsion is generally reliant on the addition of surface-active compounds that adjust the interfacial properties (such as interfacial tension [IFT], mechanical strength, plasticity, and thickness of interfacial layers). Changing the interfacial properties enhances the oil particle’s coalescence and flocculation in the emulsion [99]. On the other hand, if the magnetic nanoparticles are added to the emulsion, the demulsifying influence happens since the particles remain

covered with interfacial active NPs [100]. While specific nanoparticles such as iron oxide, iron oxide-based silica NPs have shown great efficiency in the oil removal process, the comprehensive mechanism for how the magnetic nanoparticles can improve the oil separation rate is so far to be summarized and realized. Various methods for improving the oil separation rate applying the chemical demulsification process have been introduced, involving IFT decrease, disjoining pressure and movement management, wettability alteration, viscosity management, and demulsification [101]. The aforementioned methods occur due to adsorption, desorption, and oil movement throughout the nanoparticle's pore throat [102]. The adsorption happens when the remaining attraction forces are more significant than the net repulsion force; if not, desorption happens.

Furthermore, the oil particle's transportation to the pore throat is pushed by dispersion and convection. Nevertheless, blocking might occur due to oil droplets agglomeration of bigger than the pore throat [102]. Numerous studies have demonstrated how wettability is crucial for achieving the maximum oil removal rates [77]. The wettability considerably influences the capillary pressure and comparative porousness, the point at which the oil grafted to the demulsifier can be significantly enhanced [103]. On the other hand, capillary force manages the IFT among the O/W emulsion and the demulsifier. With decreasing the IFT and adjusting the wettability of the demulsifier, the capillary pressure decreases, and the oil removal rate rises [95]. Hence, the existence of the demulsifier aid in reducing the IFT in the absence or presence of the surfactant.

Moreover, the demulsifier can enhance the emulsion mixture rheology properties and improve the impact of the surfactant in decreasing the IFT [104]. The mechanism of the disjoining pressure is a new and further methodology to comprehend the oil removal process's mechanism and describe the contact between the demulsifier and oil.

Disjoining pressure is the repulsive and attractive force among binary thin films of fluid/solid surfaces [105]. The oil removal method is complicated due to the existence of a three-phase interaction area [106]. The demulsifiers are dissolved into the emulsion to create wedge-shaped and are pushed near the oil/demulsifier interaction zone. The required formations in the wedge layer improve the dispersing and grafting of oil droplets onto the demulsifier surface [107]. The force generated through a separate molecule is comparatively insignificant. Nevertheless, the overall force of the gathered demulsifiers is very high reached more than 7.5×10^4 Pa for the nanoparticles when applied as demulsifiers in the oil recovery process.

2.6 EOR Technologies

While the oil generation rates of current fields are decreasing and the rate of a new study has come to be significantly low in the previous years, the importance of enhanced oil recovery techniques is well realized. It is well understood that there are three main types of existing technologies of the enhanced oil recovery process: thermal methods, gas methods, and chemical methods [108, 109] (see Table 2).

(1) Thermal methods generally present heat into heavy oil reservoirs thru several approaches, such for example steam flooding (SF), cyclic steam stimulation (CSS), and steam-assisted gravity drainage (SAGD), to improve the movement capability of the heavy oil or asphalt in reservoirs via altering its density and viscosity (physical characteristics).

(2) Gas methods use CH_4, C_3H_8 or natural gas (hydrocarbon gases) or N_2, or CO_2 (non-hydrocarbon gases) that disperse in oil. Thus, the inserted gas can enhance oil recovery by reducing the oil viscosity and increasing the oil amount.

(3) Chemical methods mainly include the utilization of different chemicals known as demulsifiers such as polymers, nanoparticles, ionic liquids, etc. to increase the effectiveness of the oil recovery process, or the usage of surfactants to facilitate the reduction of IFT that often inhibits oil particles from flowing via a reservoir. In summary, all these enhanced oil recovery techniques manage to recover additional oil from reservoirs through several processes: IFT decrease, wettability alteration, movement management, alteration of physical characteristics, and gravity discharge.

Table 2. The main types of existing technologies of the enhanced oil recovery process, their mechanisms, and challenges.

Oil recovery methods	Detailed procedures	Mechanisms	Challenges	Ref
Thermal methods	• Steam flooding • Cyclic steam stimulation (CSS) • In-situ combustion • Electrical heating	Decrease in the viscosity Decrease in the IFT Steam distillation Oil expansion Gravity discharge	High cost Low thermal conductivity Heat leak to the unsought films Low effective thermal degradation Heat deficiency from heat producer to the reservoir	[108]
Chemical methods	• Alkaline flooding • Surfactant flooding • Polymer flooding • Micellar flooding	Decrease in the IFT Wettability alteration Movement management Emulsification	The high cost (additional quantity required) Low efficiency on IFT and viscosity alterations Damage owing to inconsistency Un preferable movement ratio Sluggish dispersion rate	[109]
Gas methods	• Injection of hydrocarbon gas • Injection of CO_2 • Injection of N_2 • Injection of water alternating gas (WAG)	Decrease in the viscosity Oil expansion Pressure maintenance Miscibility	Gravity override CO_2 corrosion Miscible flooding requires minimum miscible pressure (MMP) Early gas permeation	[108]

2.7 Chemical Demulsification

As an effective and fast demulsification technique, chemical demulsification has been extensively utilized for several years. Demulsifiers are usually amphipathic composites along with both hydrophilic and hydrophobic groups. The oily produced water surface tension can be altered after adding the demulsifier to encourage the flocculation and aggregation of oil particles by substituting the essential interfacial active materials, hence attaining the demulsification [21, 110].

In this type of treatment, more significant amounts of alkali, surfactants, and chemicals are utilized. Surfactants are mostly liable for the stability of oil particles, decreasing oil/water interfacial tension, and zeta potential on the oil particles surfaces [111]. The stages for the process include the Ostwald ripening (i.e., change of an inhomogeneous structure over time), flocculation, coalescence, and phase separation. The film near the small drops in the O/W emulsion inhibits the water drops from merging, and the emulsion stays stable. Demulsifiers are surface-active materials that are efficient in interrupting the impacts of emulsifiers (surfactants) added to the O/W emulsion [3].

Demulsification performs an essential role in separating oil from the water phase, which is critical throughout the industrial process [45]. While crude oil contains different pollutants, they should be separated because they affect the equipment in the industry and lead to severe problems such as fouling and corrosion. This method can just be implemented when demulsifiers are applied. This chemical can cause the coalescence of oil droplets with producing film discharge and improve the surface motion as the gradient is reversed. Consequently, it implies that demulsifiers can alter the physical characteristics of the O/W interface. When demulsifiers are inserted into a diluted emulsion of insignificant concentration, a specific method known as adsorption

happens. It will adsorb the emulsion and locate it on the surface in types of droplets [42].

Moreover, the demulsifier includes organic molecules, and it will adsorb the dispersed phase so that the non-polar component will be in the crude oil. In contrast, the polar part will keep in water [112]. Demulsifiers are also identified as non-ionic that comprise two individual components of hydrophobic and hydrophilic. The hydrophobic group includes alkyls oxypropylenes or alkylphenols, while the hydrophilic group comprises amine groups, oxyethylene, carboxyl, or hydroxyl. There are also numerous techniques in separating the emulsion, including chemical separation, electrical separation, and mechanical separation [112]. Generally, it is noted that the chemical method is a widespread method applied in the industry. The studies showed that the coalescence of O/W emulsion is enhanced, and the protecting film was broken using a chemical demulsifier [113]. Therefore, researchers are searching for a method to speed up the demulsification method efficiently. Numerous techniques were used, such as polymers, nanoparticles, surfactants, and other demulsifier types. According to the study performed by [43], it was noticed that the separation rate of (O/W) emulsion was incredibly effective when microwave power was utilized in comparison to the usage of chemical non-ionic surfactants. Also, they found that the solubility of the surfactant in water declines with the assistance of a saline mixture such as seawater.

On the other hand, the use of polymers grafted with magnetic nanoparticles was very hopeful. It shows a high coalescence rate where the oil drops are settled throughout the magnetism of an external magnetic field. It is also reusable, thus decreasing the cost in the oil industry as reported by [114] using Janus magnetic submicronic molecules or P(MMAAA-DVB)/Fe_3O_4. To improve the demulsification efficiency, the parameters that can influence it should be studied and considered, such as oil concentration,

surfactant hydrophile balance (HLB), pH, surfactant concentration, salinity, and zeta potential, etc.

The influential parameters (e.g., oil concentration, HLB, pH, surfactant concentration, salinity, and zeta potential) require further study and consideration to improve the demulsification efficiency. For example, for the oil concentration, the lower concentration it has, the higher the separating rate for the emulsion. Thus, the higher oil content becomes difficult for the demulsifier to disperse in the crude oil. Additionally, an increase in the amount of HLB, surfactant concentration, zeta potential, and salinity demonstrate a decrease in the separation efficiency of this process. However, the higher surfactant amount acts as a steading agent to protect the demulsification of crude oil, which produces a dense film that affects the dispersibility of demulsifiers in the emulsion [45, 115]. Figure 4 illustrates the mechanism of the chemical demulsification process.

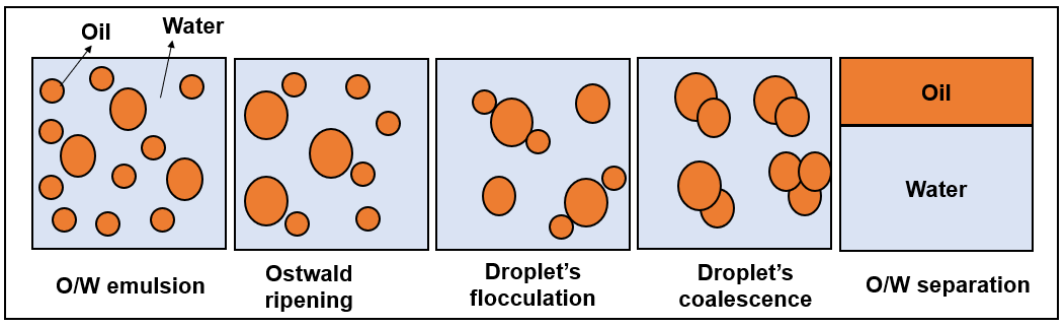

Figure 4. Representation of the mechanism of the chemical demulsification process.

2.7.1 Application of Magnetic Nanoparticles in the Oil Recovery Process

Due to the continued increase in worldwide energy need, innovative technology for improving oil recovery requirements needs to be developed [108]. The reality that obtaining creative hydrocarbon supplies is complicated, and the common oil fields have 60%-70% of non-generated hydrocarbon leads to the improvement of new techniques

for enhanced oil recovery [116]. The application of NPs in the oil recovery process has various advantages, for example (1) high stability since the surface force is more controlling than gravity; (2) the shape and size of NPs can be improved throughout the industrial method with great elasticity; (3) the chemical characteristics of the NPs surface can be altered to be hydrophobic or hydrophilic; and (4) the most common NPs used in the oil recovery process is iron oxide and silica nanoparticles (99.8% silicon dioxide), which are environmentally friendly materials [117]. Until now, the three most popular types of NPs used in the enhanced oil recovery process can be categorized into nanofluid, nano emulsion, and nano-foam types. By description, nano-fluid is a fluid including diffuse NPs and producing a colloidal suspension. Nano emulsion is a biphasic distribution of two non-miscible liquids: either water in oil or oil in water particles steadied via the NPs, which is also called Pickering emulsion. For the nanoparticles-steadied gas bubbles in a liquid, it is termed nano-foam. The different main types of NPs are grafted NPs synergized with surfactants, and the most dominant nanoparticles are silica-based, of which the surface hydroxyl amount can be altered to make them each hydrophobic or hydrophilic, resulting in oil in water and water in oil emulsions, respectively. Various experimental tests on enhanced oil recovery using NPs have been conducted previously [118]. Different types of NPs, for example, graphene, carbon nanotubes (CNTs), metallic and metal oxides, have been examined by [119], all exhibiting favourable findings in improving the oil recovery process.

The application of NPs in the oil recovery method can develop both the upstream and downstream petroleum industry, involving discovery, drilling, generation, and oil production, along with refinery methods [120, 121]. In addition, it offers a broad field of substitutes for methods and materials to be used in the petroleum industry. The number of research on NPs (nanotechnology) associated with the oil industry has

increased fast in the past few years. Figure 5 represents the number of technical papers published in this area, showing a massive quantity of studies actions, even throughout the downtime of the petroleum industry. A review of crucial research associated with the use of nanoparticles in the oil industry is shown in Figure 5.

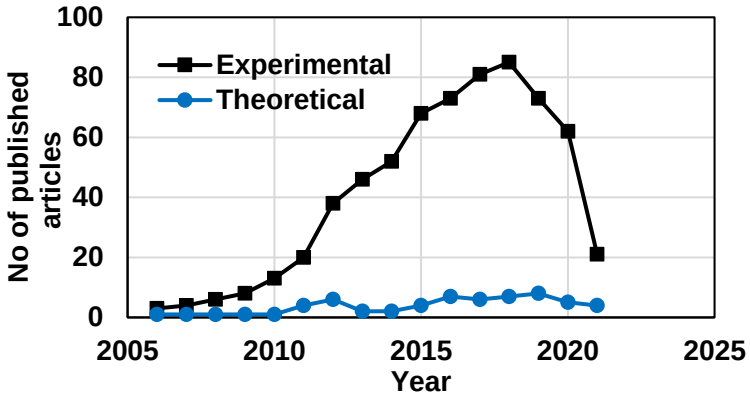

Figure 5. Research on the application of nanoparticles in the oil recovery process.

2.7.1.1 Characteristics of Magnetic Nanoparticles (MNPs)

Magnetic nanoparticle (MNPs) has become a promising material with fast improvement and great ability in the latest years. Therefore, it has been commonly utilized in several fields of advanced science, for example, thermometry [122, 123], catalysis [124], information storing [125], environmental preservation [126], and solar power production [127]. MNPs are mainly created from a magnetic core, for example, nickel, cobalt, iron, or their oxides, and an active-group shell layer. The superparamagnetic or ferromagnetism showed via magnetic core conduces to attaining movement in a specific direction and magnetic production heating below the impact of various magnetic domains. Furthermore, the active groups combined on the shell layer can be coupled to certain particles, thus achieving the grafting. Consequently, the grafted magnetic nanoparticles (MNPs) have both the properties of MNPs and shell-layer nanoparticles,

for example, surface impact, magnetization impact, magneto-mechanical impact, and magnetic induction heating.

2.7.1.2 The Most Common Nanoparticles Studied for the Oil Recovery Process

2.7.1.2.1 Iron Oxide NPs

Iron oxide (Fe_3O_4 or Fe_2O_3) nanoparticles have been suggested as nano devices [128]. Nevertheless, there is just limited research on the possible usage of iron oxides for the enhanced oil recovery process. Haroun et al. [129] examined numerous metal oxide NPs, for example, NiO, Fe_2O_3, and CuO, on the plugs of the carbonate nucleus. The outcome for the iron oxide nanoparticles was not so favourable because it could just achieve a maximum oil recovery equal to 57%, while other nanoparticles might attain more than 85%. Nevertheless, others have demonstrated that iron oxide nanoparticles could enhance oil recovery efficiency by more than 24% (extra) when dispersed in water [13]. Joonaki et al. [130] stated that Fe_3O_4 or Fe_2O_3 could remove 17% of additional oil as other nanoparticles, including the SiO_2 and Al_2O_3, were separated about 20% extra oil. Shekhawat et al. [131] examined the efficiency of magnetite Fe_3O_4 in heavy oil recovery using a magnetic field. The mechanism of magnetic recovery works by applying an external magnet to the oil in water emulsions and driving the NPs toward the magnet to assemble the highest amount of oil.

2.7.1.2.2 Silica-Based Nanoparticles

Silica-based nanoparticles are highly frequently examined for an enhanced oil recovery application. At the same time, they can be generated, have well-identified chemical and physical characteristics, and can be obtained with various properties, for example, hydrophobicity to hydrophilicity [117]. Besides, they are potent non-harmful inorganic substances [132] and have lower production costs than the other nanoparticles [133].

Several silicas nanoparticle types have been prepared and tested for oil recovery process [134]. These can be classified depending on their wettability performance into three categories [135]: lipophobic and hydrophilic polysilicon (LHP), hydrophobic and lipophilic polysilicon (HLP), and neutral-wet polysilicon (NWP). Silica-based NPs have been confirmed to alter the emulsion system wettability when adsorbed. Additionally, silica NPs have high thermal steadiness, as noted utilizing x-ray diffraction (XRD), infrared spectroscopy (IR), and scanning electron microscopic (SEM analysis), without the thermal unsteadiness for comparatively superior-temperature uses [136]. Ju et al. [102] carried out investigational and theoretical research on using hydrophilic silica nanoparticles for the enhanced oil recovery process. By adding 2.0-3.0% of silica NPs, the results showed that the nanoparticles could be adsorbed, changing the wettability of the O/W system and enhancing oil recovery. Onyekonwu and Ogolo [137] presented another study on silica nanoparticles dissolved in various fluids include ethanol, water, and alcohol. The produced silica nanoparticles dissolved in ethanol could change the wettability from water-wet to oil-wet and act as surfactants by decreasing the IFT between the O/W phases. Hendraningrat et al. [138] examined the impact of silica NPs by applying different doses of NPs (0.01 to more than 0.1 wt%) dissolved in brine (3 wt% of NaCl). They revealed that the contact angle declines when the NPs amount rises, but the greater amount enhanced the efficiency of the oil recovery process. Furthermore, silica nanoparticles were applied by [139] for the oil recovery from heavy crude oil/water emulsions. Silica nanoparticles dissolved in brine in a carbonate core sample and increased the recovery (39% to 61%) [140]. An integration of silica nanoparticles with a polymer for enhanced oil recovery was also examined by Maghzi et al. [141]. They dissolved silica nanoparticles into a PAM polymer mixture (hyperbranched polymer) in a glass micromodel to test the

polyacrylamide emulsion rheology properties when silica nanoparticles are added to the emulsion. By employing 0.1 wt % of silica NP to the emulsion, the overall viscosity of the mixture was enhanced, which resulted in further oil recovery of more than 10%. Sharma et al. and Corredor et al. [142, 143] tested the use of silica NPs dissolved in surfactant and polymer solution for chemically enhanced oil recovery and discovered that silica NPs can lesser and steady the IFT for the emulsion, resulting in 21% extra recovery in comparison to the surfactant-polymer demulsifiers. Besides, they found that the efficiency of polymers and surfactant-polymer demulsifiers is decreased when applying high temperatures to the emulsion system. In contrast, the emulsion mixture shows stable performance at greater temperatures using silica nanoparticles, making silica NPs a high potential solution for high-temperature chemical enhanced oil recovery processes [144, 145]. Recently, Kim et al. [146] and Zhong et al. [147] prepared a stable decane/brine solution with small silica NPs and silica coated HPAM polymer. They showed that at low NPs dosages, a larger size of NPs was preferred, while at high NPs dosages, a lesser size of NPs was favoured. Silica NPs are deemed the highly cost-effective and environmentally friendly NPs; however, the threat of dry silica NPs must be evaluated because they might be hazardous to people when directly breathed in [130]. An excellent oil recovery rate (R_{oil} < 90%) was achieved applying high oil concentration (C_{oil} < 2000) mg/L using Fe_3O_4 magnetic NPs grafted with silica nanoparticles (doses as low as 10 mg/L) in the study done by [148] and [149] . The developed magnetic NPs exhibited excellent oil recovery, consistent steadiness, and great magnetization values (between 46.1 and 80.2 emu/g). Adding a 5,8,10, and 15 nm silica layer on the Fe_3O_4 magnetic NPs surface preserved them from oxidation conditions, expanded their service life, and attained a high oil separation (96.3%) as stated by [95]. The magnetite (Fe_3O_4) MNPs were applied separately in the oil recovery

from oil/water emulsions in our previous study in chapter 4 [39]. The Fe_3O_4 achieved oil removal ≥ 98% for C_{oil} in the range of 200-660 mg/L. More than 98.6% of the $\%R_{oil}$ was achieved for C_{oil} in the range from 0-800 mg/L utilizing just 10 mg/L of Fe_3O_4 MNPs. A smaller dose of Fe_3O_4 (5 mg/L) recovered more than 55.6% of the oil. Table 3 summarizes the recent experimental research on the application of some nanoparticles, including iron oxide and silica nanoparticles, in the oil recovery process that has been reported. Also, the mechanism of the demulsification process using Fe_3O_4-SiO_2 hybrid nanocomposite in the oil recovery process was illustrated in Figure 6.

Table 3. Recent application of different nanoparticle types applied separately and added to other materials for the oil recovery process.

NPs type	NPs amount (wt%, mg/L)	Additive materials	Oil recovery rate (R_{oil}%)	Results and comments	Ref
SiO_2	1 wt%	Polyacrylamide	90%	Increased the emulsion viscosity and the emulsion stability after polymer addition	[140]
SiO_2, $Fe(OH)_3$, TiO_2, Al_2O_3	0.2 wt.%	Xanthan gum	80-89%	Improved the emulsion viscosity	[142]
Al_2O_3	0.05 wt.%	Anionic surfactant	88.5%	Wettability alteration of the emulsion to oil-wet.	[585]
SiO_2	0.01-3 wt.%	-	81-89	Improved oil and nanoparticles dispersion in the emulsion mixture	[138]
Fe_3O_4	10 mg/L	SiO_2	93%-94.3%	An excellent oil recovery	[40]
ZrO_2	0.1 wt%	Cetrimonium bromide surfactant	40%	Change the emulsion mixture wettability to oil-wet.	[134]

NPs type	NPs amount (wt%, mg/L)	Additive materials	Oil recovery rate (R_{oil}%)	Results and comments	Ref
Pyroxene	1 wt%	-	89.5%	Decreased the IFT and changed the contact angle between the oil and water phases	[133]
Pyroxene	1 wt%	-	89.5%	Decreased the IFT and changed the contact angle between the oil and water phases	[134]
CeO_2, ZrO_2, Al_2O_3, TiO_2, MgO, $CaCO_3$, SiO_2	5 wt%	-	91-92%	Enhancement in the emulsion mixture viscosity	[119]
TiO_2	2-2.6 wt%	Sodium dodecyl sulfate surfactant	96%	Enhanced rheological characteristics	[539]
SnO_2	2 wt%	-	78%	Reduction in IFT and wettability alteration of O/W emulsion	[134]
ZnO	1.6 wt%	-	89%	Reduction in IFT and emulsion viscosity	[136]
SiO_2	0.31 wt%	Xanthan gum polymer-surfactant	73%	Increased the oil viscosity in the emulsion	[159]
Nickel	0.005-0.02 wt%	Xanthan gum	94%	High emulsion viscosity	[134]

NPs type	NPs amount (wt%, mg/L)	Additive materials	Oil recovery rate (R_{oil}%)	Results and comments	Ref
SiO_2	1 wt%	Polyethylene glycol	92%	High rheological properties	[142]
Fe_3O_4	1 wt%	-	35% Enhancement in oil recovery	Reduction in IFT and crude oil recovery.	[134]
Fe_3O_4	10 mg/L	SiO_2 with different thicknesses in the range (5-15 nm)	93%-94.3%	An excellent oil recovery rate (R_{oil} < 90%) was achieved applying high oil concentration (C_{oil} < 2000) mg/L using magnetic NPs doses as low as 10 mg/L.	[40]
Fe_3O_4	10 mg/L	SiO_2 with different thicknesses in the range (5-15 nm)	87.5%-96.3%	Exhibited excellent oil recovery, consistent steadiness, and great magnetization values (46.1 and 80.2 emu/g). Adding a 5,8,10, and 15 nm silica layer on the Fe_3O_4 magnetic NPs surface preserved them from oxidation conditions, expanded their service life, and attained a high S_{oil}.	[95]

NPs type	NPs amount (wt%, mg/L)	Additive materials	Oil recovery rate (R_{oil}%)	Results and comments	Ref
Fe_3O_4	10 mg/L	-	≥ 98%	The Fe_3O_4 has achieved oil removal ≥ 98% for C_{oil} in the range of 200-660 mg/L. More than 98.6% of the $\%R_{oil}$ was achieved for C_{oil} in the range from 0-800 mg/L utilizing just 10 mg/L of Fe_3O_4 MNPs. A smaller dose of Fe_3O_4 (5 mg/L) recovered more than 55.6% of the oil.	[39]
SiO_2, TiO_2, Al_2O_3	0.1-0.4 wt%	HPAM	93%	Development in the rheological characteristics	[146]

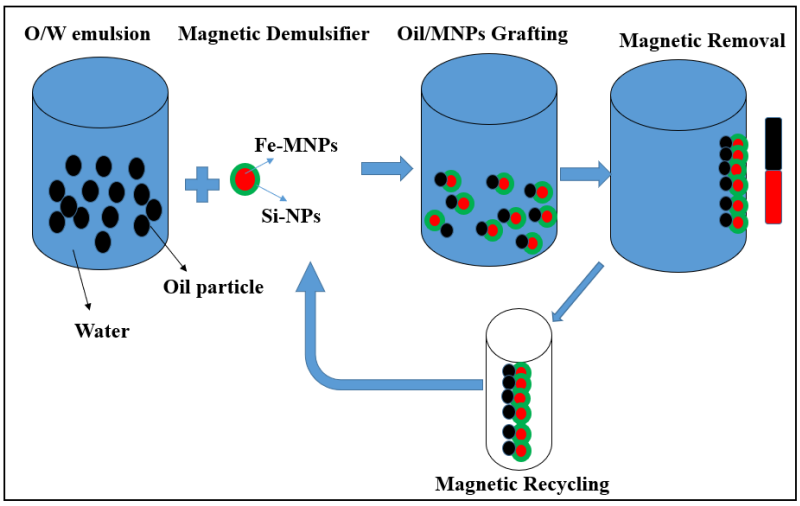

Figure 6. Application of Fe_3O_4-SiO_2 hybrid nanocomposite in the oil recovery process [40].

2.7.1.3 Parameters Affected the Application of Nanoparticles in Oil Recovery

2.7.1.3.1 NPs Size

The NPs size has a considerable effect on the demulsification process and oil production rates. For a comparable mass, a lesser NPs size will provide a greater particle force (density) and smaller contact angle among the oil and water surface. A greater particle force significantly increases the oil droplet's coalescence. It enhances the oil recovery [150], while slighter NPs will disperse further easily than larger particle molecules for fewer hydrophilic surfaces. McElfresh et al. [151] determined that lesser molecules would cause a more significant charge density and superior electrostatic repulsion, presuming the stability of the nanoparticle. As stated by Hendraningrat et al. [152], lesser nanoparticles size have been verified to improve the recovery of the oil significantly and enhance the movement efficiency of the nanoparticles inside the emulsion. Numerous previous tests determined that tinier particles would cause a greater final oil production rate [153]. Kondiparty et al. [150] showed that reducing the

nanoparticle diameter (30 nm-18.5 nm) enhanced oil recovery efficiency by around 4 times.

Consequently, small particles are often better to achieve high oil recovery [132]. On the other hand, it must be observed that the excellent surface energy might lead to an increased accumulation and adsorption of the very fine nanoparticles on the surface and thus influencing the emulsion stability. Moreover, the size of the NPs also impacts the surface functionalization (coating) method with other materials (demulsifiers). Hence, we believe that there would be an optimum value concerning the size of these NPs.

2.7.1.3.2 NPs Concentration

The NPs concentration is one of the crucial parameters that define the oil recovery method. Following the study shown by Chengara [154], the oil recovery will improve with increasing the NPs concentration, enhancing the repulsion forces inside the emulsion. Applying high NPs amounts will also enhance the oil recovery efficiency due to improved NPs dispersion in the emulsion [153]. The interfacial tension (IFT) among both phases (oil and water) can be reduced considerably by enhancing the concentration of NPs [155]. A great NPs concentration also causes a more significant wettability alteration impact. Therefore, a greater concentration is preferable to achieve greater oil recovery rates.

Nevertheless, there is a maximum limit to the NPs volume, and over that limit, NPs will be likely to affect the emulsion stability and negatively affect the demulsification process. A greater NPs amount will enhance the wettability alteration of O/W emulsions, reduce the IFT between the oil and water phases, and thus increase oil recovery efficiency. Nevertheless, when the NPs amount is very high, the accumulated NPs will gather in the emulsion and then decrease the oil recovery effectiveness[132].

Hendraningrat et al. [155] described that the oil recovery was reduced by around 2% when adding silica NPs with an amount exceeding 0.5 wt%. Consequently, an ideal amount is essential to obtain the highest production of oil. Nevertheless, this best amount differs depending on the nanoparticle type, emulsion type, and preparation conditions.

2.7.1.3.3 Salinity

The salinity of the O/W emulsion has a substantial impact on the NPs dispersion stability. High salinity values lower the nanoparticle's zeta potential values, which results in simple accumulation (agglomeration) [151]. As the surface of the emulsion is charged, it is estimated that the magnetism and collision will not occur for particle/surface but can take place for particle/particle [156]. Therefore, in a high salinity condition, functionalization of the NPs is crucial to preserve the steadiness, which can be achieved by surface grafting, ionic control through a surfactant, or an integration of both [153]. Worthen et al. [157] stated the steadying of nanoparticles by attaching polymers with low molecular weight to the nanoparticle surface in a high-salinity condition. The study found that the high salinity conditions enhanced the stability of the NPs.

Conversely, by utilizing silica NPs with high strength, Hendraningrat et al. [132] showed that adding NPs with high salinity could change the wettability further water-wet. At higher salinity conditions, the adsorption of the NPs is enhanced owing to the rise in the chemical exchanges [158]. Comparably, Kanj et al. [159] determined from their study that improving the emulsion salinity did not prevent the transfer of nanoparticles but did enhance the adsorption on the nanoparticle surface. Therefore, improving the salinity results in enhancing the NPs adsorption and thus increase the oil production rates. Nevertheless, simultaneously, the NPs stability will be decreased in

high salinity conditions. Hence, the proper salinity range and surface grafting are crucial characteristics to be studied to avoid the aggregation of the nanoparticles.

2.7.1.3.4 Wettability

Improving the wettability of the emulsion will enhance the oil production rates and vice versa [160]. Following the study done by [161], incredible water wetness is beneficial for more effective oil recovery. Nevertheless, in particular situations, it has been stated that an oil/wet emulsion [162] and neutral wettability [161] present more significant oil generation. Therefore, wettability performs an essential part in NPs dispersion, influencing the distribution and movement of the NPs in the emulsion [163]. Primary wettability will define the wettability alteration scale throughout the enhanced oil recovery process applying nanoparticles (nano-EOR). An investigational report utilizing silica nanoparticles indicated that the maximum oil generation was generated from an intermediary/wet system [155]. In an intermediary/wet situation, oil and water are instability conditions, which lowers the chance of oil removal in the emulsion [155]. Li et al. [116] revealed that wettability influences the NPs adsorption. Water/wet and neutral/wet emulsions have a greater NPs adsorption than the oil-wet emulsion mediums. In an oil/wet emulsion mixture, the adsorption zone is near the desorption region, implying that desorption is expected to occur. Therefore, the impact of nanoparticles on the oil/wet emulsions will be reduced. More innovative findings are required to examine the familiar and undetermined factors that might possibly influence the use of NPs in oil production methods. Greater knowledge of both approaches and factors is an important step to achievement in the practical application of NPs in enhanced oil recovery processes.

2.7.1.4 Surface Coating of Nanoparticles

While the greater physical and chemical characteristics shown by MNPs partially rely on their surface functionalization, surface grafting plays a crucial part in implementing the MNPs in oilfield applications. Several substances, for example, amine, polyvinylpyrrolidone (PVP), tetramethylammonium hydroxide (TMAOH), oleic acid, polymers, surfactants, and inorganic substances, have been applied for surface functionalization of the MNPs [164, 165]. In addition, several methods for example co-precipitation [166], sol-gel technique [167], hydrothermal technique [168], electrochemical [169], vapor phase procedure [170], and thermal decomposition [171] were applied for the preparation of surface-grafted magnetic nanoparticles (MNPs). Surface functionalization improves the MNP's stability and enhances their dispersibility in oil/water emulsion mixture. Additionally, it also assists in enhancing the surface activity of MNPs and developing the physical and chemical properties of MNPs [172]. By using a certain coating on the MNPs surface, the crucial requirements for MNPs have been utilized in oilfield uses can be fulfilled, which involve [173]: (i) the MNPs should stay steady for a long period without aggregate production when separately spread in the emulsion solution; (ii) the MNPs have to transference through the emulsion for a long space with slight retention; and (iii) the MNPs should only be adsorbed at the predictable places such as adsorbing at the oil/water interfaces of the remaining oil. Additionally, the type of nanoparticle, sonication (before and after the addition of dispersant), and the MNPs distribution in the emulsion, also have effects on the MNPs dispersion in the emulsion mixtures [174].

2.7.1.5 Nanoparticles Magnetization

The MNPs can be categorized into ferromagnetism and paramagnetism reliant on impulsive magnetization. These magnetic characteristics are considerably influenced

by NPs size. When the size of the nanoparticle is under a particular crucial value, it creates a separate magnetic field. Magnetic fields are the zones where each magneton in a specific amount of ferromagnetic substance aligns similarly below the impact of exchange force [175]. As the single magnetic domain nanoparticle diameter is fewer than the crucial value that superparamagnetic shows (generally from 3 to 50 nm according to the materials), the coercive force achieves zero, and these NPs demonstrate superparamagnetic performance [176]. The superparamagnetic NPs are the highly generally utilized MNPs, and thermal impacts mainly produce the superparamagnetic. Usually, the super paramagnets magnetization curve, demonstrating no hysteresis, varies from that of ferromagnets. Superparamagnetic NPs distributed in the emulsion mixture will reveal nonmagnetic performance in the non-existence of an outer magnetic domain (Figure 7a). When a low magnetic field is introduced, the thermal agitation can partly beat the movement of dipole moment alignment near the magnetic field. As the magnetic domain power rises, the superparamagnetic NPs will line up gradually. When it surpasses a specific value, the magnetization will achieve the saturation condition where the superparamagnetic NPs are aligned [177], as demonstrated in Figure 7b. The magnetization of superparamagnetic NPs, defined by the modified Langevin function (equation 1), relies on the intensity of the utilized magnetic field (H) and the saturation magnetization of superparamagnetic NPs (M_s) [178, 179]:

$$M = M_0 L \frac{(\mu_p H)}{K_B T} + X_a H \quad (1)$$

where $L(x) = coth\ -1/x$ is the Langevin function, x is the Langevin factor, μ_p is the median magnetic moment of every superparamagnetic NP, and χ_a is the linear compound of the sensitivity. With such magnetization feature, superparamagnetic NPs

can produce inducement domain when exposed to an external magnetic field, which conduces to releasing their sites and has been revealed remotely.

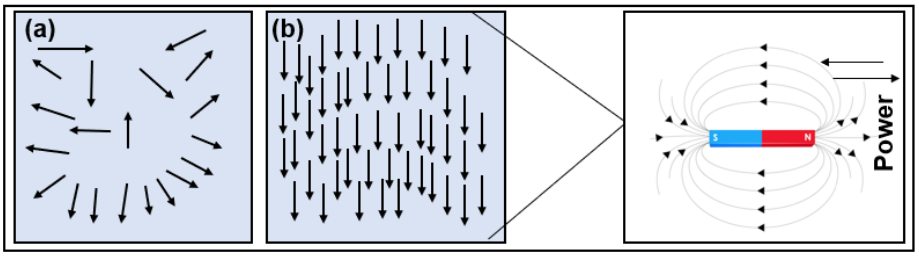

Figure 7. (a) Superparamagnetic NPs dissolved in water demonstrate non-magnetic performance in lack of outside magnetic field (b) Complete alignment of NPs when a strong magnetic field is employed.

2.7.2 Application of Hyperbranched Polymers in the Demulsification Process

Owing to the highly branched and 3D expanded structure, polymer demulsifiers are highly beneficial in oily wastewater treatment [14]. Le Follotec et al. examined the correlation between four triblock copolymers' interfacial characteristics, structures, and demulsification behavior properties. They realized that polymers with lengthy hydrophobic bonds are unproductive for both W/O and O/W emulsions, while polymers with shorter hydrophobic bonds are found to be operative in the demulsification process [180]. Furthermore, twenty polyether copolymers dependent on polyethyleneimine (PEI) were produced by Wang et al. They studied the impacts of the intermediary size and the ratio between EO/PO on the effectiveness of the demulsification process using these polyether's. The findings demonstrated that the demulsification ability enhanced with expanding the size of the hydrophobic units of the polymers [181]. Consequently, Pensini et al. analyzed the interaction between the PEO-PPO (diblock) polyether and

asphaltene in the O/W emulsion and observed that demulsification could be attained at a minimal amount [182].

In an inclusive review by [15] polymers utilized in EOR methods, they consider that there is a massive hopefulness that the usage of polymer might show an essential part in covering the present energy need since its uses in particular enhanced oil recovery fields has revealed some achievements to regenerate up to 20% extra oil from oil content. In demulsification of O/W emulsions using polymers as demulsifiers Hydrolyzed Polyacrylamide (HPAM) is one of the highly popular polymers utilized in the oil recovery process to date; it was found to be effective in enhancing O/W emulsions stability but, at the same time, complicate the water treatment process [183]. A collection of tests was applied to realize the effect of adsorbent amount on sorption efficiency. They studied the impacts of HPAM on O/W Interfacial characteristics and the stability of emulsions developed by crude oil. The study was carried out by measuring interfacial tension (IFT), Zeta potential, and the stability of the emulsion. They noticed that HPAM can adsorb at the O/W interface between the oil phase (oleic) and water with no reduction in the IFT. They were improving the concentration of HPAM polymer results in an improvement in the Zeta potential and emulsion stability. The findings from this research can assist in the proper choice of surfactants used in oil in water emulsions. [183, 184] conducted experimental investigations at separate times regarding the chemical description of the emulsions formed using paraffinic crude oil that comprises a minimal concentration of asphaltene and incredibly low acid number known as “Da Qing” crude oil. In this process, hyperbranched demulsifiers polymerized in sodium hydroxide solutions were applied to recover crude oil. The oil recovery was enhanced, but a strongly steadied O/W emulsion complemented the generated oil.

Hyperbranched polymers have particular shapes, sizes, interfacial movements and can change the basic interfacial active materials at the O/W interface. Hence, these polymers are highly hopeful for O/W emulsion separation [185]. It was previously stated that hyperbranched polymers exhibited superior demulsification behavior than linear polymers due to the additional branch bonds, greater interfacial action, better dispersion, and more significant end groups. The demulsification behavior of the hyperbranched polymers is strongly associated with different parameters, for example, the branch chains number, molecular weight, hydrophilic units, and grade of isomerism. Wang et al. [186] synthesized a hyperbranched polymer known as a "broom molecule" polymer and detected that this polymer with an innovative dendritic structure acted great demulsification behavior versus an O/W emulsion. El-Sharaky et al. [187] developed a star molecule that relied on ((nitrilotris(ethane-2,1-diyl)) tris (oxy)) tris (4-oxobut-2-enoicd) and examined its effectiveness in the demulsification process. It was noticed that the star polymer was extra effective compared to the PEO/PPO-based copolymers for crude O/W emulsions treatment. Bi et al. [188] prepared benzyl-G3 and octyl-G3 hyperbranched demulsifiers utilizing strict benzyl and elastic octyl, respectively, as the dominant cores. Both demulsifiers showed great demulsification efficiency for the O/W emulsion. Hao et al. [189] applied triethyl tetramine (TETA) as the central core to produce a hyperbranched demulsifier. They attained a demulsification rate of 96.66 % for a diesel/water emulsion using low demulsifier volume and temperature in a short time. Yao et al. [190] produced hyperbranched polymers using methyl acrylate and ethylenediamine. They demonstrated that the polymers had an excellent demulsification efficiency in a diesel O/W emulsion and produced very fine oil particles. Consequently, two hyperbranched demulsifiers were prepared by Zhang et al. [191] utilizing an enhanced "one-pot" technique by

ethylenediamine and 1,3-malonediamine as the main cores. The results showed that the demulsifier with 1,3-malonediamine as the dominant core had greater demulsification effectiveness for a diesel/water emulsion in comparison to the demulsifier including ethylenediamine as the main core.

While hyperbranched polymers (HPs) have been examined widely for the demulsification process, their usage still meets numerous challenges, such as the demand for significant amounts, great operational temperature, and sometimes complicated production procedures [188, 190, 192]. Furthermore, most of these polymer demulsifiers are utilized in diesel/water emulsions [190, 191], and there have been limited articles for the treatment of produced O/W emulsions using HPGs polymers demulsifiers. In the study reported by Kuang et al. [193], HPGs prepared with 4,4-diamino diphenyl methane as the main core was observed to separate the diesel/ water emulsion and also needed a high temperature (60°C). Also, another type of hyperbranched macromolecular demulsifier was developed and used to separate oil from oily wastewater using a one-pot technique with 1,4-phenylene diamine (PPDA) as the dominant core and ethylenediamine and methyl acrylate as the chain parts. The results showed that PPDA could separate the oil using low demulsifier amounts and exhibits excellent efficiency in the demulsification process. Significantly, it can be utilized at ambient temperature. The impacts of the demulsifier dosage, settling time, temperature, and other significant parameters on the effectiveness of the demulsification process were examined analytically and in specific by [193]. Table 4 demonstrated some types of hyperbranched polymers that were applied recently in the oil recovery process.

Table 4. Application of hyperbranched polymers in the oil recovery process.

Polymer type	Results and Comments	Ref
Triblock copolymers	Polymers with lengthy hydrophobic bonds are unproductive for both W/O and O/W emulsions, while polymers with shorter hydrophobic bonds are found to be operative in the demulsification process	[180]
Polyether copolymers dependent on polyethyleneimine (PEI)	The demulsification ability is enhanced by expanding the size of the hydrophobic units of the polymers	[181]
		[182]
PEO-PPO (diblock) polyether	The demulsification process can be attained at an extremely small concentration (as low as 1 wt%)	
Polyacrylamide	Enhancement in the demulsification process and the polymer regenerated up to 20% extra oil from oil content	[15]
Hydrolyzed Polyacrylamide (HPAM)	The O/W emulsion stability was enhanced with the polymer by steric and electrostatic stabilization Oil recovery was enhanced, but a strongly steadied O/W emulsion complemented the generated oil	[183]
Dendritic polymer "broom molecule polymer."	Excellent demulsification behavior versus an O/W emulsion and high recovery	[186]
PEO/PPO-based copolymers	PEO/PPO-based copolymers for crude O/W emulsions treatment was found to be less efficient compared to the other polymer applied called star polymer that relied on ((nitrilotris(ethane-2,1-diyl)) tris (oxy)) tris (4-oxobut-2-enoicd)	[187]
Benzyl-G3 and octyl-G3 hyperbranched demulsifiers	Great demulsification efficiency for the O/W emulsion	[188]
Amine-based dendrimer polyamidoamine (PAMAM)	Attained a demulsification rate of 96.66 % for a diesel/water emulsion using low demulsifier volume and temperature in a short time	[189]
Amine-based dendrimer demulsifier PAMAM (polyamidoamine)	The polymers had an excellent demulsification efficiency in a diesel O/W emulsion and produced very fine oil particles	[190]

Polymer type	Results and Comments	Ref
Hyperbranched poly (amido amine) (h-PAMAM)	The demulsifier with 1,3-malonediamine as the dominant core had greater demulsification effectiveness for a diesel/water emulsion in comparison to the demulsifier, including ethylenediamine as the main core	[191]
Hyperbranched poly (amido amine) (h-PAMAM) using 1,4-phenylene diamine (PPDA)	High separation the diesel/ water emulsion and needed a high temperature (60°C). it can separate the oil using low demulsifier amounts and exhibits excellent efficiency in the demulsification process	[193]
Hyperbranched polyglycerol polymers (HPGs)	The HPG demulsifiers with hydrophobic and hydrophilic features are capable of abiding by the O/W interface, decreasing the IFT, reducing the adsorption time, enhance the oil droplets separation rate, and encourage phase separation via improved flocculation and coalescence method High oil recovery rates (recover up to 90.3%)	[37]
Hydrolyzed Polyacrylamide (HPAM)	Effective in enhancing O/W emulsions stability but at the same time complicate the water treatment process The stability of emulsions was developed HPAM can adsorb at the O/W interface between the oil phase (oleic) and water with no reduction in the IFT Improving the concentration of HPAM polymer results in an increase in the Zeta potential, and emulsion stability	[183-441]

Hyperbranched polyglycerol polymers (HPGs) are another type of hyperbranched polymers commonly applied for biomedical uses but have been used so far in water treatment and oil recovery processes [14]. HPGs are biodegradable, comparatively economical, easy to develop and produce, and provide a great oil recovery rate [191, 194]. HPGs structure includes hydrophilic and hydrophobic functional groups that assist in decreasing the IFT among oil and water; this instantly enhances the flocculation and coalescence of oil particles, therefore enhancing the separation of the

two phases [190, 195]. Furthermore, HPG polymer rapidly separates the phases, which lets the oil be separated from the water fast when adding the polymer to the emulsion mixture; this consequently enhances the polymer efficiency for oil recovery in a short time. In addition, the HPG polymers present a green demulsifier (i.e., environmentally friendly), in which employing them in the oil recovery method is viable and reduce the usage of toxic compounds [16, 17].

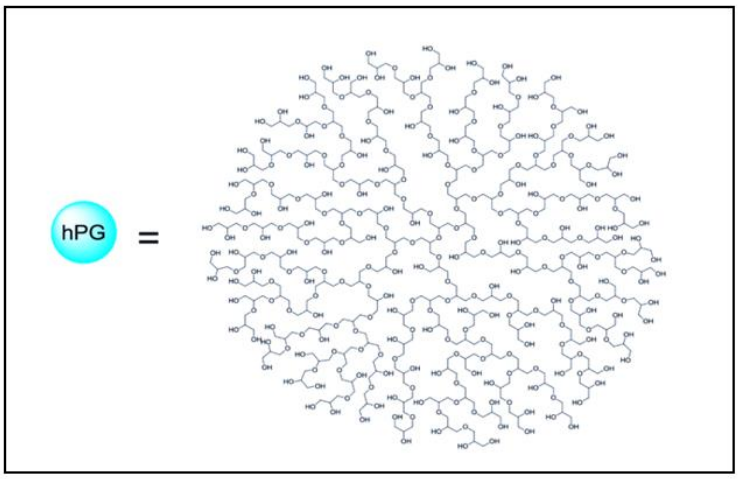

Figure 8. Structure of hyperbranched polyglycerol (HPG) polymer.

Figure 8 shows the structure of the hyperbranched polyglycerol polymer, which has presented great outcomes in the oil recovery process [37] as a green and efficient technology for oil recovery and separation from O/W emulsions.

In our work mentioned above [37], the demulsification method separates the oil from O/W emulsions into bulk phases of oil and water. The demulsification process can be characterized by four methods: destabilization, aggregation, coalescence, and gravity separation. Herein, chemical demulsification was applied with particular quantities of HPG polymer to the O/W emulsion. The HPG demulsifiers with hydrophobic and hydrophilic features can abide by the O/W interface, decrease the IFT, reduce the

adsorption time, enhance the oil droplet's separation rate, and encourage phase separation via improved flocculation and coalescence method [19, 37, 196].

2.7.3 Application of Ionic Liquids in the Oil Recovery Process

Ionic liquids (ILs) are another demulsifier type utilized effectively in enhanced oil recovery (EOR) methods. The properties of ILs are essential for the safety and health interests in industries. ILs can stay steady even at extreme temperatures (300◦C and above), but the problem is that other traditional surfactants applied to the emulsion might decompose at those temperatures. Specific properties make ILs distinctive in comparison to other demulsifiers [18]. The most common properties studied for ILs are the physical properties such as the melting point temperature. The melting point temperature for the C_2mim BF_4, C_8mim BF_4, N_{6222}mim NTf_2, C_2mim TfO, and C_6mim BF_6 ILs were found to be 15°C, -80°C, 20°C, -10.15°C, and -61°C [10].

Generally, for its application in the oil recovery process, the researchers favoured developing and producing room-temperature ionic liquids (RTILs), which are just comprised of ions (organic cations and organic or inorganic anions) showing low interactions, which generate a low propensity for crystallization. RTIL can be attained by preparing organic cations with variable organic anions, acetate, dicyanamide, trifluoromethyl sulphate or inorganic anions, chloride, bromide, hexafluorophosphate, tetrafluoroborate, and the formation of cations and anions in the emulsion mixture with the presence of the surfactant in the emulsion mixture develop the mechanism of ion exchange which causes the oil separation [197]. Figure 9 shows some prevalent ILs cations containing pyridinium, ammonium, imidazolium, pyrrolidinium, and phosphonium. While Table 5 listings few anions that are applied for preparing ILs.

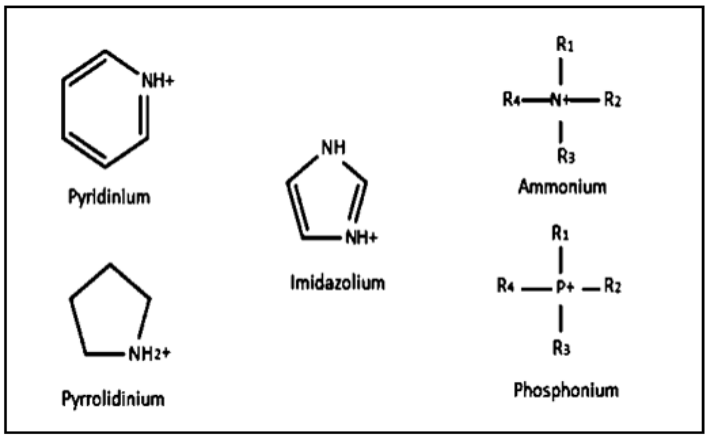

Figure 9. Common ionic liquids cations [10].

Table 5. Common ionic liquids anions [198, 199].

Anions	Abbreviation	Types (organic/inorganic)
Chloride	Cl^-	Inorganic
Bromide	Br^-	Inorganic
Fluoride	F-	Inorganic
Methane sulfonate	$R_3C\text{-}S\text{-}O_3^-$	Organic
Alkyl sulfate	$R\text{-}O\text{-}SO_3^-$	Organic
Hexafluorophosphate	PF_6	Inorganic
Tetrafluoroborate	BF_4	Inorganic
Iodide	I^-	Inorganic
Bis (trifluoromethyl sulfonyl) imide	$[(CF_3SO_2)_2N]^-$	Inorganic

Certain ionic liquids have an amphiphilic formation that attracts the two phases (oil and water) [27, 200]. The amphiphilic characteristic might be in the anion or cation portion of the structure of ionic liquids. According to the position of the amphiphilic design, ILs can be categorized into anionic or cationic ionic liquids [201]. Figure 10 demonstrates the ordinary structure of the ionic liquids.

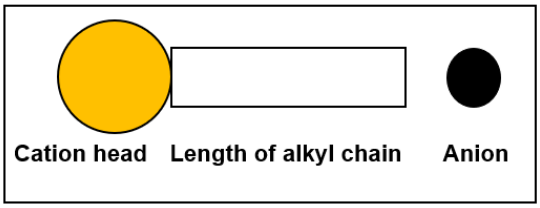

Figure 10. The general structure of ionic liquids.

Pillai et al. [202] examined the impact of various ionic liquids (C_{12}mim BF_4, C_{10}mim BF_4, and C_8mim BF_4) on the demulsification process and IFT decrease of oil in water emulsion at 30◦C. The outcomes revealed that at high concentrations of 12,000 ppm, 5000 ppm, and 2000 ppm, respectively for C_8mim BF_4, C_{10}mim BF_4, and C_{12}mim BF_4 IFT values were decreased to 14.57 mN/m, 4 mN/m, and 2.1 mN/m for each ILs, respectively. C_{12}mim BF_4 IL showed excellent performance in the oil recovery process compared to the other ionic liquids applied, which recovered about 32.28% of oil at an oil concentration of 2000 ppm.

2.7.3.1 Chemical Demulsification Using Ionic Liquids

The demulsifiers are surface-active materials utilized to weaken the emulsion phases for the separation [31, 44]. The demulsifier's surface action must be greater than that of surfactants to disrupt the emulsion [51]. The demulsifier's surface activity properties can be assessed through different methods, including electrical conductivity, proton nuclear magnetic resonance (H NMR), surface tension, etc.[203]. Chemical demulsification is applied by adding a particular volume of demulsifiers to emulsions and mixing them vigorously. Later, enough time is needed to let the Ostwald ripening (i.e., changing an inhomogeneous structure over time), flocculation, coalescence, and phase separation happen. Ostwald ripening occurs when the oil phase (dispersed phase) can disperse simply in the continuous phase (water phase) to reach simultaneously for coalescence. Flocculation is developed when the particles of oil or water gather

simultaneously in the water phase while they protect their character. Coalescence is an irrevocable method in which oil or water particles merge and produce more significant drops [48]. The separation process takes place according to the dispersed phase density [204]. The recent application of ionic liquids as demulsifiers in the oil recovery process from O/W emulsions is illustrated in Table 6. The application of two types of ionic liquids, halogenide (HIL) and nonhalogenide (Non-HIL) ionic liquids for the demulsification process and their efficiency in oil separation and recovery, was presented in Figure 11.

Table 6. Recent application of ionic liquids as demulsifiers in oil recovery from O/W emulsion.

ILs	Cation Type	Anion Type	Emuls Type	Dose (ppm)	R_{oil} (%)	Result and Comments	Ref
$C_n$mim NTf_2 n = 10,12, 14	Imidazolium	Bis (trifluoro methyl sulfonyl) imide	O/W	100-3500	90-93.6	Improving the ILs amount and the hydrophobic ILs alkyl cation chain enhanced the demulsification method.	[209]
$C_n$mim PF_6 n = 10,12, 14	Imidazolium	Hexafluo rophosph ate	O/W	500-3500	71.2-86.2	high ILs amount and the cation chain alkyl length of ILs resulted in aggregation and decrease in R_{oil}%.	[209]

ILs	Cation Type	Anion Type	Emuls Type	Dose (ppm)	R_{oil} (%)	Result and Comments	Ref
TOMAC	Ammonium	Chloride	O/W	1000-2000	95-100	Increasing ILs concentration to 1040 ppm at a pH of 7 increases the oil recovery efficiency. In addition, TOMAC had higher efficiency (100%) than the other ionic liquids since it was further hydrophobic compared to other ILs types.	[32]
C_{12}mim NTf_2	Imidazolium	Bis (trifluoromethyl sulfonyl) imide	O/W	5-125	30-70	The application of long alkyl chain lengths ILs (12 carbon atoms) was further efficient to replace the surfactants, improving the IFT and decreasing the %R_{oil}.	[210]
TOMAB	Ammonium	Bromide	O/W	1000-2000	65	Expanding IL conc and R_{oil}% from 30% to 65%.	[205]

ILs	Cation Type	Anion Type	Emuls Type	Dose (ppm)	R_{oil} (%)	Result and Comments	Ref
CTAB	Ammonium	Bromide	O/W	300-800	90.3	Rising ILs amount to 333 ppm 80°C results in high demulsification efficiency (90.3%).	[207]
$P_{666,14}$ NTf_2	Phosphonium	bis(trifluoromethyl sulfonyl) imide	O/W	-	< 95	Steady emulsions still are present in the system with $P_{666,14}$ NTf_2 ionic liquids because the surface-active area would not attain in very hydrophobic ionic liquids.	[210]
$P_{666,14}$ Phos	Phosphonium	Dicyanamide	O/W	-	< 90	Unchanging emulsions still are existent with the addition of $P_{666,14}$[Phos] ionic liquids because the surface-active area would not attain in very hydrophobic ionic liquids.	[210]

ILs	Cation Type	Anion Type	Emuls Type	Dose (ppm)	R_{oil} (%)	Result and Comments	Ref
$P_{666,14}$ NTf_2	Phosphonium	bis(trifluoro methyl sulfonyl)imide	O/W	-	< 95	Steady emulsions still are present in the system with $P_{666,14}$ NTf_2 ionic liquids because the surface-active area would not attain in very hydrophobic ionic liquids.	[210]
$P_{666,14}$ Phos	Phosphonium	Dicyanamide	O/W	-	< 90	Unchanging emulsions still are existent with the addition of $P_{666,14}$[Phos] ionic liquids because the surface-active area would not attain in very hydrophobic ionic liquids.	[210]
$P_{666,14}$ Cl	Phosphonium	Chloride	O/W	-	< 90	$P_{666,14}$[Cl] (halogenide ionic liquids) removed oil from water in an extremely short period (20 min) in comparison to $P_{666,14}$[$N(CN)_2$] non-halogenide) ionic liquid) (24 h).	

ILs	Cation Type	Anion Type	Emuls Type	Dose (ppm)	R_{oil} (%)	Result and Comments	Ref
C_8mim Cl	Imidazolium	Chloride	O/W	100-1000	> 30	Less hydrophobic cation compared to other ionic liquid cations and thus, achieved lower efficiency.	[207]
C_{12}mim Cl	Imidazolium	Chloride	O/W	100-1000	25.2	Less hydrophobicity of ILs cation results in decreasing the oil recovery rate.	[205]
N_{2224} $N(CN)_2$	Ammonium	Dicyanamide	O/W	-	< 90	Steady emulsions were achieved when adding the N_{2224} $N(CN)_2$ ionic liquids since the surface-active area would not attain in very hydrophilic ionic liquids.	[208]
$P_{666,14}$ $N(CN)_2$	Phosphonium	Dicyanamide	O/W	-	100	$P_{666,14}[N(CN)_2]$ had a great surface-active area and separated the oil from water.	[32]

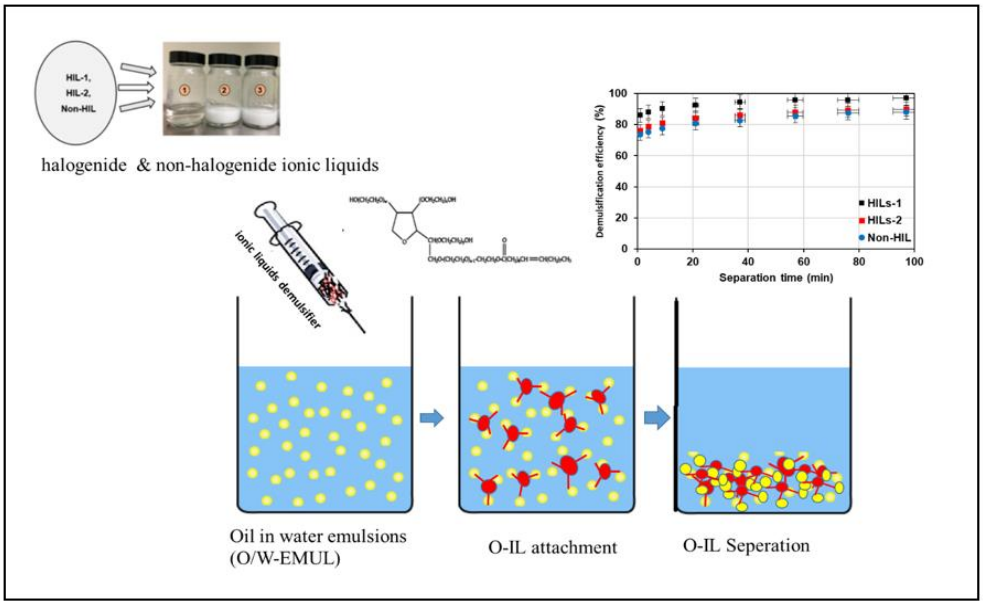

Figure 11. Application of halogenide (HIL) and nonhalogenide (Non-HIL) ionic liquids for the demulsification process.

2.7.3.2 Demulsification Mechanism of Ionic Liquids (ILs)

The method of the demulsification process using ILs includes two major phases, diffusion and adsorption. Before entering the O/W interface, the diffusion method allocates ILs particles in the continuous phase (water phase). In contrast, the adsorption procedure implies that the dispersed ionic liquid particles go over the water phase and extend the O/W interface [10, 205, 206]. The ionic liquid particles later replace the normal surfactants at the interface and alter the viscoelastic characteristics of the interfacial films. This results in separating the solid film over the O/W drops and improving the coalescence of the oil particles (i.e., dispersed oil particles) [49, 200]. Latest studies have discovered that ionic liquids with hydrophobic surface-active properties can be applied for efficient demulsification of W/O emulsions [207, 208]. A study carried out by Hazrati et al. [209] showed that hydrophobic ionic liquids such as Cnmim PF_6 provide high demulsification efficiency compared to hydrophilic ILs such as Cnmim Cl. To enable the suspension of ILs in the oil phase, organic solvents such

as methanol and xylene can be utilized and hydrophilic and hydrophobic ILs, correspondingly [51]. Dichloromethane, isopropanol, chloroform, ethanol, toluene, and benzene can also be used separately or in mixtures to accomplish a similar objective [210]. Tian et al. [211] applied C_2mim BF_4 with cyclohexane for oil production from oily sludge stable emulsion, and they showed that up to 95% of overall oil hydrocarbons were recovered using 0.1 mL/g of ILs to sludge ratio, at 10 min, and a shaking rate of 100 rpm [211].

2.8 Challenges and Future Research

This review reports the current developments in the use of different demulsifiers (NPs, hyperbranched polymers (HPs), and ionic liquids (ILs) as chemical demulsifiers for oil recovery and removal from O/W emulsions. The future expansion of oil recovery methods using chemical demulsification processes meets several challenges. The major problems for the oil industry are the constraints of technology, commercial parts, and health and environmental problems. Although many types of research have demonstrated that the application of NPs, polymers, and ionic liquid demulsifiers has shown high oil recovery rates and improved demulsification efficiency, some of the nanoparticle demulsifiers are restricted to small laboratory scales. Therefore, they are not still appropriate for large-scale field applications. Numerous restrictions that inhibit the use of nanoparticles (NPs) on a field level include the aggregation of NPs in the emulsion under certain conditions of high salinity, high temperature, etc. Also, the production of consistent NPs mixture is still a problem, the mechanisms applied for oil recovery and the factors affecting the demulsification process are not fully comprehended.

Moreover, a basic knowledge of the application of NPs in the oil recovery method is constrained due to the absence of theoretical and mathematical investigation of NPs in

oil recovery methods, which does not thoroughly explain NP performance, and most of the models used are not yet take into consideration the chemical interactions. The HPG polymer demulsifiers also meet several challenges for application in the oil recovery process. Due to the fast development of NPs in the application in EOR process application, health and safety reports are coming at the back. One of the crucial problems for NPs expansion is understanding the impacts of several nanoparticles on the human body. Owing to nano-scale size, nanoparticles can be breathed in through humans and possibly placed in the lungs.

According to these challenges, upcoming studies on oil recovery processes using NPs should concentrate on the different parts:

- The production of stable emulsions in larger amounts requires to be achieved concerning commercial sides.
- Numerous NPs have demonstrated various properties and methods for the oil recovery process. Nevertheless, limited studies have been recommended on the use of NPs in emulsion mixtures. Moreover, different uses and superior behaviour can be feasible by nanoparticle surface functionalization.
- More experimental schemes of O/W emulsions for oil recovery need to be conducted using MNPs. These schemes will enhance the knowledge in the NPs in oil recovery process nano-EOR processes in experimental conditions. Also, optimization research on the factors that affected the application of NPs in oil recovery is suggested to develop the oil recovery rates and cost-efficacy.
- Investigational study must be performed to verify the adsorption and desorption performance through NP dispersion inside the emulsion mixture since they will impact the NPs deliverability to the O/W interface.

- Combined studies on the NP's safety and health should be accomplished to avoid the hazard to humans and the environment.

The hyperbranched polymers-based (HPGs) demulsifiers are gaining the interest of researchers owing to their tunable characteristics and structures. The hyperbranched polymers can be produced to fit the nature of the contaminants inside the emulsion by utilizing proper functional moieties. Besides outer surface regions, they give greater internal surface zones for grabbing the oil from the emulsion mixture. Also, they can be applied in integration with other materials such as magnetic nanoparticles to improve the demulsification efficiency. However, from the published literature, it can be noticed that the hyperbranched polymers have not been extensively studied in oil removal. The one potential justification can be their multistep preparation which needs much knowledge, and it also requires assessing the potential of polymers structures for the application of oil removal. Moreover, a lack of evidence about characteristics of the HPG polymers and the maximum performance in the demulsification process under different conditions. The HPGs polymers are commonly used in biomedical applications. Thus, the possibility of applying HPGs demulsifiers in the oil recovery process from oil in water emulsions should be further investigated.

ILs are favourable demulsifiers, mainly under severe conditions, including high temperature, high salinity, and high viscosity. The significant properties of ILs that have drawn the interest of the researchers are their thermal steadiness, in-flammability, reusability, and low toxicity. Various parameters influencing their demulsification efficiency involve the types of ionic liquid, amounts, salinity, temperature, molecular weight, and the types of oil used in emulsions. The efficiency of the demulsification process would be improved by choosing suitable ionic liquids and volume for certain

emulsion types and detecting the optimum treatment conditions. Besides the benefits of ionic liquids, some constraints need more studies to fit general use.

2.9 Conclusions

Several reviews on applying the chemical demulsification method using different demulsifier types (NPs, HPGs polymers, ionic liquids, etc.) for oil recovery from emulsion mixtures have been conducted and have demonstrated favourable findings. The application of nanoparticles in the oil removal process from oil in water emulsions has appeared as a promising replacement for the other enhanced oil recovery process technologies to enhance and achieve the highest oil recovery rates. The most extensively used demulsifiers in the oil recovery process from O/W emulsions are the magnetic nanoparticles such as iron oxide and silica nanoparticles, which has various features including the particle size in nanoscale with an excellent surface area and great dispersion throughout the emulsion, the high ability to enhance the oil recovery behaviour applying small NPs concentrations, their ability to achieve high demulsification efficiency at room temperature and even at high-temperature conditions as reported by previous studies, their high capability in integrating and functionalized with additional materials (for example polymers and surfactants) results in achieving high oil recovery rates compared to the use of them separately. Until now, numerous nanoparticle types (organic and inorganic materials), as characterized by the greatest widespread silica, are proved to be capable of attaining further separation of oil by more than 20%, via various well-known methods containing IFT decrease, wettability alteration, and NPs dispersion in the emulsion. Multiple factors, such as NPs amount, NPs size, wettability, and salinity, have been identified to influence the behaviour of their application in the oil recovery process. Although the significantly

expanding concerns in the use of NPs in the oil removal methods, few categorized usages have been stated, and the present study stays at the laboratory scale.

Consequently, more studies are needed to meet the difference between laboratory experiments and field-level applications. Hyperbranched polymers are a great additive to the domain of adsorbents as they are hyperbranched macromolecules with distinctive three-D structures and highly grafted with responsive end groups. They have a great core and outside specific areas. Both surface and inner voids can capture and attach with the target contaminants in the emulsion (oil) via broad types of interactions. They have shown excellent potential in the oil recovery process from oil in water emulsion. They can be applied separately or functionalized on other materials and achieve the greatest demulsification efficiency with effective regeneration processes.

For ILs, the efficiency of the demulsification process would be improved by choosing suitable ILs and appropriate concentrations for the particular types of emulsion with detecting the optimum treatment conditions. Besides the advances of ionic liquids and the high oil recovery rates, some limitations still need additional research to make them suitable for comprehensive implementation. However, they are comparatively not as toxic and biocompatible, which is a valuable sign for their upcoming water treatment use, and they are cost-effective demulsifiers. Based on these findings, the study results revealed that applied demulsifiers (i.e., functionalized magnetic nanoparticles-based demulsifiers and hyperbranched polymers) were very effective, which achieved high oil recovery rates >95% and environmentally friendly material. Furthermore, the study results showed that polymers with highly hydrophilic content and molecular weight, such as hyperbranched polyglycerol (HPG) polymers, are effective demulsifiers and achieved high oil recovery rates due to their higher interfacial activity, higher dispersibility, and a significant amount of sensitive functional groups. Also, ionic

liquids were very effective and achieved high oil recovery percentages (>90%) but were expensive. Nevertheless, although they are costly, they could be recommended as future alternatives for traditional solvents for treating petroleum emulsions.

CHAPTER 3: UTILIZING ENVIRONMENTALLY FRIENDLY HYPERBRANCHED POLYGLYCEROL POLYMERS (HPG) TO SEPARATE GASOLINE FROM DEIONIZED WATER

3.1 Introduction

The development of a simple and effective oil removal process with a low cost for the recovery of traces of oil from oil/water emulsion has become increasingly important [212, 213]. However, conventional technologies employed for this purpose including, centrifugal, gravitational settling, and ultrasonic treatment, have a high energy demand, limited application volume, and ineffective recovery limits. In contrast, chemical demulsification processes have a greater potential for recovering oil from oil/water emulsion. However, a knowledge gap exists as to the type of chemicals, the maximum performance, the toxicity, and the environmental effect on water, oil, and the ecosystem. Thus, the synthesis, selection, and preparation of effective chemical demulsifiers for oil removal challenges.

Commercially available demulsifiers are polymers composed of poly oxyethylene, polypropylene, polyester, or a mixture of different surface-active materials [56, 214]. Chemicals such as ethyl cellulose (EC) and non-ionic demulsifiers were tested for their suitability in recovering bitumen oil from water. The results indicated a significant improvement for the recovery performance, which was achieved by adding 100 to 200 ppm of ethyl cellulose to the emulsion [215-217]. In their study, Feng et al., 2009, 2011 examined how ethyl cellulose attained a high oil recovery under different initial concentrations, with up to 90% of oil recovery achieved in 30 minutes [215, 218].

Non-anionic demulsifiers such as tween 80 were used to address the stability of the emulsion and separation of oil from water. Such demulsifiers were found to be effective and exhibited an adequate performance in recovering the oil on account of the

molecular structure and physical properties [219, 220]. The application of the non-anionic demulsifiers in the concentration range of 400 to 600 ppm exhibited an acceptable performance for the recovery of oil. However, the water phase was found to have traces of non-recovered oil droplets. Applying these demulsifiers at lower concentrations, such as < 300 ppm, demonstrated a substantial decrease in oil recovery under all oil concentrations [221, 222].

Similarly, soluble amphiphilic dendrimers are essential because of their suitability in various applications, such as liquid crystals, molecular encapsulation, and the preparation of micelles [223-225]. Zhang et al., 2005 demonstrated that the demulsification process contains multiple phases, beginning with destabilization, aggregation, coalescence, and lastly, separation by gravity settling [196]. Various studies have reported that the structure of the demulsifiers plays a critical role in its performance for the recovery of oil [9, 186, 196]. Wang, Hu et al., 2010 reported that dendrimers with higher branches demonstrated a better demulsification performance. However, the dendrimers are commonly formed via different stepwise growth methods, involving first, second, and third-generation expansions which require a multistep procedure of protection, de-protection, and purification. In addition, the preparation process is complex, which makes it challenging to prepare high molecular weight dendrimers [226].

Figure 10 displays the hyperbranched polyglycerol (HPG) structure, which has shown promising results as a green and effective technology for recovering oil from oil/water emulsion. HPGs are biodegradable, relatively inexpensive, and simple polymers with a high oil capacity [196, 227, 228]. The structure of the HPGs contains hydrophobic and hydrophilic functional groups that help reduce the interfacial surface tension between oil and water, which simultaneously increases the flocculation and coalescence of oils

droplets, thus improving phase separation [9, 229]. HPG polymer provides a quick phase separation, allowing the oil to be removed quickly from the water once the polymer is added, which subsequently improves the efficiency of the polymer for oil separation within a shortened length of time. Moreover, HPG polymers are green demulsifiers (i.e., environmentally friendly), wherein applying them in the oil recovery process can be cost-effective and bound the use of toxic chemicals. [56, 230, 231].

The HPG polymers have exhibited an encouraging potential for the recovery of oil from oil/water emulsion. However, there is a lack of evidence about HPG polymer's maximum performance under different emulsions concentrations, optimum polymer dose, the effect of operational conditions on the process performance, the toxicity, and the environmental impact of the chemicals on the surrounding ecosystem. As such, this chapter aims to investigate the synthesis of high and low-molecular-weight HPG polymers and test their performance on the recovery of oil from oil/water emulsion. First, an oil content analysis and interfacial tension (IFT) measurement were performed to evaluate the demulsification mechanism. Second, the efficiency of the polymer in recovering oil was assessed by measuring the oil content before and after the treatment using UV-Vis spectroscopy. Third, the environmental sustainability of the HPG polymers was determined by testing their biodegradability and toxicity.

3.2 Materials and Methods

3.2.1 Materials

Glycidol (purity 96%) and L-Ascorbic Acid (purity 99%) were purchased from Sigma Aldrich. The dialysis membrane tubing with a diameter of 15 mm and MWCO: 1000 Da were purchased from Biotech Cellulose Ester (Sigma Aldrich). Deionized water was utilized for the purification of the produced polymer. Gasoline oil was synthetic oil (95

Octane) obtained from WOQOd station located in Qatar. Polyethylene sorbitol ester (Tween-80) surfactant was purchased from Sigma Aldrich.

3.2.2 Preparation of Oil-in-Water Emulsions

Oil-in-water emulsions (o/w) were prepared by mixing 2 grams of gasoline oil, 719.7 kg/m^3 density, stabilized with polyethylene sorbitol ester (Tween-80) surfactant (Sigma Aldrich, Germany) 1.07 (25 °C) specific gravity and Hydrophile-Lipophile Balance (HLB) with a value of 15.

3.2.3 Preparation of Hyperbranched Polyglycerol Polymer (HPG)

Cationic ring-opening polymerization of glycidol at ambient conditions was used to synthesize polyglycerol polymer free from traces of toxic agents. 1.11 g of glycidol was mixed with 0.88 g of ascorbic acid under vacuum conditions at 80^{o}C. The ascorbic acid acts as an activator for the reaction. The mixture was stirred at 3500 rpm for 10–15 minutes to form polyglycerols with various structural parameters. Once the product was created, the mixing stopped because of high product viscosity, and the reaction was considered complete. After that, the mixture is dissolved in water and dialyzed for 24 hours using a dialysis tube and collected with a molecular weight cut of 2000 g/mole. The purified products are dried in a vacuum oven at a temperature of 40^{o}C and low pressure.

3.2.4 HPG Polymer Characterization

The structure of the HPG polymer was characterized using NMR spectroscopy (JEOL JNM-ECZR series 600 MHz spectrometers). The chemical shifts of NMR were measured in PPM using deuterium oxide D_2O. The chemical compositions of the synthesized HPG were analyzed using Fourier transform infrared (FTIR) spectroscopy (PerkinElmer using UATR) in the range of 4000-400cm^{-1}. The polymer composition

was analyzed using a DXR Raman microscope (Thermo Scientific 532 nm laser, object 50 x microscope). Raman intensity was in a range of 0-650 cps, and Raman shift ranged from 500-3500cm^{-1}. Other polymer properties including, glass transition temperature (T_g) and melting point temperature (T_m), carbon, hydrogen, and nitrogen contents, were tested using a differential scanning calorimetry DSC 8500 (Perkin Elmer) to confirm the preparation of the HPG and CHN analyzer (Thermo Scientific FLASH 2000 HT), respectively.

The biodegradability and toxicity of the HPG were tested by measuring the ratio of BOD_5/COD and the inhibition text. The analysis of the polymer sample for five days of the biochemical oxygen demand (BOD_5) was performed according to the procedures outlined in Standard Methods (1985) Section 5210D. Chemical oxygen demand (COD) was measured using a spectrophotometer (DR/2000 direct reading spectrophotometer) according to the Standard Methods (1985) Section 5220D [232]. The toxicity of the HPG polymer was estimated using MicrotoxTM bioassay that consists of using a marine bacterium Photobacterium phosphoreum as an indicator of sample toxicity following the procedure outlined in [233, 234]. Gel permeation chromatography (GPC) coupled to a size exclusion chromatography (SEC) was used to determine the molecular weight of the polymer. An Agilent 1100 GC equipped with a Brookhaven BIMWA7-angle light scattering detector and a 30 cm SEC column (pore size=100 Å) was used. Testes were carried out with water flow at a 1 mL/min rate with a mobile phase and column temperature of 20°C.

3.2.5 Preparation of Oil/Water Emulsion

Oil/water emulsions were prepared using gasoline and deionized water to mimic oil/water emulsion in the reservoir. This is a common approach in upstream research for oil and water emulsion. Different concentrations of polyethylene sorbitol ester

(Tween-80) surfactant (0.1, 0.3, 0.6, 0.9, 1.2, 2 g) were mixed with the oil (2 g by weight, 719.7 kg/m3) and deionized water using a shear emulsifying homogenizer (model BRH1-100) at a speed of 3500 rpm for 10–15 minutes, with the gasoline oil added dropwise. The optimum surfactant concentration for providing stable emulsions was inferred from monitoring the phase separation over 30 minutes. The stability of the emulsion was conducted using the zeta potential, IFT measurements, and viscosity analysis to determine the optimum surfactant concentration for emulsion preparation.

3.2.6 Demulsification Test

Demulsification of O/W emulsion was conducted by mixing approximately 4 grams of low molecular weight HPG polymers with 250 mL of the emulsion (2g gasoline oil) in a 300 mL beaker, using the homogenizer device with 220 volts of power and a frequency of 850/min for 60 seconds. Subsequently, the water was separated from polymer-oil, and the oil was recovered. Oil Content Analyzer (OCMA-350) was used to measure the oil concentration at each step to discern the amount of oil removed from the emulsion. Trichloro trifluoroethane was used as an extraction solvent to increase the oil and grease contents under UV measurements. Measurements were conducted at low temperatures to avoid evaporation and permit relatively volatile hydrocarbons [235, 236]. Additionally, the UV method was employed for oil content measurements because of its simplicity and ability to provide direct measurements of oil content. All the tests were performed in duplicates, and the results were reported as an average value of 90%.

3.2.7 Characterization of Oil/Water Emulsion

Emulsion IFT was measured using the pendant drop method (Drop Shape Analyzer DSA100, KRÜSS GmbH, Germany) conforming to Standard Methods [237] at surfactant concentrations of 0.1-2 grams. The zeta potential was estimated by Zetasizer

ZEN3600 (Malvern Instruments Ltd., UK) at room temperature for samples diluted 100× in DI water, with the instrument set to repeat a minimum of 12 times. Rheological measurements were carried out using an Anton Paar SVM 3000 Stabinger viscometer at a temperature of 25°C.

UV-Vis spectroscopy (Perkin Elmer Lambda 25 UV-visible series) was used to measure the oil removal ratio in the emulsion sample at different demulsifier concentrations and at different times. The results reported by the UV-Vis spectroscopy were confirmed using the Oil Content Analyzer (OCMA-350) following procedure #5520 C outlined in Standard Methods for the examination of water and wastewater, 23rd edition 2017 (APHA).

3.3 Results and Discussion

3.3.1 Polymer Characterization

Figure 12 presents the formation of HPG through the condensation polymerization reaction of glycidol and ascorbic acid. Condensation polymerization reaction or step-growth polymerization is a chemical reaction in which the polymers are formed by converting the monomer to polymer. As a result, a small molecule of a by-product with a lower molecular weight is released. The eliminated by-product is called condensate. Herein, the reaction happens between glycidol (monomer) and ascorbic acid. Ascorbic acid acts as an activator for the polymerization of glycidol at the studied conditions [238].

Additionally, ascorbic acid acts as a bi-functional hydrogen bond donor. It incorporates polyglycerol's structure by reacting with the activated glycidol monomer, containing alcohol and epoxide functional groups. The formation of HPG was verified using

analytical techniques, which included: FTIR, CHN analyzer, NMR, Raman spectrometer, and differential scanning calorimetry (DSC) (Figure 13).

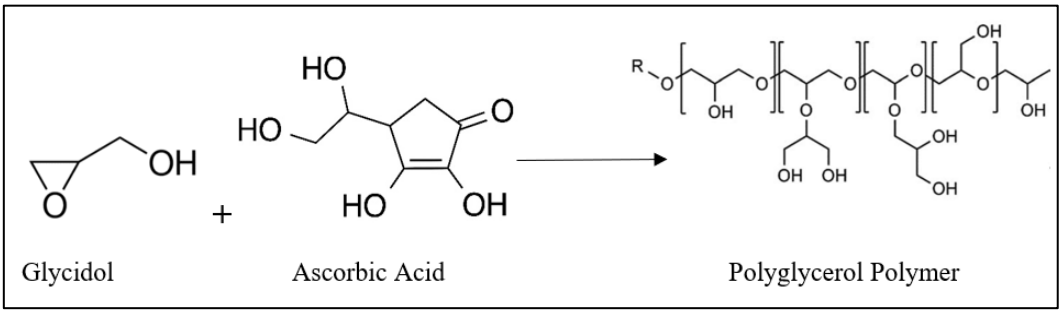

Figure 12. Condensation Polymerization Reaction of Glycidol and Ascorbic Acid.

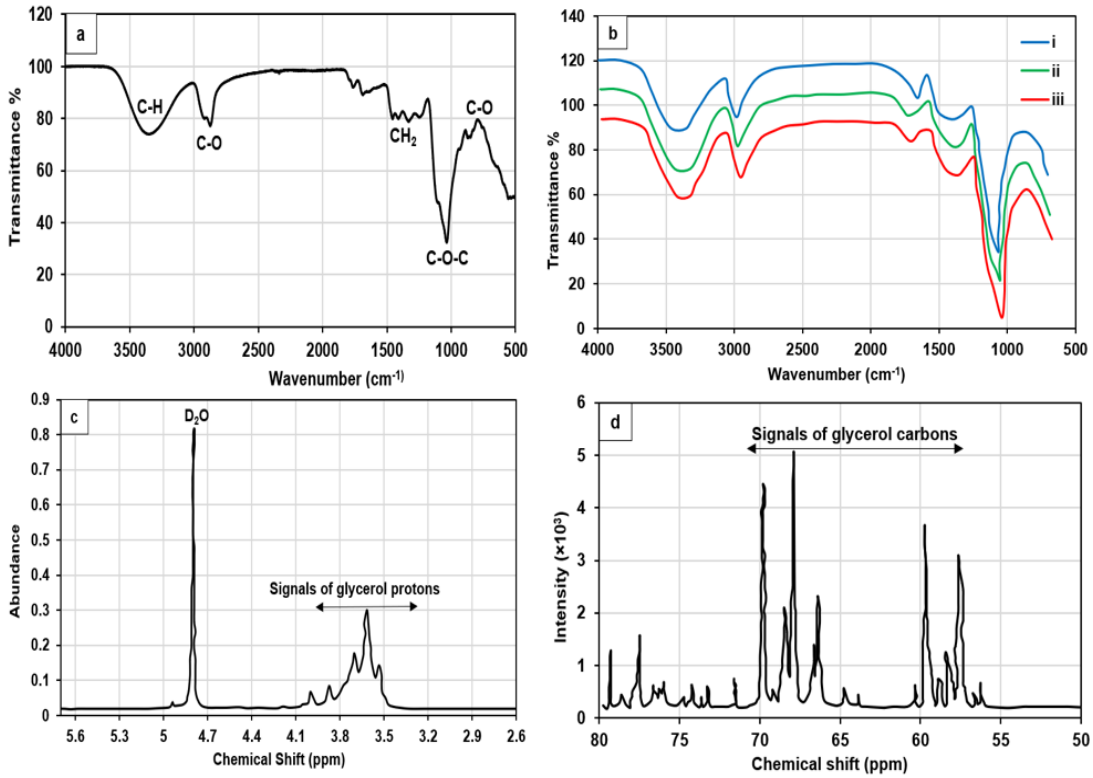

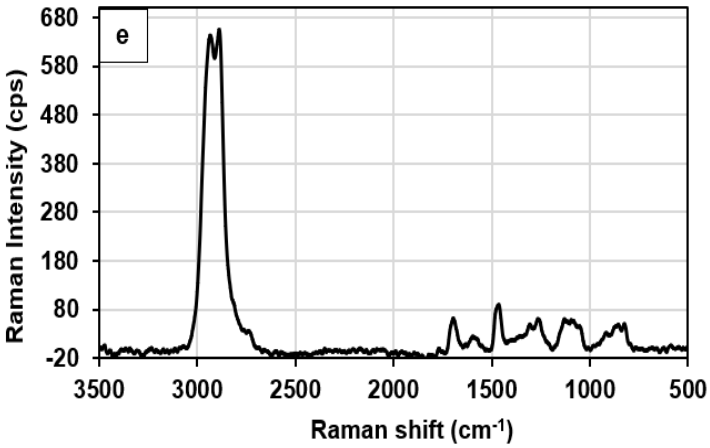

Figure 13. (a) FTIR Spectra of the synthesized polyglycerol polymer (HPG), (b) Spectra of the reference polyglycerol polymer prepared with different reactant ratios (3:40, 3:70, 5:70), (c) NMR proton spectra of the synthesized HPG polymer, (d) NMR carbon spectra of the synthesized HPG polymer, (e) Raman spectroscopy of the synthesized HPG polymer.

FTIR analysis is a qualitative and quantitative technique used to identify and quantify the presence of materials. The FTIR spectrum of the synthesized polyglycerol (Figure 13a) and the standard HPG polymer from the literature (Figure 13b) was similar in structure. In both images, the structure and the FTIR spectrum model are similar [239] and highlighted similar trends for the commercial HPG. The FTIR fingerprint spectrum of the HPG polymer is in the range of 600-1500cm^{-1}. The structure contained hydroxyl, aliphatic C–H, and C–O bonds of polyglycerols at 3300 cm^{-1}, 2891 cm^{-1}, and 1100 cm^{-1}, respectively. The peaks at 1050 cm^{-1} and 1377 cm^{-1} correspond to the asymmetric bending vibration of the C-O-C and the scissoring deformation of CH_2, respectively, comparable to the one reported by [240], which confirms the formation of the HPG polymer. The Carbon, Hydrogen, and Oxygen content of the HPG were determined using a CHN analysis and were found to be 47%, 8%, and 44.9%, respectively. The chemical formula of the HPG (known as 1, 2, 3 propanetriol) was determined using the

results from the CHN analysis. Subsequently, this was confirmed to have the chemical formula of the polymer as $(C_3H_8O_3)_x$. Furthermore, the CHN analysis found nitrogen detectable in the product, equal to 0.1%. A similar observation was reported by [241] during the synthesis and characterization of grafted hydroxypropyl guar gum by ceric ion-induced initiation. Figure 13c displays the NMR proton spectra of the HPG. The signals occurring at 3.3-4.2 ppm were allocated to the HPG protons. Given that both IR and NMR spectra do not display absorbance bands and signals of ascorbic acid, this component represents an activating agent. It is not combined into the polyglycerol polymers structure. The peak signal at 4.8 (Figure 13c) corresponds to the deuterium oxide (D_2O) solvent used in the NMR analysis. Inverse gated NMR spectra of the synthesized polyglycerols are allocated to the carbons of HPGs, and it is shown that the polymers include L1, 4 units, and L1, 3 units (Figure 13d). The L1, 3 units, is the result of the activated chain end (ACE) mechanism. Thus, L1, 4 unit's existence in the prepared HPG structure indicates that glycidol is polymerized using ascorbic acid via the activated monomer (AM) procedure as confirmed by [242, 243]. The NMR results demonstrate how the reaction between the glycidol and ascorbic acid to produce HPG occurs by protonating the glycidol and then polymerizing the protonated monomers using glycidol. Moreover, the NMR shows that the produced HPG from the reaction mostly contains glycerol blocks and a small amount of ascorbic acid, including L1, 4 units, and L1, 3 units (Figure 13d). The abundance of the L1, 4 structural units in the polymer backbone verified that the polymerization technique is the activated monomer (AM) procedure [244]. Figure 13e displays the Raman spectrum of polyglycerols, which confirms pure HPG without any secondary reactions. The intensity of the peaks at 1642 and 1738cm^{-1} normalized the whole as an internal normalization standard. The proportional reduction in carboxyl groups occurred at 1642cm^{-1}. Raman spectra

demonstrated acid (1642 cm^{-1}) and ester (1738 cm^{-1}) peaks. The carboxyl functional group peaks intensities were predicted to gradually decline during the reaction. This would occur once there was a total conversion of acid groups on ascorbic acid through each reaction as a function of glycidol, ascorbic acid ratio, and temperature. The results demonstrated clear peaks of the distinguished polymer with no noise, indicating that no additional reactions occurred. The average molecular weight of the synthesized HPG polymer was determined to be 2138±150 g/mol, and the ratio of BOD_5/COD was determined to be 0.73. Samples with a BOD/COD ratio ≥ of 0.5 are considered readily biodegradable [245]. Thus, the values presented by this work indicate that the HPG is biodegradable. The HPG was tested using Microtox® bioassays. The HPG was detected to have very low toxicity of 0.5, suggesting that the compound did not develop. The toxic effect on the bacterium Photobacterium phosphoreum indicated sample toxicity [246, 247]. Kolhe et al. and Aryal et al. [248, 249] studied the toxicity of the HPG polymer under acidic conditions (pH 5.0) over 20 days using MTT viability assay against NIH/3T3 cells. Results showed that the cell viability is higher than 90% after 24 and 48 hours of incubation with the concentration of HPG up to 10 mg/L. These results confirm that the HPG has low cytotoxicity to NIH/3T3 cells. The combination of good biodegradability and low toxicity make HPG polymers excellent materials to be used as a promising carrier for produced water treatment. The degradation behaviour of HPG polymers was estimated using ^1H NMR measurements. The polymer HPGs were dissolved in different phosphate buffered saline (PBS) and D_2O solutions (pH 7.4 and 5.0). The molecular weights of the (HPGs) polymers were measured for 10 days.

3.3.2 Oil in Water Emulsion Characterization

The stability of the emulsion was determined to be a function of the surfactant concentration (0.1 to 2g). In cases with the lowest surfactant concentration (0.1 g), the

oil separated within approximately one minute, with a progression in the emulsion stability of the surfactant concentration occurring at 0.6 g. The stability of emulsion started at a concentration of 0.6 g, after which it remained constant with no phase separation for a long time. Jha, Mahto et al. 2016 reported similar trends for diesel oil in a brine solution which was steadied using xanthan gum and aluminium stearate [250].

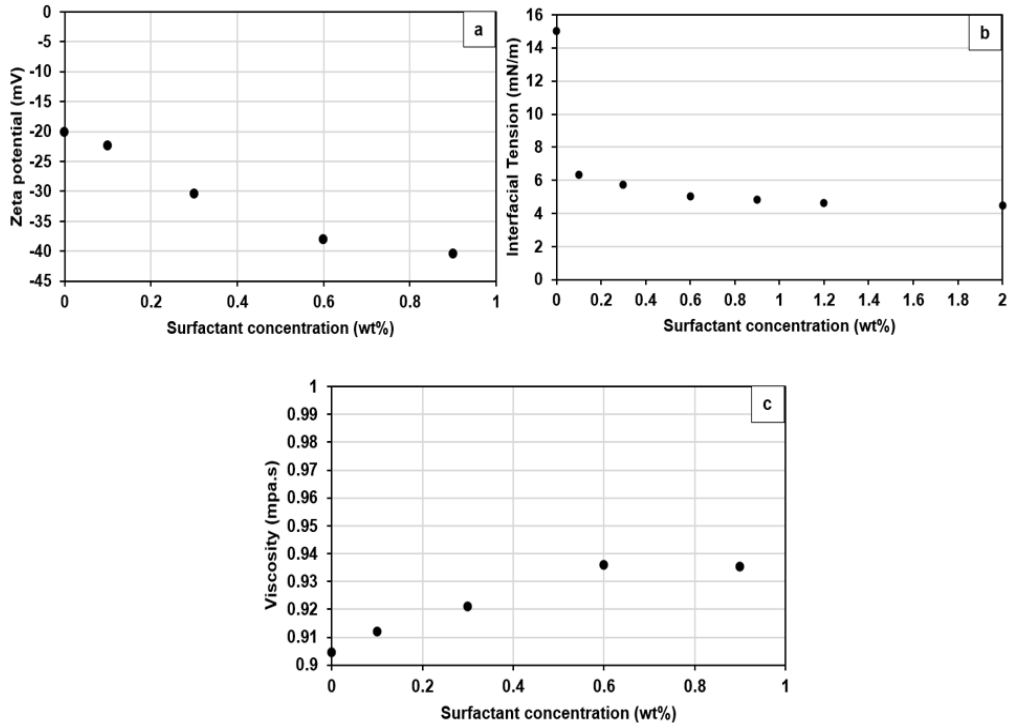

Figure 14. (a) The effect of surfactant concentration on zeta potential, (b) The effect of surfactant concentration on interfacial tension, (c) The effect of surfactant concentration on viscosity.

Figure 14a presents the zeta potential (ξ) of the emulsion as a function of the initial concentration of the surfactant ($C_{i,\ sur}$). A ξ value of -20.13 was obtained for the o/w mixture (reference sample) without using a surfactant. ξ value decreased as the surfactant concentration ($C_{i,\ sur}$) increased from 0.1 to 0.6 g and stabilized at higher concentrations. ζ has a value of -22.33 mV at $C_{i,\ sur}$ of 0.1 g, which decreased to -38.12 mV at $C_{i,\ sur}$ of 0.6 g, and stabilized at -40.4 mV for $C_{i,sur}$ > 0.6 g. The results indicate

that to produce a stable emulsion, the zeta value should be ≥ -38.12, and the optimum surfactant concentration to achieve emulsion stability is 0.6 g. This trend corresponds to the one described for engine diesel oil in a water solution stabilized with ethylene tetrakis [-CH_2N [(-CH_2CH_2O-)[-$CH_2CH(CH_3)O$-]H]$_2$]$_2$ as reported by [251].

Figure 14b displays the IFT measurements for o/w emulsion samples at different surfactant concentrations. First, there was a significant reduction in the IFT values, from 15 to 5.74 mN/m, observed for the O/W emulsion samples prepared with surfactant concentrations in the range of 0 to 0.3 g. Thereafter, a lower reduction in the IFT value reached 5.02 mN/m at a concentration of 0.6 g. Figure 14 illustrates the stability of the emulsion with a starting concentration of 0.6 g. This confirmed the zeta potential results, indicating that emulsion stability started at a surfactant concentration equal to 0.6 g. Jha et al. and Abdulla et al. [250, 251] reported similar results for diesel oil in brine solution stabilized using xanthan gum, aluminium stearate, and ethylene tetrakis [-CH_2N[(-CH_2CH_2O-)[-$CH_2CH(CH_3)O$-]H]$_2$]$_2$.

The viscosity measurement is used for the emulsion as an indirect indicator for stability and oil content within the emulsion, as stable emulsion signifies that more oil is trapped inside the water. The viscosity of o/w emulsion was measured and evaluated at different surfactant concentrations ($C_{i,\ sur}$) at a temperature of 25°C (Figure 14c). Results indicated that the increase in the surfactant concentration ($C_{i,sur}$) significantly increased the emulsion viscosity. Furthermore, the emulsion stability was associated with the observed viscosity. It was observed that at $C_{i,\ sur}$ of 0.6 g, the emulsion was stable with a viscosity value of 0.9361 mPa.s. This confirms that this surfactant concentration (0.6 g) achieved the stability of the emulsion.

Previous studies have confirmed that the viscosity increase corresponds with the increase in surfactant concentration. For example, pal et al. found that when the surfactant concentration was in the range of 1 to 50 wt.% and the water concentration was varied between 0 to 75 vol.%, the apparent and relative viscosities of the emulsions (at specific water concentration) increased with the surfactant concentration [252]. However, the effect of surfactant concentration on the relative viscosities reduced with an increase in the shear stress [252].

3.3.3 Demulsification Efficiency of HPG Polymer

The demulsification technique is applied to resolve the o/w emulsions into bulk phases of oil and water. The mechanism of demulsification can be represented by a four-stage process including destabilization, aggregation, coalescence, and gravity separation. This chapter used chemical demulsification by adding specified amounts of the HPG polymer to the o/w emulsion. The HPG demulsifiers with hydrophobic and hydrophilic properties can adhere to the oil-water interface, reduce the IFT, shorten the adsorption time, increase the rupture rate of oil droplets, and promote phase separation through phase separation an enhanced flocculation and coalescence mechanism [19, 196].

The demulsification tests were conducted with 4 grams of high and low molecular weight HPG. This demonstrated an oil recovery performance of 48.72% and 49.5%, respectively. On the other hand, the control test by gravity settling did not exhibit more than 3.35% of oil recovery. These trends confirm the suitability of HPG for the recovery of oil from water. Furthermore, the results confirm those reported by [253], which indicated that under gravity settling, the oil removal rate is very low and is increased by adding the HPG demulsifier to the oil/water emulsion.

3.3.4 Demulsification Efficiency of HPG Polymer Evaluated by UV-Vis Spectroscopy

3.3.4.1 The Effect of HPG Demulsifier Concentration

Figure 15 illustrates the effect of the initial concentration of HPG ($C_{i, HPG}$) in removing oil from o/w emulsion followed by UV-Vis spectroscopy. Different $C_{i, HPG}$ (500, 1000, 1500, 2000 mg/L) were applied, and oil removal was monitored at different time intervals of 40, 60, 80, and 100 minutes at a temperature of 45°C. In the absence of HPG polymer, the percentage of oil removal caused by gravity separation was very low, almost equal to 7%. Adding the HPG to the o/w emulsion improved the oil recovery. A trend showed that by increasing the polymer concentration up to 2000 ppm over 180 minutes, there was an improvement in oil recovery. The oil removal was 25.346%, 34.013 %, 45.238%, and % 90.39% at times of 40, 60, 80, and 180 minutes, respectively. The changes in oil removal compared with different concentrations of HPG demulsifier were measured in different studies, which confirm that when no demulsifier is added, the oil removal has a small value, equal to 17%, caused by the gravity settling. This affirms that the emulsion is stable and can be treated as the blank sample and that the oil removal will attain a value of 34% when the HPG demulsifier is added [253].

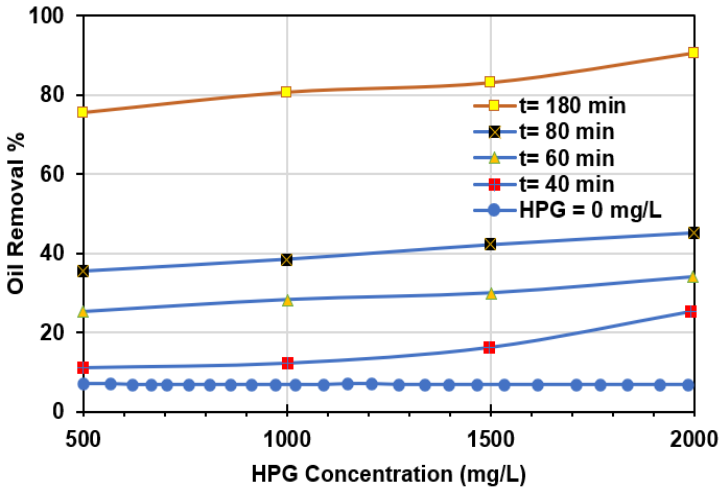

Figure 15. The effect of different demulsifier concentrations on oil removal, with a ratio at different times.

3.3.4.2 The Effect of Molecular Weight

The molecular weight of the polymer is a crucial characteristic to evaluate the demulsification efficiency. Results indicated that when the HPG polymers with high molecular weights (equal to 2138 ± 150 g/mol) were applied to different emulsions with different oil concentrations (500, 1000, 2000, 4000 ppm), high removal rates of oil were attained at 92%, 91.4%, 90.5%, and 89.7% respectively. The results from previous studies highlighted that the addition of high molecular weight water-soluble polymers would thicken the displacing fluid (i.e., oil), reduce the mobility of the aqueous phase (i.e., water), increase the carried volume of oil, and improve the efficiency of oil separation [254, 255].

3.3.4.3 The Effect of Temperature

Figure 16a and Figure 16b presents the effect of temperature on the oil removal rate. Oil separation was gradually enhanced with the temperature. Results indicated that when the demulsification occurred, the temperature ranged between 30-60°C, and settling time was 30 minutes using an HPG concentration of 500 ppm (the minimum

concentration), which increased the removal and reached a rate of 63.6%. As molecular thermodynamic motion theory stipulates, the demulsifier particles transferred more at a higher temperature. Thus, at 60°C, the movement of particles is more significant than at 30°C, as higher temperatures can aid the attachment of the molecules to the oil-water interface [256]. In addition, the temperature rise can cause the reduction of viscosity and the mechanical strength of the oil/water interface. Moreover, high temperatures increase the difference in oil-water phase density (i.e., Brownian motion). Consequently, this promotes phase separation by enhancing the flocculation and coalescence mechanisms [257].

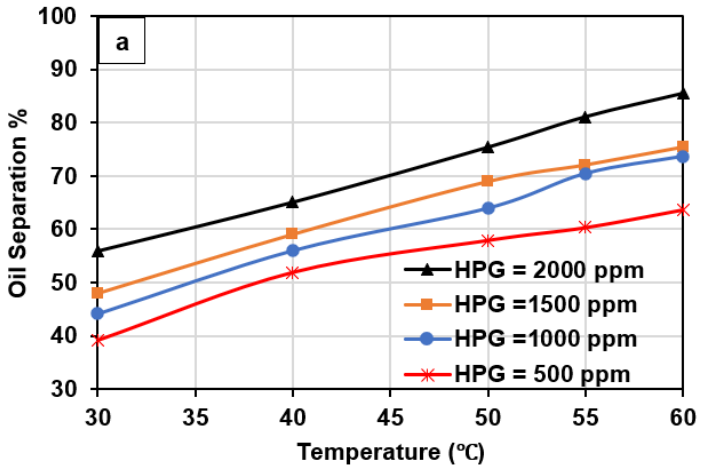

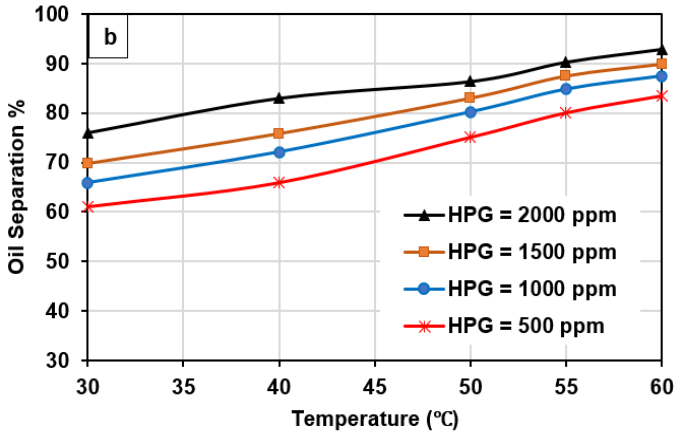

Figure 16. The effect of temperature on the oil separation from gasoline oil/water emulsions using HPG polymers as the demulsifier at: (a) settling time = 30 mins, (b) settling time = 1hour (60 mins).

3.3.4.4 The Effect of Settling Time

Settling time is a significant factor that affects the demulsification process. Figure 17 shows how when the settling time for the demulsification process is set to 30 minutes, with a temperature of 60°C, and a demulsifier concentration of 2000 ppm, there is an oil separation value of 76%. By increasing the settling time to 60 minutes (1 hour), the removal was increased to 93%, and the oil separation remained constant thereafter. This confirms that extending the settling time enhances the emulsification process. Previous studies have indicated that HPG polymers regularly need at least 90 minutes to achieve a high demulsification performance [258, 259]. This suggests that the synthesized HPG polymer is advantageous for emulsion breakup and can be an effective material for industrial applications. Considering the branched structure of HPG and the interactions between the water particles and ether bonds, it was able to quickly attach to the oil-water interface and decrease the interfacial film thickness while also shortening the adsorption time of the demulsifier to oil droplets. This is valuable for enhancing the demulsification efficiency.

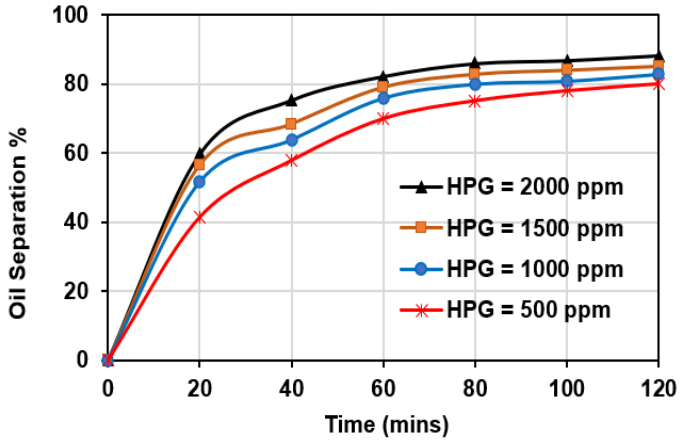

Figure 17. The effect of settling time on the oil separation from gasoline oil/water emulsions using HPG polymer as a demulsifier.

3.4 Conclusion

Hyperbranched polyglycerol green demulsifiers were effectively synthesized via the condensation reaction between glycidol and ascorbic acid. The performance of the demulsifier was managed by the two reactant ratios, which were below the conditions for the demulsification process. The demulsification of oil was evaluated through oil content measurements. The oil removal of 48.72% and 49.5% were through a low dose of low and high molecular weight HPG. Up to 90.30 % of oil recovery can be achieved at optimized conditions of dosage and time. The effect of temperature and settling time on the oil separation demonstrated how oil separation is significantly enhanced by increasing the temperature and the settling time. This chapter offered an innovative technique to study the demulsification process, which is valuable for developing high-efficient demulsifiers for oil/water emulsions within the oil industry.

CHAPTER 4: APPLICATION OF MAGNETIC NANOPARTICLES FOR THE REMOVAL OF OIL FROM OIL-IN-WATER EMULSION: REGENERATION/REUSE OF SPENT PARTICLES

4.1 Introduction

High volumes of produced water (PW) generated during the oil and gas extraction process contain significant amounts of waste oil, which drains energy resources and causes serious environmental harm. PW is the by-product of the waste produced during the production and exploration of oil and gas from onshore and offshore wells [260, 261]. There are three major types of oily wastewater, and each has different treatment processes. The first type is wastewater with very small quantities of oil dispersed in the water, and the oil present is soluble oil. For this type of wastewater, adsorption, nano-filtration, reverse osmosis, and even advanced oxidation technologies can be used as a treatment method. The second type of wastewater exhibits the presence of oil as free droplets. For the second type of wastewater, phase separation techniques such as gravity separation, absorption, and skimming can be utilized as treatment methods. The third type of wastewater is an oil-in-water emulsion (O-in-W-emu), wherein one of the phases is dispersed in the other. In such a case, the separation is difficult to achieve in comparison to the last two categories. This is especially true when particles or surfactants stabilize the emulsions. The separation and recovery of oil from PW, generally, and from oil-in-water emulsion (O-in-W-emu), specifically, is a widespread problem due to the increase in the discharge of industrial oily PW [262-265]. Reports have indicated that the immediate release of oily PW can cause serious health problems and environmental pollution [266-268] [269].

Various conventional treatment techniques have been applied for the recovery of oil from O-in-W-emu, such as settling tanks [270], burning [271], flotation [272], and

adsorption [273]. However, the efficiency and the large-scale performance of oil recovery by these processes are comparatively low. Additionally, membranes and ultrafiltration processes have been used for the separation of oil from O-in-W-emu. Nonetheless, the low flux through the membranes, difficult synthesis process, expensive raw materials, instability, and the adsorption of the surfactant or pore plugging are major limitations of these techniques as reported by Lipp et al., Xu et al, and Zhang et al. [274-276]. Other separation methods such as chemical flocculation [277, 278] and flotation [279] [280, 281] have been tested for oil recovery from O-in-W-emu. Chemical flocculation offers a simple combined physicochemical process that uses a wide range of commercially available chemicals to achieve the required separation at a low cost. However, this particular method has a low oil removal rate, generates high sludge volumes, requires a highly sophisticated pH control, and is an energy-intensive process [282, 283]. Furthermore, flotation techniques have several limitations for oil separation, including low efficiency, high-energy demand, metal selective rather than oil selective, and the requirement for extended time to achieve the expected separation efficiency [282, 284, 285]. As such, there is a crucial need to develop a cost-effective and high efficiency method that will help to recover oil from O-in-W-emu.

More recently, there has been a growing body of research on magnetic nanoparticles in enriched oil recovery due to their potential to increase oil recovery. This is despite the high salinity of PW, high pressure and temperature, and unnatural pH of the reservoirs. It has been previously reported that the MNP has a high surface area, excellent oil adsorption capacity, and can be 30% less costly than the other available methods [286]. Furthermore, magnetic nanoparticle's fast and simple separation procedure utilizing an external magnetic field is an additional advantage of this technology [100, 287].

Furthermore, magnetic demulsifiers are eco-friendly substances for handling oil droplets in water and vice versa [288, 289].

Multiple magnetic materials can be used for oil recovery. Fe-MNP is an excellent choice among these magnetic materials due to their high dispersion in O-in-W-emu, low toxicity, strong magnetic response, and low cost as reported by Bagheri et al. [290], Lu et al., Mirshahghassemi et al., and Liang et al [291-293]. The Fe-MNP can be dispersed in the emulsion to attach oil droplets and then separated from the water phase using an external magnetic field [294, 295]. Fe-MNP were employed alone or were combined with demulsifiers such as triethoxysilane [295], and in both cases, they achieved $\%R_{oil}$ up to 90%. Although these magnetic nanoparticles were previously used for the demulsification process, they still need to maintain their high oil separation efficiency under an extended time of operation (i.e., extended re-usability) and address their environmental impacts.

The various methods that were used for the preparation and synthesis of Fe-MNP include the co-precipitation method (Co-PM) [296], hydrothermal method (HTM) [297], microwave irradiation method (MIRM) [298], and combustion synthesis method (CSM) [299]. The Co-PM is the simplest and most cost-effective synthesis process for the production of Fe-MNP. Primarily, the Co-PM can generate MNP in large quantities. However, the size distribution is still relatively non-uniform, and it does not produce consistent nanoscale Fe-MNP immediately without further separation. Thus, it is not recommended if a uniform Fe-MNP is required. Additionally, this method needs a highly sophisticated pH control for the reaction mixture during the precipitation stage to avoid side reactions and transform the magnetite to maghemite (γ-Fe_2O_3) [300, 301]. HTM is another effective method that can be employed for MNP preparation [302]. The HTM can produce high crystallinity and controlled morphology particles, but the

resulting MNP has a larger diameter than the Co-PM. Notably, the large-sized Fe-MNP (≥50nm) exhibited ferromagnetic performance instead of superparamagnetic performance, which may be problematic for their separation [303, 304]. The MIRM method was previously used for Fe-MNP preparation because of its advantages: phase purity with a greater yield, fast kinetics, and elevated reproducibility [298]. However, the MIRM method has drawbacks, including the selectivity and evaporation of solvent due to microwaves. Additionally, the reactions develop a gas that can build up pressure which require special attention to avoid an explosion [305]. Conversely, the Co-PM and HTM methods produce nanoparticles with a very low suspension in aqueous media (i.e., water) due to high crystallinity. Moreover, the Co-PM and HTM methods are complex and require high temperatures and an inert environment throughout the preparation process which takes many hours.

The combustion synthesis method (CSM) is an energy-saving and effective method, which can occur in the liquid, gas, and solid phases. Over 500 materials have been synthesized using the CSM process due to their simplicity, quick preparation, ability to produce high purity products, and stability at high temperatures compared to other traditional methods [306]. External resources consistently heat the reactive medium to ignition temperature [307]. The reaction begins at every point of the medium, which effectively and homogeneously causes the production of several products [307]. Among all the other techniques, the CSM was chosen to prepare the Fe-MNP because it produces high purity homogeneous MNP for a low cost [308].

The primary advantage of the CSM technique is that it allows the creation of the MNP varying size distribution. Other advantages of the CSM method include a low to medium reaction temperature that can be easily controlled and a short preparation time, significantly lower and shorter, respectively than the Co-PM and HTM preparation

methods [309]. Additionally, monodispersed MNP with varying morphologies and surface functionalization can be prepared for extensive applications [310]. Parameters including flame type, produced gases, temperature, the ratio of air-fuel-oxidant, and the precursor reagent's chemical composition must be optimized when applying the CSM to generate specific MNP for special applications [308, 311]. Previous research has exemplified that a temperature in the range of 150ºC to 200ºC is optimum for the production of magnetite MNP [312, 313]. Higher temperatures (> 400°C) may result in the formation of other types of iron oxides, such as hematite (α-Fe_2O_3) and maghemite (γ-Fe_2O_3). The formation of hematite and maghemite would not be helpful as they have very low magnetism properties, limited stability, and low dispersibility in the emulsion; thus, they are not recommended for the recovery of oil from O-in-W-emu [314]. Other studies have highlighted the need to provide a proper surface coating for the Fe_3O_4 MNP because of the high surface activity with a water solution. The magnetite (Fe_3O_4) nanoparticles can accept various chemical coatings, such as polymers and surfactants, specialized for produced water treatment applications [315].

The literature above highlights how a well-formed and cost-effective oil recovery system must remove oil from water and ensure a clean and sustainable environment. However, presently, there is a lack of literature about the impact of the surface properties of the Fe-MNP, the operational parameters of the process on the demulsification efficiency ($\%\eta_{dem}$), and the percentage oil recovery ($\%R_{oil}$) from the O-in-W-emu. Moreover, the reusability performance of the oil recovery system under varying operational conditions needs further examination. Similarly, there is also a lack of research on the impact of the preparation conditions of the Fe-MNP on the $\%\eta_{dem}$, $\%R_{oil}$, and the process kinetics. As such, in this chapter, magnetite (Fe_3O_4) MNP (Fe-MNP) was synthesized using the vacuum CSM method at differing temperatures

(150ºC, 250ºC, and 350ºC). The as-synthesized Fe-MNP was then used to recover oil droplets from the O-in-W-emu and analyzed for their demulsification efficiency ($\%\eta_{dem}$) and the percentage mass of oil recovered ($\%R_o$). In addition, the impact of various parameters such as pH, surfactant concentration (C_{sur}), and reusability were assessed and compared with other research literature. Additionally, the mechanism, adsorption isotherm and kinetics, and separation ability of the developed MNP were evaluated. The Fe-MNP were synthesized using simple and safe chemical compounds, including iron nitrate $(NO_3)_2$ and glycine (CH_2NH_2COOH), producing a uniform combustion reaction.

4.2 Experimental Methods

4.2.1 Chemicals

The materials used in the present chapter include Iron (III) Nitrate $(NO_3)_2{\cdot}6H_2O$, Ethanol (CAS Number: 64-17-5), and glycine CH_2NH_2COOH, purchased from Merck-Qatar, commercially available gasoline (95 Octane, density = (719.7 kg/m^3) obtained from a local petroleum supplier (WOQOd Co. in Doha, Qatar), and Polyethylene sorbitol ester (Tween-80) surfactant bought from Sigma Aldrich. All of the materials were laboratory grade and applied as received with no purification.

4.2.2 Preparation of the Magnetite (Fe_3O_4) MNP

The Fe-MNP was synthesized using the combustion synthesis method (CSM) as presented by [316]. Initially, a homogeneous aqueous solution of iron nitrate hexahydrate Fe $(NO_3)_2{\cdot}6H_2O$, iron nitrate trihydrate, Fe $(NO_3)_2{\cdot}3H_2O$, and glycine NH_2CH_2COOH as fuel were mixed at a specific molar ratio. The number of precursors was assessed depending on the formation of 3g of pure metal/metal-oxide following the stoichiometric values in the reaction described by (Equation 1). All of the reagents were dispersed in deionized water (DI) (75 ml) at room temperature for 1 h and continuously

stirred to make a homogenous solution with the same transparency. The formulated mixtures were placed on a hot plate heater (Barnstead Thermolyne, model no. sp 46925). After that, the mixtures were heated for 1 h until the water evaporated and the temperature rose to reach the ignition temperature, which produced Fe-MNP (equation 2).

$$Fe\,(NO_3)_2.6H_2O + Fe\,(NO_3)_2.3H_2O + NH_2CH_2COOH \xrightarrow{at\ 300℃} Fe_3O_4 \quad (2)$$

The generally accepted arrangement for the stoichiometric equilibrium reaction between the oxidizer (metal nitrates) and the fuel (glycine) is explainable by the response presented in equation (3) [299].

$$M^v(NO_3)_v + \left(\frac{5}{9}v\varphi\right)NH_2CH_2COOH + v\frac{5}{4}\,(\varphi - 1)O_2$$

$$M^vO_{\frac{v}{2}}(s) + \left(\frac{10}{9}v\varphi\right)CO_2(g) + \frac{25}{18}\varphi H_2O(g) + v\frac{5\varphi+9}{18}N_2(g) \qquad (3)$$

Where M^v is a v-valent metal, based on reaction 2 (equation 3), a $\varphi > 1$ symbolizes a fuel-rich environment, a $\varphi < 1$ is a fuel-lean environment, and $\varphi = 1$ represents the stoichiometric conditions where no outer oxygen is required for preparation.

4.2.3 Synthesis of Oil-in-Water Emulsion (O-in-W-emu)

The O-in-W-emu was prepared by dissolving the gasoline oil in deionized water (DI) to simulate the performance of the reservoir O-in-W-emu. This is a common practice in oil and water emulsion upstream research. The preparation of O-in-W-emu was conducted by dispersing 0.05 g/L of Tween-80 surfactant into a specified volume of deionized water and mixed with a shear emulsifying homogenizer (model BRH1-100, USA) for 2 min at a speed of 3500 rpm. Thereafter, a specific concentration of the gasoline oil (0-800) mg/L was added, drop by drop, and mixed for 10 to 15 min with water to generate a consistent O-in-W-emu.

4.2.4 Characterization of the Fe-MNP

Fe-MNP was studied applying the Fourier Transform Infrared Spectrum (FTIR) (400 PerkinElmer FTIR Spectrometer, US). The ultraviolet-visible spectroscopy (Perkin Elmer Lambda 25 UV-visible series, US) was used to evaluate the absorption spectra of the magnetite iron oxide MNP. The X-ray diffractometer spectroscopy (XRD, Minifix II Japan) was applied to define the Fe-MNP phase structure, and the rays were radiated at a wavelength of (ג= 0.154 nm). Conversely, the particles' morphology was examined using the Scanning Electron Microscope (FEI model Nova Nano SEM 450, US). The Scanning Electron Microscope (SEM) analysis supported by the Energy Dispersive X-ray spectrometer (EDX) system was used to identify the material's elemental composition and check the availability of the Fe-O group. This process was carried out to confirm the formation of magnetite MNP. The surface morphology of the Fe-MNP was also examined using a high-resolution transmission electron microscopy (HRTEM, Hitachi H-600, Japan). To exemplify the three-dimension (3D) profile of the configuration made by the Fe-MNP, an atomic force microscope (AFM MFP-3D Infinity AFM Asylum Research Oxford Instruments, US) was used. The use of the atomic force microscope (AFM) allows for the 3D analysis of the Fe-MNP with sub-nanometer resolution. The purpose of this particular test is to provide information on the size, distribution, surface morphology, and roughness of the MNP. The AFM analysis was carried by drying the Fe-MNP and then placing them on glass for further analysis. Lastly, the Fe-MNP sample's magnetization was assessed using a vibrating sample magnetometer (VSM, Lakeshore, 7407, US) with a magnetic field range from -10000 to 10000 Oe. The Mössbauer spectra were verified using a standard transmission Mössbauer spectrometer at T 300 °K in a constant acceleration mode. A ~100 mCi of

a ^{57}Co (Rh) source was used, and the spectrometer was adjusted using α-iron at room temperature.

4.2.5 Experimental Procedure

The oil recovery was performed by mixing the O-in-W-emu at varying C_{oil} with different D_{MNP} (5-100 mg/L) and then mixing at 3500 rpm for an additional 10 min. All of the experiments were performed at room temperature unless specified. The pH of the O-in-W-emu was not controlled and was able to develop and stabilize around 4.0 freely. Once the mixing was completed, the mixture was left for an additional 10 mins, allowing the Fe-MNP to adsorb oil droplets. Thereafter, the Fe-MNP was removed by the magnetic field, and the $\%\eta_{dem}$ was assessed. The oil concentrations before and after the addition of the Fe-MNP were associated with the total organic matter (TOM) in the water with a verified detection limit at 0.03± 0.005 wt%. The UV analysis was used for the oil content measurements. This analysis was chosen due to its ease and direct measurements for the oil concentration (C_{oil}). All of the experiments were repeated multiple times, and the results were determined as an average value of 90%. The recycling tests for the Fe-MNP were conducted by consecutively washing the Fe_3O_4 MNP with deionized water and ethanol to eliminate the grafted droplets of oil. The reproduced Fe-MNP have dissolved again in water and used in the following cycles for oil recovery.

4.2.6 Equilibrium and kinetic Experiments

The Fe-MNP was used to calculate the amount of oil recovered by presenting a mass balance of the treatment method. At any time, the volume of oil recovered using the Fe-MNP was equivalent to the oil volume separated from the O-in-W-emu according to equation (4).

$$q_t = \frac{(C_{i,oil} - C_{t,oil}) * V}{D_{MNP}} \quad (4)$$

Where q_t is the volume of oil removed using the Fe-MNP during specified periods (mg/mg), $C_{i,\ oil,}$ and $C_{t,\ oil}$ denote the initial and final concentrations of dissolved oil droplets in O-in-W-emu in mg/L, and V is the initial volume of the O-in-W-emu (L). The efficiency of the demulsification process ($\%\eta_{dem}$) was defined following equation 5 below.

$$\%\ demulsification\ efficiency\ (\%\eta_{dem}) = \frac{C_{i,oil} - C_{f,oil}}{C_i, oil}\ x\ 100\% \quad (5)$$

Where $C_{f,\ oil}$ indicates the final oil concentration in O-in-W-emu (mg/L). The equilibrium adsorption capacity Q_e (mg/mg) was determined by applying the mass balance outlined in Equation (6). The experimental results from the oil recovery process were fitted to Langmuir and Freundlich isotherms, outlined in (equation 7) and (equation 8), respectively.

$$Q_e = \frac{C_{i,oil} - C_{e.oil}}{S} \quad (6)$$

$$q_e = \frac{q_{max} K_L C_{e,oil}}{1 + K_L C_{e,oil}} \quad (7)$$

$$q_e = K_f (C_{e,oil})^{\frac{1}{n}} \quad (8)$$

Where q_{max} denotes the maximum oil recovery for each unit mass of Fe-MNP (mg/mg), K_f is the Fe-MNP recovery capacity, and n is the intensity of the recovery.

4.3 Results and Discussion

4.3.1 Fe-MNP Characterization Methods

Figure 18a Presents the infrared (IR) spectra of the Fe-MNP synthetized at varying temperatures (150, 250, and 350 °C). At 476cm-1, 519cm-1, 688cm-1,743cm-1, and 875cm-1 IR, the peaks were assigned to anhydrous iron (II), O-C-O in-plane bending, C-O CO_3^{2-} ν4 in-phase bending modes, and the strained ring structures with an exocyclic $=CH_2$ group. The peaks ranging from 1069 cm^{-1} to 1600 cm^{-1} and 2606 cm^{-1} to 2941cm^{-1} are allocated to O-H, C-H, C=C, C=O, and C-O extending groups. The presence of such groups with the possibility of free hydrogen protons demonstrates the acidity (medium acidic condition) of the Fe-MNP arrangement. Similar results were observed by Abinaya et al. and Jin et al [317, 318] using IR spectra, confirming that the peaks ranging from 400 cm^{-1} to 1600 cm^{-1} were assigned and attributable to the Fe-O vibration and COO^- vibration, respectively. Conversely, the peaks at 3226 cm^{-1}, 3293cm^{-1}, and 3325cm^{-1} were correlated to the absorption band in the position of the Fe^{2+}, O-H, and N-H stretching vibrations. The vibrating likely originated from ethylene glycol and iron nitrate structures, as suggested by [319]. The FTIR supports the presence of Fe_3O_4 monomer inside the MNP structure as indicated by [298, 320, 321].

The effect of the preparation temperature exhibited a discernible impact on the surface of the Fe-MNP. As the preparation temperature increased, the peaks either reduced or shifted. The peaks in the range of 476 to 875 cm^{-1} exhibited a significant reduction and slight shift by expanding the preparation temperature from 150°C to 350 °C. As previously discussed, these particular peaks are assigned to anhydrous iron (II), O-C-O bending, C-O, CO_3^{2-}, and $=CH_2$ group; their decrease at high temperatures is aimed at the oxidation of the components and deformation to produce the final nanoparticles. The peak at 1069 cm^{-1}, assigned to O-H, significantly increased by simultaneously

increasing the preparation temperature, suggesting the formation of more O-H bonds and an increase in the acidic properties of the Fe-MNP. The peaks in the range of 3226 to 3325cm^{-1} exemplify the permanent presence of Fe^{2+} and O-H. For these peaks, there was a decrease in the N-H as the preparation temperature increased. Additionally, while the Fe-MNP prepared at 150ºC exhibited maghemite properties, a significant change to hematite (Fe_2O_3) was observed for the Fe-MNP prepared at 350℃. The last change is likely the result of oxidation of the Fe-MNP. Similar results were reported by [322, 323]. Moreover, [324, 325] reported similar results for the preparation of Fe-MNP using the sol-gel method, which employed ethylene glycol, $FeCl_3$, and $FeCl_2$. The sol-gel method resulted in the formation of low productivity Fe-MNP at a temperature ≥ 400ºC. In this chapter, the results confirm that the synthesis of Fe-MNP at 150℃ produced pure magnetite. At the same time, the Fe-MNP prepared at higher temperatures (>150℃) contained a mixture of hematite (γ–Fe_2O_3) and maghemite (α-Fe_2O_3) MNP. The obtained results indicated that the structure of the Fe-MNP is well established at a temperature of 350°C.

Figure 18b shows the absorption spectra of the MNP prepared at varying temperatures. The ultraviolet-visible (UV-Vis) spectrum indicated that the absorption peaks between 300 and 450 nm could be assigned to the iron oxide MNP. These adsorption peaks were linked to the as-synthesized Fe-MNP [313, 326]. In their study, [327] demonstrated how the UV-Vis spectrum with peaks in the wavelength (λ) range of 200-500 nm support the formation of the Fe-MNP. In our study, the peak at 370 nm was associated with the Fe-MNP, while the absorption edge for the Fe-MNP lies between 375 and 650 nm. The normal lower retention at λ of 261.9 nm and 231 nm are apportionable to the Fe_3O_4 MNP absorption bands, which were noted in the MNP prepared at a temperature of

150℃. The UV-Vis spectrum of the Fe-MNP synthesized at high temperatures of ≥ 250℃ exhibited a shift in absorption in the range of 300-500 nm. This absorption shift was aligned with the change in the structure of the Fe-MNP. This is due to the low productivity of the Fe_3O_4 MNP at a temperature of ≥ 200ºC, as well as the oxidation of the Fe-MNP to maghemite and hematite with the MNP at high temperatures.

Identical results and conclusions were noted by [328]. The mobility of electrons from the valence band to the conduction band is determined by calculating the energy gap (E_g) as per equation (9). [328]. The results indicated that the expected band gap energy is 5eV. A comparable value of 4.7eV was determined for the Fe-MNP by [328, 329].

$$Eg = \frac{hc}{\lambda} \tag{9}$$

Where c is the light speed, h is blank constant, and ƛ is the light wavelength.

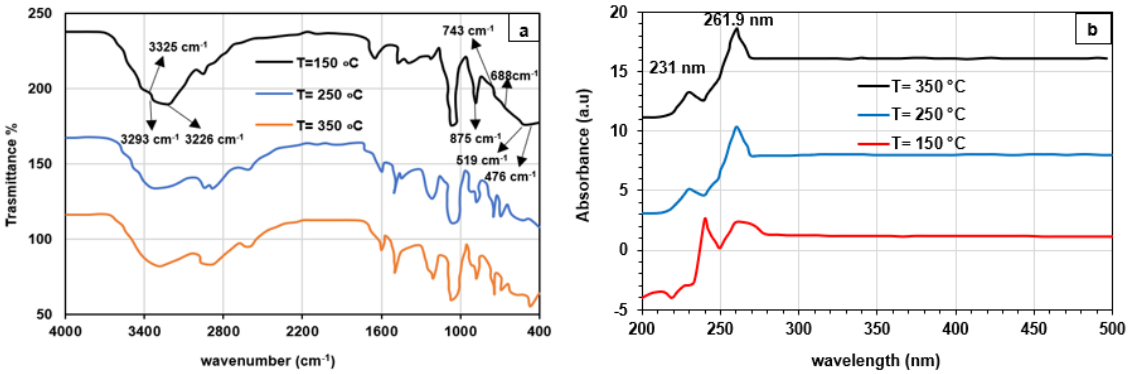

Figure 18. (a) FTIR Spectra of the synthesized Fe-MNP at different temperatures (b) UV-visible spectra of the synthesized Fe-MNP at varying temperatures.

The XRD pattern of the Fe-MNP synthetized at three different temperatures is presented in Figure 19a. The Fe-MNP prepared at 150ºC exhibited diffraction peaks at 2θ values of 26.5º, 32º, 35º, 56º, and 62.4º. These values were allocated to specific intensity values of the magnetite nanoparticles, including (310), (110), (311), (440), and (330). The values mentioned above support the appearance of the Fe-MNP structure as proposed by [298, 324]. Two peaks appeared at 46.54º, and 55.98º for the Fe-MNP prepared at 250 ºC and 350 ºC, which were allocated to the planes (240) and (331) for the α-Fe_2O_3 (ICDD card no. 33-0664) and γ–Fe_2O_3 (JCPDS card no. 25-1402), respectively. Corresponding conclusions were described by [312, 330] during Fe_3O_4 and Fe_3O_4/polyaniline nanocomposite preparation.

The differences in the XRD spectrum indicate that the Fe-MNP prepared at 150ºC is pure magnetite, while the Fe-MNP prepared at a higher temperature contains a mixture of γ–Fe_2O_3 and α-Fe_2O_3 MNP. These results are compatible with those published by [331, 332]. The XRD results demonstrate that the composition of the Fe-MNP prepared at 150ºC coordinated exceptionally well with the Fe_3O_4. However, increasing the preparation temperature to 250ºC shifted the peak to a higher angle. This shift was due to the formation of γ–Fe_2O_3 because of the Fe_3O_4 oxidation [332-334]. The composition of the Fe-MNP prepared at 350ºC was compatible with the α-Fe_2O_3 MNP (JCPDS card no. 25-1402). As such, the oxidation of Fe_3O_4 at 350ºC leads to the transformation of Fe_3O_4 to α-Fe_2O_3 MNP [335]. Scherer's equation (10) was used to calculate the size of the crystalline particles for the prepared Fe-MNP at differing temperatures [335]:

$$D = \frac{K.\lambda}{\beta.Cos\ \theta} \qquad (10)$$

Where K is a dimensionless number equal to 0.94; λ represents the X-ray wavelength, β is the half- of maximum intensity value, and θ is the Bragg angle.

The particle sizes of the Fe-MNP prepared at various temperatures are presented in Figure 19b. It was observed that the size of the MNP increased by correspondingly increasing the synthesis temperature from 150ºC to 350ºC. Increasing the reaction temperature would likely increase the degree of aggregation of the Fe-MNP and increase their size, which would result in larger nanoparticles [336]. Moreover, it is also likely that increasing the reaction temperature would provide more energy to the solution. This, in turn, would increase the mobility of the nanoparticles, ultimately causing a greater chance for a collision between the particles, thus producing a larger particle size [337]. The particle sizes for the three Fe-MNP were prepared at 150ºC, 250ºC, and 350ºC, and they were 2 nm, 6 nm, and 8.2 nm, respectively.

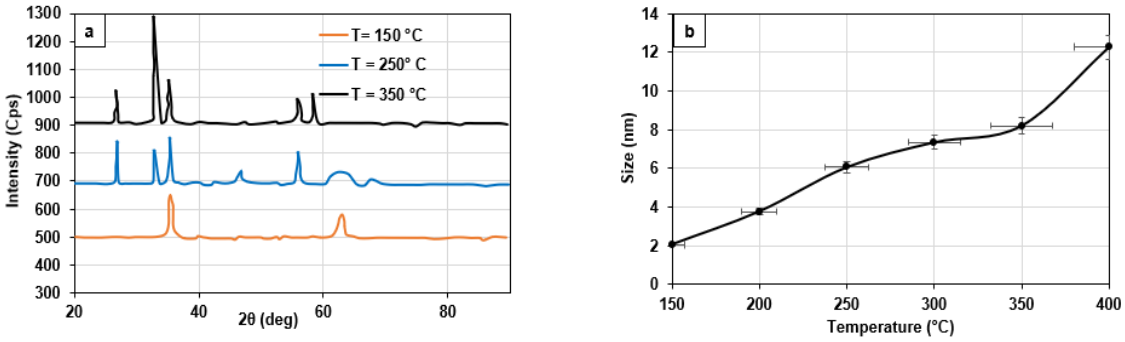

Figure 19. (a) XRD analysis of the Fe-MNP obtained at the temperatures 150°C, 250°C, and 350°C, respectively (b) Fe-MNP particle size as a function of temperature calculated by Scherer's formula.

The morphology of the Fe_3O_4 MNP sample prepared at 150ºC was characterized using a Scanning Electron Microscope (SEM) (Figure 20a) followed by an Energy Dispersive X-Ray (EDX) analysis (Figure 20b). The results showed that the Fe-MNP has a spherical agglomerated structure due to the effect of the Van der Waals force in the

solid phase. The spherical structure of the Fe-MNP is advantageous as it provides a superior internationalization rate and cellular take-up compared to the other shapes such as nano-disk or nano-cube shapes [332]. The particle size measured using the SEM analysis was approximate ~13 nm. As the preparation temperature increased, the shape of the Fe-MNP morphed into irregular particles due to the aggregation of the particles, as presented in Figure 20c. The reaction temperature raises the degree of aggregation of the Fe_3O_4 MNP and subsequently increases the size of the Fe-MNP, which results in larger nanoparticle sizes. As investigated by [317, 330], the size of the magnetite nanoparticles increases as the temperature increases from 200ºC to 400ºC. As such, the average particle size calculated using Scherer's formula is 2.02 nm, 5.58 nm, and 8.35 nm for Fe-MNP prepared at 150, 125, and 350 °C, respectively. This indicates that by increasing the temperature, the size of the Fe_3O_4 nanoparticles gradually increases.

The EDX images (Figure 20b) demonstrated the appearance of the Fe-MNP by exemplifying how the Fe-O gathered on the iron oxide MNP. The calculation from the EDX pattern showed that the Fe-MNP contains 76% iron and 18% oxygen, which is comparable to the results [338].

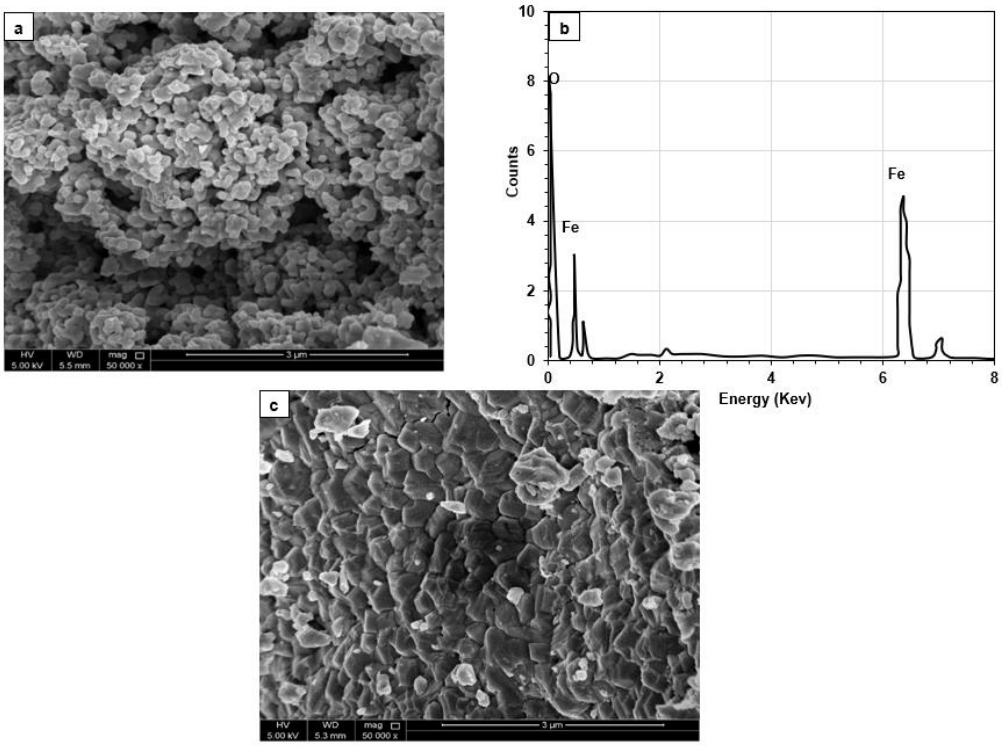

Figure 20. (a) SEM image of the Fe_3O_4 MNP obtained at a temperature of 150°C (b) EDX analysis of the Fe_3O_4 MNP (c) SEM image of the Fe_3O_4 MNP at 350°C.

Figure 21a presents the three-dimensional image of the Fe-MNP as obtained from the atomic force microscope analysis. The AFM images indicate that the particle of the magnetite Fe-MNP was uniformly distributed in size range of 10 to 20 nm, which was consistent with the results from the SEM analysis. The yellow region on the AFM image indicates a small agglomeration of the Fe-MNP as proposed by [167, 323]. The AFM image was analyzed using J image software to interpret the diameter of the individual nanoparticle (Figure 21b). The results showed that the MNP is spherical, with a diameter in the range of 10 to 20 nm and an average diameter of ~10 nm. These values are similar to those estimated using the SEM and TEM analysis with a percentage difference of ~ 0.5%. The research conducted by Chicea et al. [339] demonstrated similar results, with a range for the Fe-MNP size between 11-15 nm using an AFM

analysis (in this study), which is compatible with the size obtained by DLS and an effective crystallite mean size evaluated by XRD.

The magnetization of the Fe-MNP was examined using a vibrating sample magnetometer (VSM), as exemplified in Figure 21c. The shape of the vibrating sample magnetization curve (VSMC) exhibited a hysteresis loop, which supports the ferromagnetic performance of the Fe-MNP prepared at 150°C with a high magnetic saturation (M_S) value (51 ± 0.4 emu g^{-1}), and a St. Dev = 0.67. The results indicated that the Fe-MNP has the greatest magnetization value compared to the other samples at 250°C and 350°C, with low magnetization values. The decrease in M_s for the Fe-MNP prepared at higher temperatures is due to the weakening of the coupling force between the octahedral and tetrahedral sites. The octahedral and tetrahedral sites undergo an exchange interaction caused by the thermal fluctuations that can change the direction of the magnetic moment, as suggested by Pati et al. [340]. Additionally, it was observed that the Fe-MNP moved faster when using the magnetic field and spread apart again after shaking when the magnetic field was eliminated. This reaction indicates that the Fe-MNP has the essential characteristics of an adsorbent with efficient dispersion and separation characteristics for oil separation from water with a comparatively small magnetic field.

The Fe-MNP Mössbauer spectrum at 300°K is highlighted by the broad line exhibited in Figure 21d. which indicates the non-existence of an external magnetic field (H_{ext}). The spectra contains: an isomer change of δ = 0.321 mm/s, a line width of Γ = 1.355 mm/s, a quadrupole splitting (ΔEQ = -0.071 mm/s), a doublet including an isomer move δ = 0.38 mm/s, Γ= 0.992 mm/s, ΔEQ = 0.755 mm s^{-1}, and a sextet including a magnetic hyperfine field of B_{hf} = 474 kOe [341]. The components of the Fe-MNP area without the H_{ext} are in the doublet/sextet ratio of 34.2 to 65.8%. In contrast, the quadrupole

component is allocated to the superparamagnetic fraction. The Fe-MNP Mössbauer spectrum is associated with the particle size in the range of 2-10 nm, consistent with data described by Lehlooh et al., and Vijayakumar et al. [342, 343] and matched with the data from the XRD, SEM, and TEM characterization analyses. In the presence of ultrafine particles, the sub-lattices of iron do not settle, and approximately one-third of the samples remain suspended in the solution under a superparamagnetic state. The superparamagnetic components hide when H_{ext} = 0.17 T is used because of the produced magnetization of the sample. With the presence of H_{ext}, the Fe-MNP Mössbauer spectrum is estimated by one sextet with a considerable line width of Γ = 5.466 mm/s), ΔEQ = -0.056 mm/s, B_{hf} = 328 kOe, and δ = 0.332 mm/s. The line expanding the sextet is caused by the Fe-MNP particle size distribution and the several types of iron atom crystallographic surroundings. This coincides with a spinel structure where Fe^{2+} and Fe^{3+} ions are placed in different crystallographic locations (octa- and tetrahedral). The Fe_3O_4 MNP Mössbauer spectra exhibited two sextets, including an isomer change at δ = 0.27 mm/s for Fe^{3+} ions in tetrahedral A sites and δ = 0.65 mm/s for Fe^{2+} and Fe^{3+} ions in octahedral B sites [344]. The iron atoms (Fe^{2+} and Fe^{3+} ion) state will not be observable at room temperature because of the rapid electron-hopping process [345]. The iron cation's random distribution in the octahedral B sites causes an average valency case of $Fe^{2.5+}$. Furthermore, the isomer shift value likely reduces due to the nonstoichiometric phase of Fe-MNP [346].

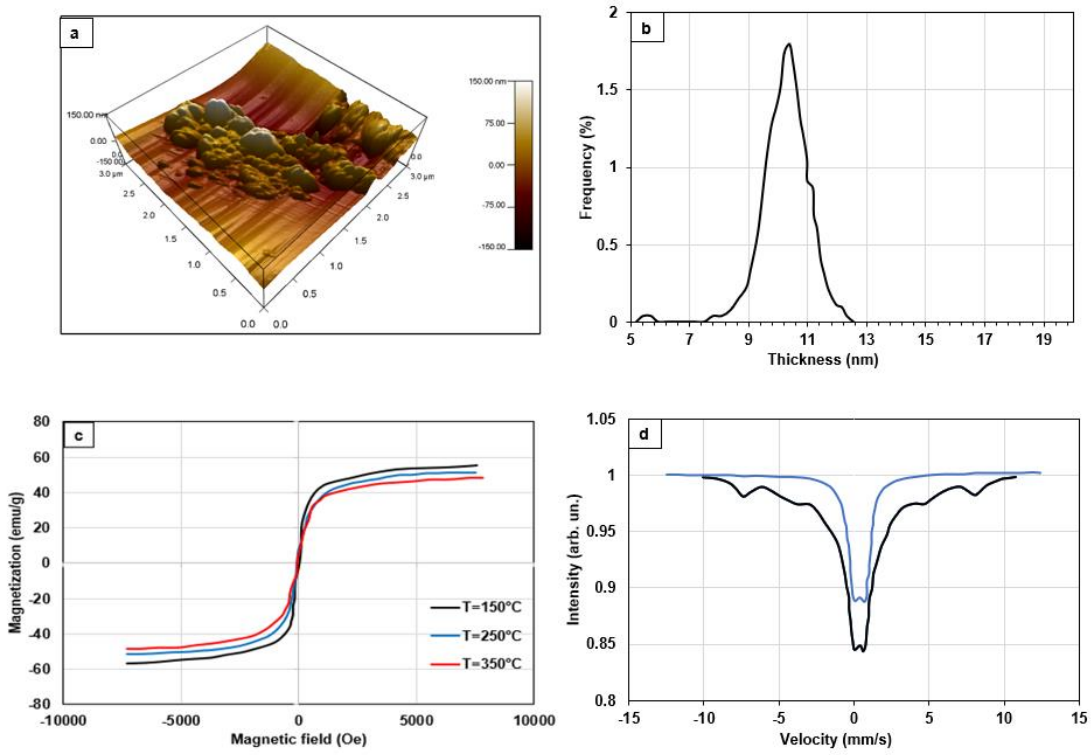

Figure 21. (a) AFM three-dimensional (3D) image of the synthesized Fe-MNP (b) AFM analysis histogram of the Fe_3O_4 MNP (c) Magnetization curve of the Fe-MNP at differing temperatures (d) Mössbauer spectra of the Fe-MNP in the absence of an external magnetic field.

The morphology and size of the produced Fe-MNP were investigated using high-resolution transmission electron microscopy (HRTEM). The samples used for the HRTEM studies were formed by dissolving the particles in deionized water for 30 min with mixing. Then a drop of the dispersion was added onto the copper grid, grafted with an amorphous carbon layer.

Figure 22 shows the TEM of the Fe-MNP and the Fe-MNP images using the HRTEM at two different magnifications. Both the HTEM image and the SEM analysis indicate that the shape of the particles is spherical. The images also highlight how the prepared Fe-MNP are dispersed consistently throughout, and the spheres are consistent in size to other another [327]. Additionally, it was observed that the particles have an average

size of approximately 8 nm. This observation is compatible with the results from the XRD analysis.

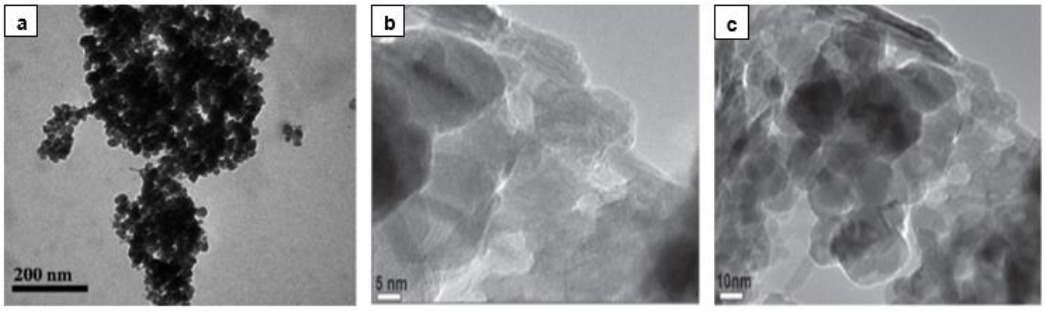

Figure 22. (a) TEM images of synthesized Fe-MNP (b) and (c) (HRTEM) images of the prepared Fe-MNP at a scale bar of 5 and 10 nm.

4.3.2 Oil Recovery Using Fe-MNP Demulsifier

4.3.2.1 The Effect of Fe-MNP Demulsifier Dose

Figure 23a presents the effect of the D_{MNP} in the range of 5 to 100 mg/L on the $\%\eta_{dem}$ of oil from O-in-W-emu. The high hydrophilic properties of the Fe-MNP indicate a strong attachment to the oil droplets dispersed in water, which aid in the removal from the emulsion and subsequently enhance the oil recovery performance. When the D_{MNP} increases from 5 to 10 mg/L for the O-in-W-emu with C_{oil} in the range of 0-800 mg/L, the demulsification efficiency improves from 55.66% to 69.6%. However, with a D_{MNP} of 30-50 mg/L, the removal rate reached up to 98%, after which the demulsification efficiency remained constant with high values ($\geq$ 98%) at high C_{oil}. Similar conclusions were observed by Lu et al. [291], whose research indicated that as the D_{MNP} increased from 25 g/L to 30 g/L, the $\%\eta_{dem}$ increased from 80.85% to 92.41% (after the removal rate remained constant at high C_{oil} ranges).

Figure 23a demonstrates that the oil demulsification is linearly dependent upon the D_{MNP} for the doses in the range 5 and 7 mg/L. As the D_{MNP} increased from 5 to 7 mg/L,

the $\%\eta_{dem}$ linearly increased from 55.7% to 69%. Conversely, for $D_{MNP} \geq 10$ mg/L, the $\%\eta_{dem}$ relationship concerning D_{MNP} is not linear and significantly increased to reach a maximum removal efficiency of $\geq 98\%$ at all the studied C_{oil}. These trends suggest that the Fe-MNP is appropriate for removing oil from O-in-W-emu. The adsorption capacity for low doses is significant under numerous conditions (including different C_{oil} and D_{MNP}). The results in Figure 23a also suggest that the $\%\eta_{dem}$ is not a function of C_{oil} when sufficient D_{MNP} is used. Therefore, under the studied conditions, the process can be conducted with the minimum required D_{MNP}, which should not be lower than 10 mg/L. Given this, a review of the research literature indicates that the Fe-MNP are thermally stable, recyclable, environmentally friendly, highly selective to oil, and exhibit a good dispersibility in O-in-W-emu. The dispersibility of the Fe-MNP indicates that the material can be examined as a potential magnetic sorbent for the water treatment process [347].

4.3.2.2 Effect of pH on the Demulsification Process

The pH is an essential factor that impacts the performance of the oil removal process. As such, Figure 23b. exemplifies the influence of the pH on the $\%\eta_{dem}$ at different C_{oil}. As demonstrated in Figure 23b. the $\%\eta_{dem}$ was evaluated as a function of pH by adding 10 mg/L of Fe-MNP to the emulsion samples (500 ml) with C_{sur} of 0.05 g/L, and oil concentrations from 0-1000 mg/L. After adding the Fe-MNP to the emulsion, the droplets of oil attached to the Fe-MNP, and no free droplets of oil appeared clearly in the mixture. Additionally, some aggregation in the Fe-MNP was observed, which indicates that the emulsified oil droplets were absorbed into the Fe-MNP. [348] reported similar observations during the separation process of oil/water mixtures using iron oxide magnetic nanoparticles. The results indicated that the corresponding oil removal efficiency decreased with a low pH (4), the $\%\eta$dem has a high value (~ 95%). The effect

of the pH is likely associated with the change in the surface charge at differing pH. For instance, at a lower pH, the presence of H protons improves the aggregation of oil droplets in the O-in-W-emu, making the negative charges dominant, thereby decreasing the zeta potential and enhancing the attachment between the oil and the Fe-MNP. Thus, the $\%\eta_{dem}$ increased even when at a low D_{MNP}.

The decrease in the $\%\eta_{dem}$ at a higher pH (~91% at a pH of 7 and 90.4% at a pH of 10) is correlated to the increase in the negative charge of the O-in-W-emu, which also leads to an increase in the negative Zeta potential and a decrease the attraction force and the $\%\eta_{dem}$. Similarly, Chen et al. [349] noted that the demulsification efficiency is significantly reduced at a high pH value (3.4). Further, the decrease in the pH during the water phase to a value of 1.2 by adding acid can cause significant oil droplet coalescence, leading to more than 85% of the oil phase separation. However, the concept of pH must be cautiously considered, especially during a non-aqueous phase such as the oil phase. During the PW treatment process, an alteration in the pH can be made by adding acidic or basic chemicals [350]. As such, the pH permits the removal of dissolved oil from water through the demulsification process. The water comprises both negatively charged hydroxide ions and positively charged hydrogen ions, which improves the separation process as reported by Lu et al. [278]. Stachurski et al. [351] noted that the OH^- ions in the aqueous phase (i.e., water phase) with the addition of acids would generate further positive charges in the surrounding area of the O-in-W-emu interface, which will ultimately change the stability of the O-in-W-emu. Given that, the existence of some materials in the O-in-W-emu mixture will affect the purity of the MNP and thus slightly decrease the ability of the oil to absorb onto the MNP. Moreover, it was found that at a high pH, the electrostatic repulsion between the oil

droplets and the MNP was significantly more potent than at a medium or low pH, which negatively affected the demulsification process [352].

4.3.2.3 Effect of Surfactant Concentration (C_{sur}) on the Demulsification Process

Given that the O-in-W-emu samples commonly include surface-active substances called surfactants [100], it is crucial to examine the impact of these material concentrations (C_{sur}) on the $\%\eta_{dem}$. The presence of surfactants combined with the Fe-MNP in O-in-W-emu will impact the $\%\eta_{dem}$ by disrupting the chemical and physical bonds of the surface-active agents (surfactants) that keep oil emulsified in produced water. Accordingly, the Fe-MNP were tested and selected based on their high performance in PW treatment, owing to their large surface area and high $\%R_{oil}$ [111]. In this chapter, the efficiency was tested with and without adding various amounts of surfactants. The tests with the surfactant were conducted under two concentrations, C_{sur} 0.1 and 0.5 g/L, using a D_{MNP} = 10 mg/L and O-in-W-emu with C_{oil} from 0-1000 mg/L as shown in Figure 23c. The results indicated that under all the studied C_{oil} (0-1000 mg/L), the $\%\eta_{dem}$ slightly reduced by increasing the C_{sur}. These results are due to the increase in the O-in-W-emu stability. A high C_{sur} enhances the oil droplet distribution inside the emulsion, while decreasing the forces of the surface tension leads to a reduction in the absorption over the Fe-MNP.

Prior research focused on the demulsification of O-in-W-emu showed that oil droplets could graft onto the Fe-MNP due to the attractive hydrophobic forces [353]. Hence, the existence of the surfactant improves the oil droplet's dispersion, decreasing the surface tension forces and reducing the Fe-MNP oil absorption.

Additionally, as the electrostatic repulsion between the surfactant and oil droplets decreases, these factors will consequently influence and decrease the $\%\eta_{dem}$ of the Fe-MNP. The experimental results further show that for most of the (used) demulsifiers, the $\%\eta_{dem}$ significantly dropped at $C_{sur} \geq 0.65$ g/L. This result is in contrast with previous studies of oil removal by natural organic macromolecules [352]. In this chapter, it was noted that the Fe-MNP could disturb the chemical and physical bonds between oil- surfactants, which maintain the emulsified oil in water and obtained a high $\%\eta_{dem}$. The substantial $\%\eta_{dem}$ maybe associated with the significant Fe-MNP surface area, the greater attraction force of oil-Fe-MNP, and the efficient removal using an external magnetic field. As magnetic nanoparticles have direct contact with the stabilized oil droplets, the high surface area of the MNP leads to the rapid separation of oil droplets from the water phase using an external magnetic field. The separation can occur in the absence of a magnetic field, though much slower [354, 355].

4.3.2.4 Effect of Salinity on the Demulsification Process

The effect of the salinity of the O-in-W-emu on the $\%\eta_{dem}$ was evaluated, and the results are presented in Figure 23d at a pH of 4. The $\%\eta_{dem}$ was examined with an added 10 mg/L Fe-MNP to the emulsion sample with varying C_{oil} from 0 to 1000 mg/L and a salinity range of 0.1, 0.3, and 0.5 M NaCl. The results demonstrated that as the salinity of the O-in-W-emu increased, the $\%\eta_{dem}$ correspondingly improved. Further, when the salinity of the O-in-W-emu increased from 0.1 to 0.5 M NaCl, the $\%\eta_{dem}$ increased from 88.2% to 95.4% at a C_{oil} of 100 mg/L. Similar trends were observed at other concentrations. Primarily, this was caused by a “salting-out” effect, which reduced the stabilizing surfactants' hydrophilicity and consequently lowered O-in-W-emu's interfacial tension [356].

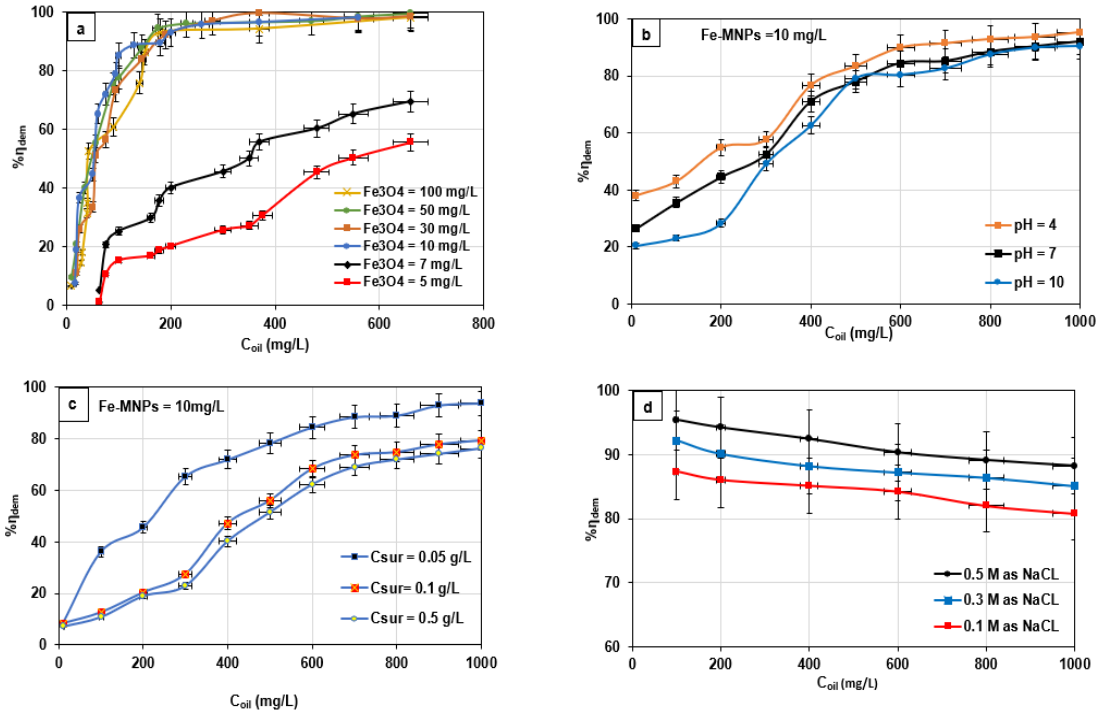

Figure 23. Evaluation of $\%\eta_{dem}$ as a function of (a) D_{MNP}, (b) pH, (c) C_{sur}, (d) salinity.

4.4 Reusability of the Fe-MNP Demulsifiers

In addition to the high performance of the Fe-MNP during the demulsification process, they can also be recycled and reused many times over. As such, Figure 24a presents the recyclability of the Fe-MNP at different pH (4, 7, and 10). The results exemplified how at a pH of 4, the $\%\eta_{dem}$ in the 1st cycle was ~ 95.11% and slightly decreased during the 4th cycle, as it reached 86.6%, then reduced to 83.19% during the 7th cycle. However, for the tests carried out at a pH of 7 and a pH of 10, for the 1st cycle, the $\%\eta_{dem}$ decreased to 92.9% and 90.7%, respectively. The $\%\eta_{dem}$ of the Fe-MNP was recently examined at a pH of 4 by [291], whose research showed a $\%R_{oil} \geq 90$ after being recycled five times. The $\%\eta_{dem}$ declined by expanding the pH in the O-in-W-emu. These results were comparable with the work of [357] for the treatment of oily-micro-contaminated water using magnetic nanoparticles. The study found that the oil removal value was

approximately 87% during five cycles and that the removal began to decrease after five cycles as it reached roughly 80% during the 8th cycle.

From the previous results of the reusability of the Fe_3O_4 MNP examined at different pH, it was observed that at a pH ≤ 4, the oil removal rate (%R_{oil}) has a significant value of ~ 95%. Therefore, the recyclability test was carried out again at this pH level to achieve a more effective oil removal and enhance the demulsification efficiency (%η_{dem}). Thus, the reusability of the MNP was improved at specific conditions. After that, the statistical analysis (ANOVA calculations) was applied to define the impact of all process variables on the oil removal rate. These analyses only consider the factors that have a statistical consequence on the demulsification process with a P-value ≤ of 0.05 are set as a cut-off limit to accept or reject parameters. To achieve the best conditions for reusing large amounts of the Fe-MNP, a 10 mg/L of Fe-MNP and a maximum of 20 mL of ethanol at a separation time of 8 min were required for reproducing approximately 20 mL of Fe-MNP. As exemplified in Figure 24b, under these conditions (C_{oil} 500 mg/L and D_{MNP} 10 mg/L), the Fe-MNP can be reused for a minimum of 7 cycles with no considerable drop in the oil removal rate (%R_{oil}). The demulsification efficiency decreases and reaches 83.6% during the 6th cycle, which is still considerably higher than other oil removal rates achieved by different demulsifiers. The reduction in the demulsification efficiency is caused by the grafting of certain remnants of the organic materials onto the surface of the Fe-MNP. The grafting affected the percentage of oil removed in the 7th cycle as it decreased to 83.19%. Prior research has demonstrated that the Fe-MNP exhibited high oil removal values under an expanded operating time, and the Fe-MNP demulsifiers were found to be effective regenerate [353, 358]. Further, the Fe-MNP demulsifiers were reused for seven cycles

of oil recovery from O-in-W-emu, indicating that these demulsifiers are greatly impactful for reducing the cost of the oil recovery process [353, 358].

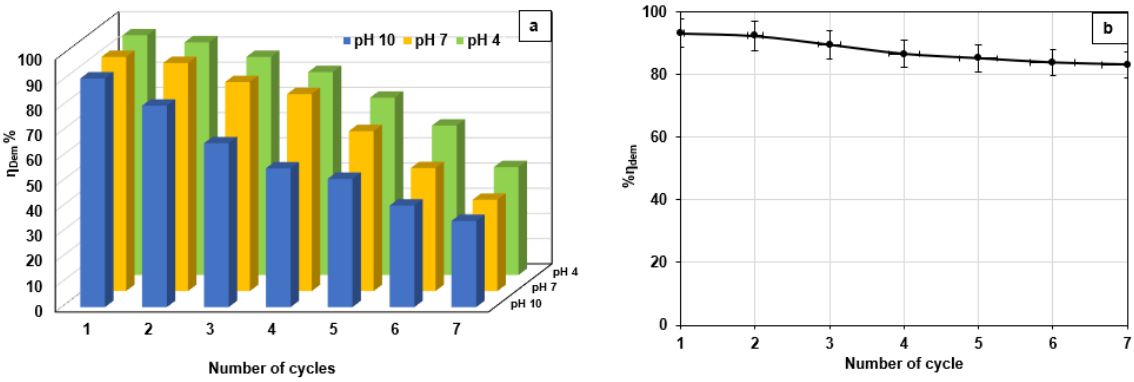

Figure 24. (a) Recyclability of the Fe_3O_4 MNP in O-in-W-emu at different pH, (b) The $\%\eta_{dem}$ of the Fe_3O_4 MNP at a pH=4 under different cycles

4.5 Adsorption Isotherm of the Fe_3O_4 MNP

The adsorption isotherms of the demulsification process using Fe_3O_4 MNP were conducted at room temperature with oil concentrations ranging from 0-800 mg/L. The initial and most common models used in this type of research are the Langmuir (equation 7) and Freundlich isotherms (equation 8) [359]. The Langmuir isotherm assumes single-layer adsorption of contaminants onto solid adsorbent surfaces (in this chapter, oil adsorption onto the Fe-MNP surface), after which no additional adsorption will occur. The parameters q_{max} and K_L represent the maximum adsorption capacity and the energy needed for the adsorption process, respectively. In contrast, the Freundlich isotherm presumes adsorption within multiple combined layers with a different distribution in adsorption heat and high identical surfaces [360]. The parameters K_f and n represent the model coefficients, both of which are associated with adsorption capacity and the adsorption process favourability, respectively. A non-linear regression analysis based on the Marquardt Levenberg algorithm using Microsoft Excel solver was used to determine the parameters of each isotherm following the procedure established

by Ashrafi et al. [361]. The regression analysis was assessed based on the R^2 values, and the method with the greater R^2 value was chosen.

Table 7 presents the isotherm parameters following the Langmuir and Freundlich isotherms for the Fe-MNP adsorbent, and representative regression analysis of the experimental data is shown in Figure 25. It was determined that the Fe-MNP achieved a maximum adsorption capacity (q_{max}) of 15.051 mg/g using the Langmuir model. Further, the oil removal from the O-in-W-emu using the Fe-MNP demulsifier is supported by the Freundlich isotherm with R^2 = 0.998 and a high K_f value of 1.836. While this model cannot predict the saturation level of the oil droplets in the Fe-MNP surface, the mathematical analysis indicates that the coverage of the Fe-MNP demulsifier surface reaches infinity. However, the values of the 1/n can be used to evaluate the high capacity of the adsorption process, where a value ≤ 1 denotes the favourability of the adsorption process. The 1/n value for the Fe-MNP demulsifier is 0.380 (see Table 7), which signifies a high level of attraction for oil removal using Fe-MNP demulsifiers. Similar results were exhibited for the adsorption onto the Fe_3O_4 MNP for heavy metal removal. The estimated parameters achieved from the Freundlich equation show a high adsorption efficiency of the synthesized Fe-MNP to the examined heavy metal ions, wherein the calculated values of the 1/n are 0.3259, 0.3383, and 0.3191 (all $\leq$ 1). The values mentioned above indicate the favourability of the adsorption process [362].

Table 7. Langmuir and Freundlich model parameters for the adsorbed oil on the synthesized Fe_3O_4 MNP demulsifier.

Isotherm model	Parameter	Fe_3O_4
Langmuir Isotherm	Q_{max} (mg/g)	15.051
	K_L (L/mg)	0.105
	R^2	0.908
Freundlich Isotherm	K_f	1.836
	1/n	0.380
	R^2	0.998

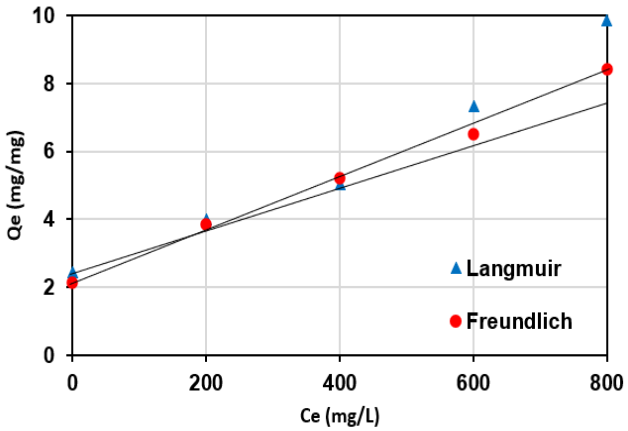

Figure 25. Adsorption isotherm for the adsorption process onto the Fe_3O_4 MNP at a temperature of 25°C, pH 4, and initial oil concentration (C_{oil}) of 100 mg/L.

4.6 Adsorption kinetic Studies

Pseudo-first-order and pseudo-second-order models were used to assess the kinetic of the demulsification process. The pseudo-first-order model, equation (10) [363], assumes that the adsorption process rate is directly correlated to the number of empty places by the adsorbate [364].

$$Ln\,(Q_e - Q_t) = LnQ_e - K_1 t \qquad (10)$$

Figure 26a exemplifies the regression analysis of the experimental data following equation (10) for the tests carried out at different time lengths with a temperature of 25°C, a pH of 4, a D_{MNP} of 10 mg/L, 30 mg/L, 50 mg/L, and 100 mg/L. The kinetic constants k_1 and Q_e were determined and briefly outlined in Table 8. The experimental data did not match correctly with the pseudo-first-order model, except the D_{MNP} = 100 mg/L, where the correlation coefficient R^2 was 0.984. A high R^2 value signifies that the adsorption of oil droplets on the Fe-MNP follows the pseudo-first-order model. However, the oil adsorption on the D_{MNP} = 10, 30, and 50 mg/L have R^2 values that are comparatively low, which indicates that they do not adhere to the pseudo-first-order model. The pseudo-second-order model is also a kinetic model that is applied in the adsorption process. The pseudo-second-order model is typically used to characterize kinetic equations based on their adsorption capacity from the solution concentration [365]. The pseudo-second-order model is presented in equation (11). The regression analysis following equation (11) is shown in Figure 26b. The experimental data correctly matched with the pseudo-second-order model for all tested D_{MNP} with $R^2 \sim 1$, indicating that this adsorption method largely supports this kinetic model.

The high Fe-MNP dosage of 100 mg/L exhibited fast adsorption kinetic for an equilibrium achieved after 1 h, after which time no additional adsorption occurred. When the adsorbent dosages were improved, further surface area sports were accessible for adsorption, which caused an uptick in the adsorption values. This is caused by the oil particle's saturation of the surface sites (that exist on the adsorbent). This reaction leads to an equilibrium condition between the oil adsorbed on the surface along with the solution. Furthermore, a larger dosage of the adsorbent may cause aggregation of the MNP, thus becoming less accessible for the adsorbate (oil) effective-binding sites to attach to the surface.

Consequently, at lower dosages of the adsorbent, there was a decrease in the oil adsorption capacity. Similar results were noted by Yu et al. [366] for the use of Fe_3O_4 MNP as sorbents of oil from wastewater in a wastewater treatment application. Furthermore, the study [366] highlighted how a maximum adsorption capacity for different types of oil applied has greater values, ranging from 0.09-3.77 g/g, which is 7.15 times its weight.

$$\frac{1}{q_t} = \frac{1}{K^2{}_2\, q^e{}_e} + \frac{t}{q_e} \tag{11}$$

Table 8. Kinetic parameters for the adsorbed oil on the produced Fe-MNP demulsifiers.

Kinetic model	Qe (mg/g)	K1 (1/min)	R^2
Pseudo-first-order			
D_{MNP} 10 mg/L	1.230	0.0598	0.718
D_{MNP} 30 mg/L	0.4101	0.0124	0.834
D_{MNP} 50 mg/L	0.4703	0.0118	0.899
D_{MNP} 100 mg/L	6.817	0.0107	0.948
Pseudo-second-	Qe (mg/g)	K2 (1/min)	R^2
order	1.217	0.226	0.997
D_{MNP} 10 mg/L	1.378	0.229	0.998
D_{MNP} 30 mg/L	902.1	0	0.999
D_{MNP} 50 mg/L	5.652	0.288	0.999
D_{MNP} 100 mg/L			

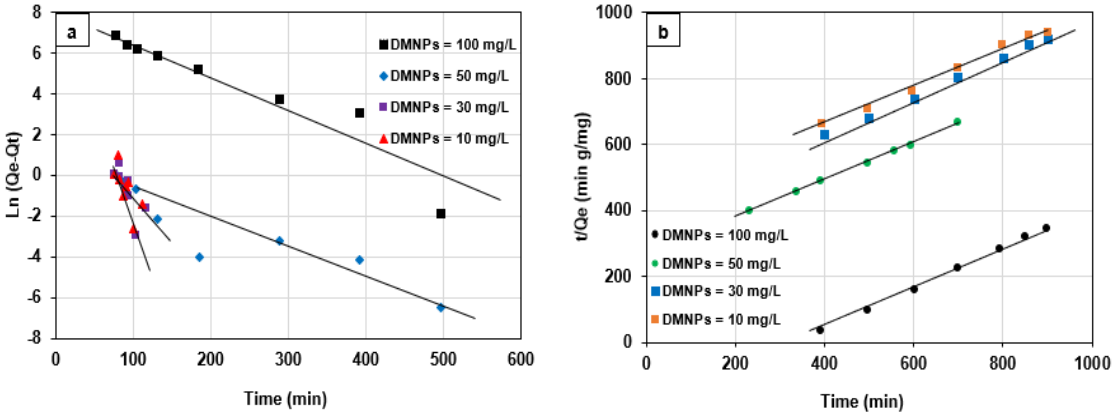

Figure 26. (a) Pseudo-first-order and (b) Pseudo-second-order kinetic models for the adsorption process applying different dosages of the Fe-MNP.

4.7 Discussion/Summary

Table 7 outlines how the oil adsorption with the Fe-MNP was best predicted using the Freundlich isotherm model compared to the Langmuir model. As such, Table 7 present the estimated parameters for each model and compares the two isotherm models. The Freundlich isotherm properly fits with the experimental data under the studied concentration (100 mg/L). The correlation coefficient values (R^2) indicate that the adsorption of oil droplets on the Fe-MNP follows both the Langmuir and Freundlich models. However, the adsorption was found to be faster using the Freundlich isotherm. The correlation coefficients were estimated to be 0.908 for the Langmuir model and 0.998 using the Freundlich model. The value of the exponent 1/n provides a sign of the adsorption favourability (≥1.0), and the value suggests conditions of favourable adsorption [367]. Table 7 indicates that the calculated value of exponent 1/n is 0.380 for Fe-MNP adsorbents. The value of the R_L for the Fe-MNP following the Langmuir equation was determined using the relation: $R_L = 1/1+KLC_0$ and was found to be = 0.23. The R_L values exhibited favourable adsorption of oil on the Fe-MNP surface. Given

that, the Fe-MNP are favourable adsorbents. Table 9 summarizes the comparison between the Langmuir and Freundlich models in oil adsorption using Fe-MNP.

Table 9. Comparison between the Langmuir and Freundlich models in oil adsorption using Fe-MNP.

Model	Key parameters	Assumption	Other parameters
Langmuir	Q_{max}: is the maximum adsorption capacity. Q_{max} = 15.051 mg/g R^2 = 0.908	Assumes single-layer adsorption of contaminants onto solid adsorbents surface	K_L: is the energy needed for the adsorption process. K_L= 0.105 L/mg R_L: dimensionless constant separation factor R_L = 0.23
Freundlich	K_f: is the adsorption capacity. K_f = 1.836 R^2 = 0.998	Presumes the presence of adsorption with multiple layers combined with a different distribution in adsorption heat and identical high surface	1/n: the favourability of the adsorption process 1/n = 0.380 ($\leq$ 1)

4.8 Conclusion

This chapter has investigated the preparation of Fe_3O_4 MNP using a CSM at temperatures of 150ºC, 250ºC, and 350ºC. Various analysis methods were applied to verify the synthesis of the magnetite (Fe_3O_4 MNP). The SEM analysis successfully defined the crucial characteristics of the MNP, including morphologies, molecular structure, size, and roughness. The results indicated that when the temperature changed, different MNP sizes were obtained. The morphology analysis of the Fe-MNP exhibited how the sample prepared at 150ºC is more spherical and partially agglomerated than the samples prepared at 250ºC and 350ºC. The CSM is effective for the preparation of

Fe_3O_4 MNP and economically feasible and environmentally friendly. Further, the temperature variation offers different Fe_3O_4 MNP size samples, effectively controlled by shifting the temperature. Then, the $\%\boldsymbol{\eta_{dem}}$ of the as-synthesized Fe-MNP were evaluated. The application of the MNP exemplified a significant improvement in the efficiency of the demulsification process, although only a small amount of the MNP was used.

This chapter also examined the parameters that would affect the demulsification process. As such, it was noted that the $\%\boldsymbol{\eta_{dem}}$ declined when there was an increase in the pH and the concentration of tween-80 surfactant. Additionally, the prepared Fe-MNP were still effective after being recycled for 7 cycles and had a high removal rate ($\%R_{oil}$) ~ 90%. This indicates that the MNP is a reliable technique for the recovery and separation of oil from O-in-W-emu.

The adsorption kinetic analysis was carried out using pseudo-first-order and pseudo-second-order kinetic models. The highest Fe-MNP dose (100 mg/L) indicated the highest adsorption capacity and exhibited the fastest adsorption kinetics. Given that, the experimental data are accurately fitted to the pseudo-second-order model.

CHAPTER 5: APPLICATION OF Fe_3O_4 MAGNETITE NANOPARTICLES GRAFTED IN SILICA (SiO_2) FOR OIL RECOVERY FROM OIL IN WATER EMULSIONS

5.1 Introduction

Large amounts of produced water (PW) contaminated with oil and other constituents are generated during gas and crude oil extraction, which would pollute the environment if discharged without proper treatment [368, 369]. Primarily, PW contains solids (suspended and dissolved), organic matters (soluble and non-soluble), and the chemicals used during the production process [370]. Various technologies have been successfully developed and applied for the effective treatment of solids. However, treatment processes used to recover chemicals and oil still require further investigation [371]. Nevertheless, proper treatment of PW allows for the reuse and recycling of high volumes of treated water and the recovery of oil [37], which subsequently improves the economic and environmental sustainability of the whole process [372].

Oil in PW appears as a small-sized droplet, known as oil in water (O/W) emulsion [289, 373], which is difficult to treat in comparison to other types of contaminates [374, 375]. The chemicals used during oil and gas processing reduce the interfacial surface tension and decrease the zeta potential of the mixture, thus increasing the stability of the emulsions [212]. Various treatment processes [376] including flotation [377], chemical coagulation-flotation [378], electrochemical separation [379], chemical demulsification [380], membrane separation [381, 382], electrocoagulation, adsorption processes [383] and biotechnologies [384] were employed for the separation and recovery of oil from O/W emulsion. However, the low removal efficiencies, high cost, excessive generation of sludge, and difficult process operational conditions limit the large-scale application of these processes. Recently, the use of MNPs in environmental

applications such as electro-catalysis, metals recovery, and oil removal has gained significant attention as noted by Kong et al., Wang et al., Kokate et al., Zhang et al., Almomani et al., and Liu et al. [375, 385, 386], [387, 388], [389-394]. Studies showed that the successful use of MNPs in such application is related to the well-defined surface morphology, excellent adsorption capacity, well-determined physical properties, biocompatibility, high dispersion, low cytotoxicity, and simple separation from multiphase composite [395-398].

With the progress of nanotechnology, the use of MNPs has expanded to applications in water and wastewater treatment processes [399]. Shen et al. [400] prepared and used Fe_3O_4-MNP for the treatment of the wastewater polluted with metal ions. The synthesized MNP demonstrated an excellent removal efficiency of different metal ions (Ni, Cu, Cd, and Cr) from wastewater. This chapter highlighted the importance of the chemical reactivity of the Fe_3O_4-MNP during the treatment process. The work recommended future work to focus on improving and enhancing the removal efficiency while keeping the Fe_3O_4-MNP chemically stable. Lu et al. [401] proposed the development of a core-shell structure, which includes forming Fe_3O_4-MNP covered by a protective shell. Organic compounds such as polymers and surfactants or inorganic coating compounds such as silica, carbon, and expensive metals were proposed to coat the MNP. In such a configuration, the properties of the Fe_3O_4-MNP and the stability against oxidation are maintained.

Coating the Fe_3O_4-MNP with functional materials (e.g., silica) has shown excellent stability and allowed various functional groups on the surface MNPs to enhance the treatment and separation efficiencies [402]. For instant, amines and carboxyl groups can enhance the attraction-repulsion force and improve ions removal. Coated Fe_3O_4-MNPs were successfully used in protein isolation [403], electron therapy [404], medical

applications [405], and wastewater treatment [406]. [407] demonstrated the preparation of Fe_3O_4-MNP grafted with an inner layer of dense, nonporous silica and an outer layer of miso porous silica. The developed nanoparticles exhibited an excellent removal efficiency (~ 85%) of pollutants from oil field wastewater through the superconducting magnetic separation technique. Peng et al. [212] prepared an MD by grafting ethyl cellulose onto the surface of amino-functionalized Fe_3O_4 nanoparticles coated with silica. The developed nanoparticles recovered up to 90 % of the water from a diluted bitumen emulsion. Furthermore, Calcagnile et al. [408] prepared a novel composite material based on the functionalizing of polyurethane foam and colloidal Fe_3O_4-MNP. Singh et al. [409] synthesized Fe_3O_4-SiO_2 nanoparticles with hydrophilic properties by adding hydroxyl groups on the surface of the SiO_2 shell, which could simply be attached to hydrophobic constituents. Recently, [410] have synthesized core-shell γ-Fe_2O_3/MnO_x MNPs with a core diameter of ~31 ± 3 nm and saturation magnetization ranging from 55 to 70 emu/g. The new composite was effectively used to separate contaminants from oil field wastewater and achieved $\%R_{oil}$ in the range of 75.5% to 94.9% due to hydroxyl groups. Mirshahghassemi et al. [411] studied the recovery of oil using polyvinylpyrrolidone (PVP)-coated iron oxide MNPs from oil-water mixtures. The results showed an excellent removal efficiency of up to 100 % from synthetic and natural water samples.

The literature mentioned above indicated that the development of chemically stable MD with a high capacity for the separation and recovery of oil is crucial. Additionally, the mechanism, reusability, removal capacity, and the effect of operational conditions on the developed MD must be assessed and analyzed. A review of the relevant research literature highlights the need for further studies related to oil separation from PW using stable MD. As such, this chapter aimed at developing an MD consist of magnetite

nanoparticles (Fe_3O_4) coated with silica (SiO_2) with extended durability for the demulsification of oil from PW. This synthesized MD was used to recover oil from O/W emulsion at different doses (MD_{dose}) and tested for their demulsification efficiency ($\%\eta_{dem}$) and the percentage oil recovery ($\%R_o$). Additionally, the mechanism, adsorption isotherms, reusability, and separation ability were assessed. The newly developed MD will open a new opportunity to recover valuable material from an aqueous solution.

5.2 Materials and Methods

5.2.1 Chemicals

Analytical grade of Tetraethyl Orthosilicate (TEOS, Merck, CAS Number: 78-10-4), Ammonium hydroxide solution (25 wt% CAS Number: 1336-21-6), Ethanol (CAS Number: 64-17-5), and the Fe_3O_4 nanoparticles (99.9%, size 8 nm) were purchased from Merck-Qatar. These chemicals were used as received without further purification. Gasoline oil was prepared from synthetic oil (95 Octane, density = 719.7 kg/m^3) purchased from a local fuel oil provider (WOQOd, Doha, Qatar). Polyethylene sorbitol ester (Tween-80) surfactant was purchased from Sigma Aldrich and used to prepare O/W emulsion.

5.2.2 Preparation of Fe_3O_4-SiO_2 Magnetic Demulsifier (MD)

The modified Stober procedure [289] was used for the preparation of Fe_3O_4-SiO_2 MD. Figure 27 summarizes the chemical reaction involved in the preparation process and the proposed shape of the MD. The procedure includes dissolving 0.5 g of Fe_3O_4 in 25 mL of deionized water (18.2 MΩo-cm and 0.055 µS); the mixture was then transferred to a three-neck round-bottom flask and mixed with 100 mL of ethanol and 1.0 mL ammonia solution (28 wt%). The mixture was vigorously mixed at room temperature for 15 min. Then a 0.5 mL of tetraethyl orthosilicate (TEOS) was added to the mixture

and left to react at room temperature for an additional 6 h under continuous mechanical stirring. The produced Fe_3O_4-SiO_2 MD were collected using an external magnetic field, washed with ethanol and water numerous times, and dried for 8 h at 70°C.

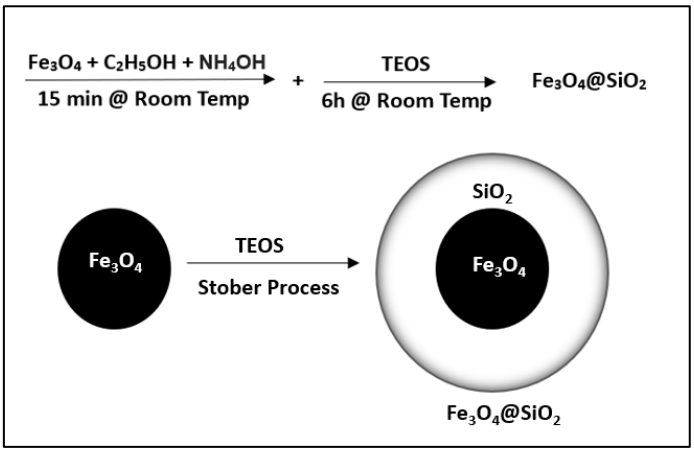

Figure 27. The chemical reaction for the preparation of the MD and the proposed shape.

5.2.3 Preparation of O/W Emulsions

The oil in water (O/W) emulsions used in the experiments were prepared by mixing gasoline oil with deionized water to mimic the behavior of O/W emulsion in the reservoir. This is a common approach in upstream research for oil and water emulsions. The O/W emulsions were prepared by dissolving 0.6 g of surfactant with 1000 mL deionized and mixed in a shear emulsifying homogenizer (model BRH1-100, USA) at a speed of 3500 rpm for 2 min. According to the stability test performed, this surfactant concentration was the proper dosage that produces a homogeneous O/W emulsion. Subsequently, a specific concentration of the gasoline oil was added dropwise and mixed with water for 10-15 min to produce homogenous O/W emulsion with C_{oil} in the range 500 to 4000 mg/L.

5.2.4 Characterization of the Fe_3O_4-SiO_2 MD

The surface morphology of the MD was characterized using transmission electron microscopy (TEM, Hitachi H-600, Japan). The X-ray diffraction (XRD, Minifix II Japan) patterns were verified using a Rigaku D/MAX-R diffractometer with a copper target at 40 kV and 30 mA. Fourier transform infrared (FTIR, PerkinElmer Spectrum 400, USA) spectra were obtained at room temperature with a spectrometer using KBr pellets. The thermal analysis tests were conducted in a TGA (TA Q-600, AUST) apparatus at a heating rate of 10 K/min in the presence of nitrogen as a spacer gas. Magnetic hysteresis loops were measured using a vibrating sample magnetometer (VSM, Lakeshore 7407, US) with an applied magnetic field between – 20,000 Oe and 20,000 Oe at 300 K. The nanoparticle's morphology, structure, and elemental composition were characterized by Scanning Electron Microscope (SEM FEI model Nova Nano SEM 450, US), followed by Energy Dispersive X-ray spectrometer (EDX). Lastly, the particle size distribution was detected using Dynamic Light Scattering measurements (DLS, Zeta PALS, Brookhaven Instrument Corp, US).

5.2.5 Experimental Procedure

The procedure used for the recovery and separation of oil from O/W emulsions entails adding a specified dose (MD_{dose} ~10, 20, 50, and 100 mg/L) of the MD to 500 mL of O/W emulsion, followed by sonication for 2 min and subsequently mixed for an additional 10 min at 3500 rpm. All tests were conducted at room temperature unless otherwise specified. The pH of the O/W emulsion was left to evolve freely without adjustment, and it was observed to be approximately 4.0 ± 0.1 (Std. Dev. = 0.89). Thereafter, the mixing was stopped for an additional 10 min, which allowed oil droplets to adsorb on the Fe_3O_4-SiO_2 MD. Then, the MD-oil was separated using an external magnetic field, and the $\%\eta_{dem}$ and $\%R_o$ were subsequently evaluated. Tests carried out

at different pH were adjusted by adding a concentrated amount of phosphoric acid and/or sodium hydroxide. Quality measurement conformed that the added acid/base did not interfere with the volume of the solution or the reported $\%\eta_{dem}$. Experiments carried out to determine the effect of time on the $\%\eta_{dem}$ were carried out in 15 L reactors, and the samples were withdrawn at different 10-second intervals and used for analysis.

The initial and final concentrations of the oil in the O/W emulsion were determined using UV analysis coupled with trichloro-trifluoroethane (TCTFE) extraction. The use of TCTFE as an extraction solvent amplifies the absorbance of the carbon-hydrogen bond in the infrared region and allows for accurate measurements of oil in O/W emulsion. Quality assurance tests were performed to determine the minimum detection limit of the C_{oil}, and it was determined to be 0.15 ± 0.06 mg/L (standard deviation (Std. Dev.) ~0.88). The tests were performed at 20°C to eliminate the chance for hydrocarbon evaporation and achieve accurate measurements. Additionally, quality assurance tests were carried to verify the initial and final concentrations of the oil in O/W emulsion using TOC measurements. The C_{oil} was correlated to the TOC in water with the detection limit of 0.03± 0.005 wt% (St.Dev. ~1.3). Predetermined calibration curves were established between the C_{oil} and the TOC at different surfactant concentrations.

The recycling tests for the MD were conducted using sequential cleaning of the MD with ethanol and deionized water to remove the attached oil droplets. The procedure used for regeneration and cleaning involves sequential soaking of the used MD with ethanol (2 mL ethanol/5mg MD) five times each with a duration of 8 min. The MD was then washed with 20 mL of deionized water (18.2 MΩo-cm and 0.055 μS) 10 times, separated by a magnetic field, and reused for subsequent oil recovery cycles.

Adsorption experiments were conducted using the batch approach. Briefly, at room temperature, 50 mL an O/W solution at different C_{oil} concentrations (50, 100, 200, 300, 400, 500, 1000 and 2000 mg/L) was mixed with different MD_{dose} (10, 20, 50, and 100 mg/L) in 60 mL flasks. The pH of the mixture was fixed to 4, and a shaker mixed the flasks for 2 h. Once the test was completed, the MD was separated from the mixture, and the oil concentration in the water solution was determined. The amount of oil lost in all cases was checked and did not exceed 0.3%. All tests were repeated three times, and the average values at 95% confidence were presented and discussed.

5.2.6 Mathematical Manipulation

The amount of oil recovered by the MD was calculated by performing a mass balance on the treatment system. The mass of oil recovered at any time by the MD is equal to the amount of oil removed from the O/W emulsion as per equation (11).

$$q_t = \frac{(C_{i,oil} - C_{t,oil})}{S} \tag{11}$$

Where q_t represents the amount of oil recovered by the MD at any specific time (mg_{oil}/mg_{MD}), $C_{i,\,oil}$, and $C_{t,\,oil}$ represents the initial and final oil concentration in O/W emulsion (mg/L) at a specific time. S represents the slurry dosage defined as the ratio between the MD (mg) mass to the initial volume of O/W emulsion (L). The percent demulsification efficiency ($\%\eta_{dem}$) was determined as per equation (12).

$$\%\, demulsification\ efficiency\ (\%\eta_{dem}) = \frac{C_{i,oil} - C_{f,oil}}{C_i, oil}\ x\ 100\% \tag{12}$$

Where $C_{f,\,oil}$ represents the final concentration of oil in O/W emulsion (mg/L). The equilibrium adsorption capacity Q_e (mg_{oil}/mg_{MD}) was calculated using equation (13), and the experimental results for the oil recovery were fitted to Langmuir (equation 14),

Freundlich (equation 15), and combining Langmuir-Freundlich (L-F) (equation 16) isotherms.

$$Q_e = \frac{C_{i,oil} - C_{e.oil}}{S} \quad (13)$$

$$Q_e = \frac{q_{max} K_L C_{e,oil}}{1 + K_L C_{e,oil}} \quad (14)$$

$$Q_e = K_f (C_{e,oil})^{\frac{1}{n}} \quad (15)$$

$$Q_e = \frac{q_{max} K_L (C_{e,oil})^n}{1 + K_L (C_{e,oil})^n} \quad (16)$$

Where q_{max} is the maximum recovery of oil per unit mass of MD (mg_{oil}/mg_{MD}), K_f is the recovery capacity of the MD, and n is the recovery intensity.

5.2.7 Statistical Analysis

The oil recovery results at different operational conditions (MD_{dose}, C_{oil}, pH, C_{sur}, and t_{sep}) were judged based on standard deviation and one-way analysis of variance (ANOVA). The test was conducted to verify statistical differences in the reported $\%\eta_{dem}$ at a significance level of 5%. The statistical analysis was performed using Prism GraphPad statistics software (Version 7.04, USA).

5.3 Results and Discussion

5.3.1 Characterization of the Magnetic Demulsifier (MD)

The morphology of the Fe_3O_4-MNPs grafted with the silica particles (i.e., the MD) was examined using Transmission Electron Microscopy (TEM). Figure 28a shows that the MD consists of the core MNPs covered with a uniform layer of silica. The formation of the uniform silica layer on a single magnetite particle was achieved using the modified Stober method. A uniform-smooth shell of SiO_2 played a crucial role in

shielding and preventing the MD from reacting with oxidants in the aqueous solution. In addition, the uniform-smooth shell of SiO_2 enabled an effective attaching with oil and other functionalized nanomaterials. The well-controlled condensation and hydrolysis reactions of tetraethyl orthosilicate (TEOS) in the deionized water-ammonia-ethanol mixture [412] contributed to forming a uniform silica layer over the magnetite nanoparticles.

TEM analysis (Figure 28a) shows that the MD consists of identical and monodisperse sphere-shaped particles with clear-core shell structures. Calculations indicated that the mean diameter of the MD is 28.0 ± 3 nm with a standard deviation (Std. Dev.) of ~1.34. The MD is larger than the diameter of the Fe_3O_4 nanoparticles because of the addition of the silica layer. The thickness of the silica layer on the surface of the magnetite nanoparticles was found to be in the range of 19-15 nm, with an average value of 13.0 ± 2 nm (Std. Dev ~ 0.88).

The XRD of the MD (Figure 28b) exhibited diffraction peaks at 2θ values of 30.0°, 35.5°, 43.5°, 56.7°, and 62.4°. These were associated with the presence of crystal planes of (220), (311), (400), (511), and (440), as per the standard peaks of Fe_3O_4 (JCPDS file number 19-0629), respectively. Similar results were reported by Reddy et al. [413] during the preparation of monodispersed Fe_3O_4-SiO_2 core-shell nanoparticles. The diffraction peak at 22.3∘ corresponded to the amorphous SiO_2, which confirms the formation of a thin layer of silica over the Fe_3O_4 nanoparticles [414, 415]. The diffraction peaks in the Fe_3O_4-SiO_2 support the sample highlighted in Figure 28b, which indicates that the magnetite nanoparticles were kept on the silica surface.

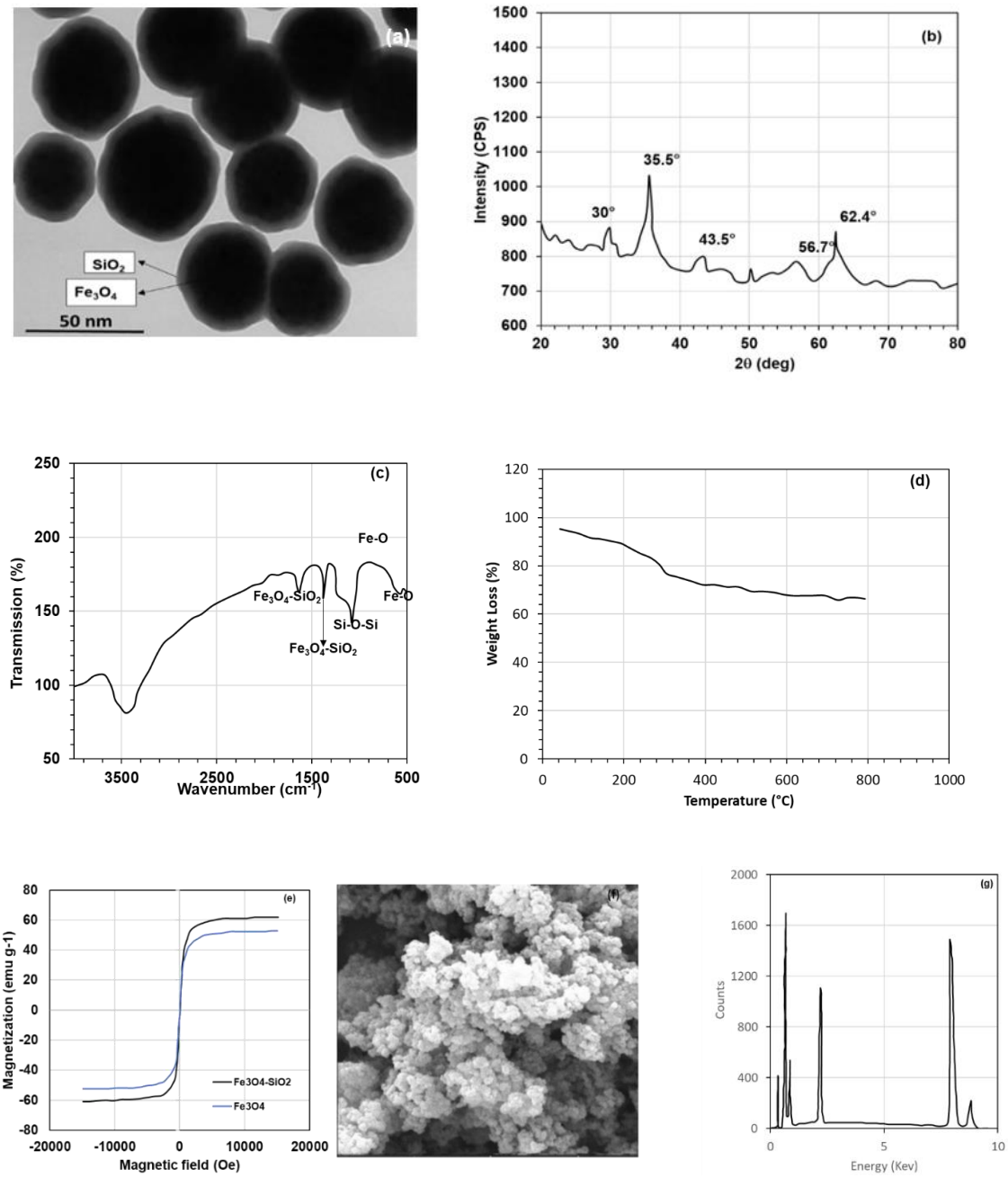

Figure 28. Characteristics of the Fe_3O_4-SiO_2 MD (a) TEM image, (b) the XRD analysis, (c) FTIR Spectra, (d) TGA analysis, (e) Magnetization curve, (f) Scanning Electron Microscope (SEM), (g) EDX analysis of MD.

Figure 28c presents the FTIR spectra of the MD. Prototypical Fe–O bands were noted at 573 and 970 1/cm originating from the magnetite phase. The peaks at 1635, 1384, and 1055 1/cm were associated with H-O-H binding, =C-H vibration, and C-O

stretching [416]. Due to the existence of the nitrate group, Fe_3O_4 nanoparticles have a high dispersibility in polar solvents, which is helpful for the coating and modification process of SiO_2. Furthermore, a peak was observed around 1083 1/cm, which is linked to the asymmetric stretching vibration of Si–O–Si. This indicates that there is a coating of the silica on the surface of the magnetic nanoparticles. The peak at 2850 1/cm represents the C-H stretching vibration initiated by the hydrocarbon during the preparation stage.

Figure 28d presents the MD's thermogravimetric analysis (TGA) in the temperature range 50 to 790°C under a nitrogen atmosphere. The TGA analysis allows for calculating the weight loss that occurs due to the decomposition of the organic compounds. Results revealed that the MD exhibited a maximum weight loss of 7.67 wt% at temperatures ≤ 300°C, related to the water loss and the volatile organic compound. Increasing the TGA temperature to 800°C led to the decomposition of the remaining organic compound marking a maximum weight loss of 11.69 wt%. The TGA curve of the MD seems to have two stages of decomposition. The first stage, which was observed to be fast and starts from 70 to 300 °C. This stage was correlated to removing the physically adsorbed water or volatile organic compounds (e.g., ethanol). The second stage, which was slow and located in the temperature range 310 to 790°C. This stage characterized the decomposition of any crystalline water, partial decomposition of the amorphous hydroxyl and/or the organic matter. The low weight losses and the shape of the TGA curve revealed the formation of stable MD that can be used under different operational temperatures. In addition, the low weight loss from the MD suggests a stable structure and a strong connection between the Fe_3O_4 and silica. Similar observations were reported by Feyzi et al. [417].

Figure 28e presents the vibrating sample magnetization curve (VSMC) of the Fe_3O_4-SiO_2 and Fe_3O_4 at 300°K. The shape of the VSMC exhibited a hysteresis loop, which confirms the ferromagnetic behavior of both. The magnetic saturation (MS) value for the MD was found to be ~ 42.3 ± 0.3 emu g^{-1} (St. Dev =0.67), which is lower than that of Fe_3O_4 (77.2 ± 0.4 emu g^{-1} (St. Dev.= 0.67). The lower MS value for the Fe_3O_4-SiO_2 is due to the silica cover, which is a non-magnetic material. This property (lower magnetization) supports the silica nanoparticles easily grafting onto the surface of the Fe_3O_4 nanoparticles. It was observed that the MD coagulate rapidly once the magnetic field is applied and re-dispersed after shaking when the magnetic field was removed. This suggests that the MD has the essential feature of being an adsorbent with effective separation and dispersion properties for removing oil from water under a relatively low magnetic field.

Figure 28f presents the Scanning Electron Microscope (SEM) analysis of the prepared MD. The MD has a spherical shape and an average size of approximately 29.21 ± 0.2 nm (Std. Dev ~4). The SEM images also showed that the morphological properties of the Fe_3O_4 nanoparticles still exist after being coated with the silica (excluding the slightly larger particle size). The EDX spectrum (Figure 28g) supports the existence of Fe and O as fundamental elements for Fe_3O_4 nanoparticles. Moreover, the figure demonstrates that the elemental composition of the core-shell MD is (Fe, O, and Si). The size distribution of Fe_3O_4 and Fe_3O_4-SiO_2 nanoparticles was measured using Dynamic Light Scattering measurements (DLS). Results indicated that the MD has the size distribution within the average size of 32.1 ± 0.1 to 22.8 ± 0.1 nm (Std. Dev. ~ 1.34). The small sizes measured by DLA were found to be comparable with the values using XRD and TEM. This size difference is likely due to the hydration effect.

5.3.2 Oil Recovery Using Fe_3O_4-SiO_2 MD

5.3.2.1 Effect of Oil Concentrations (C_{oil})

Figure 29a presents the reported $\%\eta_{dem}$ at different C_{oil} (500, 1000, 2000, and 4000 mg/L) for tests carried out with MD_{dose} of 10 mg/L. It was observed that after adding the MD to the O/W emulsion, the oil droplets were adsorbed on its surface, resulting in an effective separation. [27] suggested that the Fe_3O_4-SiO_2 develop hydrophobic properties that can facilitate the attachment of oil droplets. The paramagnetism properties support easy separation making the MD an effective demulsifier to recover and separate oil from O/W emulsion. The proposed MD achieved an excellent recovery of oil as the reported $\%\eta_{dem}$ under all the studied concentrations were higher than 88.5± 0.2% (Std. Dev. ~0.89). The $\%\eta_{dem}$ were 93.4 ± 0.2% (Std. Dev. ~0.89), 90.8 ± 0.2% (Std. Dev. ~0.99), 90.24± 0.2% (Std. Dev. ~0.89), and 88.5 ± 0.2% (St.Dev. ~0.89) for tests carried out with $\boldsymbol{C_{oil}}$ of 500, 1000, 2000, and 4000 mg/L, respectively. The results further indicate that the effective demulsification efficiency was achieved using a small amount (10 mg/L) of the MD, suggesting high oil adsorption affinity at such low concentrations. The demulsification efficiencies reported in the present chapter are comparable to the results reported by Mirshahghassemi et al. [418]. However, the MD_{dose} applied in the present chapter is 3 orders of magnitude lower than the MD_{dose} used by Mirshahghassemi and Lead. While the present study achieved ≥ 88.5± 0.2% (Std. Dev. ~0.89) using only 10 mg/L of the MD, up to 32.5 mg/L was required by the previous study to achieve 100% removal.

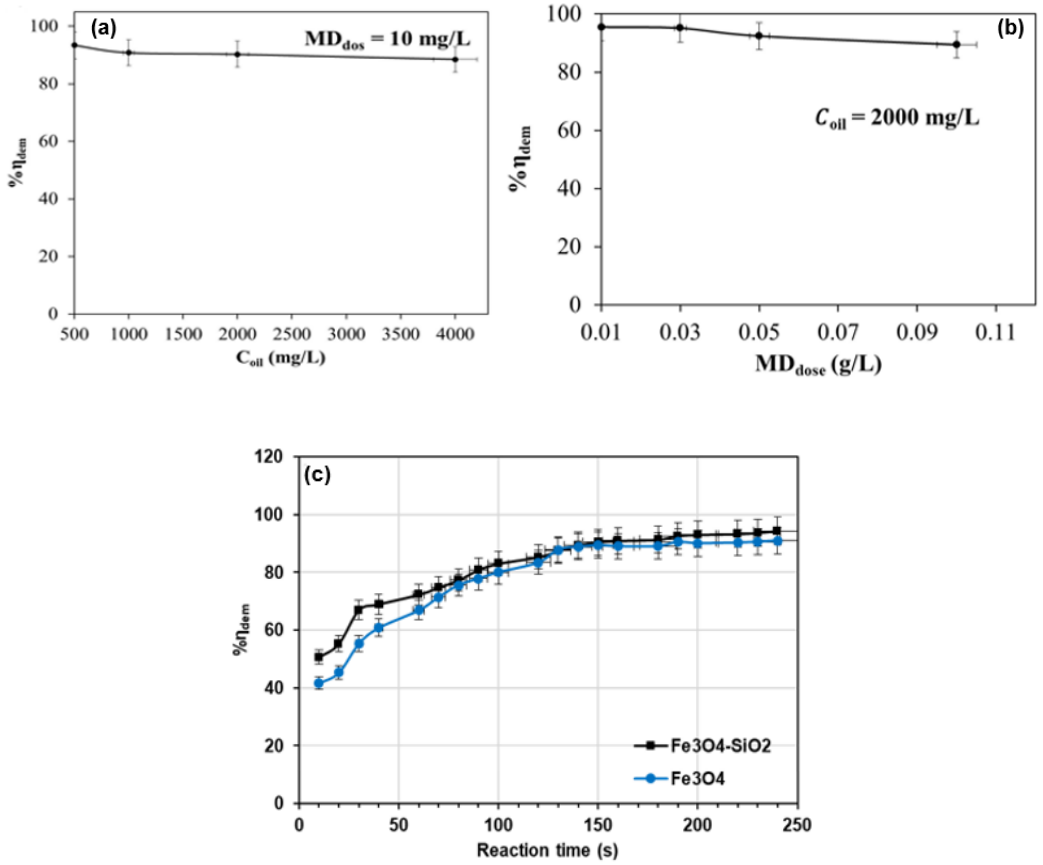

Figure 29. (a) The $\%\eta_{dem}$ at different C_{oil}, (b) the effect of MD_{dose} on $\%\eta_{dem}$ with C_{oil} = 2000 mg/L, (c) $\%\eta_{dem}$ as a function of reaction time for the MD and Fe_3O_4.

5.3.2.2 Effect of MD Dosage (MD_{dose})

Figure 29b presents the effect of MD_{dose} (10, 30, 50, and 100 mg/L) on the $\%\eta_{dem}$ for the tests carried out a C_{oil} of 2000 mg/L. Under all the studied MD_{dose}, the $\%\eta_{dem}$ was higher than 89.3 ± 0.2 (Std. Dev ~1.32), with a maximum $\%\eta_{dem}$ of 95.5 ± 0.2 (Std. Dev ~1.32) achieved at MD_{dose} of 10 mg/L. Although the dispersion of the MD was excellent at MD_{dose} 30 mg/L, the reported $\%\eta_{dem}$ was slightly lower than at MD_{dose} =10 mg/L. The results confirm the removal of a significant amount of oil in this short period using a very low dosage of the MD. The oil recovery of the MD was determined to be in the range of 12.1 ± 0.3 mg-oil/mg-MD (Std. Dev ~ 1.5) to 18.9 ± 0.3 mg-oil/mg-MD (Std. Dev ~ 2.0) which achieved a $\%R_{oil}$ of 90 ± 0.1 to 96 ± 0.1%, respectively.

This oil recovery capacity is 10 to 15 fold higher than the results reported in the literature [27, 418, 419]. [420] showed oil removal efficiency of 96% using a significantly higher MD_{dose} of 29 g/L, which indicated that the developed MD has an outstanding oil separation efficiency. The slight decrease in $\%\eta_{dem}$ at higher MD_{dose} can be related to self-aggregation. By increasing the MD_{dose} in the aqueous solution, the chance for self-aggregation increases, followed by a reduction in the surface area of the MD and a significant reduction in absorption capacity. Therefore, the reported $\%\eta_{dem}$decreased. A similar phenomenon was observed by [420] during the demulsification of crude oil from water emulsion. In their research, [420] demonstrated that increasing the MD_{dose} from 25 g/ L to 29 g/L increased the $\%\eta_{dem}$ from 88.88% to 95.63%. However, an additional dosage greater than 29 g/L resulted in a slight decrease in $\%\eta_{dem}$due to self-aggregation. Therefore, it was it is recommended to operate the demulsification process at lower MD_{dose} to limit the chance for self-aggregation and achieve significant $\%\eta_{dem}$. In addition, the observed trends suggest that the MD should be mixed with O/W at high speed enhance the dispersion and enable effective contract with oil before the application of the magnetic field to complete the separation process.

A comparison between the $\%\eta_{dem}$using Fe_3O_4 and Fe_3O_4-SiO_2 MD was done. The capacity of the Fe_3O_4-SiO_2 to remove oil from O/W emulsion was estimated to be in 101.25, 63.4, 37.1, and 17.9 mg_{oil}/mg_{MD} for the tests carried out with an MD_{dose} of 10 30, 50, and 100 mg/L, respectively, which is equivalent to a removal efficiency of 95.53%, 95.15%, 92.43%, and 89.48% from the original emulsion (C_{oil} =2000 mg/L). Fe_3O_4 showed lower $\%\eta_{dem}$ by 5-12% under the same previous conditions. The lower removal efficiencies achieved by Fe_3O_4 suggest a lower adsorption capacity and high self-aggregation properties. In addition, considering the expected short service life of the Fe_3O_4 due to the absence of the protective layer, the application of this MD will

have several limitations. On the other hand, the Fe_3O_4-SiO_2 MD was produced with significant properties to protect the susceptible magnetic cores that enable fast and facile separation under an external magnetic field. This kind of MD tends to stay stable at the interface of O/W and thus attach to the oil droplets from the emulsion interface, realizing high removal efficiency. It was reported that MD with such properties tends to be hydrophobic to superhydrophobic due to their interfacial activities and the differentiated dispersion in the water phase. Further research work is recommended to verify the contribution of the hydrophobic properties on oil removal efficiency. The performance of uncoated (Fe_3O_4) and silica-coated (Fe_3O_4-SiO_2) MD for the removal of oil was investigated by [421]. Results revealed that coated MD achieved 35% of oil recovery, while only 17 % was reported for uncoated MD. The enhancement in the oil removal after coating was attributed to the reduction in interfacial tension between MD and oil particles and the hydrophobic properties of the coated MD.

The obtained results indicate that the prepared silica-coated MD can remove oil from O/W emulsion with the support of an easy separation process using an external magnetic field. Additionally, results demonstrated that the lower removal percentage at higher MD_{dose} is likely due to the self-aggregation, which reduces the MD's surface area and absorption capacity. Although the uncoated Fe_3O_4 MD demonstrated acceptable results, the stability against a strong oxidation aqueous environment can be a challenge for large-scale applications.

5.3.2.3 Effect of Reaction Time on the Demulsification Process

Figure 29c presents the effect of reaction time on the $\%\eta_{dem}$ of Fe_3O_4 and the MD. The MD exhibited excellent performance in recovering oil from O/W emulsion in a short time compared to Fe_3O_4. This is due to the high dispersion rate, excellent adsorption capacity, and fast separation in a short period, as proposed by [422]. The fast and

excellent oil removal efficiency achieved using the external magnetic field can compensate for the long time required for natural settling. The relationship between the settling time and oil removal rate was studied by [289]. In the present chapter, the oil removal was tested at different settling times (0.5 h, 1 h, 1.5 h, 2 h, 2.5 h, and 3 h) using high and low $MD_{dose.}$ The results revealed that significant ($\geq 90 \pm 2$ %) oil removal at low $MD_{dose.} \leq 30$ mg/L required at least 4h, while higher $MD_{dose} \geq 59$ mg/L needed between 1.5 and 2h to achieve the same percentage removal. It was required 2 h settling time with MD_{dose} of 163 mg/L to achieve $\%\eta_{dem}$ 94.9%, while this efficiency can be achieved in 8 min using an MD_{dose} of 10 mg/L if the magnetic field is used. Thus, the proposed treatment methodology has lower MD_{dose} requirements and shorter separation and treatment time, which will significantly affect the performance and economy of the oil recovery from O/W.

5.3.2.4 Effect of Surfactant Concentrations (C_{sur})

Oil in water (O/W) emulsion may contain a surfactant material that can stabilize the emulsion and decrease in oil-water interfacial tension leading to a reduction in the $\%\eta_{dem.}$ Thus, the performance of the MD will be affected by the presence of these surfactants [100, 423]. As such, it is essential to study the effect of the concentration of these materials on the $\%\eta_{dem}$. Figure 28a presents the $\%\eta_{dem}$ as a function of surfactant concentrations. Tests were carried out under three different concentrations of surfactant (C_{sur}) of 0.05, 0.1, and 0.5 g/L using an MD_{dose} of 10 mg/L and C_{oil} in the range 20-1000 mg/L. Under all the studied C_{oil}, the $\%\eta_{dem}$ slightly decreased by increasing the C_{sur} in O/W emulsions. Previous research has reported that oil droplets in O/W emulsion can attach to the MD due to the attractive force of the hydrophobic bond [419, 424]. Therefore, the presence of the surfactant increases the dispersion of oil droplets, increasing the surface tension forces and reducing the absorption on the MD. In addition

to the increase in the hydrophobicity of the oil droplets, the interaction between the oil droplets and the surfactant will decrease the electrostatic repulsion between them, and these parameters will subsequently affect the performance of the oil sorption into the MD. Thus, the $\%\eta_{dem}$decrease. In addition, The surfactant could also interfere with acidic components in the oil and generate new compounds that can increase the density of negative charge on the surface of oil droplets and enhance their stability [111]. In the present chapter, it was observed that the MD could disrupt the chemical and physical bonds between oil-surfactants, which keep the oil emulsified in water and achieve high $\%\eta_{dem}$. The significant $\%\eta_{dem}$ may be associated with the large surface area of the MD, the strong oil-MD attraction forces, and the effective separation process using an external magnetic field. As exemplified in Figure 30a, although the $\%\eta_{dem}$ decreased by increasing the C_{sur}, the reported removal efficiency still ≥ 77%. The observed effective removal efficiency can be attributed to the effect of MD on the zeta potential of oil droplets in water, which is expected to increase after the addition of the MD leading to a decrease in electrostatic repulsion between oil droplets and enhance the removal efficiency as proposed by Deng et al. [111].

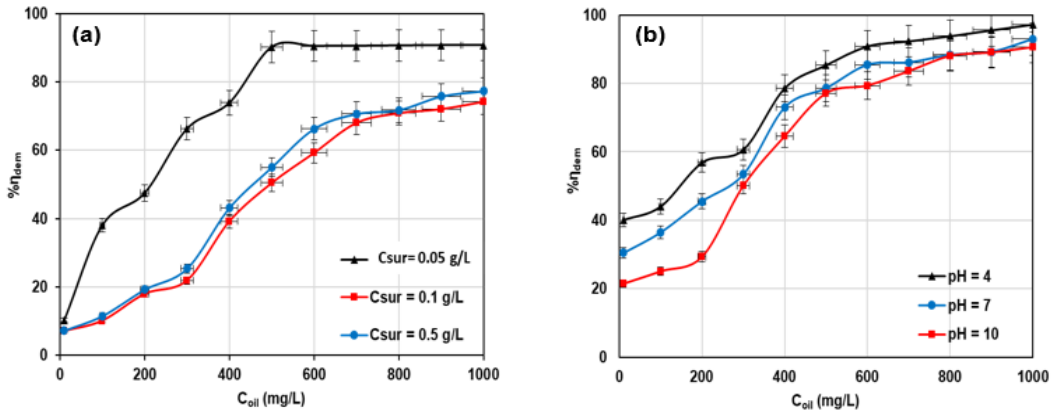

Figure 30. (a) Effect of C_{sur} on $\%\eta_{dem}$ using Fe_3O_4-SiO_2 MD, (b) Effect of pH on the $\%\eta_{dem}$ using Fe_3O_4-SiO_2 MD.

5.3.2.5 Effect of pH on the Demulsification Process

Figure 30b presents the effect of pH on the $\%\eta_{dem}$ using Fe_3O_4-SiO_2 MD. The pH is a major factor that can impact oil recovery performance from O/W emulsion [425]. The general trends show that the $\%\eta_{dem}$ slightly dropped by increasing the pH ≥ 7. The $\%\eta_{dem}$ was decreased from ~ 98% at pH =4 to ~ 95% at 7 and 94% at 10. The decrease in the $\%\eta_{dem}$ higher pH can be related to the increase in the repulsion force due to ionization of acids, which influenced the density of negative charge on the surface of oil droplets and reduced their removal efficiency.

The adsorption of oil droplets onto the Fe_3O_4-SiO_2 MD at the three different pH levels indicates that the surface charge in the emulsion is completely negative at higher pH. Then there is an electrostatic repulsion force between the MD and oil droplets. Lower pH leads to an increase in the positive surface charge, decreases the repulsion force, and enhances the $\%\eta_{dem}$ as proposed by [426]. The pH is generally altered during the wastewater treatment process by adding an acidic/basic chemical, an integral part of the O/W treatment system. This change in pH allows for the separation of dissolved waste from water during the treatment process. Water dissociation comprises a positively charged hydrogen ion and a negatively charged hydroxide ion which assists in the oil removal process [278]. Wai et al. [420] showed similar trends during crude oil recovery from water emulsion using magnetite–reduced graphene oxide nanocomposites. The study showed that the maximum $\%\eta_{dem}$ of 96% was achieved at pH ≤ 4, confirming the proposed electro-attraction mechanism.

5.4 Process Optimization and Reusability of the Fe_3O_4-SiO_2 MD

As previously analyzed and reported in the relevant literature [36, 295], the highest $\%\eta_{dem}$ was found to be at pH 4. As such, the recycle test for the Fe_3O_4-SiO_2 MD was conducted at this pH value. The recyclability was developed under controlled

conditions that were determined using analysis of variance (ANOVA) calculations. Under these conditions, the ANOVA determined the effect of process variables on $\%\eta_{dem}$. The statistical analysis was based on considering the parameters that have statistical significance on the removal efficiency. The ANOVA manipulation accepted the model terms with a P-value ≤ of 0.05, whereas values greater than 0.05 were considered insignificant. Under these conditions, it was determined that an MD_{dose} of 10 mg/L, t_{sep} of 8 min, and a maximum amount of chemical (ethanol) used for regeneration of 2 mL/5mg MD are the optimum conditions. With these conditions implemented, the Fe_3O_4-SiO_2 MD can be used for at least 9 cycles without a significant decrease in the reported $\%\eta_{dem}$ as exemplified in Figure 31. In the 8th cycle, the $\%\eta_{dem}$ begins to decrease to a value of 86.43%, which is still more significant than the removal efficiencies reported for other demulsifiers (≤86%). The slight decrease in $\%\eta_{dem}$ is associated with the attachment of some traces of other organic matter on the surface of the MD and/or the loss of the active site on the surface of the MD, which results in a decrease in the removal efficiency to 85.6% in the 9th cycle. Liu et al. [427] suggested that the decay in the $\%\eta_{dem}$ is likely due to the attachment of small oil droplets on the surface of the MD that cannot be easily removed by the ethanol regeneration stage, leading to a gradual decrease in the $\%\eta_{dem}$ during the recycling process. However, the TEM measurements of the used MD showed no such droplets on the surface, excluding this hypothesis. Moreover, it is believed that the sequential regeneration of the MD results in loss of the active site from the surface of MD or change in the surface charge of the MD, resulting in a slight decrease in its $\%\eta_{dem}$. In conclusion, the proposed MD has extended service life as it can be used for at least 9 cycles with no more than 2% drop in the $\%\eta_{dem}$. The extended service life and the reusability of the Fe_3O_4-SiO_2 to recover oil from O/W emulsion suggest a significant reduction in the process cost.

The mechanism of oil removal using the MD was investigated by analysing the FT-IR before and after the adsorption. Results showed that the spectrum of the MD after oil adsorption remained intact, with few additional peaks detected at 2901, 1467, and 13331/cm. These peaks were consistent spectral peaks of diesel fuel, suggesting that the oil was removed via surface adsorption.

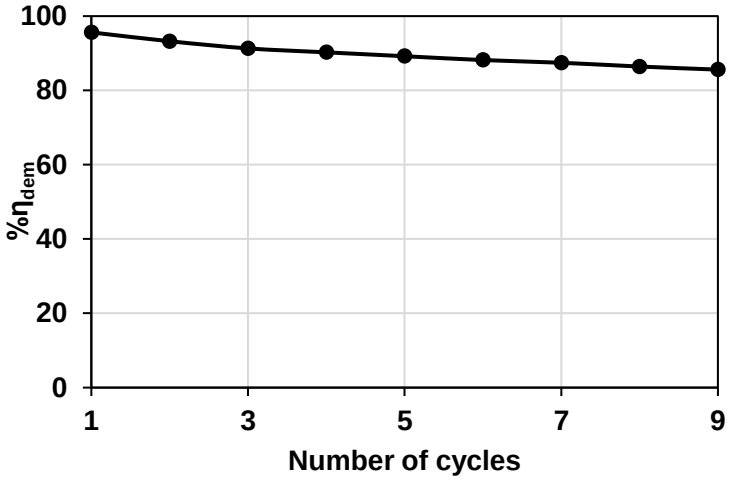

Figure 31. The $\%\eta_{dem}$ of Fe_3O_4-SiO_2 MD under different cycles.

5.5 Adsorption isotherm of the Fe_3O_4-SiO_2 nanoparticles

Different isotherms were used to study the oil removal from O/W emulsion [428]. Among them, Langmuir and Freundlich are the most used isotherms [359, 429, 430]. The adsorption isotherm of O/W was performed to determine and compare the maximum adsorption capacity of Fe_3O_4-SiO_2 in comparison with Fe_3O_4 at ambient conditions. Figure 32a-d presents the oil recovery process adsorption isotherms using Fe_3O_4-SiO_2 and Fe_3O_4 following Langmuir and Freundlich with the corresponding linear regression residual (inner graph). The adsorption isotherm coefficients were determined using the linear regression of the experimental data using graph Pad Prism V9 software and summarized in Table 10. The oil recovery process follows both Langmuir and Freundlich isotherms with a maximum R^2 of 0.921 and residuals

distributed around the horizontal zero-line in the range -0.4 to 0.55. This suggests that the proposed isotherms can be used to represent the recovery of oil. It is known that Langmuir isotherm presumes monolayer adsorption of impurities (oil in this study) onto the surface of MD, after which no more adsorptions can occur. This can be explained by the adsorption taking place on particular homogenous sites on the MD surface. Once these sites are occupied, a saturated adsorption capacity is reached, limiting the adsorption.

On the other hand, Freundlich isotherm represents an empirical representation of the heterogeneity of the surface of the adsorbent and the exponential distribution of adsorption sites with the corresponding energies. Thus, Freundlich isotherm assumes the adsorption occurs onto heterogeneous surfaces following both monolayer (chemisorption) and multilayer (physisorption) adsorption mechanism [360]. Table 10 summarizes the results of isotherm regression following Langmuir and Freundlich isotherms at different ranges of MD_{dose}. The kinetic data show that oil adsorption on Fe_3O_4-SiO_2 and Fe_3O_4 depends on the $MD_{dose,}$ with the highest occurring at a lower dose due to the self-aggregation problem. Moreover, it was observed that the Q_{max} of the Fe_3O_4-SiO_2 (187 ± 7 to 27 ± 3 mg_{oil}/mg_{MD}) is 1.7 to 1.2 folds higher than Fe_3O_4 (95 ± 3 to 14 ± 4 mg_{oil}/mg_{MD}) due to the high adsorption capacity of the first.

Although the calculations show that both Langmuir and Freundlich isotherms can represent the adsorption isotherm of oil, the determined correlation coefficients are low. Therefore, it was decided to check the validity of an integrative model combining both Langmuir and Freundlich isotherm (L-F) following equation (16). The L-F isotherm combines the characteristics of the Freundlich isotherm with an asymptotic consideration of the maximal adsorption value. Fitting the experimental data using the L-F isotherm, equation (16), generated well-fitted lines (Figure 30e), with a correlation

coefficient (R^2) of 0.999 and very low residual in the range -0.05 to 0.05, confirming that the L-F is the most suitable model to describe the adsorption isotherm compared to the separate Langmuir and Freundlich isotherms. Table 10 presents the average Q_{max} at different MD_{dose}, which was determined to be in the range 186 ± 5 to 35 ± 5 mg_{oil}/mg_{MD} for Fe_3O_4-SiO_2 in the MD_{dose} in the range 10-100 mg/L, compared with 86 ± 5 to 23 ± 5 mg_{oil}/mg_{MD}, revealing the significantly high adsorption capacity of the proposed MD. The maximum adsorption capacity values for Fe_3O_4-SiO_2 MD are 1.2 folds higher than Fe_3O_4 due to higher surface, high adsorption affinity to oil, and will form surface area. Moreover, the high capability of the adsorption process can be judged based on the values of the 1/n, where a value ≤ 1 suggests a favorable adsorption process. Based on the values in Table 10, the 1/n value for the Fe_3O_4-SiO_2 is twice lower than Fe_3O_4, which indicates a high affinity for oil removal.

Table 10. Langmuir, Freundlich and L-F isotherms parameters for Fe_3O_4 and Fe_3O_4-SiO_2 at different MD_{dose}.

Langmuir						
	Fe_3O_4-SiO_2			Fe_3O_4		
MD_{dose} Range	Q_{max} (mg_{oil}/mg_{MD})	$K_L x10^{-3}$	R^2	Q_{max}	K_L $x10^{-3}$	R^2
10-30	187 ± 7 to 87 ± 5 (Std. Dev. = 0.9)	5.4±0.1 to 5.8 ±0.2	0.921	95 ± 3 to 76 ± 2 (Std. Dev. = 2.1)	3.6±0.1 to 0.78±0.01	0.921
30-50	87 ± 5 to 45 ± 5 (Std. Dev. =1.3)	5.8 ±0.2 to 6.8 ±0.1	0.909	76 ± 2 to 30 ± 3 (Std. Dev. = 1.9)	0.78±0.01 to 0.78±0.01	0.921
50- 100	45 ± 5 to 27 ± 3 (Std. Dev. = 1.3)	6.8 ±0.1 to 7.1 ±0.1	0.919	30 ± 3 to 14 ± 4 (Std. Dev. = 1.9)	0.73 ±0.01 to 0.78±0.01	0.901
Freundlich						
MD_{dose}	1/n	Kf	R^2	1/n	Kf	R^2
10-30	0.41 ± 0.07 to 0. 33 ± 0.02 (Std. Dev. = 0.12)	2.10 ± 0.03 to 2.20 ± 0.04 (Std. Dev. = 0.55)	0.906	0.71 ± 0.04 to 0.77 ± 0.07 (Std. Dev. = 0.10)	1.70 ± 0.03 to 0.43 ± 0.03 (Std. Dev. = 0.22)	0.905
30-50	0.33 ± 0.02 to 0.26 ± 0.03 (Std. Dev. = 0.10)	2.20 ± 0.04 to 0.90 ± 0.03 (Std. Dev. = 0.10)	0.906	0.77 ± 0.07 to 0.75 ± 0.02 (Std. Dev. = 0.02)	0.43 ± 0.03 to 0.11 ± 0.02 (Std. Dev. = 0.72)	0.891
50- 100	0. 26 ± 0.03 to 0.22 ± 0.01 0.22 ± 0.01 (Std. Dev. = 0.08)	0.90 ± 0.03 to 0.50 ± 0.03 (Std. Dev. = 0.08)	0.906	0.75 ± 0.02 to 0.73 ± 0.05 (Std. Dev. = 1.12)	0.11 ± 0.02 to 0.06 ± 0.01 (Std. Dev. = 0.44)	0.910

	L-F							
MD_{dose}	Q_{max}	$K_L x10^{-3}$	1/n	R^2	Q_{max}	$K_L x10^{-3}$	1/n	R^2
10-30	186 ± 5 (Std. Dev. = 0.9)	5.2± 0.1	0.39 ± 0.07	0.999	86 ± 5 (Std. Dev. = 0.9)	4.2± 0.1	0.69 ± 0.07	0.999
30-50	65 ± 3 (Std. Dev. = 0.9)	5.5 ± 0.3	0.29± 0.03	0.998	35 ± 3 (Std. Dev. = 0.9)	1.5 ± 0.3	0.79± 0.03	0.998
50-100	35 ± 5 (Std. Dev. = 0.9)	6.9 ± 0.2	0.24± 0.04	0.999	23 ± 5 (Std. Dev. = 0.9)	0.8 ± 0.2	0.84± 0.04	0.999

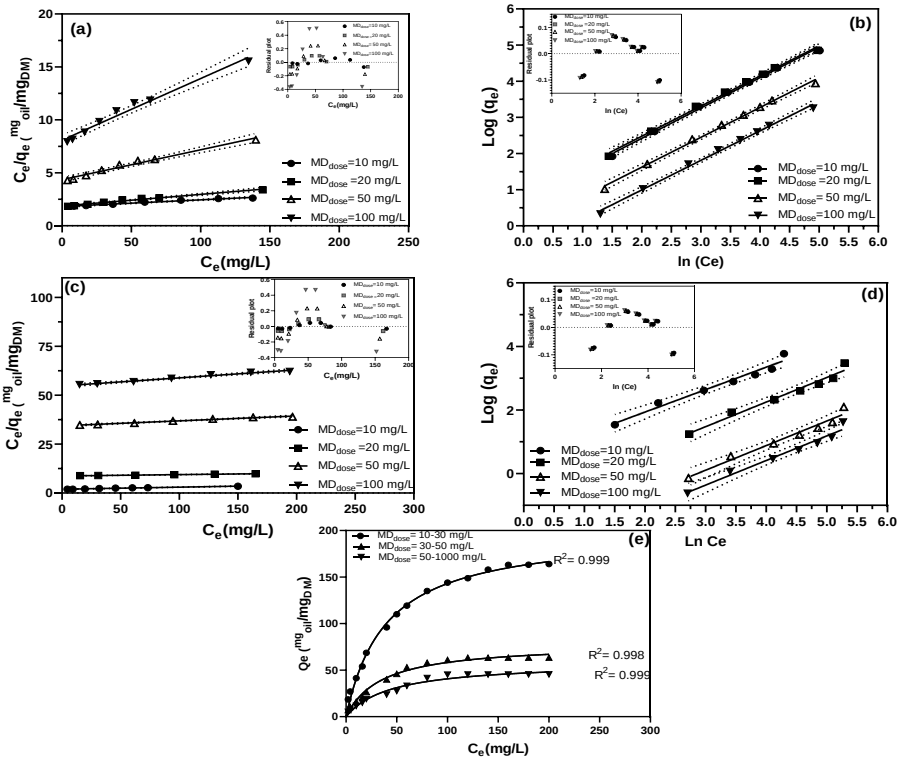

Figure 32. Langmuir, Freundlich, and L-F isotherms for the adsorption process onto the Fe_3O_4 and Fe_3O_4-SiO_2.

5.6 Conclusion

This chapter has highlighted the preparation of Fe_3O_4-SiO_2 nanoparticles as a magnetic demulsifier (MD) using a modified Stober process at room temperature. The analytical techniques, TEM, SEM, and EDX, supported the formation of grafted magnetite Fe_3O_4 nanoparticles covered with a silica surface using the modified Stober method under a well-controlled reactant (TEOS, Ammonia, and Ethanol) stoichiometry. The $\%\eta_{dem}$ increased by increasing the MD_{dose} to 30 mg/L and subsequently decreased at a high dosage. This was aimed at the aggregation of the MD at higher concentrations, which led to a significant reduction in the surface area. Using an MD_{dose} as low as 10 mg/L attained a $\%\eta_{dem}$ in the range of 93% to 94.3% for O/W mixtures with $C_{oil} < 2000$ mg/L, which decreased to ~ 90%

for higher concentrations. The $\%R_{oil}$ was > 90 ± 0.1, which declined by increasing the pH to 7 and the concentration of C_{sur} to 0.1 g/L.

The proposed MD has an excellent oil recovery performance in comparison to similar research results. The Fe_3O_4-SiO_2 can be reused numerous times (9 cycles) and achieved high recyclability at an effective, stable $\%R_{oil}$ ~ 90% after 9 cycles. The kinetic of the oil removal by the MD follows L-F isotherms, as it has the highest adsorption capacity and a higher kinetic constant in contrast to the Fe_3O_4 nanoparticles. The adsorption capacity values reached 186 ± 5 to 35 ± 5 mg_{oil}/mg_{MD} and 86 ± 5 to 23 ± 5 mg_{oil}/mg_{MD} for the Fe_3O_4-SiO_2 and Fe_3O_4 MNPs, respectively. It is recommended for future work to revise the regeneration methods and explore the use of the MD in other applications such as industrial and biomedical.

CHAPTER 6: FUNCTIONALIZATION OF SILICA-COATED MAGNETIC NANOPARTICLES AS POWERFUL DEMULSIFIER TO RECOVER OIL FROM OIL-IN-WATER EMULSION

6.1 Introduction

Research literature has been dedicated to the development of materials and methods to separate and recover oil from produced water (PW) emulsions to save energy (i.e., recover the oil), protect the environment, and enhance the water treatment process [431]. Compared to other types of wastewater, PW formed from the oil and gas industry is especially challenging to handle as it includes several remaining chemicals in addition to the oil [432]. Typically, the oil-in-water emulsion (O/W-emul) contains a considerable amount of stable oil droplets, surfactants, and co-surfactants [433]. The presence of surfactants decreases the interfacial tension and the zeta potential of the oil droplets and contributes to the stability of the O/W-emul [212]. Moreover, the O/W-emul generated from the PW is complex and challenging to treat because of the development of an electrical dual layer on the surface, reducing the likelihood of treatment using conventional processes [372]. Various approaches have been employed for the treatment of PW, including electrochemical [434], biotechnology [435], membrane separation [381], coagulation and flotation [377, 378], and demulsification process [380]. However, their large-scale applications are limited due to high cost, low performance, and complicated operational conditions. Thus, there is an urgency to develop efficient treatment methods to recover oil and recycle or reuse high volumes of PW.

The use of magnetic nanoparticles (MNP) in wastewater treatment processes has been applied in the wastewater purification process due to their adsorption capacity [40, 286, 436, 437]. The unique magnetic properties of the MNP allow them to be simply removed from the complicated poly-phase systems within a brief amount of time. For example, Shen

et al. [400] used the Fe-MNP to treat wastewater contaminated with metal ions. The researchers noted that the MNP successfully removed all of the contaminants from the wastewater. However, the chemical stability of the Fe-MNP was not suitable due to a rust problem [400], which highlights the importance of increasing the Fe-MNP chemical stability. Lu et al. [310] proposed a solution for improving the chemical stability of the Fe-MNP with the formation of a core-shell covered by a protective layer. The shells protect the MNP from corrosion and can be used for additional grafting of the nanoparticles by functional groups such as carboxyl and amines [438].

There are two magnetic coating procedures for the Fe-MNP outlined in the research literature [439, 440]. The first includes adding organic composites such as surfactants and polymers to the MNP. The second includes coating with inorganic elements such as carbon, silica, or valuable metals. Kamgar et al. [441] exhibited how coating Fe-MNP with silica is advantageous because it has abundant surface hydroxyl groups that can improve the oil removal process without changing the iron properties. Additionally, silica is stable and resistant to different environments, which contributes to the stability and service life of the Fe-Si MNP [441, 442]. [443] presented the preparation of Fe-MNP functionalized with an inner layer of thick nonporous silica and a layer of mesoporous silica as an outer layer. The procedure used the complicated plasma polymerization method for grafting the Fe-MNP with polymethyl acrylate. The results indicated that the magnetic nanoparticles could remove significant amounts of contaminants from oily wastewater. Peng et al. [212] exemplifies how preparing a magnetic demulsifier by functionalizing ethyl cellulose onto the surface of amino-grafted Fe-MNP coated with silica was used to remove water from a diluted bitumen emulsion. Calcagnile et al. [408] produced a new synthesis material that relied on grafting the colloidal Fe-MNP and polyurethane foam. The results exemplified a high oil removal efficiency and extended service life. The materials indicated high

contaminant removal from oily wastewater, though they cannot effectively recover oil from oil field PW. Within this context, (Xie et al. 2020) suggested an interfacially active porous Fe-MNP with double silica shells. This type of MNP has a high adsorption capacity for oil and can act as an oil adsorbent from water. Additionally, these MNP are likely to remain steady and stable at liquid/liquid or air/water interfaces and are able to achieve a significant demulsification efficiency of O/W-emul [444].

Fe-Si MNP are preferred for oil recovery applications because they are easily synthesized with well-known physical-chemical properties and engineered with different characteristics (e.g., hydrophobic to hydrophilic) [117]. Fe-Si MNP is also a non-toxic inorganic material and has a low production cost than other nanoparticles [132, 133]. Additionally, the Fe-Si MNP exhibited appropriate thermal stability for temperatures up to 650°C, as reported by [445]. Lastly, Ju et al. [135] prepared and classified polysilicon nanomaterials based on their wettability behaviour into three categories: lipophobic and hydrophilic polysilicon (LHP), hydrophobic and lipophilic polysilicon (HLP), and neutral-wet polysilicon (NWP).

The literature above suggests that various MNP are suitable for wastewater treatment applications, though large-scale applications for removing and reusing oil from O/W-emul are limited. As such, there is an urgency to develop a well-established and stable MNP that has an appropriate oil adsorption capacity and facile separation process for use in the demulsification of oil from O/W-emul. However, understanding the effect of different operational conditions in the oil separation process still poses challenges. Moreover, there is a knowledge gap in analysing and optimizing the key operating parameters of oil separation at maximum performance. In addition, limited research investigates and addresses the technical issues related to the synthesis of the Fe-Si MNP, their use for oil

recovery, and analysis on the impact of the importance of the synthesis process on the properties of the produced MNP.

Given that, this chapter aims to produce different Fe-Si MNP with variable silica layer thicknesses (5 nm [Fe-Si-1], 8 nm [Fe-Si-2], 10 nm [Fe-Si-3], and 15 nm [Fe-Si-4]) that can be used for the recovery of oil from O/W-emul. A review of the relevant literature indicates that few studies focus on oil removal from PW that apply this magnetic demulsifier. The Fe-Si MNP were synthesized using the modified Stöber process. The thickness of the silica layer was controlled by varying the volume of the tetraethyl orthosilicate (TEOS) used to prepare the Fe-Si MNP. The as-prepared Fe-Si MNP were tested for their ability to recover oil from O/W-emul. Furthermore, this chapter investigates the properties of the Fe-Si MNP, the effect of different operational conditions, the percentage of oil separation ($\%S_{oil}$), and the recyclability of the MNP.

6.2 Materials and Methods

6.2.1 Materials

The chemicals used in the present chapter were tetraethyl orthosilicate (TEOS, Merck, CAS Number: 78-10-4), ammonium hydroxide (25 wt% CAS Number: 1336-21-6), ethanol (CAS Number: 64-17-5), and magnetite (Fe_3O_4), MNP (99.9% and size 8 nm). The chemicals were obtained from Merck-Qatar and were used as received. The gasoline oil used in the preparation of the O/W-emul was a synthetic oil (95 Octane, density = [719.7 kg/m^3]) bought from a local supplier (WOQOd, Doha, Qatar). The surfactant applied in the test for O/W-emul is Polyethylene sorbitol ester (Tween-80) obtained from Sigma Aldrich. All the chemicals are analytical grade and were used with no purification.

6.2.2 Preparation of Fe-Si MNP Demulsifiers

Four different Fe-Si MNP (Fe-Si-1, Fe-Si-2, Fe-Si-3, and Fe-Si-4) were prepared for this study. The detailed synthesis procedure is described in our previous study [446] (chapter 5). In summary, the method includes dissolving 0.5 g of Fe-MNP in 25 mL deionized water. Then, the solution is shifted to a three-neck round-bottom flask and mixed with 100 mL ethanol and 1.0 mL ammonia solution (28wt%) under strong mechanical stirring for 15 min at room temperature. Later, differing volumes (0.5, 1.0, 1.5, and 2.0 mL) of tetraethyl orthosilicate (TEOS) were added to the mixture and left to react for an extra 6 h under continuous mechanical stirring at room temperature. Finally, the formed Fe-Si MNP were gathered applying an external magnetic field, cleaned with ethanol 10 times, dried at 70°C for 8 h, and then used in experiments. In this chapter, according to the volume of TEOS and the synthesis, four different types of Fe-Si MNP were prepared and are denoted as Fe-Si-1, Fe-Si-2, Fe-Si-3, and Fe-Si-4 for the MNP prepared with 0.5, 1.0, 1.5, and 2.0 mL of TEOS, respectively.

6.2.3 Synthesis of O/W-emuls

The preparation of the O/W-emul used in the tests was achieved following the method applied in the previous chapter [446]. In summary, 0.05 g of Tween-80 surfactant was mixed with deionized water for 2 min at a rate of 3500 rpm using a shear emulsifying homogenizer (model BRH1-100, USA). After that, a specified amount of gasoline oil was added to the water, drop by drop, and mixed for 10-15 min to generate a consistent oil/water emulsion with concentrations of 500, 1000, 2000, and 4000 mg/L.

6.2.4 Characterization of the Fe-Si MNPs Demulsifier

The X-ray diffraction (XRD, Minifix II Japan) patterns were tested using a Rigaku D/MAX-R diffractometer with a copper target at 40 kV and 30 mA. The surface morphology, structure, and elemental composition of the Fe-Si MNP were analyzed using

transmission electron microscopy (TEM, Hitachi H-600, Japan). This was followed by an energy dispersive x-ray spectrometer (EDX). The Fourier transform infrared (FTIR, PerkinElmer Spectrum 400, USA) spectra were obtained with a spectrometer applying KBr pellets at room temperature. Finally, the magnetic hysteresis loops were assessed using a vibrating sample magnetometer (VSM, Lakeshore 7407, US) at 300°K with two practical magnetic field ranges between –15000 Oe to +15000 Oe and –10000 Oe to +10000 Oe.

6.2.5 Demulsification Tests

The demulsification process involves adding differing D_{MNP} (10-100 mg/L) to O/W-emul (500 mL) and subsequent sonication for 2 min with mixing at 3500 rpm for an additional 10 min. All of the experiments were conducted at room temperature, if not otherwise stated. The pH of the O/W-emul was left to develop spontaneously without modification and was noted to be nearly 4.0. Once the mixing had stopped, the mixture was left to react for an additional 10 min, which allowed for the adsorption of oil droplets onto the Fe-Si MNP. Subsequently, the Fe-Si MNP/oil was removed with external magnetism, and the $\%S_{oil}$ was then assessed. The oil concentration in the emulsion before and after the treatment was associated with the overall amount of organic material in the water (with a detection limit of 0.03± 0.005 wt%). Finally, the reusability of the Fe-Si MNP was studied by serially cleaning the Fe-Si MNP with deionized water and ethanol to eliminate the droplets of oil attached to the MNP. After that, the recycled MNP demulsifier is dispersed in water and applied to the following cycles for the oil recovery process. All the tests were performed in triplicate, and the average at 95% confidence level was used in reporting the results. In addition, the statistical significance of the results was confirmed using the student's paired t-test.

6.2.6 Contact Angle Measurement

The Fe-Si MNP/oil/water contact angle measurements were conducted following the procedure established by Rezvani et al. [447]. The measurements were carried out using the DSA100 contact angle meter (Kruss, Germany) with an accuracy of 0.3° within the measurement range of 0-180° [448]. To examine the impact of the synthesized MNP demulsifiers on the O/W-emul wettability a 10 mL of the four Fe-Si MNP demulsifiers (Fe-Si-1, Fe-Si-2, Fe-Si-3, and Fe-Si-4) were added to the samples of O/W-emul and prepared with an oil dose of 500 mg/L under ultrasonication with 250 watts of power for 15 min. For comparison purposes, the tests were performed using each MNP separately, and contact angles helped assess the hydrophobic performance of the O/W-emul after the addition of the nanoparticle. The contact angle measurements were conducted after treating oil/water emulsion surfaces with various magnetic demulsifiers.

6.2.7 Interfacial Tension (IFT) Measurement

The interfacial tension (IFT) measurements for the pendant drop method were applied for measuring the IFT between gasoline oil and 10 mg/L of Fe-Si MNP demulsifiers using the DSA100 (Kruss, Germany). This procedure was adapted from the work of [447]. The measurements included a range between 0.01 to 2000 mN/m and an accuracy of 0.3 mN/m. The equilibrium IFT was evaluated at the time the oil droplet was released. The ultrasonication process was achieved before each measurement with 250 watts of power for 15 min.

6.3 Results and Discussion

6.3.1 Characterization of the Fe-Si MNPs

Figure 33a demonstrates the XRD of the Fe-MNP and the as-synthesized Fe-Si MNP (Fe-Si-1, Fe-Si-2, Fe-Si-3, and Fe-Si-4). The Fe-MNP were characterized with crystal planes of (220), (311), (222), (400), (422), (511), and (440), respectively. The sharp and vigorous

peaks of the Fe-MNP represent their spinel structure, which supports the formation of magnetite nanoparticles. Furthermore, the diffraction patterns of the Fe-Si MNP are identical to the Fe-MNP, which suggests that the crystallinity of the Fe-MNP was preserved after the silica layer was coated. For all of the samples, the Si amorphous hump was around 2θ of 22°, and the characteristic peaks for the Fe were around 2θ of 35.4° (311). Furthermore, there was a trend showing an increase in the intensity of the peak at 2θ of 22° for Fe-Si-1< Fe-Si-2< Fe-Si-3< and Fe-Si-4 due to the accumulation of Si on the surface of the nanoparticles. Therefore, it was concluded that the Fe-Si MNP crystalline structure was conserved, and the Si layer depends on the volume of TEOS used during the preparation stage. Further, the increase in the intensity of the amorphous hump suggests that the Si content accumulates on the surface of the nanoparticles by increasing the TEOS volume in the reaction medium. This leads to the formation of a protective layer which helps to sustain an excellent oil separation rate.

Figure 33b presents the additional verification for the as-prepared Fe-Si MNP using an EDX analysis. The elemental composition of the Fe-Si MNP indicates the presence of oxygen, iron, and silicon without the appearance of any impurities. This trend suggests that the Fe-Si MNP only formed Fe and SiO_2. As highlighted in Figure 31b, the intensity of the silicon (Si) peak suddenly increased and reached 1100 cps.

The FTIR analysis of the Fe-MNP and the as-synthesized Fe-Si-1, Fe-Si-2, Fe-Si-3, and Fe-Si-4 nanoparticles (Figure 33c) exhibit an adsorption peak near 542 cm^{-1}. This peak corresponds to the Fe-O functional group vibration band, which is commonly observed for Fe-MNP. However, the wide absorption peaks around 1130 cm^{-1} correspond to the irregular Si-O-Si vibration band, while the peak at 900 cm^{-1} represents the Si-OH bond. The results indicate that the peak intensities at 1130 and 900 cm^{-1} are the maximum for the Fe-Si-4 and decrease for Fe-Si-3> Fe-Si-2 >Fe-Si-1. This result suggests a greater silica deposit on the

surface of the MNP through the use of high volumes of TEOS during the preparation stage. Conversely, the peaks in the range of 3500-3000 cm^{-1} were assigned to the –OH functional group expanding curve of chemisorbed water. Thus, the peaks were enhanced because of an increase in the TEOS volume due to silica nanoparticles.

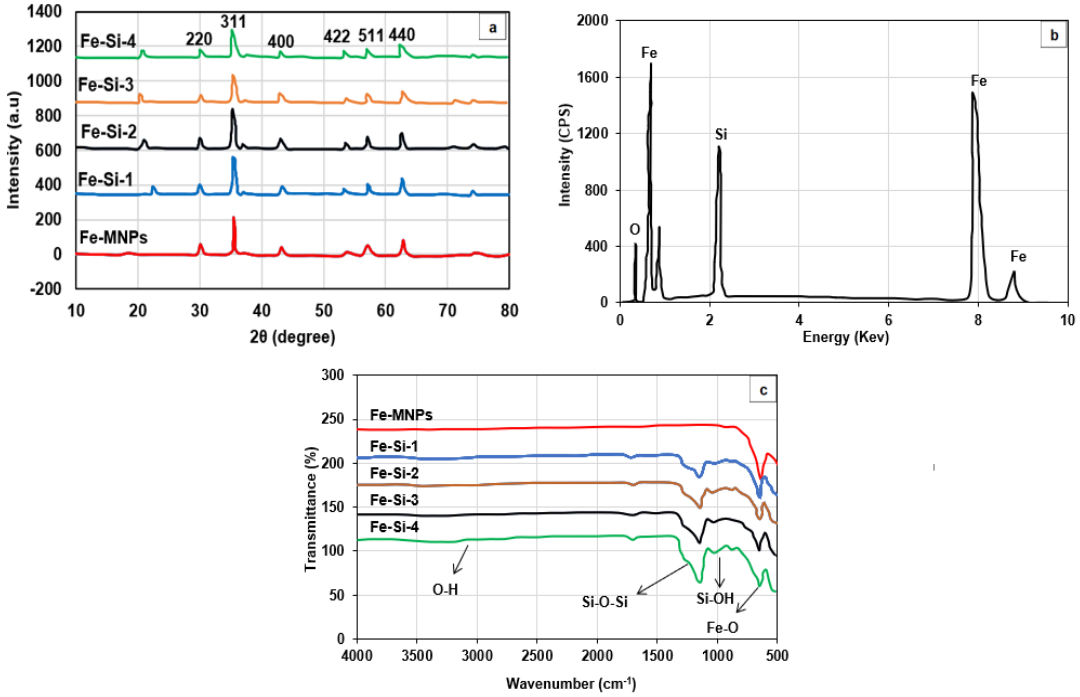

Figure 33. Characteristics of the Fe-MNP and Fe-Si-MNP demulsifiers (a) XRD pattern, (b) EDX analysis, and (c) FTIR spectra.

In comparison to the Fe-MNP, the TEM method was applied to define the morphology of the prepared Fe-Si-1. As outlined in Figure 34a, the Fe-MNP has a spherical shape with a particle size of ~40.0 nm. Further, after the silica layer was deposited, the size of Fe-Si-1 slightly increased to ~50 nm, which indicated that an additional 5 nm was added to the Fe-Si-1 silica layer (Figure 34b). [449] reported similar observations in the significant increase in the Fe-MNP size after grafting with silica nanoparticles. Figure 34c presents the magnified micrograph of the Fe-Si-1 from Figure 34b. The core and shell structure of the Fe-Si-1 is represented with the grey and dark areas. The dark area was assigned to the Fe-

MNP; the grey area represents the SiO_2 layer. It is evident that the Fe-MNP surfaces are completely coated with the SiO_2 shell layer.

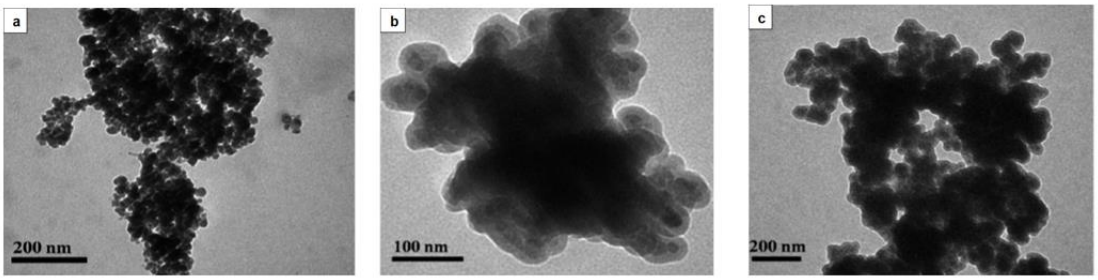

Figure 34. TEM analysis of (a) Fe-MNP and (b, c) Fe-Si-1 at 100 and 200 nm, respectively.

Figure 35 exhibits the TEM images for the Fe-MNP, Fe-Si-1, Fe-Si-2, Fe-Si-3, and Fe-Si-4. The accumulated silica layer with varying thicknesses (5-13 nm) on the Fe-Si-1, Fe-Si-2, Fe-Si-3, and Fe-Si-4 is exemplified in Figure 35a-35e compared to the uncoated pure Fe-MNP (Figure 35a). As such, Figure 35a shows how the Fe-MNP exhibited a well-defined crystalline cubic shape structure consistent with the sharp peaks observed in the XRD analysis. The size of the Fe-MNP before the coating is approximately 40 nm with small and identical size distribution. The Fe-Si-1, Fe-Si-2, Fe-Si-3, and Fe-Si-4 were coated with silica to form the core/shell nanocomposites. As previously indicated, varying the volume of the TEOS used in the reaction medium from 0.5 mL to 2.0 mL increased the silica shell thickness from 5 to 15 nm. As a result, the thickness of the silica layer was 5 nm, 8 nm, 10 nm, and 15 nm for the Fe-Si-1, Fe-Si-2, Fe-Si-3, and Fe-Si-4, respectively. Thus, increasing the volume of TEOS in the reaction medium led to Fe-Si MNP with a greater silica thickness and a larger diameter. This change is ascribable to the higher volume of TEOS, which increased the quantity of the Si deposit on the surface of the Fe-MNP.

Given that, the grafting and thickness of the silica layer on the Fe-Si MNP correlate to the volume of TEOS. Typically, the MNP with a greater surface area tends to have a higher

attraction force to the oil droplets, which achieves a higher $\%S_{oil}$ as indicated by Tang et al. and Di et al. [450, 451]. However, a slight aggregation between the nanoparticles is possible even after the coating process, as indicated from the TEM images.

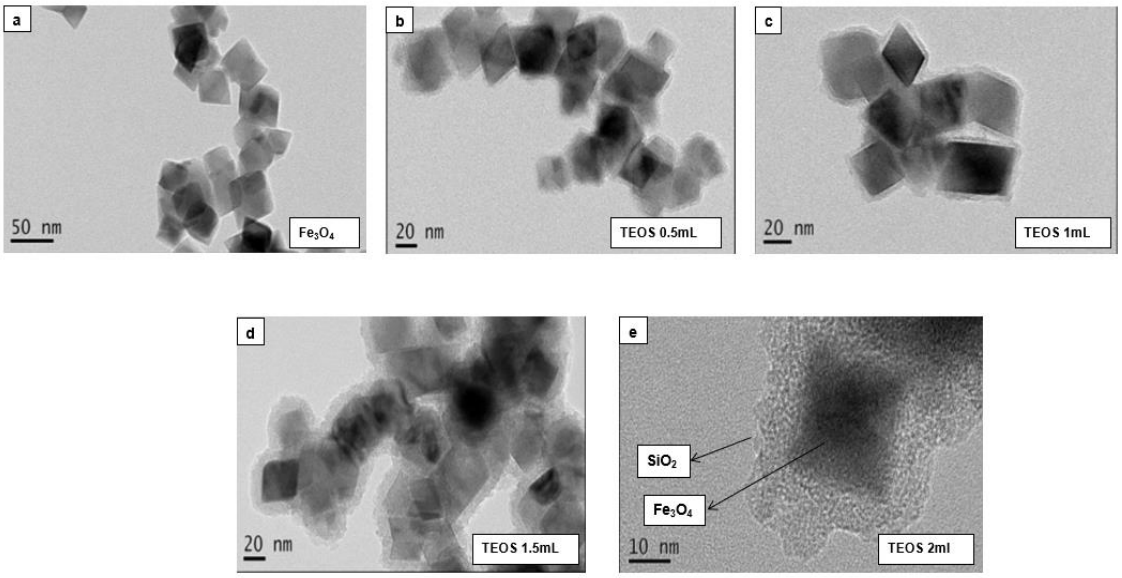

Figure 35. TEM images of the Fe-MNP and the Fe-Si-MNP prepared with different volumes of TEOS; (a) Fe-MNP (b) Fe-Si-1 (c) Fe-Si-2, (d) Fe-Si-3, and (e) Fe-Si-4.

Figure 36a illustrates the magnetism curves of the Fe-MNP, Fe-Si-1, Fe-Si-2, Fe-Si-3, and Fe-Si-4. The studied MNP exhibits hysteresis behaviour with superparamagnetic properties, consistent with previous research that indicated that Fe-MNP with sizes smaller than the critical size of 29-36 nm exemplified high superparamagnetic properties. The greatest saturation magnetization (M_s) value was observed for the Fe-MNP (~76·38 emu/g), which was similarly reported by Tan et al. [452] and Ge et al. [453]. The Fe-Si MNP remained superparamagnetic even after the silica coating. Due to the presence of the SiO_2 shell, the M_s values slightly decreased to ~ 50.7, 46.1, 43.8, and 42 emu/g for the Fe-Si-1, Fe-Si-2, Fe-Si-3, and Fe-Si-4, respectively. However, the M_s values for the Fe-Si MNP can be separated by applying an external magnetic field as suggested by [451, 454]. The decrease in the magnetization values after the nanoparticles are attached may be due

to the integration of non-magnetic silica shells over the Fe-MNP surface. Additionally, the reduction in magnetization is due to the presence of chemical bonds such as Fe-O-Si, which occurred because of surface functionalization with SiO_2 nanoparticles. [455] demonstrated how silica could bond with Fe to generate Fe-O-Si to maintain the magnetic properties and protect the MNP. Moreover, Singh et al. and Kolhatkar et al. [456, 457] reported similar results for decreasing the magnetic value after grafting with silica nanoparticles. As previously indicated, the thickness of the Si layer increased by simultaneously increasing the volume of TEOS during the synthesis process, and as a result, the magnetism value was reduced. Thus, the magnetism of the composite particles (Fe-Si MNP) is controllable by altering the volume of TEOS.

Figure 36b exhibits the maximum magnetization values of Fe-Si-1, Fe-Si-2, Fe-Si-3, and Fe-Si-4 prepared with varying amounts of TEOS. As previously noted, the TEOS volume is a crucial parameter that influences the silica layer thickness and the magnetic properties of the Fe-Si MNP. First, the TEOS in the reaction medium is transferred and hydrolyzed to be adsorbed onto the surface of the Fe-MNP. After that, the hydrolyzed surface of the MNP produces the silica shell through a condensation reaction [458]. As suggested by Ding et al. [458], this procedure helps the Fe-Si MNP retain a small size and preserve excellent dispersion properties.

Figure 36c illustrates a decrease in magnetization by 8.1%, 41.8%, 45.3%, and 49.1% for Fe-Si-1, Fe-Si-2, Fe-Si-3, and Fe-Si-4, respectively, in comparison to the Fe-MNP. Conversely, Figure 36c demonstrates that the applied volume of TEOS contributes to the silica shell thickness. The thickness of the silica shell ranged from 5 to 15 nm. The Fe-Si-1 nanoparticles have the lowest silica thickness (5 nm) in comparison to the MNP prepared with high TEOS amounts (1.0 mL to 2.0 mL). For the MNP prepared with high TEOS amounts, the thickness of the silica layer increased to ~ 15 nm for the Fe-Si-4 MNP. These

results are compatible with those outlined by [459], whose research indicated that a high TEOS volume (> 5 mL) generates a silica layer with a thickness of > 10 nm. At the same time, the amount of Fe-MNP did not substantially impact the silica shell thickness.

The stability of the Fe-Si MNP is crucial when used for a produced water treatment for oil and water separation. Figure 36d presents the stability of the Fe-Si MNP, which was evaluated by measuring the magnetization curve after two months of exposure to normal air and a strong reducing agent (hydrogen gas). For the Fe-MNP, the M_s significantly decreased from 80 emu/g to ~ 55.4 emu/g, while the M_S reduction for the Fe-Si MNP was 50.4 emu/g to ~ 48.5 emu/g. Similarly, the magnetization value for the Fe-Si-1 MNP with the presence of hydrogen gas decreased to only 48.5 emu/g. As such, the results indicate that the Fe-Si MNP improved with the addition of the silica layer, which supports the practical applications of the MNP.

Figure 36e exemplifies the relation between the M_s and the thickness of the SiO_2 shell. The saturation magnetization values for the Fe-Si MNP (Fe-Si-1, Fe-Si-2, Fe-Si-3, and Fe-Si-4) decreased as the silica shell thickness increased and have the corresponding values: 81.2, 75.2, 65.3, and 47.5 emu/g with a silica shell thickness of 5, 8, and 10, and 15 nm, respectively. In all samples, the decrease in the magnetization value after the silica coating is attributed to the integration of nonmagnetic silica shells over the Fe-MNP. Additionally, the decline in the magnetization value for the Fe-Si MNP is due to certain chemical bonds, such as Fe-O-Si, resulting from surface functionalization with SiO_2. Moreover, [460] suggested that the magnetization value is affected by the shape of the nanoparticles with a lower M_S for cubic-shaped MNP compared to those with a spherical shape. The Summary of the properties of the four different Fe-Si-MNPs used in the chapter is presented in Table 11.

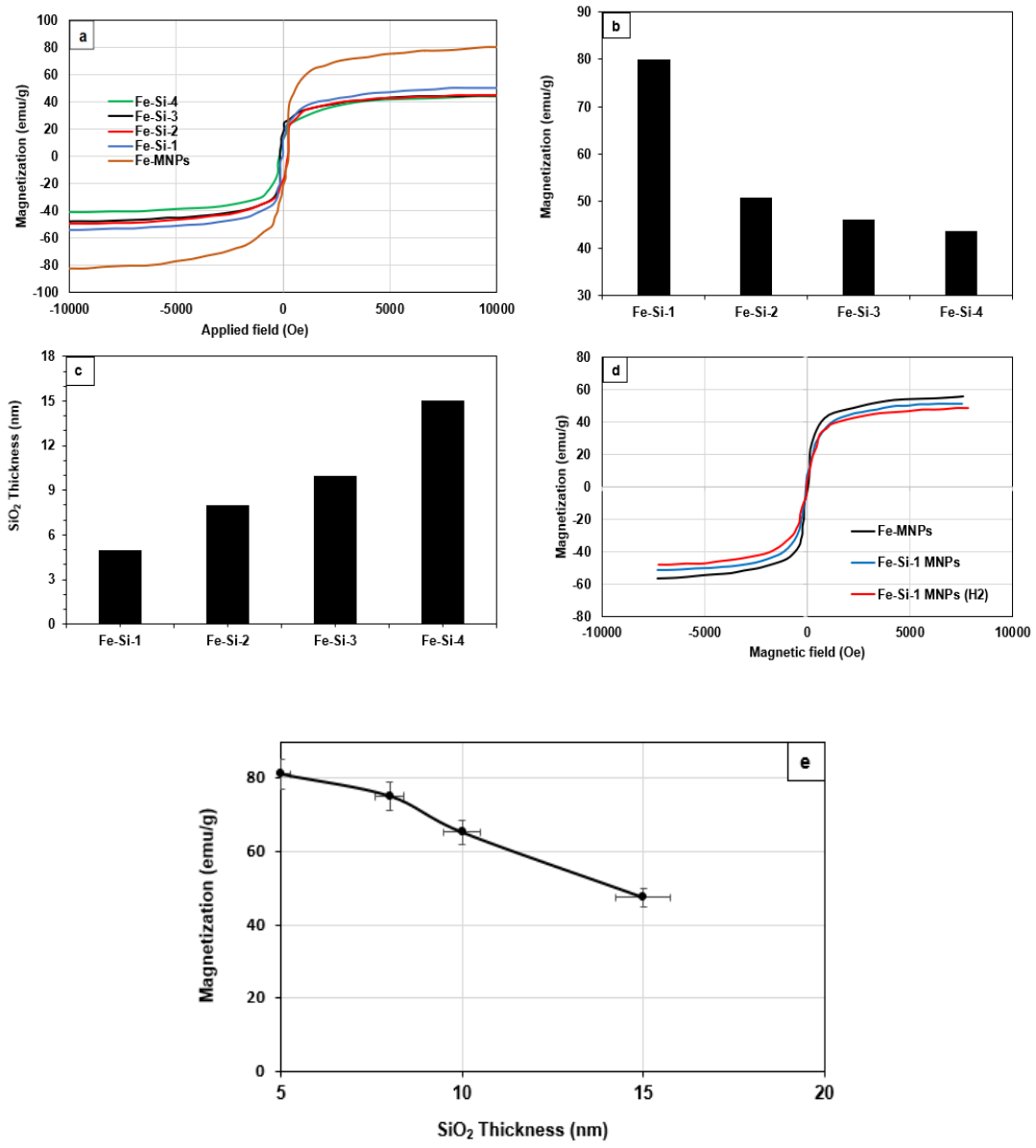

Figure 36. Properties of the Fe-MNP and Fe-Si MNP demulsifiers (a) magnetization curve at 300°K (b) maximum magnetization values, (c) the thickness of silica layer, (d) magnetization curve (i) after 2 months of exposure to air, and (ii) in the presence of H_2 gas.

Table 11 Summary of the properties of the four different Fe-Si-MNPs used.

NP	Structure	Function group	TEOS (ml)	NP size (nm)	Thickness of silica layer (nm)	Ms (emu/g)	IFT (mN/m)	Contact angle (degree)
Fe-NP	Crystalline cubic shape	C=O, COO, CH, Fe-O, CH_2, C=C,	-	40	-	76.38	-	-
Fe-Si-1	Crystalline spherical shape	Si-O-Fe, Fe-O, Si-O-Si, SiO, OH, Si-OH	0.5	45	5	50.7	23.8 ± 2.3	115°
Fe-Si-2	Crystalline spherical shape	Si-O-Fe, Fe-O, Si-O-Si, SiO, $^{-}$OH	1.0	55	8	46.1	20.5 ± 1.3	109°
Fe-Si-3	Crystalline spherical shape	Si-O-Fe, Fe-O, Si-O-Si, SiO, $^{-}$OH	1.5	64	10	43.8	16.8 ± 1.3	104°
Fe-Si-4	Crystalline spherical shape	Si-O-Fe, Fe-O, Si-O-Si, SiO, $^{-}$OH	2.0	75	15	42	13.2 ± 1.1	100°

6.3.2 The Application of the Fe-Si MNP for Oil Separation

6.3.2.1 Effect of Oil Concentration (D_{oil}) on Oil Separation Performance

Figure 37a presents the effect of D_{oil} on $\%S_{oil}$ at a fixed dosage of 10 mg/L for Fe-Si-1, Fe-Si-2, and Fe-Si-3. The results indicated that Fe-Si-1 provided the highest $\%S_{oil}$ in the range of 88.2% to 96.3%. For the Fe-Si-2 and Fe-Si-3, the $\%S_{oil}$ decreased to the range of 86.3% to 95.0% and 83.6% to 92.3%, respectively. The results are consistent with the results reported by Tang et al., Di et al., and Gao et al. [450, 451] [461], whose research showed that the MNP with a greater surface area tends to have a higher attraction force to oil droplets to achieve a higher $\%S_{oil.}$ In contrast, the $\%S_{oil}$ is higher than the values reported by Gao et al. [461], as their experiments were conducted with Fe-Si MNP particle sizes in the range of 45-75 nm. In this chapter, the results indicate that the amount of TEOS used in the synthesis of the Fe-Si MNP has a substantial influence on the $\%S_{oil}$. With a TEOS volume < 1 mL, coating the Fe-MNP with silica is quick. This reaction is due to high dispersion conditions that produce a small Fe-MNP covered with a SiO_2 layer. As a result, the particles have a high surface area and exhibit a high $\%S_{oil}$. However, a low TEOS concentration can cause direct adsorption of the hydrolyzed silica by TEOS onto the agglomerates (i.e., Fe-MNP) to create particles with a high dispersion rate. As suggested by [462], when the TEOS volume increases (> 1 mL), the particle size subsequently increases, and a large amount of the TEOS is hydrolyzed to form adhesions, which causes particle distribution and reduces the $\%S_{oil.}$ Thus, the favourable nanoparticle sample is prepared using a small volume of TEOS ~0.5 mL (i.e., Fe-Si-1), which obtained an oil separation rate of ~ 96%. Additionally, a significant $\%S_{oil}$ was achieved with a low Fe-Si-1 dosage of 10 mg/L for the oil concentration range between 0-800 mg/L.

6.3.2.2 Effect of Demulsifier Dosages (D_{MNPs}) on Oil Separation Performance

Figure 37b presents the $\%S_{oil}$ as a function of D_{MNP} (10, 30, 50, and 100 mg/L) for the Fe-Si-1, Fe-Si-2, and Fe-Si-3 during the treatment of O/W-emul with a D_{oil} of 750 mg/L. The Fe-Si-1 exhibited the highest $\%S_{oil}$ under all the studied $D_{MNP,}$ followed by Fe-Si-2 and Fe-Si-3. For all of the studied nanoparticles, there was a trend indicating the highest $\%S_{oil}$ for $D_{MNP} \leq 30$ mg/L, after which the $\%S_{oil}$ decreased to stabilize at a constant value. First, the Fe-Si MNP was gradually dispersed into the O/W-emul. Then, the oil was quickly absorbed onto the Fe-Si MNP surface and separated using the external magnetic field. It is estimated that the hydrophobicity and superparamagnetic properties of the Fe-Si MNP improved the oil removal and separation process as suggested by Shehzad et al. [27].

Similarly, Kamgar et al. [441] observed that a small amount of Fe-Si MNP (10 mg/L) was used to recover oil from the O/W-emul. The results indicated that the $\%S_{oil}$ of Fe-Si-1 was estimated to be 95.53%, 95.15%, 92.43%, and 89.48% for the D_{MNP} of 10, 30, 50, and 100 mg/L, respectively. The $\%S_{oil}$ decreased for the Fe-Si-2 and Fe-Si-3 at varying D_{MNP} compared to the results achieved by the Fe-Si-1 due to the increase in the nanoparticle size. In comparison to the results achieved by the Fe-Si-1, the $\%S_{oil}$ decreased for the Fe-Si-2 and Fe-Si-3 due to the increase in the MNPs size and decrease of MS. Wang et al. [402] suggested that using high volumes of TEOS increases the Si hydrolysis on the surface of the Fe-MNP, which subsequently increases their size and reduces the $\%S_{oil}$. Moreover, [151] highlighted how smaller MNP result in a higher density and a stronger electrostatic attraction force (assuming the MNP have stable conditions). The results indicated that the as-prepared Fe-Si MNP could separate the oil from the emulsion mixture and easily carry the oil under the external magnetic field.

Further, the results showed that the low $\%S_{oil}$ at a higher D_{MNP} is likely due to the aggregation of the nanoparticles. This commonly occurs at higher concentrations following the decrease in the adsorption capacity and the surface area of the nanoparticles [418, 419].

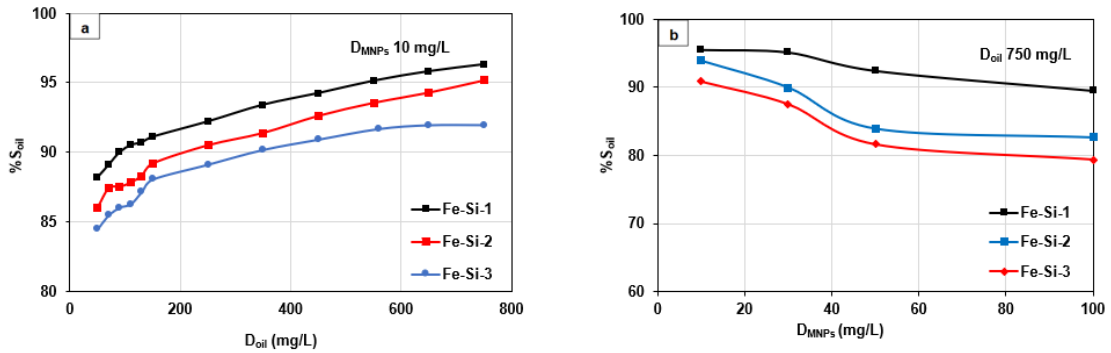

Figure 37. (a) The $\%S_{oil}$ using varying D_{MNP} demulsifiers with D_{oil} = 750 mg/L (b) the effect of Fe-Si MNP demulsifiers on the $\%S_{oil}$ with a D_{MNP} of 10 mg/L.

6.3.2.3 Oil Separation Performance at Different Surfactant Concentrations (D_{sur})

As the prepared emulsion samples commonly include surface-active substances, called surfactants [463], it is essential to evaluate the impact of the material concentrations on the $\%S_{oil}$. A tween-80 surfactant was used for the synthesis of the O/W emulsion. First, the removal rate was tested without adding a surfactant. After that, the surfactant concentrations (0.05, 0.1, and 0.5 g/L) were tested with D_{oil} in the range of 0-1000 mg/L using a D_{MNP} of 10 mg/L for Fe-Si-1, Fe-Si-2, and Fe-Si-3. As exhibited in Figure 38 (a-c), the $\%S_{oil}$ is Fe-Si-1> Fe-Si-2> Fe-Si-3 and decreased with the addition of the surfactant. The oil particles in the emulsion can be absorbed into the Fe-Si MNP via hydrophobic interaction [419]. After the addition of the surfactant, most of the oil particles disperse onto the surface. However, part of the oil particles is absorbed into the Fe-Si MNP and attached to the hydrophobic site on the Fe-Si MNP due to the hydrophobic attraction force. Apart

from the increase in the oil droplets hydrophobicity, the oil absorption by the tween-80 surfactant decreased, which created an electrostatic repulsion force. As such, all of these factors influence the oil sorption behaviour on the Fe-Si MNP. [419, 424] highlighted how the addition of the surfactant increases the hydrophobicity of oil particles, decreasing the oil absorption, and subsequently influences the $\%S_{oil}$. [464] reported the effect of natural organic macromolecules on oil removal, the efficiency diminished at a high concentration of the surfactant for most demulsifiers. Conversely, the volume of TEOS, which controlled the final size and structure of the Fe-Si MNP, was highly influential on the $\%S_{oil.}$ [442].

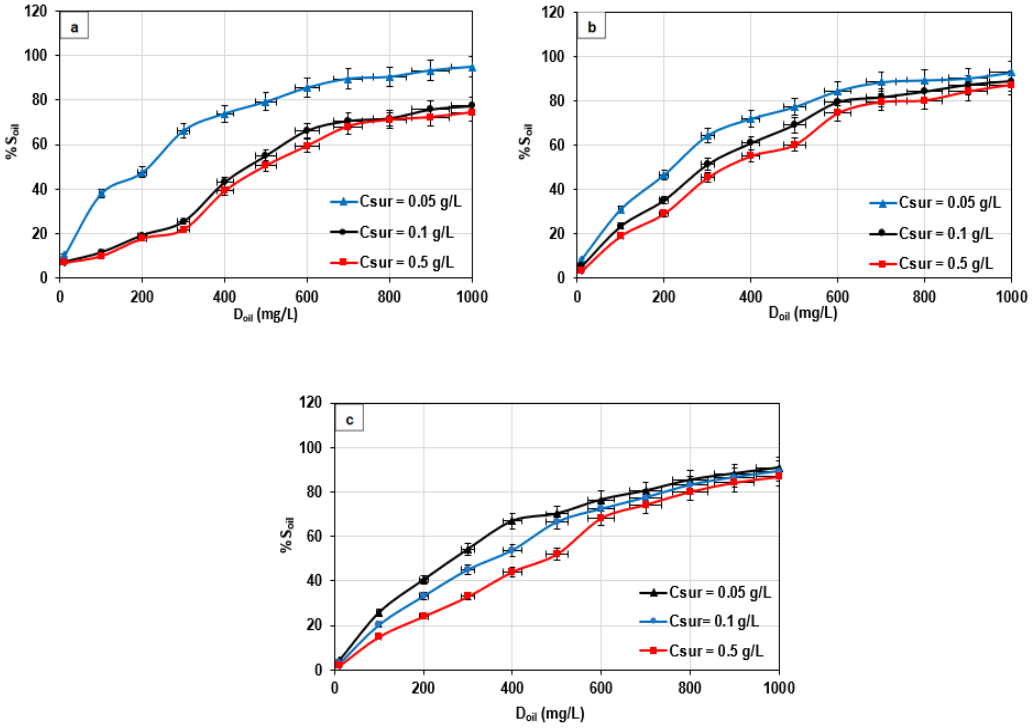

Figure 38. The effect of (a) Fe-Si-1 (b) Fe-Si-2 (c) Fe-Si-3 MNP on the $\%S_{oil}$ at different D_{sur}. Conditions: D_{MNP} of 10 mg/L and D_{oil} in the range of 0-1000 mg/L.

6.3.2.4 Effect of pH on Oil Separation Performance

Figure 39 (a-c) highlights the effect of pH on the $\%S_{oil}$ from the O/W-emul using Fe-Si-1, Fe-Si-2, and Fe-Si-3. The pH is one of the primary factors affecting the oil removal performance from O/W-emul [465]. The $\%S_{oil}$ was examined at a pH of 4, 7, and 10. Under

all of these pH values, the $\%S_{oil}$ diminished by increasing the pH of the emulsion samples. The oil removal by the Fe-Si MNP is governed by electrostatic interaction forces between the demulsifier and the O/W-emul that change by manipulating the pH [466]. Under basic and neutral pH, the $\%S_{oil}$ was found to be lower than at acidic conditions. This is likely because the surface functional groups are partially separated under basic and neutral conditions, which causes a decrease in the $\% S_{oil}$ [467, 468].

Moreover, the pH has a significant effect on the oil recovery mechanism. The electrostatic repulsion between the Fe-Si MNP and the oil droplets increases by correspondingly increasing the O/W-emul pH. The goal is to reduce the electrostatic repulsion between the demulsifier and the oil droplets to enhance the $\%S_{oil}$. Under acidic conditions, the Fe-Si MNP has a positively charged functional group, while the O/W-emul exhibited a negative charge. Thus, the oil droplets can be adsorbed onto the surface of the MNP via electrostatic attraction force, which causes a significant improvement in the $\%S_{oil}$. For the neutral and alkaline conditions, the positive surface charge of the Fe-Si MNP decreased, and interfacial adsorption was limited, thus reducing the $\%S_{oil}$. In addition, the absolute zeta potential for the Fe-Si MNP at an acidic pH is highly positive compared to the alkaline and neutral pH, which indicates a decrease in the electrostatic repulsion between the Fe-Si MNP and the O/W-emul.

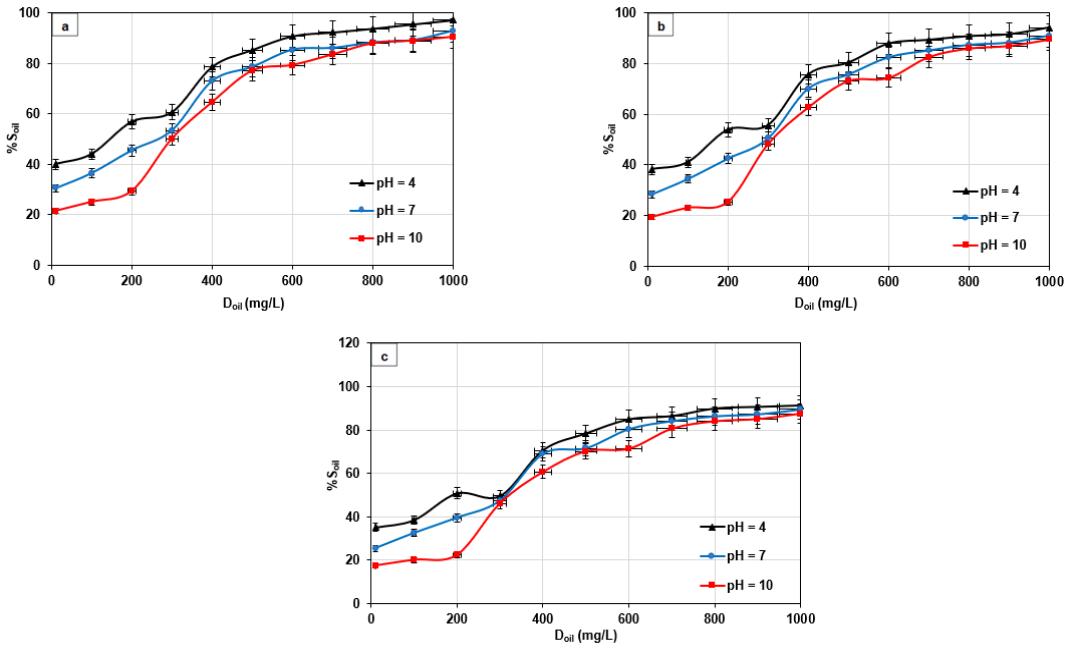

Figure 39. The effect of pH on the $\%S_{oil}$ with different demulsifiers at varying D_{oil} (a) Fe-Si-1 (b) Fe-Si-2 (c) Fe-Si-3 MNP. Conditions: D_{MNP} =10 mg/L.

6.3.2.5 IFT and Contact Angle Measurements

At ambient conditions, figure 40a exemplifies the IFT values between the gasoline oil and the MNP (Fe-Si-1, Fe-Si-2, Fe-Si-3, and Fe-Si-4). The reduction in the IFT largely contributes to the improvement in the oil recovery. As Figure 40a indicates, all of the MNP (Fe-Si-1, Fe-Si-2, Fe-Si-3, and Fe-Si-4) exhibited smaller IFT values in comparison to the IFT value of distilled water (DW) without additional demulsifiers (the value was equal to 39±2 mN/m). For example, the Fe-Si-1 exhibited a reduction of 38.9% (23.8 ± 2.3 mN/m). Adding a greater silica layer on the Fe-MNP (i.e., Fe-Si-3 and Fe-Si-4) resulted in a decrease in the IFT to 20.5 ± 1.3 for Fe-Si-2, 16.8 ± 1.3 mN/m for Fe-Si-3, and 13.2 ± 1.1 mN/m for Fe-Si-4. The lower IFT values are likely the consequence of the synergistic impact of separate MNP demulsifiers as a nanocomposite structure. However, this is an improvement for the demulsification process of O/W-emul at ambient pressure. As such, synergistic influences are the consequences directly produced by each nanoparticle to

create the nanocomposite (i.e., Fe-Si MNP). The results outlined in prior research literature indicate that adding the Fe-Si MNP demulsifiers to the O/W-emul ought to lead to a more significant improvement in the IFT and wettability.

It is imperative to evaluate the effect of pH on the interfacial tension and zeta potential as they greatly influence the demulsification process for the O/W-emul. For the IFT measurements, a decrease in the pH increases the interfacial tension of the O/W-emul. The demulsification process and oil separation were most effective at monodispersed emulsions with a pH of 5 or less. However, a higher pH caused the particle size to increase and reduced the dispersity of the nanoparticles [469]. For the zeta potential, the experimental data indicates that the O/W interface is negatively charged at a pH > 4, though it can be positive at a lower pH [36, 470]. The results exemplify for the first time how the increase in the pH of the emulsion changes the zeta potential and Van Der Waals force to decrease the oil attachment and reduce the $\%S_{oil}$. Results are in good agreement with data published by [471], who showed that the zeta potential of the emulsion decrease by increasing the pH, and the corresponding electrostatic force repulsive tends to stabilize oil droplet in the emulsion. In contrast, the Van Der Waals force tries to flocculate the oil droplets and increase removal efficiency.

Figure 40b presents the measurements for the contact angle of the water and the MNPs/oil/water surface systems after treatment for 5 h. The results exhibit a decrease in the contact angle values for 10 mg/L for the Fe-Si MNP O/W surface compared to the water without adding the Fe-Si demulsifier. The wettability alteration from the condition of oil/wet to water/wet likely contributes to the improvement in oil production through flooding, accompanied by a decrease in the IFT. The contact angles of water were measured at 137°. A significant reduction in the contact angle values was noted. There was a substantial decrease in the contact angle values after adding various volumes of MNP

demulsifier to the O/W-emul. The MNP overcame the adhesion force between the gasoline oil droplets and the water surface. The MNP removed oil droplets from the water surface by using disjoining pressure on the surface, which caused the alteration in water wettability. Disjoining pressure is needed to overcome the oil adhesion force on the water's surface for oil separation [472]. When a difference in pressure between the thin film of fluid and bulk on the water's surface occurs, a wedge film with discontinuous fluid is formed at the interface through the configuration of the MNP [473]. This reaction causes oil separation and is a mechanism for wettability alteration [473]. This method is influenced by Brownian motion and electrostatic repulsive forces between the MNP. The arrangement of MNP in the wedge layer develops a greater force to the interface, which improves with a greater volume of the MNP and creates pressure higher than 50 000 psi. When these forces are employed against the interface, the oil begins to move to a stable condition, consequently affecting the enhancement of the oil separation process.

As such, there are two crucial factors for determining the wettability alteration: the properties of the phases presented in the system and particle size [474, 475]. As highlighted in Figure 40b, compared to the other MNP demulsifiers, the greatest wettability alteration for the oil/wet occurred when the Fe-Si-1 MNP was applied. The greatest contact angle was measured for the Fe-Si-1 MNP/O/W surface, which was 115°. The results indicate a slight contact angle reduction for the systems with demulsifiers prepared with a TEOS concentration ranging from 1-2 ml compared to the first system. The contact angles measured for Fe-Si-2, Fe-Si-3, and Fe-Si-4/MNPs/O/W surfaces were 109°, 104°, and 100°, respectively. The results indicate that the hydrophobicity of the surface is Θ = 90-150°.

The pH impacts the contact angle between the oil and nanoparticles. The value of θ rises slowly as the pH increases due to the decrease in the thickness of the silica nanoparticle

layer. The decline in the nanoparticle's zeta potential results in an increase in the hydrophobicity of the nanoparticles. When the pH is 4, the measured value of θ with an improving pH is small (40.5◦). Further, even with a pH of 10, the value of θ is 49.5◦ (still much less than 90◦). [476] have examined the content angle between the oil, nanoparticles, and emulsion droplet sizes using statistics modelling at specified conditions. The estimated θ value is similarly found to be smaller than 90◦.

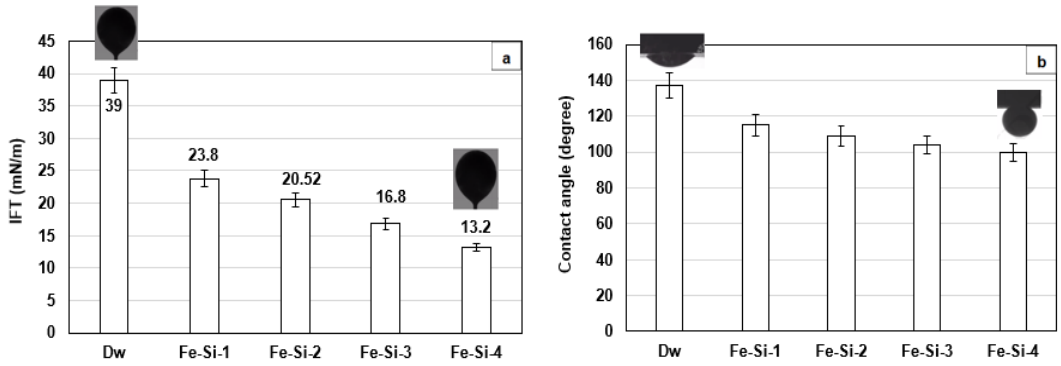

Figure 40. (a) IFT measurement of water and IFT between gasoline oil and 10 mg/L of Fe-Si MNP demulsifiers (b) Contact angle measurements of the water and the MNPs/oil/water surfaces using 10 mg/L of the four Fe-Si-MNP demulsifiers at O/W-emul with a D_{oil} of 500 mg/L.

6.3.2.6 Oil Separation Performance at Different Salinity

The effect of the salinity of the O/W-emul on the $\%S_{oil}$ was evaluated. Figure 41 presents the results with a pH condition of 4. The $\%S_{oil}$ was examined with 10 mg/L to the Fe-Si MNP demulsifiers for the emulsion sample with varying oil dosages (D_{oil} from 0 to 1000 mg/L) and a salinity range from 0.1 to 0.5 M NaCl. The results demonstrated how both the salinity of the O/W-emul and the $\%S_{oil}$ increased. At a high salinity value of 0.5 M NaCl and D_{oil} 100 mg/L, the Fe-Si-1 nanoparticles exhibited the highest oil separation rate of 93.3% (Figure 41a). Conversely, with the same $D_{oil,}$ the $\%S_{oil}$ using Fe-Si-2 (Figure 41b), Fe-Si-3 (Figure 41c), and Fe-Si-4 (Figure 41d) nanoparticles have lower values of 90.3%,

88.03%, and 86.3%, respectively. When the salinity increased from 0.1 to 0.5 M NaCl, the $\%S_{oil}$ increased from 87.3% to 93.3% (Fe-Si-1), 85% to 90.3% (Fe-Si-2), 84.13% to 88.03% (Fe-Si-3), and 82.2% to 86.3% (Fe-Si-4) with a D_{oil} 100 mg/L. Similar trends were observed with other oil concentrations (200, 400, and 600 mg/L). This was primarily due to the "salting-out" effect, which reduced the hydrophilicity of the stabilizing surfactants and consequently lowered the interfacial tension of the O/W-emul [356].

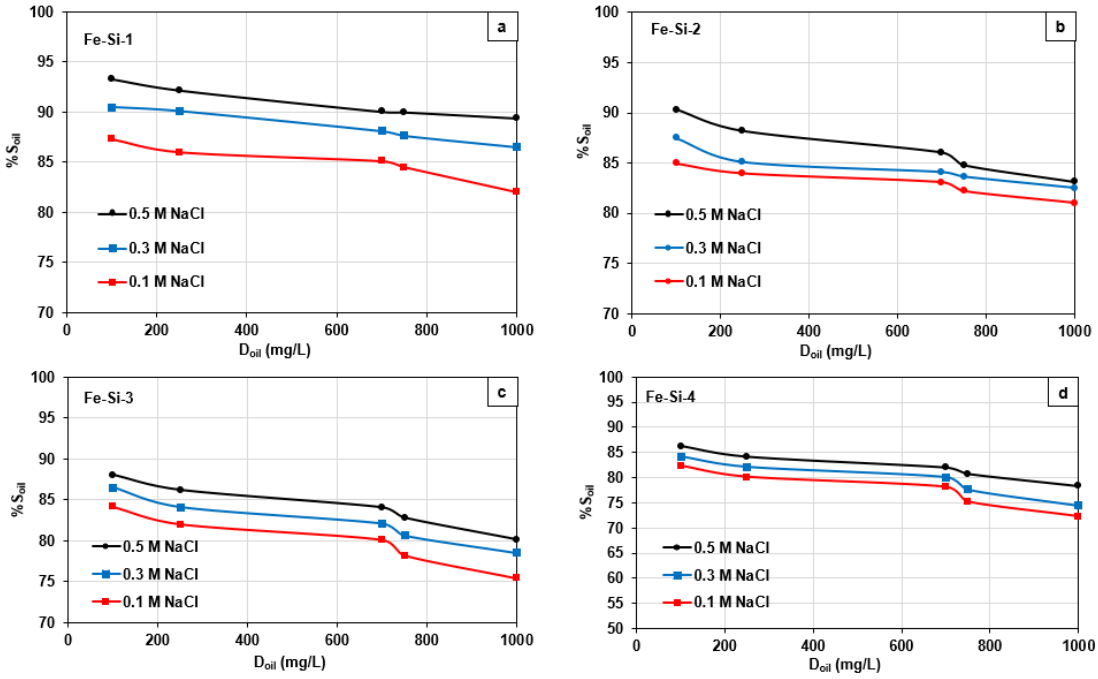

Figure 41. The effect of 10 mg/L (a) Fe-Si-1 (b) Fe-Si-2 (c) Fe-Si-3 (d) Fe-Si-4 MNPs demulsifiers on the $\%S_{oil}$ at different salinity (0.1,0.3,0.5 M NaCl) at D_{oil} ranging from 0-1000 mg/L.

6.4 Oil Removal Mechanism

The mechanism for the oil recovery process is centred on electrostatic attraction forces between the oil and the Fe-Si MNP. In summary, the negatively charged oil droplets from the O/W-emul can attach to the positively charged functional groups on the surface of the nanoparticles by the electrostatic attraction force of the hydrophobic bond. Many of the

separation methods for the MNP include the dispersion of the nanoparticles into the medium. After that, the targeted chemicals, ions, surface of functional groups are adsorbed onto the nanoparticle's surface. Lastly, a magnetic field is presented, and the nanoparticles with the adsorbed material are separated from the medium.

Moreover, oil recovery from O/W-emul is commonly dependent upon adding the surface-active composites that alter the interfacial characteristics (e.g., interfacial tension [IFT], mechanical potency, flexibility, and interfacial films thickness). Altering the interfacial characteristics improves the coalescence and flocculation of oil droplets in the emulsion. In contrast, if the MNP is inserted into the emulsion, the demulsifying impact occurs because interfacial active nanoparticles are coating the droplets.

Although the developed nanoparticles have demonstrated an excellent efficiency for oil recovery, the detailed mechanism for how the Fe-Si MNP could increase the $\%S_{oil}$ is yet to be clearly outlined and understood. Numerous mechanisms for enhancing the $\%S_{oil}$ have been proposed, including interfacial tension reduction, disjoining pressure and mobility control, wettability alteration, viscosity control, and demulsification. The mechanisms above occur because of adsorption, desorption, and oil transport through the MNP pore throat [102]. Five types of energy can be responsible for the interaction between the oil from the O/W-emul and the MNP: (1) London-van der Waals attractive potential energy, (2) electric double layer attraction-repulsion energy, (3) Born repulsion, (4) acid-base interaction, and (5) hydrodynamic energy [477]. The adsorption occurs when the net attraction forces are larger than the net repulsion force. Otherwise, desorption occurs. Additionally, the movement of the oil droplets to the pore throat of the MNP is driven by diffusion and convection. However, blocking may occur due to an aggregation of oil droplets larger than the pore throat [102].

Several research works have exemplified how wettability is crucial for obtaining the highest $\%S_{oil}$ [77, 478]. The wettability significantly affects the capillary pressure and relative permeability, the stage at which the oil attachment to the MNP can be considerably improved [103]. Conversely, capillary force controls the IFT between the O/W-emul and the MNP [479]. By reducing the interfacial tension and altering the MNP wettability, the capillary pressure reduces, and the $\%S_{oil}$ increases [480]. Thus, the presence of the MNP helps to decrease the IFT with or without the surfactant. Furthermore, the MNP can improve the rheology of the solution and enhance the effect of the surfactant to reduce the IFT [104].

The disjoining pressure mechanism is a novel concept to explain the interaction between the MNP and oil [481, 482] is an additional approach to understanding the oil removal mechanism. Disjoining pressure is the attractive and repulsive forces between two thin layers of fluid-solid surfaces [483]. The oil recovery process is complex because of a three-phase contact region [106]. First, the MNP is dispersed into the mixture to develop wedge-shaped structures and is forced towards the oil-solid contact area. Second, the ordered structures in the wedge film enhance the spreading and attachment of oil onto the solid surface [107]. The force created by a single particle is relatively small. However, the total force of the accumulated nanoparticles can reach up to 7.5×10^4 Pa. The mechanisms that cause this phenomenon are the Brownian motion and the electrostatic attrition-repulsion forces. Essentially, the disjoining force is responsible for the attachment and detachment of oil on the solid surface while also aiding in its recovery.

The disjoining pressure is affected by several parameters, including the size and concentration of the MNP, the surface charge density, temperature, salinity, and surface characteristics [151]. The size of the MNP and the associated charge density significantly affect the disjoining pressure strength. It is estimated that the smaller particles would result

in a higher charge density and a stronger electrostatic attraction force (assuming stable particle conditions). As such, [152] assert that smaller particles have been shown to increase the recovery considerably. The results indicate that both the oil recovery and displacement efficiency increased because of the smaller-sized nanoparticles. Similarly, several other experiments concluded that the smaller particles lead to a higher total oil recovery [484, 485]. Moreover, research by [150] exemplified how decreasing the MNP diameter from 30 nm to 18.5 nm changed the structural disjoining pressure by a magnitude of roughly 4.3 times. The concentration of the MNP is a primary determining factor for the $\%S_{oil}$. Chengara et al. [154] noted that increasing the concentration of MNP will increase the repulsion forces. Increasing the MNP concentration will subsequently decrease the interfacial tension between the oil and MNP [155]. Given this, there is indeed an optimal MNP concentration that will produce a favourable oil recovery.

The salinity of the O/W-emul significantly affects the $\%S_{oil}$. Therefore, increasing the salinity can reduce the zeta potential of each particle, which ultimately creates a more accessible aggregation [151]. In addition, high ionic strength in the O/W-emul is due to salt, which leads to a lower electrical repulsion between the oil and particles and creates a higher $\%S_{oil}$. Thus, a high salinity environment is necessary to maintain stability, achievable with surface modification, ionic control via surfactant, or both [153].

6.5 Reusability of the Fe-Si MNP Demulsifiers

Figure 42 presents the recyclability of the Fe-Si MNP as a function of the TEOS volume used in the preparation process for emulsions, with D_{oil} in the range 0-1000 mg/L using D_{MNP} of 10 mg/L of Fe-Si MNP tested over 9 cycles. The sample Fe-Si-1 exhibited the highest $\%S_{oil}$ in comparison to the values for the Fe-Si MNP prepared with high TEOS volumes (> 1 mL). The optimum operating conditions for reusing the magnetic demulsifiers were obtained at a pH of 4, D_{MNP} of 10 mg/L, and 20 mL of ethanol used for washing the

MNP for 8 min. It was observed that the $\%S_{oil}$ had a high value when using the Fe-Si-1 MNP demulsifier. However, the demulsification efficiency decreased from 87.09% to 85.43% when TEOS increased from 1 to 2 ml (Fe-Si-2 to Fe-Si-4). As highlighted in Figure 42, the high volume of TEOS influences the oil separation, although the demulsification efficiency does not considerably decline. Instead, the oil separation still has high values in the following cycles. However, the efficiency decreased during the 8^{th} cycle, reaching 87.43%, 87.09%, 86.43%, and 85.43% for all demulsifier samples. These percentages are still significant, suggesting that the Fe-Si MNP remains efficient and utilized in the following cycles. [289] had comparable results and recommended that the decline in the oil recovery rate is likely due to the grafting of tiny oil drops onto the MNP surface that cannot simply be eliminated through the ethanol regeneration stages, which results in a gradual reduction in the efficiency of oil separation through the reusing method.

Following the 9^{th} cycle, there was a slight decrease in the $\%S_{oil}$ for the demulsifiers prepared with high TEOS volumes (i.e., Fe-Si-3 and Fe-Si-4 MNPs). This could be attributed to some of the surface functional groups after the sequential cleaning process. Further discussion is required to confirm this observation. Nevertheless, the results indicate that the application of coated Fe-Si MNP for the oil recovery from O/W-emul maintains paramagnetic particle properties for easy separation. These results are compatible with research by [486]. The advantage of the MNP in comparison to other conventional chemical demulsifiers is their ability to: (a) achieve separation via an external magnetic field and (b) regenerate after the demulsification process [212, 288]. The application of the Fe-Si MNP demulsifiers with varying TEOS volumes in the oil recovery process exemplified how the demulsification efficiency decreased when the TEOS amount increased.

Further, a high oil separation rate was achieved at a low TEOS concentration (0.5 ml). The low TEOS aided in the adsorption of the silica hydrolyzed by the TEOS onto the Fe-Si

MNP to create small particles that achieved a greater dispersibility into the O/W-emul [358, 442]. In contrast, the emulsions with a larger particle size tended to be unstable after only a few hours with a greater amount of TEOS. This is likely due to unadopted nanoparticle distribution and the ineffective proportion of oil and water phases [487]. The expanded service life and recovery of the Fe-Si MNP to remove oil from the O/W-emul indicates a substantial decrease in the process cost. As such, Table 12. summarizes the reusability results for Fe-Si-1, Fe-Si-2, Fe-Si-3, and Fe-Si-4 nanoparticle demulsifiers during the 9th cycle.

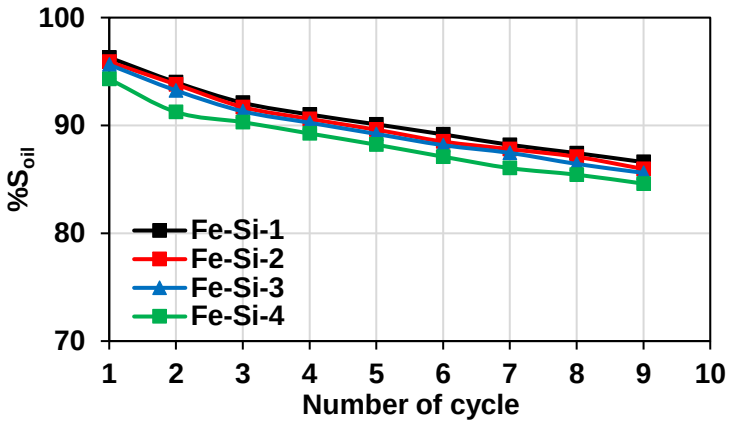

Figure 42. The reusability of the Fe-Si MNP demulsifiers prepared with TEOS ranging from (0.5-2.0 mL) at optimum conditions of t_{sep} 8 min, ethanol 2 mL/5mg MNP and D_{MNP} of 10 mg/L as well as the effect on the $\%S_{oil}$ for emulsions with D_{oil} in the range 0-1000 mg/L.

Table 12. Summary of the reusability results for Fe-Si-1, Fe-Si-2, Fe-Si-3, and Fe-Si-4 nanoparticle demulsifiers.

NPs	Oil separation efficiency ($\%S_{oil}$) at the 9th cycles								
	1	2	3	4	5	6	7	8	9
Fe-Si-1	96.3	94.00	92.1	91.01	91.10	89.17	88.2	87.43	86.60
Fe-Si-2	95.9	93.80	91.70	90.60	89.60	89.50	87.80	87.09	85.09

NPs	Oil separation efficiency (%S_{oil}) at the 9th cycles								
	1	2	3	4	5	6	7	8	9
Fe-Si-3	95.63	93.24	91.31	90.25	89.21	88.17	87.45	86.43	85.60
Fe-Si-4	94.3	91.24	90.30	89.25	88.21	87.10	86.04	85.43	84.60

6.6 Adsorption Kinetic

Pseudo-first order and pseudo-second-order models were applied to evaluate the kinetic of the oil separation process using four nanoparticle adsorbents (Fe-Si-1, Fe-Si-2, Fe-Si-3, and Fe-Si-4). The pseudo-first-order model equation (17) [363] assumes that the adsorption process rate directly relates to the volume of empty spaces by the adsorbate.

$$Ln\,(Q_e - Q_t) = LnQ_e - K_1 t \qquad (17)$$

Figure 43a presents the regression analysis of the experimental data following equation (17) for the experiments conducted with separate temperature periods of 25℃, a pH of 4, and a D_{MNP} of 10 mg/L. Table 13 presents the estimates of the kinetic constants k_1 and Q_e. The experimental data was poorly fitted to the pseudo-first-order model, except for the Fe-Si-1 MNP, where the correlation coefficient R^2 was 0.984. A high R^2 value indicates that the adsorption of oil droplets on Fe-MNP is appropriate for the pseudo-first-order model. However, the R^2 values for the oil adsorption for Fe-Si-2, Fe-Si-3, and Fe-Si-4 were relatively low, which signifies that they do not adhere to the pseudo-first-order model. The pseudo-second-order model (i.e., the kinetic model employed in the adsorption process) is commonly used to characterize kinetic equations dependent upon the adsorption capacity from the solution concentration [488]. The pseudo-second-order model is represented by equation (18). Figure 43b presents the regression analysis following equation (18). The experimental data were appropriate for the pseudo-second-order model. All examined Fe-

Si MNP had an $R^2 \sim 1$, suggesting that the adsorption method significantly favours this kinetic model.

As previously noted, the Fe-Si-1 MNP demonstrated fast adsorption kinetic for equilibrium, which was achieved after 1h. After this time, no further adsorption occurred because as the TEOS volume declined, additional surface area spots were accessible for adsorption, which increased adsorption values. This happened because of the saturation of all of the surface spots on the adsorbent by the oil particles, which produced an equilibrium condition between the adsorbed oil on the surface along with the mixture. [40] observed that the adsorption capacity of the Fe-Si MNP prepared with TEOS of 0.5mL reached a higher value of 186.0 ± 5 mg_{oil}/g_{MNP} compared with 86.0 ± 5 mg_{oil}/g_{MNP} for the Fe-MNP alone. Moreover, lower dosages of the TEOS may initiate an aggregation of the MNP. Thus, there can be less availability for the adsorbate (oil) efficient-binding sites to graft onto the surface. Given that, there was a reduction in the oil adsorption capacity for the MNP prepared with higher TEOS concentrations.

$$\frac{1}{q_t} = \frac{1}{K^2{}_2\, q^e{}_e} + \frac{t}{q_e} \tag{18}$$

Table 13. Kinetic parameters for the adsorbed oil on the developed Fe-Si MNP demulsifiers.

Kinetic models	Qe (mg/g)	K_1 (1/min)	R^2
Pseudo-first order			
Fe-Si-1	6. 817	0.0107	0.948
Fe-Si-2	0.4703	0.0118	0.899
Fe-Si-3	0.4101	0.0124	0.834
Fe-Si-4	1.230	0.0598	0.718

Kinetic models	Qe (mg/g)	K_1 (1/min)	R^2
Pseudo-second order	Qe (mg/g)	K_2 (1/min)	R^2
Fe-Si-1	5.652	0.288	0.999
Fe-Si-2	902.1	0	0.999
Fe-Si-3	1.387	0.229	0.998
Fe-Si-4	1.217	0.226	0.997

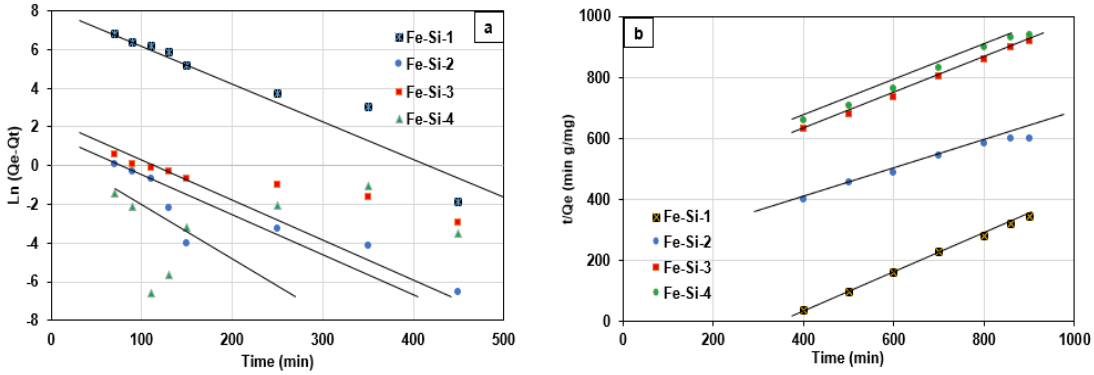

Figure 43. (a) Pseudo-first order, and (b) Pseudo-second order kinetic models for the adsorption process using 10 mg/L of the Fe-Si-1, Fe-Si-2, Fe-Si-3, and Fe-Si-4 MNP demulsifiers with a pH of 4 and temperature of 25℃.

6.7 Conclusion

This chapter developed a novel and efficient approach to synthesize the Fe-MNP covered with a silica layer at varying thicknesses following the Modified Stöber method. The significant advantages of this method include high yields, a short separation time, and easy preparation and handling of the magnetic nanoparticles. Moreover, the Fe-Si MNP can be regenerated by purification and recycled for successful use in the oil recovery process. The grafting of the magnetite nanoparticles (Fe-MNP) with the SiO_2 layer, morphologies, molecular structure, particle size, and roughness was examined and confirmed using different characterization methods, including TEM, scanning electron microscopy (SEM),

and x-ray spectroscopy (EDX). Even with small MNP concentrations, the as-synthesized Fe-Si MNP demulsifiers were successfully applied to remove oil from O/W-emul.

Furthermore, the chapter highlighted how the demulsification efficiency is low with high nanoparticle concentrations and high pH values. This is likely due to the nanoparticle's aggregation that decreases the active surface area and absorption capacity. Small-sized Fe-Si MNP significantly improved the oil recovery process, likely because of the high dispersion rate. Increasing the thickness of the silica layer simultaneously decreased the oil adsorption capacity, reduced the saturation magnetization (M_s), and ultimately decreased the demulsification efficiency. The as-prepared Fe-Si-1 were effective ($\%S_{oil} > 95\%$) for removing oil after 9 cycles. Lastly, the results indicated that the development of these nanoparticles presents an excellent method for recovering oil from oily-produced water.

6.8 Recommendations and Future Prospective

Many oil recovery process mechanisms using magnetic nanoparticles are not yet fully understood; further examination through rigorous scientific experiments should be conducted. However, the oil separation process for the functionalized nanoparticles may be helpful in the oil and gas industries and for biomedical applications. The findings in this chapter can be developed to provide a highly efficient and recyclable demulsifier that can be used for the demulsification process to reduce the process cost significantly.

CHAPTER 7: ENHANCED OIL RECOVERY USING HYPERBRANCHED POLYGLYCEROL POLYMER-COATED SILICA NANOPARTICLES

7.1 Introduction

The ever-growing development in the exploration and extraction of crude oil and gas is combined with the production of huge volumes of wastewater known as produced water (PW) contaminated with organic matter (hydrocarbons) and heavy metals [489, 490]. The presence/escape of these toxic and non-biodegradable contaminants in PW creates severe environmental impacts, energy resource losses, and human health [491, 492]. Therefore, it is crucial to design a sophisticated treatment, recovery, and reuse for these chemicals from the wastewater to prevent their release into the environment [493].

Various technologies have been employed for the treatment of PW and the recovery of valuable materials. These technologies have included: extraction [494], flocculation, precipitation [495], chemical demulsification [37, 496], adsorption [497], and membranes [498, 499]. However, most of these technologies generate additional harmful waste and face familiar issues for recovering the reagents, ultimately reducing their efficiency [500]. This chapter investigates an effective treatment process for wastewater and the reuse of valuable materials in the wastewater.

More recently, there has been ongoing development in research on the use of Fe_3O_4 magnetic nanoparticles (Fe-MNPs) to treat water and wastewater due to their superparamagnetic behaviour, dynamic morphology, and small size [501-503]. Unfortunately, though, at this time, possible dissolution, rust, and oxidation of the Fe-MNPs bound their ability to be used widely [504, 505]. To fix these issues and widen the area of applications, the surface modification of the Fe-MNPs and/or coating of the Fe-MNPs with specified functional groups or materials were recommended and extended

service life. With this improvement, functional substances and reagents can be added to the surface of the Fe-MNPs to facilitate the removal of contaminants while also maintaining the maximum separation efficiency [506, 507]. Furthermore, this practice could contribute to the recycling and reusing of the Fe-MNPs and lower the corresponding operating cost.

We recently showed that coating the Fe-MNPs with functional materials, such as silica, formed a protective layer without affecting the removal capacity or altering the separation process [40]. Nonetheless, the reported $\%\eta_{dem}$ of the prepared Fe-Si-MNPs was limited under a high $C_{oil,}$ and the capacity per gram of Fe-Si-MNPs was limited. Conversely, in other work, we synthesized and used hyperbranched polyglycerol (HPG) as an efficient demulsifier for the recovery of oil from oil in water (O/W) emulsions [37]. Moreover, various studies have indicated that HPG could modify and add active groups on the surface of the Fe-MNPs for effective wastewater treatment with minimal production of secondary contaminants [508, 509]. As such, it has been noted that adding polymer to the surface of the Fe-MNPs will increase the density of rich active groups that can be successfully used to eliminate heavy metal and/or organic materials from wastewater. Therefore, covering the surface of the Fe-Si-MNPs with chemical legends (i.e., functional groups) would help to improve the oil recovery performance and increase the capacity of the Fe-Si-MNPs (even with higher oil concentrations). The type and properties of the polymer determine the attachment characteristics and the targeted functional groups. Synthetic or natural polymers can be used in the oil recovery process. Natural biopolymers have the advantage of a low cost, extensive resources, and are biodegradable [510]. In contrast, the synthetic polymers contain polyvinyl alcohol, polyethylene glycol, polystyrene, polyacrylamide, and polypeptide polymers that can be used for the surface modification of the Fe-MNPs [511-513].

Our previous research experiments [151, 406] exemplified how both the Fe-Si-MNPs and HPG can effectively recover oil from O/W. However, the separation of HPG from the water medium was not effective, and the performance and capacity of the Fe-Si-MNPs require further improvements. Thus, this chapter offers a procedure to attach the chemically stable Fe-Si-MNPs to the HPG. The HPG was used to replace the multitude of materials that would otherwise be necessary, enhance the oil removal and recovery, maintain a simple and easy separation procedure, and increase the adsorption capacity at a high C_{oil}. In this context, the Fe_3O_4 nanoparticles were coated with a layer of silica and then attached with HPG to further enhance oil removal from the emulsion. The purpose of the silica is to protect the Fe_3O_4 nanoparticles and expand their stability. The resulting demulsifier (hyperbranched polyglycerol attached to Fe_3O_4-SiO_2 magnetic nanoparticles) was (denoted as PSiMNPs) and was characterized through various analytical methods (FTIR) and XPS) to verify its functional groups and structure.

Additionally, the mechanism, recyclability, and removal efficiency were evaluated. Therefore, this present chapter offers a novel technique for oil recovery from O/W emulsions using PSiMNPs. The effect of pH, C_{oil}, and C_{sur} on the $\%\eta_{dem}$ was investigated. The developed PSiMNPs can be easily separated via an external magnetic field and then successfully generated and reused for up to 15 cycles with stable performance (i.e., high $\%\eta_{dem}$) and high adsorption capacity. The new demulsifier provides an effective, simple, and environmentally friendly option for O/W emulsions.

7.2 Materials and Methods

7.2.1 Materials

All of the chemicals were purchased from Merck-Qatar in analytical grade and used as received. The chemicals included: glycidol ($C_3H_6O_2$, with a density of 1.11 g/cm^3 and a molecular weight of 74.08 g/mol), potassium methylate (CH_3OK, with a density of 0.95

g/cm^3 at 20°C and a molecular weight of 70.13 g/mol), and anhydrous dioxane (CAS Number: 123-91-9, with a density of 1.033 g/cm^3 and a molecular weight of 88.11 g/mol). The gasoline oil (95 Octane, with a density of 719.7 kg/m^3) was obtained from a local fuel oil supplier (WOQOd, Doha, Qatar). The polyethylene sorbitol ester surfactant (Tween-80) was purchased from Sigma Aldrich and applied for the O/W emulsion preparation. All of the solutions were synthesized using deionized water.

7.2.2 The Preparation of PSiMNPs Demulsifier

The PSiMNPs were prepared by attaching the HPG polymer to the Fe-Si-MNPs surface. Figure 44 highlights the stage of synthesis used in the production of the PSiMNPs demulsifier. In summary, the procedure consists of dissolving 0.5 g of Fe-Si-MNPs in 80 mL of toluene and 0.9 mmol of CH_3OK with the addition of 10 mL of anhydrous dioxane. Thereafter, 2 mL of $C_3H_6O_2$ was added dropwise throughout a 1 h time to the mixture with continuous stirring for 4 h. Finally, the produced material was cleaned with deionized water and then dried at 50°C.

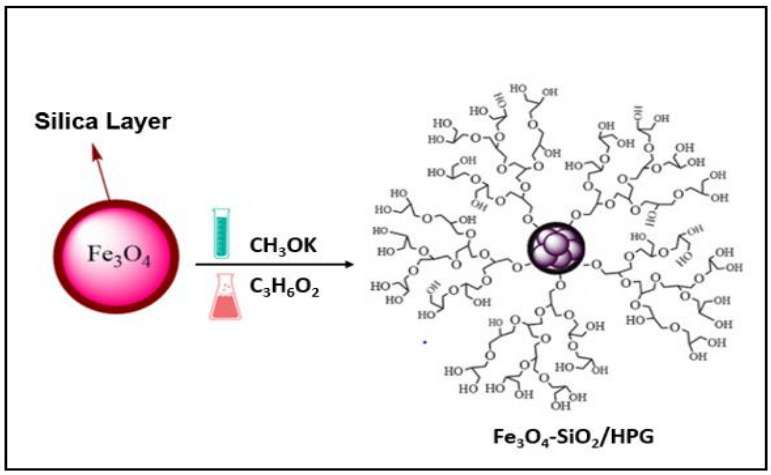

Figure 44. The preparation stages for developing the PSiMNPs demulsifier.

7.2.3 Synthesis of the O/W Emulsions

The O/W emulsions used in the tests were synthesized by mixing gasoline and deionized water to simulate the performance of the O/W emulsion in the reservoir. The emulsions were produced by dispersing 0.05 g of Tween-80 surfactant into a specified volume of deionized water and mixed in with a shear emulsifying homogenizer (model BRH1-100, USA) for 2 min at 3500 rpm speed. Thereafter, a specified gasoline oil concentration in the range of 100, 250, 700, 750, 1000, 2000, and 4000 mg/L was added drop by drop and mixed for 10-15 min with water to generate consistent O/W emulsions.

7.2.4 Characterization of the PSiMNPs

The surface morphology and the size of the PSiMNPs demulsifier were determined using transmission electron microscopy (TEM, Hitachi H-600, Japan). The crystallographic structure of the material was determined using x-ray diffraction (XRD, Minifix II Japan). The tests were conducted at 40 kV and 30 mA with a copper target using a Rigaku D/MAX-R diffractometer. The Fourier transform infrared (FTIR, PerkinElmer Spectrum 400, USA) spectra was achieved using KBr pellets with a spectrometer at room temperature. The thermal analysis experiments were conducted at a heating heat of 10 K/min using thermogravimetric analysis (TGA, TA Q-600, AUST) equipment with nitrogen as an inert gas. The magnetic hysteresis loops were evaluated at 300°K with the application of a vibrating sample magnetometer (VSM, Lakeshore 7407, US) with a magnetic field ranging from -20,000 Oe to 20,000 Oe. The carbon-hydrogen and nitrogen (CHN) analyzer (Thermo Scientific FLASH 2000 HT) was applied to assess the carbon, hydrogen, nitrogen, and oxygen contents. The analyzer uses a combustion process to break down substances into simple compounds, which are then measured.

The atomic ratio and binding energy on the surface of the demulsifier were examined using an x-ray photoelectron spectroscopy (XPS) gathered on a PHI-Quantera SXM system

(Perkin–Elmer Co., USA) with monochromatic Al Ka radiation (1486.6 eV) and C1 and C1s peaks were applied as an internal standard calibration peak at 284.8 eV. The electrophoretic properties of the nanoparticles (i.e., Z-potential values) were obtained with the electrophoretic light scattering instrument (Zetasizer Nano ZS, Malvern Instruments). The experiments were carried out at 25°C. The diameter was identified using dynamic light scattering measurements (DLS, Zeta PALS, Brookhaven Instrument Corp, US) to confirm the stability of the PSiMNPs demulsifier at various times and after different days.

7.2.5 Demulsification Experiments

The method used for the oil removal and recovery from the O/W emulsion incorporates the addition of a specified dosage of $D_{PSiMNPs}$ (2.5, 5.5, 7.5, 10, 30, 50, and 100 mg/L) to the 500 mL O/W emulsion under 2 min sonication with mixing at 3500 rpm for an additional 10 min. After that, the mixing was stopped for 10 min to allow oil droplets' adsorption onto the PSiMNPs. Then, the PSiMNPs-oil was removed using an external magnetic field, and the $\%\eta_{dem}$ was consequently assessed. The C_{oil} in the emulsion before and after the treatment was measured using the UV absorption technique. The procedure involves establishing a calibration curve between the total organic carbon (TOC) and C_{oil} in the emulsions [514, 515]. All tests were carried out in triplicate, and the average value and standard deviation (St.Dev.) at a 95% confidence level were used in reporting the data. The absorption of UV radiation @ 254 nm was linearly correlated to organic carbon (TOC) content in the solution following Beer's law. Quality assurance and the detection limit of the absorption technique were confirmed by performing frequent solvent extraction measurements. The procedure involves selecting random samples and extracting the oil from water into carbon tetrachloride to determine the oil content using an NDIR analyzer [516]. The results obtained from the extraction were compared with that of the absorption technique. Based on that, the detection limit of the C_{oil} measuring technique was estimated

to be 0.03± 0.005 wt% (St.Dev. ~1.3). All the experiments were performed at room temperature if not otherwise stated. The oil recovery process was studied at varying pH values, including 4, 7, and 10. The $\%\eta_{dem}$ was determined following equation (19):

$$\%\eta dem = \frac{C_{oil,i} - C_{oil,f}}{C_{oil,i}} \times 100\% \quad (19)$$

Where $C_{oil,i}$ (mg/L) and $C_{oil,f}$ (mg/L) are the initial and final C_{oil} before and after the addition of the PSiMNPs, respectively.

7.2.6 Recyclability of the PSiMNPs

The PSiMNPs were used in a series of experiments after regeneration to evaluate their efficiency and feasibility in the oil recovery under extended service life. The regeneration process involves mixing the PSiMNPs-oil with 20 mL of ethanol for 8 min to recover the oil. Then, the PSiMNPs were gathered using a magnetic field and cleaned with water. Finally, the regenerated PSiMNPs were reused for oil recovery in the subsequent 15 cycles.

7.2.7 Influence of Operational Parameters

The influences of operating parameters on $\%\eta_{dem}$ were investigated by conducting the tests at different $D_{PSiMNPs}$ of 2.5 mg/L, 5.5 mg/L, 7.5 mg/L, 10 mg/L, 30 mg/L, 50 mg/L, and 100 mg/L, C_{sur} in the range of 0.05 to 0.5 mg/L and C_{oil} in the range 100-4000 mg/L. In addition, the effect of pH (4, 7, and 10) and salinity (0.1 - 0.7 M NaCl) was studied at a constant $D_{PSiMNPs}$ of 10 mg/L. Furthermore, the effect of separation time on the process was examined at different times (2.5, 5, 7, 10, 20, 30, and 50 min).

7.2.8 Adsorption Studies

The equilibrium adsorption capacities (q_e), outlined in equation (20) for the Fe-Si-MNPs, HPG, and PSiMNPs have been assessed for C_{oil} in the range of 100 to 1000 mg/L and an adsorbent dose of 10 mg/L.

$$qe = \frac{(C_{oil,i} - C_{oil,e})v}{m} \quad (20)$$

Where $C_{oil,i}$ and $C_{oil,e}$ are the initial oil and equilibrium concentrations (mg/L), m is the mass of the demulsifier (g), and V is the volume of the solution (L). The adsorption kinetics was examined at C_{oil} of 500 mg/L and 300 °K. The oil adsorption isotherms were determined to be at pH 4 and 300°K. The adsorption experiments were replicated twice, with average values reported at a confidence level of 95%.

7.3 Results and Discussion

7.3.1 Characterization of the PSiMNPs Demulsifier

Figure 45a exemplifies the FTIR spectra of the Fe-Si-MNPs and the synthesized PSiMNPs. The peak at 3420 cm^{-1} was assigned to the –OH group and at 590 cm^{-1} to the Fe-O bond, which confirms the existence of Fe_3O_4 within the synthesized nano-particles as confirmed by [517]. The peak at 1090 cm^{-1} represents the Si-O-Si group confirming the presence of silica in the structure. The peaks observed at 3470 cm^{-1} and 2950 cm^{-1} (Figure 45a, line ii) were connected to the –OH and C-H aliphatic groups due to adding HPG. It should be noted that the peak 2950 cm^{-1} represents the polymerized structure of the C–H stretching, which was increased by adding HPG on the surface of magnetic nanoparticles. These results are in good agreement with the findings reported by [517], where similar peak intensities were observed at 3470 cm^{-1} and 2950 cm^{-1} after the functionalization of the HPG polymer to the nanoparticles. The differences between the FTIR spectra of the Fe-Si-MNPs and PSiMNPs confirm the formation and growth of branched structures consisting of a core Fe element covered with and attached to polymer legends as proposed in Figure 44.

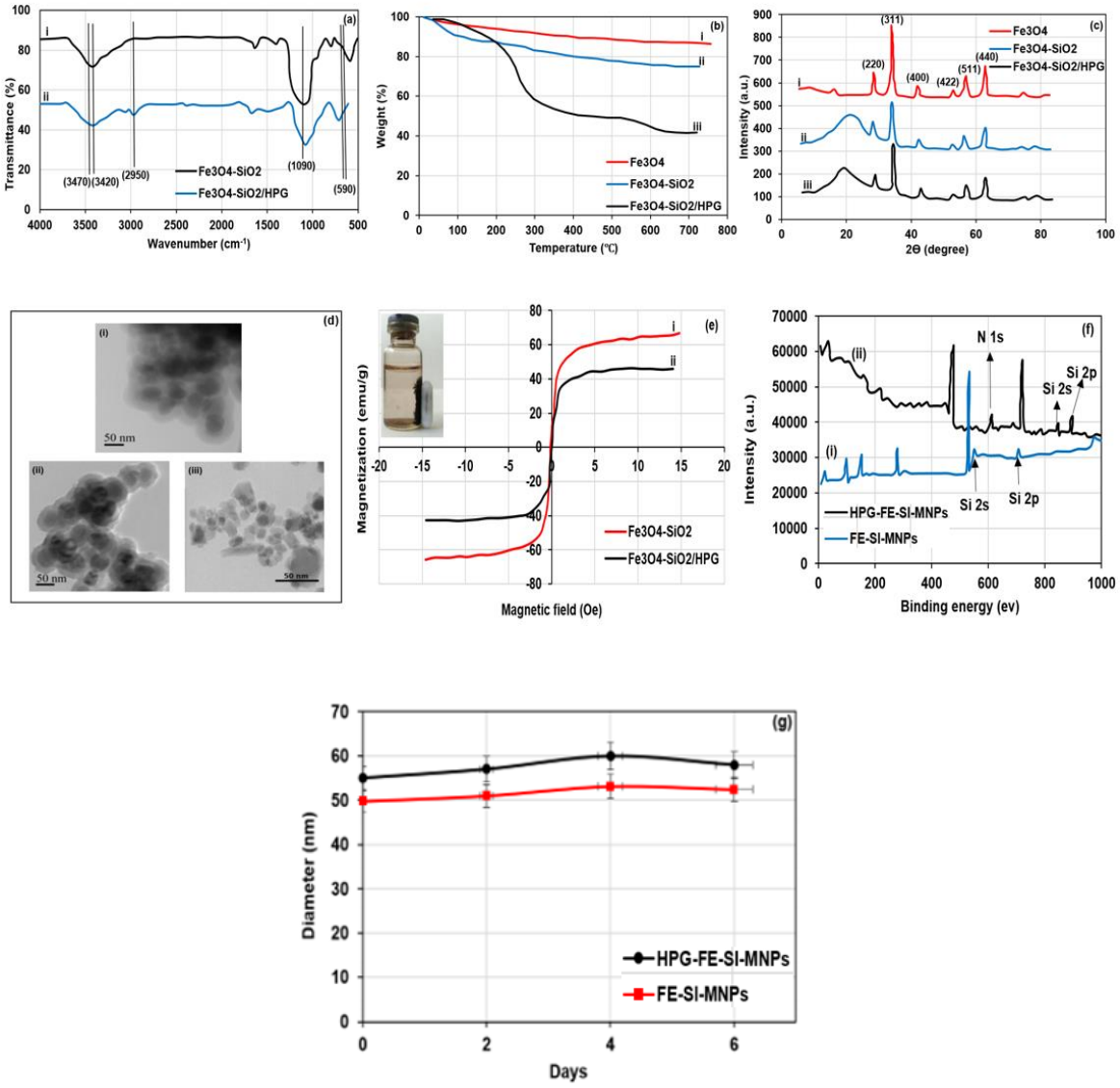

Figure 45. Characterization of the Fe-Si-MNPs and PSiMNPs (a) FTIR Spectra, (b) TGA thermograms, (c) XRD pattern, (d) TEM images, (e) magnetization curves of (i) Fe-MNPs (ii) Fe-Si-MNPs (iii) synthesized PSiMNPs demulsifier, (f) XPS spectra of (i) Fe-Si-MNPs (ii) PSiMNPs, and (g) the stability of the PSiMNPs in water measured by DLS.

Figure 45b presents the TGA analysis and the thermal degradation profiles of the Fe_3O_4 (i.e., Fe-MNP), Fe-Si-MNPs, and PSiMNPs. The TGA of the Fe-MNPs (line i) indicates a total weight loss of 4%, which is attributable to water particles evaporating from the Fe_3O_4 surface. This low weight loss suggests a stable MNPs structure under all of the studied temperatures. In contrast, for the Fe-Si-MNPs, the maximum weight loss was estimated to

be approximately 9%, higher than the weight loss of the Fe_3O_4. The rate of weight loss is relatively higher in Fe-Si-MNPs due to the loss of the SiO_2 amorphous structure (silica shell and functional groups), as exhibited in Figure 45b line ii. This trend occurs due to the loss of residual water adhering to the sample surface and could slightly reduce the functionalized nanoparticle's magnetic content and magnetic properties. The TGA of the PSiMNPs exhibited a three-time transitional phenomenon: (1) A slight decrease in the weight ~ 5% at a temperature ≤ 190 °C, which was aimed at the evaporation of water as well as the start of degradation of the HPG ligand attached to the surface of the Fe-Si-MNPs (Figure 45b line iii); (2) A moderate decrease in the weight ~ 23% with temperatures in the range 200-300°C. This moderate decrease in the PSiMNPs is associated with the degradation of the HPG polymer and (3) a stable and low weight ~ 3% for temperatures in the range of 300-500°C, which is linked to low material loss and stable Fe-Si-MNPs structure. Similar results were reported by He et al. [518] for their study of HPG coated Fe-MNPs, which were an efficient adsorbent to remove cationic dyes from water using an external magnetic field. The weight loss of the PSiMNPs sample from 100°C to 750°C exhibits a 38wt% suggesting that the HPG ligand effectively covered the surface of the Fe-MNPs.

The x-ray diffraction (XRD) was used to define the structural changes in the Fe-Si-MNPs after adding the polymer (i.e., PSiMNPs), as exemplified in Figure 45c. The PSiMNPs (line iii) exhibited numerous reflection peaks in the 2θ ranging between 20°-70°, comparable to the Fe-MNPs and Fe-Si-MNPs described by [519]. The diffraction peaks at line i were associated with (220), (311), (400), (422), (511), and (440), which fit into the Fe_3O_4 database in JCPDS (JCPDS card No. 19-0629) folder. Moreover, line ii in Figure 45c shows the Fe-Si-MNPs as core/shell pattern. The wide peaks at a slight diffraction angle indicated that the SiO_2 shells had an amorphous structure in reference to the JCPDS card No. 29-

0085. However, after adding HPG to the Fe-Si-MNPs core/shell, the large peak near 21° was moved to 19° due to the connection between SiO_2 and polymer legends (see line iii in Figure 43c); further work is required to confirm these observations.

The structure and size of the PSiMNPs were evaluated using TEM analysis, as shown in Figure 45d. In the previous chapter, the average size of the Fe_3O_4 as an MNP was determined to be in the range of 10-15 nm. After coating the Fe with the silica shell, the generated Fe-Si-MNPs core/shell structure exhibited an enhanced dispersion property and increased average particle size between 20-30 nm [446]. The results mentioned above support the results reported by [517, 520]. The average size of the PSiMNPs was evaluated using the same technique and found to be approximately between 35-50 nm, with a clear accumulation of the HPG branched legend attached to the surface of the Fe-Si-MNPs. Their research [521] presented a comparable size for the Fe-MNPs before coating within the range of 4-16 nm. The study examined the use of Fe-MNPs in biological treatment, which illustrated the high efficiency of the iron oxide magnetic nanoparticles and the effect of the coating layer on the structural and magnetic properties of the iron oxide [521].

Figure 45e exemplifies the magnetic properties of the Fe-Si-MNPs and PSiMNPs as determined by the vibrating sample magnetometer (VSM) analysis. The magnetization curves showed the superparamagnetic behaviour of all of the samples at room temperature. The Fe-Si-MNPs and PSiMNPs saturation magnetization (Ms) values were 66.7 and ~ 45 emu/g, respectively. The results indicated that the addition of the silica layer and the HPG to the Fe-Si-MNPs caused a slight decrease in the Ms. However, this decrease will not affect the separation efficiency of the new PSiMNPs by an external magnetic field. The carbon, hydrogen, and nitrogen content of the grafted Fe-Si-MNPs and PSiMNPs were verified using elemental analysis (CHN). The CHN tests indicated that the Fe-Si-MNPs contains 30.232 mg/g of C, 2.071 mg/g of H, and 0.1 mg/g of N. The elemental analysis of

PSiMNPs shows an increase in the amount of C and H to 36.9 mg/g and 4.98 mg/g due to the addition of the HPG to the surface of Fe-Si-MNPs. In addition, the EDX analysis showed that the Fe-Si-MNPs contain 12.9 wt% of Si, 43.9.1% of Fe, 41.3 % O, and 1.9% of N. Conversely, the PSiMNPs contain 10.1 % of Si, 34.4% of Fe, 22.1% C, 12.0 % O, 20.4% H, and 1.0 % N. The grafting of HPG polymer on the surface of Fe-Si-MNPs is evident by the increase in the carbon and hydrogen. Similar results in the carbon, hydrogen and nitrogen contents were reported by Shaabani et al. [522] during the synthesis and characterization of Cu, GA, and Fe-Si-MNPs, which were determined to be an efficient catalysts for preparing imidazole and benzodiazepines in biomedical applications.

Figure 45f highlights the effective grafting of the HPG polymer onto the Fe-Si-MNPs surface as determined using the XPS bands after the surface modification. As exhibited in Figure 45f line i, the Fe-Si-MNPs contain C 1s at 285 eV, O 1s at 530 eV, and Fe at 710 eV. The N 1s element peak does not appear on this scale. However, the PSiMNPs exhibited a peak at a binding energy of 400 eV because of the presence of the N 1s signal. Moreover, the Si 2p signal at 100 eV and the Si 2s signal at 150 eV reliably indicate the presence of Tetraethyl orthosilicate (TEOS) coating (Figure 45f line ii) [523]. After the HPG functionalization, the O 1s/C 1s intensity improved, illustrating that the surface polymerization enhanced the O content on the MNP surface [522]. This is important to note as it concerns the chemical structure of the HPG.

The stability of the Fe-Si-MNPs and PSiMNPs was evaluated using DLS measurements. Figure 45g presents the Fe-Si-MNPs and PSiMNPs after 6 days in water. The hydrodynamic diameters of the two demulsifiers showed no major diameter change throughout the 6 days. A significant lack of change indicates the high stability level in the water. Moreover, after this extended storing period, the demulsifiers were kept for months in the water at 4°C and still exhibited the same fresh properties.

7.3.2 Demulsification Using PSiMNPs Demulsifier

The demulsification test was used to investigate the behaviour of the PSiMNPs demulsifier during the demulsification process, as well as the oil recovery from the O/W emulsion interfacial film. Two emulsions with a C_{oil} of 100 mg/L were formed and stored for 6 h below ambient conditions. The observations indicated that the emulsions remained stable without any discernible phase separation. After that, $D_{PSiMNPs}$ of 2.5, 5.5, 7.5, 10, 30, 50, and 100 mg/L of Fe-Si-MNPs and PSiMNPs were added to the O/W emulsion Sample 1 and Sample 2, respectively, under mechanical shaking. After approximately 5 min or less, the emulsion color changed and broke the emulsion stability in both samples. Moreover, it was observed that the tiny oil floccules combined and created larger oil droplets. This reaction led to a fast attachment to the demulsifier after a maximum of 5 and 3 min to the added Fe-Si-MNPs and PSiMNPs, respectively. After that, a very light-yellow color was observed with the freshly produced water phase in Sample 1. This color may be attributed to the oil droplet separation because of the Fe-Si-MNPs in the water phase. Conversely, magnetic separation was applied to Sample 2, and the PSiMNPs demulsifier separated along with the absorbed oil droplets at the base of the mixture. The assembled water mixture was then removed and placed into separate bottles. Each sample was then examined to determine the efficiency of the Fe-Si-MNPs and PSiMNPs after removing the oil from the O/W emulsion. The $\%\eta_{dem}$ were found to be 72.4%, 80.3%, 84.1%, and 92.7% for the tests carried out with 2.5, 5.5, 7.5, and 10 mg/L of Fe-Si-MNPs. On the other hand, tests carried out with PSiMNPs showed a $\%\eta_{dem}$ of 77.3%, 85.2%, 88.2%, and 95.3% using similar dosages. Although the Fe-Si-MNPs were an effective and affordable chemical demulsifier, the PSiMNPs exhibited favourable results under the same conditions, confirming the importance of adding the HPG for a higher oil removal rate. Moreover, it was observed that the $\%\eta_{dem}$ improved by correspondingly raising the demulsifier dosage

>10 mg/L, which enabled the PSiMNPs to reach up to 95.3% 96%, and 98.09%, and the Fe-Si-MNPs to achieve 93%, 95%, and 96% for dosage of 30, 50, and 100 mg/L for O/W emulsion samples with a C_{oil} of 100 mg/L. In contrast to the Fe-Si-MNPs, the PSiMNPs demonstrated a significant efficiency in the demulsification process for O/W emulsions. They accomplished a higher oil removal of ~95.3% using a $D_{PSiMNPs}$ of 10 mg/L with a similar C_{oil}.

Additionally, the significant $\%\eta_{dem}$ achieved by the PSiMNPs is attributed to the magnetic response's unique surface properties, monitored stabilization, and emulsion separation. The magnetic nanoparticles (MNPs) have a great magnetic separation efficiency, while the HPG functional groups on the surface offer extensive binding sites for oil. This unique hyperbranched structure of the PSiMNPs is very favourable to capturing nano-sized particles in the arrangement of good dispersion. Furthermore, it can efficiently improve oil separation and emulsion stability [524].

Other factors that contributed to the $\%\eta_{dem}$ are the hydrophobic and hydrophilic polar oxygen functionality present on the outer edge of the Fe-Si-MNPs, as well as the affinity of the HPG to absorb oil. Taken together, these factors make the Fe-Si-MNPs an excellent material for emulsion applications, including demulsification procedures and stabilization of the emulsion systems [525, 526]. Furthermore, in the emulsion mixture, the gasoline O/W emulsion's stability depends upon the electrical double layer repulsive force between the oil droplets and the protection film [3]. Thus, reducing the repulsive force or damaging the viscoelastic film is necessary for the demulsification to remain stable in the O/W interfaces.

The Fe-Si-MNPs is a hydrophobic nanoparticle that can be dissolved during the water phase [527]. When the Fe-Si-MNPs are inserted into the O/W emulsion, they can be equally

spread into the water phase under high mechanical agitation. After that, the Fe-Si-MNPs in the emulsion can attach to the oil particles when it reaches the O/W interfaces [468]. Because of the high attraction between the Fe-Si-MNPs and oil, the oil droplets cortical protective film in the emulsion are partially broken with the collision between oil and water, which creates a non-continuous protection film at the interface of the oil and water. As a result, part of the covered oil droplets will move away from the partial broken protecting film to combine with other oil droplets. The tiny oil droplets begin to combine and accumulate to convert into larger droplets of oil creating an oil phase and becoming adsorbed by the demulsifier.

The dispersed oil droplets were effectively removed from the emulsion by adsorption on the surface or the attachment to polymer legend in the PSiMNPs. Although the Fe-Si-MNPs achieved a $\%\eta_{dem}$ of 72.4%, 80.3%, 84.1%, and 92.7%, the PSiMNPs achieved 77.3%, 85.2%, 88.2%, and 95.3% using a $D_{PSiMNPs}$ 2.5, 5.5, 7.5 and 10 mg/L, respectively, for the tests carried out with a C_{oil} of 100 mg/L. Thus, the PSiMNPs were able to achieve higher oil recovery rates in comparison to the Fe-Si-MNPs alone. A comparison between the demulsification efficiency of Fe-Si-MNPs and PSiMNPs at different dosages and C_{oil} was presented in Table 14.

Table 14. Comparison between the demulsification efficiency of Fe-Si-MNPs and PSiMNPs at different dosages and C_{oil}.

C_{oil} (mg/L)	Dosage (mg/L)	$\%\eta_{dem}$ of the Fe-Si-MNPs	$\%\eta_{dem}$ of the PSiMNPs
100	2.5	72.4%	77.3%
100	5.5	80.3%	85.2%
100	7.5	84.1%	88.2%
100	10	92.7%	95.3%
100	30	93%	95.3%
100	50	95%	96%
100	100	96%	98.09%

7.3.3 Demulsification Performance Using PSiMNPs Demulsifiers

7.3.3.1 Demulsification Performance Using PSiMNPs at Different Oil Dosages (C_{oil})

Figure 46a presents the $\%\eta_{dem}$ at various C_{oil} in the range of 100-4000 mg/L for the experiments conducted with $D_{PSiMNPs}$ in the range of 2.5-100 mg/L. The high hydrophobicity and paramagnetism properties of the PSiMNPs is an excellent demulsifier for recovering oil from O/W emulsions [27]. Following the addition of the PSiMNPs to the O/W emulsion, the oil particles attached to the nanoparticles and removed from the mixture. After that, the adsorbed oil droplets combined with the PSiMNPs aggregation to facilitate the manganic separation. The developed PSiMNPs achieved a $\%\eta_{dem}$ exceeding 95%. The $\%\eta_{dem}$ attained at a very small $D_{PSiMNPs}$ of 10 mg/L was 99.45%, 98%, 97.01%, 96.5%, 94.6%, 94.3%, and 93.07% for the experiments conducted at C_{oil} of 100, 250, 700, 750, 1000, 2000, and 4000 mg/L, respectively. The results confirmed that an efficient $\%\eta_{dem}$ was obtained using $D_{PSiMNPs}$ in the range of 2.5 to 100, which indicates that a small demulsifier amount is enough to adsorb and recover all the oil from the O/W emulsion.

When the concentration of $D_{PSiMNPs}$ increased within the range of 30-50 mg/L in the O/W emulsions with a C_{oil} in the range of 0-800 mg/L, the demulsification efficiency correspondingly improved. As such, with a high $D_{PSiMNPs}$, the removal rate achieved higher than 98%, after which the demulsification efficiency remained steady, and the demulsification process took approximately 10 min to recover oil drops from the O/W emulsion. The application of the Fi-Si-MNP exemplified an effective separation ~ 88.5 ± 0.2% compared to the Fe using a small demulsifier dosage of 10 mg/L. Additionally, the removal rates were 93.4 ± 0.2%, 90.8 ± 0.2%, 90.24 ± 0.2%, and 88.5 ± 0.2% for tests carried out using a high C_{oil} of 500, 1000, 2000, and 4000 mg/L, respectively. For these rates, the demulsification was achieved in 5 minutes, about half the time it took using the

Fe. In contrast, the developed PSiMNPs demulsifiers achieved a demulsification efficiency exceeding 95 ± 0.1% using a demulsifier dosage of 2.5 mg/L. Further, the completed demulsification process took approximately 3 min, indicating that the PSiMNPs have the greatest efficiency for the demulsification of the O/W emulsions.

7.3.3.2 Effect of PSiMNPs Dosages on Demulsification Efficiency

The experimental results indicated that the efficiency of the demulsification process was affected mainly by the $D_{PSiMNPs}$ that were added to the O/W emulsion mixture. The $\%\eta_{dem}$ reached ~99.45% using $D_{PSiMNPs}$ of 100 mg/L. Further, a $\%\eta_{dem}$ of 96%, 98.09%, and 95.3% was achieved with the application of fewer $D_{PSiMNPs}$ of 50 mg/L, 30 mg/L, and 10 mg/L, respectively. However, the removal rates started to decrease when the $D_{PSiMNPs}$ decreased to 2.5 mg/L, 5.5 mg/L, and 7 mg/L, which reached 88.2%, 85.2%, and 77.3% for emulsions with a C_{oil} of 100 mg/L. Moreover, as presented in Figure 46b, the PSiMNPs achieved a higher demulsification capacity than the Fe-Si-MNPs. Given that, both high and low $D_{PSiMNPs}$ exhibited a greater $\%\eta_{dem}$ in comparison to the results obtained with the Fe-Si-MNPs.

7.3.3.3 Demulsification Performance at Different Reaction Times

Figure 46c illustrates the influence of the reaction time ranging from 2.5 to 50 min on the $\%\eta_{dem}$. The PSiMNPs exhibited excellent behavior in the oil recovery process from the O/W emulsion in a short period compared to the Fe-Si-MNPs at a low dosage of 10 mg/L. This is due to the high dispersion rate, high adsorption capacity, and fast separation within a short time [422]. As exemplified, the oil removal improves by increasing the reaction time to 10 min, after which the reaction time does not affect the $\%\eta_{dem}$. However, the results indicated that with a reaction time of ~1 min, the separation of O/W was more effective, as it achieved 98.4%. This reaction suggests that the developed PSiMNPs demulsifier has excellent performance for O/W removal.

7.3.3.4 Demulsification Performance Using Different Surfactant Concentrations

The O/W emulsions consist of surfactant substances that are responsible for O/W stability and reduce O/W interfacial tension. Thus, the behavior of the PSiMNPs demulsifier will be influenced by the existence of these surfactants [423]. As such, it is essential to examine the impact of these material amounts on the demulsification process. The stability of the emulsion was observed to be a function of the C_{sur} in the range of 0.05-2 g/L. At a low C_{sur} of 0.05 g/L, the oil was removed within 1 min, with high development in the emulsion stability. The emulsion stability began at a C_{sur} value of 0.05 g/L, after which it remained constant with no phase separation for an extended period of 24 h. [250] reported comparable tendencies for a brine solution that included diesel oil stabilized using aluminium stearate and xanthan gum.

Moreover, Figure 46d presents the $\%\eta_{dem}$ as a function of different surfactant dosages. The experiments were conducted with three surfactant concentrations (C_{sur} = 0.05, 0.1, and 0.5 g/L) using a $D_{PSiMNPs}$ of 10 mg/L with O/W emulsion samples with C_{oil} in the range of 10-1000 mg/L. However, the $\%\eta_{dem}$ was only slightly reduced by rising the C_{sur} in the O/W emulsions. It was previously noted that the O/W emulsion oil droplets could graft onto the magnetic demulsifier due to the attractive force of the hydrophobic bond [419, 424]. As such, the presence of the surfactant material improved the oil droplet dispersion, increased the surface tension forces, and decreased the magnetic demulsifier absorption. As well as the improvement in the oil droplet's hydrophobicity, the interaction between the surfactant and the oil droplets will decline with the electrostatic repulsion. These factors will consequently influence the behavior of the adsorption of oil into the magnetic demulsifier.

In this chapter, it was observed that the PSiMNPs could interrupt the physical and chemical bonds among the oil surfactants, which keeps the oil emulsified in water to achieve an oil removal rate and a high $\%\eta_{dem}$. The development of the $\%\eta_{dem}$ is likely associated with the significant PSiMNPs demulsifier surface area, the attraction forces of the oil-PSiMNPs, and the effective separation process that utilizes an external magnetic field. Moreover, as highlighted in Figure 46d, the $\%\eta_{dem}$ reduced with an increase in the surfactant concentrations in the O/W emulsions. The results indicated that the demulsification efficiency reached a value of 98.8% with a C_{sur} 0.05 g/L and 96.3%, 94.2% when the surfactant concentrations increased to 0.1 and 0.5 g/L, respectively, with a C_{oil} of 10-1000 mg/L and a PSiMNPs dose of 10 mg/L.

7.3.3.5 Demulsification Performance at Various Salinity Values

The emulsion salinity was analyzed because of its effect on the performance of the demulsification process [528]. The increase in the efficiency of the demulsification behaviour of the PSiMNPs demulsifier was examined at a pH 4, according to the rise in the salinity of the produced O/W emulsion. Figure 46e demonstrates how as the O/W emulsion salinity enhanced, the demulsification efficiency correspondingly improved. Moreover, the demulsification efficiency was tested with the addition of 10 mg/L PSiMNPs to the emulsion samples with differing oil concentrations in the range of 100-4000 mg/L and salinity range of 0.1, 0.3 0.5, and 0.7 M NaCl. As observed, when the O/W emulsion salinity improved to 0.7 M NaCI, the oil removal rates increased from 95.2% to 98.4% for samples with an oil concentration of 500 mg/L. This was likely due to the “salting-out” impact, which decreased the stabilizing surfactant's hydrophilicity. As a result, the “salting-out” effect reduced the O/W emulsion interfacial tension [356].

7.3.3.6 Demulsification Performance at Different pH

The interfacial activity of the MNPs was responsive to the pH value mixture. As such, the pH performance of the Fe-Si-MNPs was primarily assigned to the degree of deprotonation of its hydroxyl groups [529]. The influence of the emulsion pH on the demulsification behaviour of the PSiMNPs was investigated. Figure 46f presents the different pH levels of 4, 7, and 10. The results indicated that the $\%\eta_{dem}$achieved high values of 98.5%, 97.9%, and 95.5% with pH values of 4, 7, and 10, respectively, with C_{oil} in the range of 0-1000 mg/L as well as $D_{PSiMNPs}$ of 10 mg/L. It was observed that with low pH levels, the PSiMNPs were less hydrophilic. This reaction occurs as the PSiMNPs move into the oil phase through the absorbed oil droplets after demulsification. However, some of the MNPs attached to the HPG polymer were first separated at the bottom of the mixture (when applying the magnetic separation). After that, the MNPs began to move to the O/W interface or float into the removed water phase when the pH value was low (i.e., 4), which led to better residual oil concentrations [468]. The results indicated that the PSiMNPs achieved a greater demulsification efficiency in the acidic conditions than the alkaline conditions (i.e., high pH), which indicated that the surface activity level of the PSiMNPs raised with more acidic conditions [530]. Further, the demulsification efficiency improved visibility when the pH slowly decreased. Thus, the low pH value of 4 was the optimum condition for the demulsification process for the PSiMNPs demulsifier.

The pH has a considerable impact on the stability of the emulsion and the demulsification process. The electrostatic repulsion between the Fe-Si-MNPs and the oil particles increases by increasing the pH of the O/W emulsion. Therefore, for effective separation, it is essential to decrease these electrostatic repulsion forces between the oil droplets and the PSiMNPs and thus enhance the $\%\eta_{dem}$. The O/W emulsions have a negative charge at low pH conditions, while the PSiMNPs exhibited positively charged, functional groups.

Consequently, the oil particles can be adsorbed on the PSiMNPs surface through the electrostatic attraction force resulting in increasing the $\%\eta_{dem}$ [467]. In the neutral and higher pH conditions, the positive surface charge of the Fe-Si-MNPs decreased, and the interfacial adsorption was reduced; hence the stability of the emulsion was being reduced, and e the $\%\eta_{dem}$was also negatively affected. In addition, the Fe-Si-MNP's absolute zeta potentials at low pH are highly favourable compared to neutral and higher pH, which indicates a reduction in the electrostatic repulsion between the Fe-Si-MNPs and O/W emulsions [40].

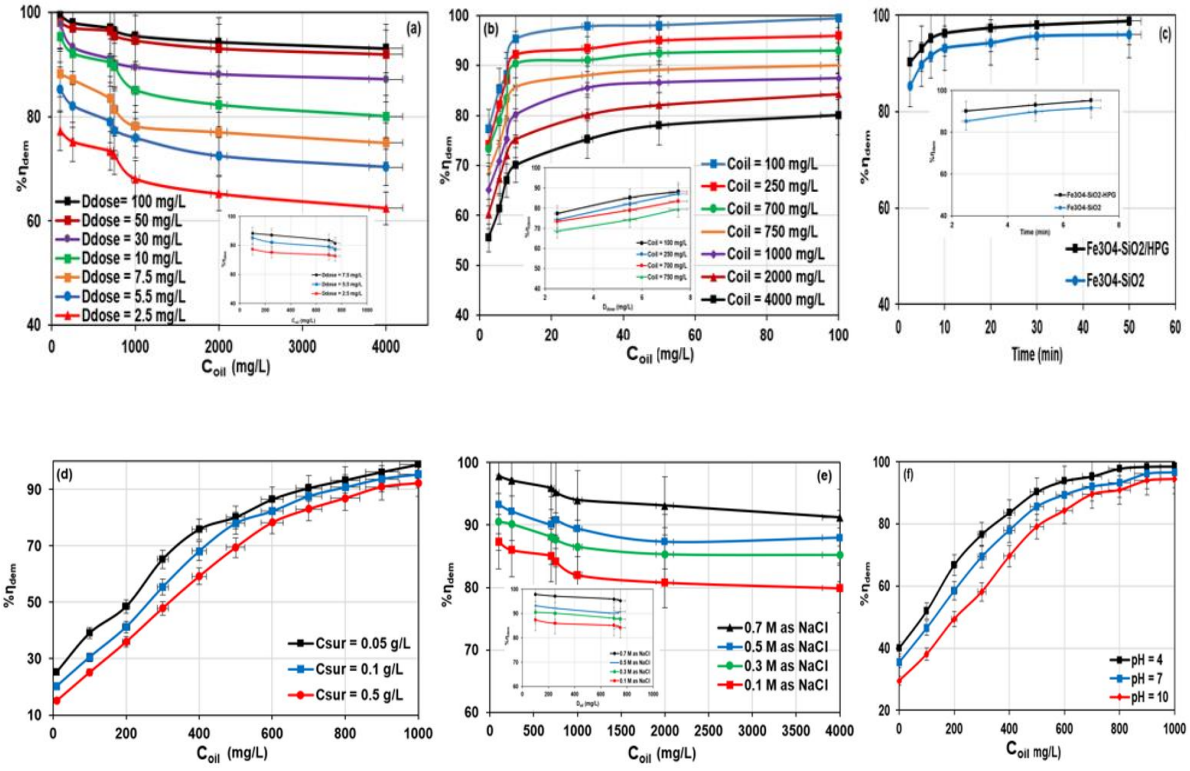

Figure 46. The $\%\eta_{dem}$ (a) at different C_{oil}, (b) at different demulsifier doses ($D_{PSiMNPs}$), (c) as a function of reaction times, (d) at different surfactant concentrations, (e) at different salinity, and (f) at varying pH levels.

7.3.3.7 Influence of Zeta Potential on the Demulsification Performance

The particle adsorption onto the interface of the O/W droplets appeared to be strongly associated with the particle's charge [531]. The zeta potential values of several demulsifiers used in the emulsion water phase were measured. A significant increase in the zeta potential (without considering the sign) occurred when the nanocomposites were added to the emulsion mixture. This reaction indicates a successive increase in the repulsive forces between the particles. The zeta potential values of all of the nanoparticles are >30 mV, which indicates that the nanocomposites are all stable [532]. Typically, in emulsion mixtures, at the interface, the electrostatic repulsion between the charged particles improves when they are stable at an oil/water interface [533]. Thus, to create a steady mixture, the particle's electrical charge should not be extremely high, which indicates why high-charged demulsifiers (i.e., Fe-MNPs, Fe-Si-MNPs, and PSiMNPs) cannot transfer at the surfaces of the oil droplets. Initially, the MNPs in the aqueous suspension avoid the precipitation instigated by the van der Waals because of the charged carboxylic acid group's electrostatic repulsive and hydration forces on their surfaces [534]. At the beginning of the process, the particle's high negative potential hinders the adsorption process because of the powerful hydration forces and electrostatic repulsion. However, to encourage the adsorption of the particles on the O/W interface, the amount of their surface charge must be decreased [535]. Thus, the water-soluble Fe-MNPs were grafted with a thin silica layer to produce the Fe-Si-MNPs, then grafted with the HPG polymer (to create the PSiMNPs) to reduce the surface charge and enhance the hydrophobicity.

The TEM images presented in Figure 45d demonstrate the average size of the Fe-Si-MNPs around 20-30 nm and 35-50 nm after grafting with the HPG polymer. The hydrophobicity of the Fe-Si-MNPs and the PSiMNPs improved as their zeta potential is $\geq \pm$ 25 mV, both of which were greater than the Fe-MNPs. The demulsifiers are highly hydrophobic as their

zeta potential values are -21.5, -25.3, and -29.6 mV for the PSiMNPs, Fe-Si-MNPs, and Fe-MNPs, respectively. The PSiMNPs demulsifier exhibited the greatest stability. When the zeta potential is high ($\geq \pm 25$ mV), the repulsive forces go above the attractive forces to distribute the particles. After that, the system deflocculated, and the oil removal rate improved. Their research [536] indicated that when the zeta potential exhibited low values ($\leq \pm 25$ mV), the attractive forces exceeded the repulsive forces. As a result, the particles were agglomerated, which caused flocculation and then negatively impacted the demulsification efficiency.

7.4 Mechanism of the Oil Recovery Process

The oil recovery method from the O/W emulsion typically depends on the addition of surface-active composites that change the interfacial properties, such as the interfacial tension (IFT), mechanical power, elasticity, and thickness interfacial films. These surface-active composites can improve the oil droplet's coalescence and flocculation in the emulsion. However, if the MNPs are added to the emulsion, the demulsifying effect occurs as the remaining drops graft with the interfacial active nanoparticles. As such, the method of the oil recovery process relies on the electrostatic attraction forces between the oil droplets and the MNPs. The negatively charged oil droplets from the O/W emulsion can be grafted onto the positively charged functional groups on the nanoparticle’s surface with the electrostatic attraction force of the hydrophobic bond. Many of the separation methods for the MNPs include the dispersion of the nanoparticles within the medium. After that, the targeted chemical, ion, surface, or functional group is adsorbed onto the surface of the nanoparticles. While the developed nanoparticles coated with the HPG polymer have exhibited high efficiency for oil recovery, the whole mechanism through which the demulsifiers enhance the demulsification rate is not yet identified. Several methods for the oil recovery process are suggested, including interfacial tension decrease, disjoining

pressure and mobility management, wettability alteration, viscosity management, and the demulsification process.

The MNPs have a high specific surface area, and the recovery of particles is assigned to their reaction to the magnetic field. The structure, surface charge, and nanomaterial create the distinctive properties of the MNPs, which indicate a high possibility for their ability to separate oil from produced water. Oil separation from produced water using the demulsifiers mentioned above impacts the electrostatic adsorption and the capacity for the MNPs to be magnetically separated. The hydrophobicity and positive surface charge of the MNPs provide an appropriate interaction within the oil. Moreover, the most common method for nanoparticle addition to the O/W emulsions is initially dispersing the particles into a water solution. The ultra-sonification demonstrated the highest results for nanoparticle dispersion, specifically those that aggregate when collected (such as the Fe-MNPs). With subsequent dispersion, the nanoparticles mixed with the emulsion for 10 or more. After that, a strong magnet was used on the solution to ensure that a removed layer was produced. The negatively charged dispersed oil remains in the positively charged MNPs surface, and the nanoparticles with the adsorbed materials are separated from the medium.

7.5 Reusability of the PSiMNPs Demulsifier

As the PSiMNPs exhibited high superparamagnetic characteristics, it was regenerated and reused after the demulsification process using an external magnetic field for the separation process. During the removal process, it was observed that the oil was adsorbed using a PSiMNPs demulsifier and then separated at the base of the mixture, which occurred because of the magnetic field. Ethanol was used to eliminate the adsorbed oil from the PSiMNPs demulsifier as the adsorbed oil (i.e., gasoline) may stay on the surface of the PSiMNPs after the demulsification process.

As exemplified in Figure 47, the reusability tests have effectively reused a total of 15 times. The PSiMNPs removed the oil from the water phase in the initial nine cycles to accomplish a demulsification efficiency of ~95.3%. However, the efficiency of the PSiMNPs began to decline after the tenth cycle, which achieved ~ 96.1%. Moreover, during the 15th cycle (the last cycle), the oil separation from the water phase decreased, and the efficiency declined to 89.19% with a C_{oil} of 100 mg/L. The ethanol was able to separate the adsorbed oil particles that were grafted onto the surface of the PSiMNPs after several more cycles of the process. The produced PSiMNPs demulsifier was recycled multiple times for the demulsification process due to its high superparamagnetic features. The recyclability of the PSiMNPs is cost-effective and creates a less negative environmental impact than other non-reusable chemical demulsifiers used.

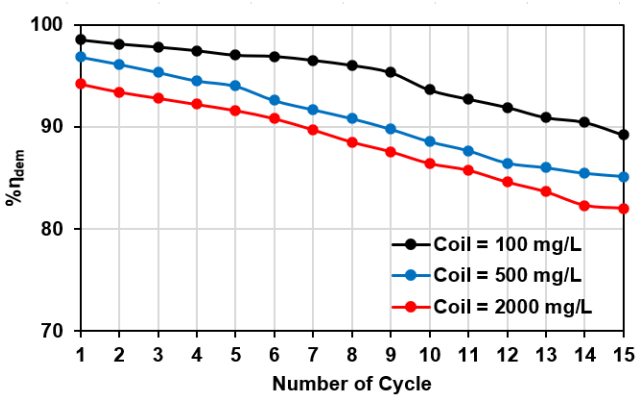

Figure 47. The $\%\eta_{dem}$ of the PSiMNPs demulsifier at different cycles and different C_{oil}.

7.6 Oil Adsorption on the PSiMNPs Demulsifier

7.6.1 Kinetics Discussion

The adsorption kinetic of the oil recovery from the O/W emulsion was checked against pseudo-first-order (PFO) (equation 22) and pseudo-second-order (PSO) model (equation 23).

Values for the q_e, k_1, and K_2 were obtained from the linear regression of equation (22) and equation (23). The PFO resulted in a poor fit (R^2= 0.488) and was rejected. Figure 48 demonstrates the adsorption kinetic of the oil recovery from the O/W emulsion following PSO.

$$\log(q_e - q_t) = \log q_e - \frac{k_1 t}{2.303} \quad (22)$$

$$\frac{t}{q_t} = \frac{1}{k_2 {q_e}^2} + \frac{t}{q_e} \quad (23)$$

Where q_e (g/mg) represents the equilibrium adsorption capacity, q_t (g/mg) signifies the adsorption rate for oil on the PSiMNPs at a time (t min), and k_1 and k_2 indicate the PFO and PSO rate constants, respectively. The PSO kinetic model provided a good fit for the experimental data and had a correlation coefficient (R^2) equal to 0.97. The regression analysis resulted in an average K_2 (R^2~ 0.96) of 0.0169 g/mg. min and q_e = 22.57 g/mg

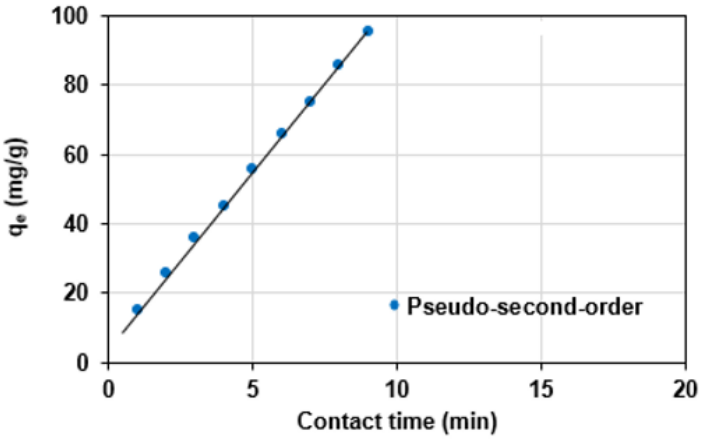

Figure 48. The oil's adsorption kinetic curve on the PSiMNPs uses pseudo-second-order, Conditions: 500 mL O/W emulsion and DPSiMNPs of 10 mg/L.

7.6.2 Adsorption Isotherm

After the modification of the HPG polymer on the surface of the Fe-Si-MNPs, the oil was adsorbed and attached to the PSiMNPs demulsifier with the hydrophobic interaction

between the oil droplets and the PSiMNPs. Typically, the equations for the Langmuir and Freundlich isotherms are applied to define the adsorption of the liquid-solid phase. Langmuir model, equation 24, assumes that adsorption occurs on the solid surface

$$\frac{C_e}{q_e} = \frac{C_e}{qmax} + \frac{1}{bqmax} \quad (24)$$

Where q_e (g/mg) is the equilibrium adsorption capacity of oil, C_e (mg/L) is the concentration of oil at the equilibrium, b (mg/L) is the Langmuir constant which demonstrates the comparative attraction of adsorbent-adsorbate (PSiMNPs-oil) in the adsorption process, and q_{max} (g/mg) is the maximum adsorption capacity of the PSiMNPs. Further, the q_{max} and b values can be found using the slope and the intercept, respectively, in a linear plot of C_e/q_e versus C_e. Freundlich model, equation 25, assumes that multilayer adsorption occurs on a heterogeneous surface.

$$Lnq_e = Ln\, k_F + \frac{1}{n} LnC_e \quad (25)$$

Whereby K_F and n represent experimental constants, which indicate the capacity and strength of the adsorption, respectively.

Adsorption results did not fit well with the Freundlich isotherm and were thus ignored. Figure 49 demonstrates how the Langmuir model successfully fit the experimental results with a q_{max} of 192.8 g/mg, b of 28.06 mg/L, and R^2 =0.994 for the test conducted with a C_{oil} of 900 mg/L.

Consequently, it was observed that the oil adsorption process on the developed PSiMNPs surface exemplified a multilayer accumulation. This suggests that the functionalization of the HPG polymer on the surface of the MNP significantly enhanced the oil adsorption, thus increasing the adsorption capacity.

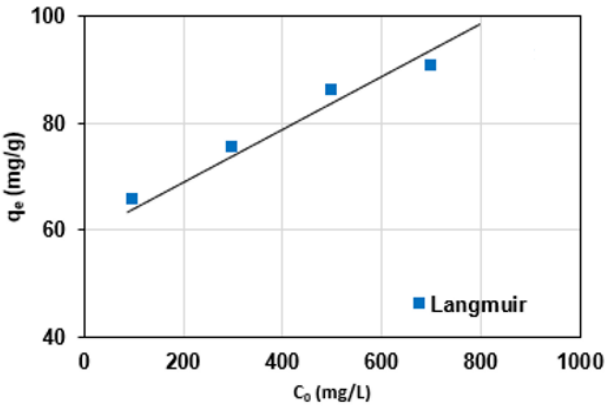

Figure 49. The adsorption isotherms for oil on the PSiMNPs. Conditions: 500 mL O/W emulsion and $D_{PSiMNPs}$ of 10 mg/L.

7.7 Recyclability of PSiMNPs Demulsifier as an Adsorbent

The FTIR spectra of fresh PSiMNPs, HPG polymer, and oil-PSiMNPs were used to compare and identify the connection between oil and PSiMNPs or HPG (see Figure 50). After the oil adsorption occurred on PSiMNPs, a peak at 813 cm^{-1} was observed on the spectra of PSiMNPs, which was associated with the connection between oil and PSiMNPs. As exemplified in Figure 50, line (d), the peak at 813 cm^{-1} was missed after the oil removal from the demulsifier using ethanol. The observed results showed that the oil is attached to the surface of PSiMNPs via chemisorption that could be easily separated by ethanol. On the other hand. The HPG spectra did not show any change suggesting that the connection between oil and HPG is via physical attachment and entrapment with the branched structure.

In summary, the oil is attached to the PSiMNPs in two different mechanisms that lead to higher capacity. Further work is required to explain and explore the trends. The equilibrium adsorption of oil on the PSiMNPs was evaluated after the 15^{th} cycle and was found to be 96.08 mg/g, which is similar to the initially developed demulsifier (97 mg/g).

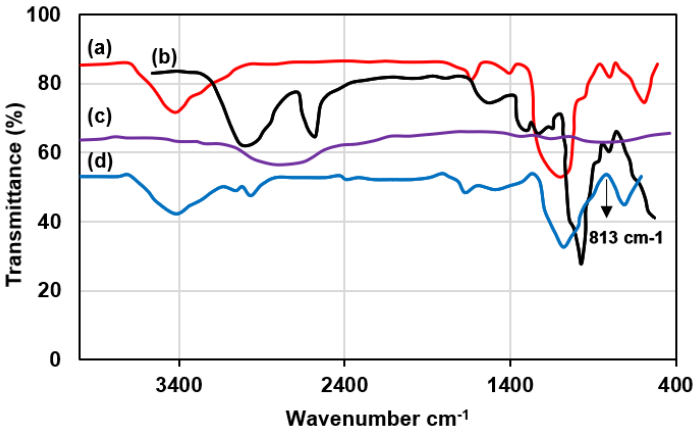

Figure 50. FTIR spectra of (a) PSiMNPs, (b) PSiMNPs after oil adsorption, (c) HPG polymer, and (d) PSiMNPs regenerated with ethanol.

7.8 Comparison Between the Efficiency of the Fe-MNPs, Fe-Si-MNPs, and PSiMNPs Demulsifiers in Oil Adsorption

Chapter 5 [396] tested the efficiency of the Fe-MNPs and the Fe-Si-MNPs in the oil adsorption and oil recovery process using varying dosages of Fe-MNPs and Fe-Si-MNPs (10, 30, 50, and 100 mg/L). The average Q_{max} values were in the range of 186 ± 5 to 35 ± 5 mg/mg for Fe-Si-MNPs and 86 ± 5 to 23 ± 5 mg/mg for Fe-MNPs using MNPs concentrations in the range of 10-100 mg/L. Therefore, the kinetic of the oil removal by the Fe-Si-MNPs follows the Langmuir and Freundlich isotherms, as it has the greatest adsorption capacity and a higher kinetic constant than the Fe-MNPs. Moreover, the maximum adsorption capacity values for the Fe-Si-MNPs were 1.2-fold higher than the Fe-MNPs because of the higher surface, high adsorption attraction to oil, ability to form the surface area. Further, the values of the 1/n for the Fe-Si-MNPs were ≤ 1 (ranging from 0.26 ± 0.03 to 0.41 ± 0.07) and in the range from 0.75 ± 0.02 to 0.71 ± 0.04 for Fe-MNPs dosages in the ranges of 10-30, 30-50, and 50-100 mg/L, which indicates the high capability of the adsorption process. Based on these values, the 1/n value for the Fe-Si-MNPs is two times lower than that of the Fe-MNPs, which suggests that the Fe-Si-MNPs have a greater oil

removal capability. However, after adding the HPG polymer to the Fe-Si-MNPs (i.e., PSiMNPs), the results indicated that the equilibrium adsorption capacity reached 192.8 g/mg. As such, the adsorption capacity of the PSiMNPs significantly improved and has a higher order of magnitude compared to the Fe-MNPs and the Fe-Si-MNPs, even at a high C_{oil}.

The kinetic of the demulsification process using the Fe-MNPs demulsifiers was examined in chapter 4, which presented the application of the Fe-MNPs in the oil recovery process [537] using PFO and PSO models. Unfortunately, though, the experimental data for the Fe-MNPs did not appropriately fit with the PFO, except for the high MNPs concentration (100 mg/L) with an R^2 of 0.984. A high R^2 value implies that the oil adsorption on the Fe-MNPs adhered to the PFO. On the other hand, the oil adsorption on the MNPs at concentrations of 10, 30, and 50 mg/L have relatively low R^2 values, which suggests that they do not follow the PFO model. The Fe-MNPs kinetic fits the PSO for all examined concentrations with an R^2 of ~ 1, indicating that this adsorption method supports this kinetic model strongly. Moreover, a high Fe-MNPs dosage of 100 mg/L exemplified fast adsorption kinetic, though, for the equilibrium process, it took an extended period (approximately 1 h) [537]. Further, the kinetic of the demulsification process applying the developed PSiMNPs follows PSO with a high kinetic constant of 0.0169 g/mg. min.

The above comparison concludes that the addition of HPG polymers to the Fe-Si-MNPs developed a novel and efficient demulsifier that can recover high volumes of oil from water emulsions and be applied at a large scale in the petroleum industry. Therefore, the proposed demulsifier can decrease the cost of the demulsification process within the petroleum industry. Furthermore, the characteristics of PSiMNPs can lessen the hazard of contaminating the environment owing to the demulsifier's ability to be recycled reused several times in the demulsification process. Besides, the developed PSiMNPs demulsifier

exhibited an excellent adsorption capacity for the oil in the O/W emulsion, which was connected to the solubilization of the HPG.

7.9 Conclusions and Recommendations

The PSiMNPs demulsifier was produced by performing surface functionalization of the Fe-Si-MNPs to the HPG polymer. The properties and characteristics of the produced PSiMNPs were studied using various characterization analyses. The results indicated that the prepared PSiMNPs demulsifier with essential oxygen functionalities was effectively coated with the Fe-Si-MNPs and exhibited high superparamagnetic performance. Furthermore, the demulsification experiments exemplified how adding small dosages of PSiMNPs to the O/W emulsion achieved a high demulsification efficiency of ≥ 90% in 5 min for emulsion samples with an oil concentration of oil 500 mg/L. Moreover, the demulsification behaviour of the PSiMNPs was excellent compared to the Fe-Si-MNPs as the suspended small oil droplets that were grafted onto the PSiMNPs were able to be easily removed from the water phase by applying magnetic separation using an external magnetic field.

Furthermore, the demulsification process optimizations were conducted to study the impact of oil concentration, demulsifier dose, pH, and salinity, and considerable results were shown. Further, the recyclability tests for the demulsifier exemplified how the PSiMNPs can be reused up to 15 times for the demulsification process. The results indicated that the proposed demulsifier could decrease the cost of the demulsification process within the petroleum industry. Furthermore, the characteristics of PSiMNPs can lessen the hazard of contaminating the environment due to the demulsifier's ability to be recycled and reused several times in the demulsification process.

After grafting the HPG, the Fe-Si-MNPs exhibited an excellent adsorption capacity for the oil in the O/W emulsion, which was connected to the solubilization of the HPG. Following

the Freundlich model, the adsorption of oil onto the PSiMNPs exhibited a higher adsorption capacity. The equilibrium adsorption capacities were 192.8 mg/g at a high C_{oil} of 900 mg/L using the Langmuir and Freundlich models. Moreover, the kinetic studies were examined using the pseudo-second-order model with an R^2 value of 0.99, which was more efficient than the pseudo-first-order model, which exhibited a K_2 of 0.0169 g/mg. min. As such, the results of this study confirm the oil adsorption onto the HPG and MNPs surface and thus onto the produced PSiMNPs demulsifier. Because of the accessibility of the Fe-Si-MNPs, the ease of attachment with the HPG polymer, and the simple magnetic separation, the PSiMNPs are a favourable adsorbent for the adsorption of various contaminants found in water environments.

CHAPTER 8: A NEW INSIGHT INTO THE SEPARATION OF OIL FROM OIL/WATER EMULSION BY FE_3O_4-SIO_2 NANOPARTICLES

8.1 Introduction

In general, the primary and secondary methods for oil recovery are ineffective, and the techniques are often complicated. Therefore, much attention has been given to efficient new technologies [503, 538]. For example, nanotechnology has been studied to enhance oil recovery from reservoirs [128, 539]. Approximately only one-third of primary oil can be generated through initial and secondary techniques. The residual oil remains in the pores of the reservoir rock due to interfacial forces and the surface [494, 538]. The oil can be uprooted by decreasing the capillary forces that inhibit the oil motion in the reservoir pores [540, 541]. The total effectiveness of each oil production method contains macroscopic and microscopic efficiencies [542]. The former is ascribed to the oil motion on the pore level, and the latter is associated with the amount of fluid replaced in the reservoir [543].

A micro model is a synthetic two-dimensional porous medium that mimics the pore-scale porous medium [544]. The required power to push the tiny, trapped hydrocarbon drops in the throat pores is caused by the capillary force, which reduces corresponding wettability alterations or IFT [495, 545]. In contrast, the nanoparticles offer a distinctive method to manage oil recovery [103, 546]. The nanoparticles have specific features that provide the required characteristics, including stability at high temperature and pressure conditions [547], chemical reactivity, high specific area, and effective surface properties, and more environmentally friendly in comparison to other chemical substances [548, 549], reduce the precipitation of oil [540]. Furthermore, the appropriate sizes (ranges from 1-100 nm) let them push the oil in the pores of the reservoir rock and remove oil without blockages [550] and alter the fluid properties causing high adsorption capacity and thus high mobility ratios [551].

A review of the relevant research literature indicates that various studies have been conducted using nanoparticles to improve the oil generation conditions from reservoirs. For example, Ogolo et al. (2012) observed that specific nanoparticles, including iron oxide and silica nanoparticles, can increase oil production and oil recovery rates using ethanol. Additionally, Ogolo et al. indicated that these nanoparticles could enhance oil recovery efficiency by reducing the IFT, alternating the wettability and penetrability, decreasing oil viscosity, and decreasing the movement ratio [13]. Suleimanov et al. (2011) examined the application of metal NP nanofluids (Fe_2O_3, Fe_3O_4, FeO, and SiO_2) in the oil production process. They indicated that a nanoparticle-surfactant scheme could improve the oil production rates to greater than 35%.

In comparison, the oil production rates were 17% in a scheme that only included surfactants which ascribed to the decrease in the IFT in the existence of the nanoparticles [421]. Similarly, [496, 552] examined the productivity of iron oxides and silicon NPs by evaluating the contact angle and IFT. They observed a significant reduction in the surface tension and a more remarkable improvement in oil production by applying the silicon NPs. Moreover, Wei et al. used a functionalized nanofluid to enhance the oil generation from the oil reservoirs. It was highlighted that the modified NPs dispersed well in 1 wt % brine forming active groups that change the dynamic interfacial tension (oil-nanofluid) and achieve high oil recovery rates reached more than 85% [553].

Additionally, [155] examined the productivity of floating mixtures with hydrophilic silica NP. The researchers described a decrease in the IFT of oil and water in the NPs and how the solid surface becomes water-wet. The oil recovery rate approximately increased by 5% with the addition of the nanoparticles. Lastly, [554] studied the improvement in the emulsion stability before the influence of the different NPs, including the iron oxide and silica NPs in two-dimensional micromodel with the structure of a real reservoir rock. The

results demonstrated an ability for the NPs to improve the emulsion layer thickness and the flow ratio. The remaining oil became emulsified through the injection of stabilized emulsions-surfactant-nanoparticles. They indicated that specified emulsions could generate up to 40% of the oil in the oil recovery process.

In this chapter, the effect of a novel nanocomposite on enhanced oil recovery from reservoirs is examined utilizing a two-dimensional micromodel taken from the real formation of the reservoir rock. The results showed that the NPs initiate various EOR methods according to their separate chemical and physical structures. The developed nanoparticles include several nanoparticles. The synergistic effect of nanoparticles in improving effective mechanisms of oil generation was detected in the case of Fe_3O_4@SiO_2 NPs. The performance of the Fe_3O_4@SiO_2 and the other nanofluids (seawater, Fe_3O_4, and SiO_2) in the enhanced oil recovery process is assessed and compared with other flooding scenarios.

8.2 Experimental Approaches

8.2.1 Chemicals

Ammonia (28 wt%), Tetraethyl Orthosilicate (TEOS), and Ethanol were purchased from Sigma Aldrich without further purification. The magnetite nanoparticles (Fe_3O_4) and the silica nanoparticles (SiO_2) were bought from Sigma Aldrich company in analytical grade and used as received, without further purification. Table 15 presents the overall characteristics of the magnetite nanoparticles (Fe_3O_4) and silica nanoparticles (SiO_2). The crude oil came from a reservoir in southern Sudan. Its fluid characteristics, assessment findings, and compositions of Saturate, Aromatic, Resin, and Asphaltene (SARA) are outlined in Tables 15 and 16. The crude oil resin and asphaltene concentrations were 2.6% and 7.7% (wt%), respectively, indicating its colloidal instability index (CII) value is

approximately 0.9. However, for the asphaltene thermodynamic compounds, the oil was unsteady and vulnerable to sedimentation.

8.2.2 Characteristics of Formation Water and Seawater

Table 18 outlines the characteristics and structure of the formation water for a reservoir in Sudan and the injected seawater. However, the nanoparticles used in the oil recovery process were synthesized with deionized water.

Table 15. The nanoparticle's properties.

NP	Purity (%)	Average (mean) diameter (nm)	Surface area, (m^2/g)	Density (g/cm^3)	Color	Structure	Chemical properties
Magnetite (Fe_3O_4)	98	40 ± 3.04	30-70	7.874	Blackish brown	Spheral	Amphoteric
Silica (SiO_2)	99.8	28.9 ± 3.01	570	2.65	White	pored	Acidic
Fe_3O_4@ SiO_2	99.5%	45 ± 3.52	296	2.77	Dark brown	Spheral	Acidic

Table 16. Applied crude oil properties.

Oil gravity °API	Density at 25°C (g/mL)	Viscosity at 25°C (cP)	Structure of SARA, (wt%)			
			Saturates	Aromatics	Resins	Asphaltenes
20.5	0.9250	140	40.9	48.8	7.7	2.6

Table 17. Crude oil composition.

Element	C_2	C_3	i-C_4	n-C_4	i-C_5	n-C_5	C_6	C_7	C_8	C_9	C_{10}	C_{11}	C_{12+}
Conc mole%	0.5	0.7	0.48	0.5	0.6	0.59	7.6	7.2	6.4	5.0	5.7	5.1	60

Table 18. The reservoir water and seawater properties and composition.

Water type	Composition of ion, (ppm)							TDS (mg/L)	pH
	Na^+	K^+	HCO^{3-}	Ca^{2+}	Mg^{2+}	Cl^-	$SO4^{-2}$		
formation water	64,440	1190	990	7440	1580	122,950	430	202,1	6.2
seawater	18,800	730	230	1300	1550	300	3380	26,15	7.4

8.2.3 Preparation of Fe_3O_4@SiO_2 NPs

A modified Stöber process was used in the previous chapter [555] to prepare the Fe_3O_4 magnetic nanoparticles functionalized with silica NP by dispersing approximately 0.5 g of Fe_3O_4 in 25 mL of an aqueous mixture. This solution was subsequently added to a flask (three-neck round-bottom flask) under mixing with vigorous mechanical stirring with the ethanol (100 mL) and ammonia solution (28 wt%) of 1.0 mL for 15 min at room temperature. After that, tetraethyl orthosilicate (TEOS) (0.5 mL) was added to the mix, and the reaction was left to maintain the mechanical mixing for 6 h at room temperature. The generated Fe_3O_4@SiO_2 NP were collected using an outside magnet and then cleaned 10 times using ethanol and dried at 70 °C for 8 h.

8.2.4 Characterization Methods of Fe_3O_4@SiO_2 NPs

The sample morphology and particle size of the Fe_3O_4@SiO_2 NP were tested applying transmission electron microscopy (TEM, Hitachi H-600, Japan) working at 200 KV. The scanning electron microscope (SEM) analysis was performed using a Hitachi-S100 scanning electron microscope. The Fourier transform infrared (FTIR, PerkinElmer Spectrum 400, USA) spectra were obtained with a spectrometer applying KBr pellets at room temperature. The magnetization experiments were conducted at room temperature using a vibrating sample magnetometer (VSM Lakeshore-7407).

8.2.5 Statistical Analysis

The TEM image and their size distribution of the Fe_3O_4 and the $Fe_3O_4@SiO_2$ were analyzed for their size changes (before and after surface modification) using the student t-test given by statistical software Minitab 14. The oil recovery results were judged based on standard deviation and one-way analysis of variance (ANOVA). The test was conducted to verify statistical differences in the reported oil recovery rates at a significance level of 5%. The statistical analysis was performed using Prism GraphPad statistics software (Version 7.04, USA).

8.2.6 Application of Glass Micromodel in the Oil Recovery Process

The patterns applied are from visualized rock surface structures or synthetic patterns such as the reservoir rock pores and throats. The current scheme was created using CorelDraw software. To draw the design on the glass, corrosion-resistant glue was used. Once the glue bonded to the glass, the pattern was inscribed utilizing a laser. Consequently, the glue-coated glass was placed into hydrofluoric (HF) acid. As such, the HF acid was applied at varying time intervals to provide the appropriate corrosion. Initially, for 3 min the glass was placed into the acid and then washed for 10 min with water to eliminate the residual acid from the glass. Following that, the glass was placed into the acid for an additional 3 min and then gently cleaned with water for another 10 min. In the third stage of the design process, for 4 min the glass was placed into the acid and then cleaned for 15 min using high-pressure water. Lastly, the micromodel was placed back into the acid for an additional 4 minutes and subsequently washed in water for 4 minutes to eliminate the residual acid. After that, the micromodel was placed into a high-temperature furnace to ensure that the two glass portions were concurrently affixed. Table 5 presents the general micromodel characteristics.

Table 19. The physical characteristics of the glass micromodel.

Wide (cm)	Length (cm)	Pore Dia. range (µm)	Throat Dia. (µm)	Porosity (%)	Permeability (D)
0.8	4	50-600	200	50	5

8.2.7 Experimental Arrangement of Glass Micromodel

Figure 51a presents the scheme for evaluating the behaviour of the nanoparticles. To inject the seawater and nanoparticles (Fe_3O_4, SiO_2, and Fe_3O_4-SiO_2) at very low rates, a Quizix pump was used. The operational rate was set to 0.6 mL/h to mimic the porous medium's applied fluid laminar flow. A camera was placed at the top of the micro model to take photos and record saturation differences and phase movement at various periods (for 1 min each). The picture assessment captured the rate of oil generation. The volume of oil remaining in the micromodel was determined using ImageJ software. The unoccupied space volume (Vp) was simply achieved, and the oil recovery factor was estimated following equation 26 below:

$$F_R = \frac{\text{Vremoved}}{\text{VT}} = \frac{\text{VT} - \text{Vremained oil}}{\text{VT}} \quad (26)$$

Where F_R represents the oil recovery factor; V removed is the oil volume removed after flooding from the micromodel; V remained oil is the oil volume remaining after flooding in the micromodel, and Vt is the total oil volume included in the throats and pores when the micromodel is filled with oil. In addition, the pendant drop method was implemented to evaluate the contact angle between the oil and glass and the wettability alterations (Figure 51b).

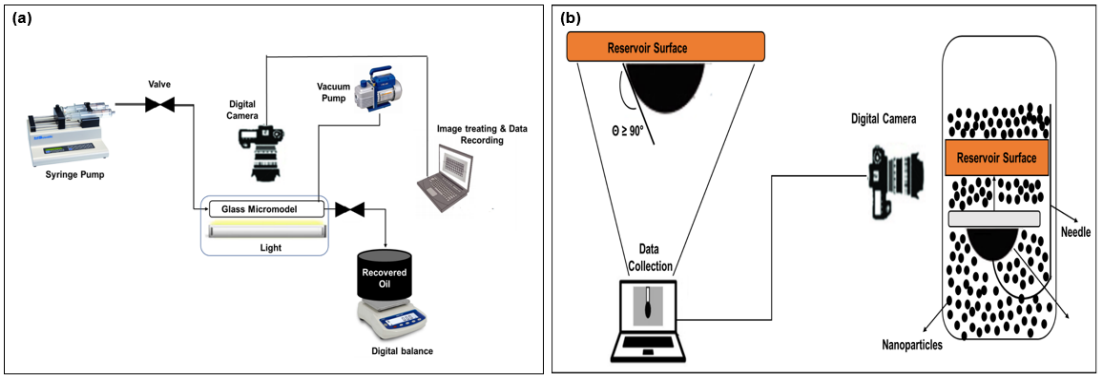

Figure 51. (a) Representation view of the glass micromodel setup [540, 556]. (b) Wettability assessment using the pendant drop method [557].

8.2.8 Injection Methods

The procedure for evaluating the differing injection methods of nanoparticles into reservoirs is outlined below.

1. Initially, the micromodel was washed with distilled water (DW) and acetone. Then, the micromodel surface was adjusted to oil-wet with 0.02 M stearic acid ($C_{18}H_{36}O_2$) and normal heptane (C_7H_{16}).
2. The injection of formation water was achieved at a rate of 0.6 mL/h. Then, full dosage of formation (Pore Volume (PV) = 2) was inserted into the micromodel.
3. For saturating the micromodel, oil was added at 0.6 mL/h.
4. The seawater and nanoparticles (Table 20) were injected at 0.6 mL/h. After that, the recovery factor and EOR methods were evaluated. However, it is essential to highlight that these nanoparticles are produced with deionized water.

Table 20. Replacing nanofluids applied during the tests.

Replacing fluid	NP amount (mg/L)	Viscosity (cp)
Seawater	-	1
Silica (SiO_2)	10	1.2
Magnetite (Fe_3O_4)	10	1.15
Fe_3O_4@SiO_2	10	1.19

8.3 Results and Discussion

8.3.1 Fe_3O_4@SiO_2 NP Characterization Analysis

8.3.1.1 TEM Analysis

The microstructure and morphology of the magnetite (Fe_3O_4) and magnetite/Silica (Fe_3O_4@SiO_2) NP were analyzed via transmission electron microscopy (TEM). Figure 52 exemplifies the TEM images of the two nanoparticles. As demonstrated in Figures 52a and 52b, spherical nanoparticles with the proper distribution and a mean particle size of ~40.0 ± 3.04 nm were observed. After grafting the Fe_3O_4 with the silica (Figure 52c and 52d), the size of the Fe_3O_4@SiO_2 NP slightly increased to ~45 ± 3.52 nm. The particle exhibited a properly-characterized core/shell structure with light difference silica shells and dark disparity cores of Fe_3O_4. This indicates that the Fe_3O_4 NP was effectively grafted with the silica shell [558]. TEM analysis of the Fe_3O_4 NPs and Fe_3O_4@SiO_2 NPs was measured in this study and compared with the values reported by Wang et al. [559]. The mean particle sizes for the Fe_3O_4 NPs and Fe_3O_4@SiO_2 NPs are about 40 ± 3.04 nm and 45 ± 3.52 nm, respectively. The mean particle sizes were statistically accepted based on the 95% confidence level of the measurements on more than 200 particles selected randomly during the analysis.

The core/shell structure of Fe_3O_4@SiO_2 nanoparticles was clearly shown. The experimental results showed that the surfaces of Fe_3O_4 nanoparticles were fully covered with SiO_2 shells, and the thickness of the silica layer was about 6 nm. Thus, fe_3O_4 nanoparticles are presented as dark dots and covered with an asymmetric SiO_2 shell.

8.3.1.2 SEM Analysis

The scanning electron microscope (SEM) examined the surface morphology, particle size distribution, agglomeration state of the particles. Figure 53 presents the typical SEM images of the magnetite (Fe_3O_4) and magnetite/Silica (Fe_3O_4@SiO_2) nanoparticles. The uncoated Fe_3O_4 nanoparticles with appropriate dispersion have a rough surface and a mean particle size of approximately 40 ± 3.04 nm (Figures 53a and 53b). These results are compatible with the TEM analysis. As demonstrated in Figures 53c and 53d, the Fe_3O_4@SiO_2 nanoparticles maintained similar morphological characteristics to the Fe_3O_4 NP, though they exhibit a significantly smoother surface and greater particle size (around 45 ± 3.52 nm). This difference is due to the surface functionalization with the silica shell layer [522].

Moreover, a non-aggregation was observed, which was consistent with the TEM images. Similarly, Wang et al. [559] showed that single Fe_3O_4 nanoparticles were aggregative due to their dipole-dipole interactions. After coating with silica, the aggregation of the magnetic nanoparticles was reduced significantly, and the dispersibility was increased due to the repulsion forces. The particles are almost spherical and had an overall mean diameter similar to those obtained by TEM analysis (40 ± 3.04 nm and 45 ± 3.52 nm) for the Fe_3O_4 nanoparticles Fe_3O_4@SiO_2, respectively.

8.3.1.3 Infrared Spectra (IR) Analysis

Figure 54a presents the IR bands of magnetite (Fe_3O_4) and magnetite/Silica ($Fe_3O_4@SiO_2$) nanoparticles. The adsorption peak at 590 cm^{-1} was assigned to the Fe-O bond, which confirms the presence of Fe_3O_4 nanoparticles. The bands correlated to 3431.1 cm^{-1}, 1635.3 cm^{-1}, and 1384.3 cm^{-1}, respectively, have been allocated to adsorbed water's O-H expanding, bending, and deforming vibrations. The peaks at 472.7 cm^{-1} and 956.4 cm^{-1} were assigned to the Si-O bond bending vibration and the Si-O-H extending vibration, respectively. Conversely, the peak at 1088.8 cm^{-1} matches the irregularity widening vibration of the Si-O-Si, which indicated that the SiO_2 was effectively coated onto the surface of the Fe_3O_4 nanoparticles [560].

8.3.1.4 VSM Analysis

Figure 54b illustrates the magnetization analysis of the magnetite (Fe_3O_4) and magnetite/Silica ($Fe_3O_4@SiO_2$) nanoparticles. For the Fe_3O_4, the magnetic saturation (Ms) value is 58.110 emu $g^{-1,}$ and the coercivity (Hc) is 45.245 Oe. The magnetic saturation value was reduced to 33.479 emu/g for the $Fe_3O_4@SiO_2$ nanoparticles because of the silica layer on the Fe_3O_4 NP surface. Moreover, the corresponding coercivity (Hc) was reduced to a value of 41.684 Oe. The corresponding coercivity (Hc) values for the Fe_3O_4 and $Fe_3O_4@SiO_2$ microspheres were low and less for the theoretical value ($Hc \leq 50Oe$) for the superparamagnetic molecules ranging between (29-30 Oe), which suggests the presence of well-formed superparamagnetic properties [561].

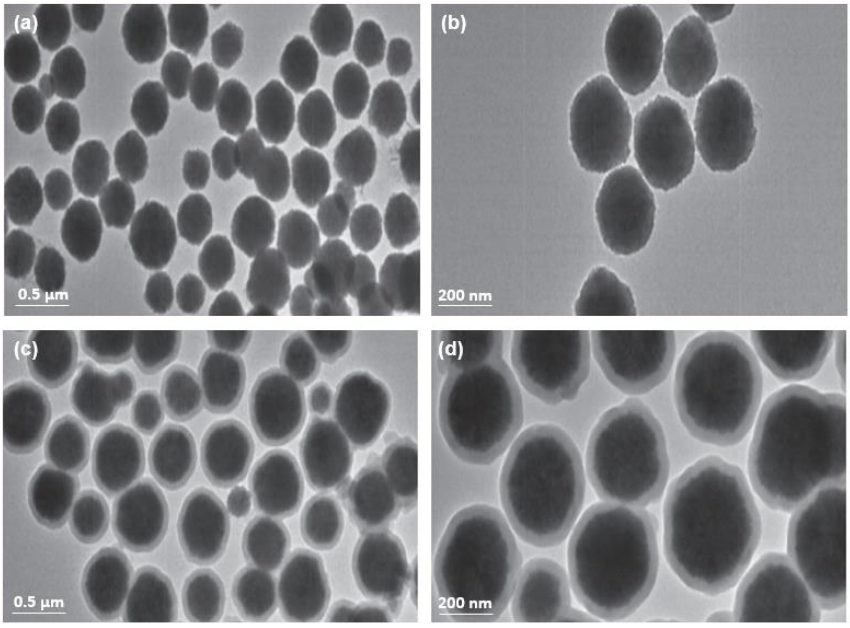

Figure 52. TEM images of (a) Fe_3O_4 NP at low enlargement (100 KX) (b) at high enlargement (200 KX) (c) Fe_3O_4@SiO_2 NP at low enlargement (100 KX) (d) Fe_3O_4@SiO_2 NP with high magnification (200 KX).

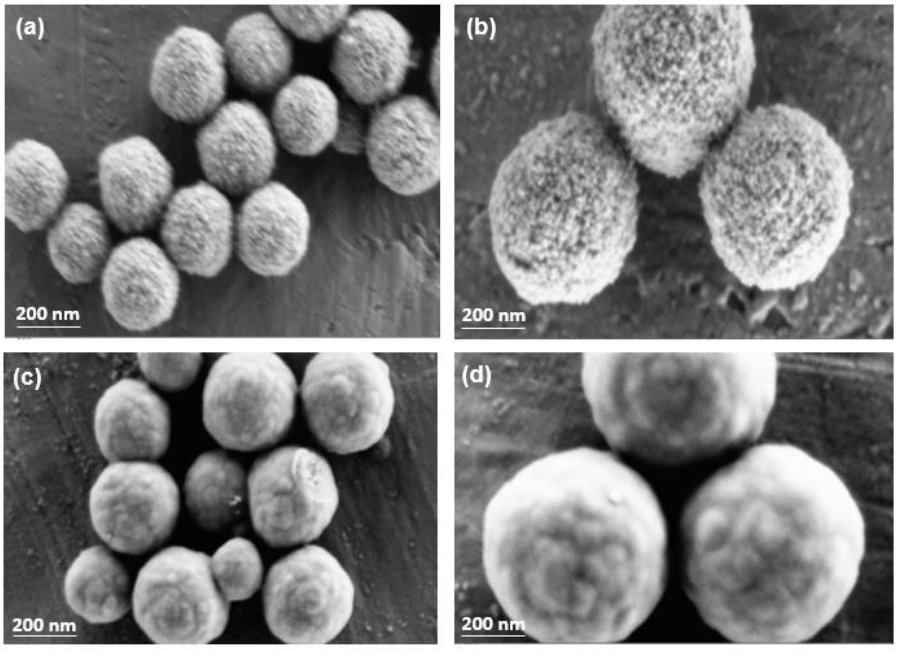

Figure 53. SEM images of (a) Fe_3O_4 NP at low enlargement (100 KX) (b) Fe_3O_4 NP at high enlargement (200 KX) (c) SEM images of Fe_3O_4@SiO_2 NP at low enlargement (100 KX) (d) Fe_3O_4@SiO_2 NP with high enlargement (200 KX).

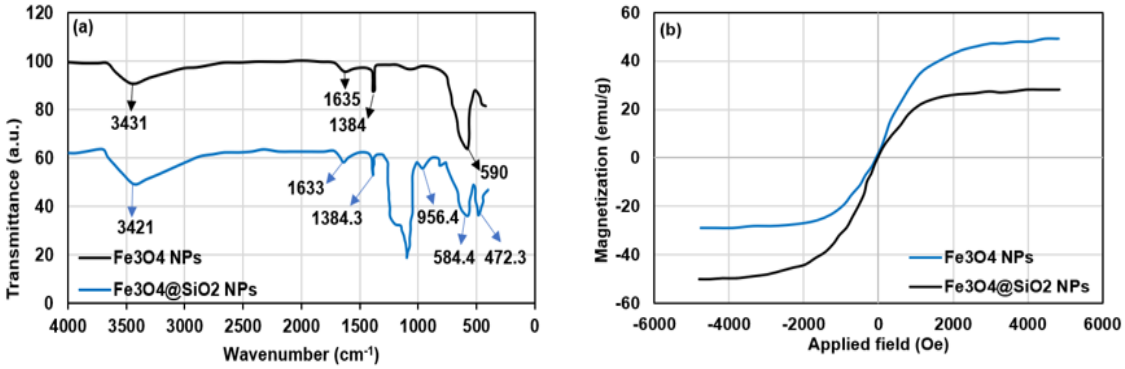

Figure 54. (a) FTIR spectra of Fe_3O_4@SiO_2 and Fe_3O_4 NP (b) the magnetization analysis of two nanoparticles.

8.4 Oil Recovery Using the Glass Micromodel

As described for the injection methods, the formation water was inserted into the micromodel and subsequently injected with crude oil (Nile blend) at a rate of 0.6 mL/h. Figure 55 exhibits the micromodel oil-saturated photo. The colors (black, white, and grey) correspond to the oil, water, and emulsion, respectively. As noted in Figure 55, the micromodel was filled with oil and a small amount of formation water, which indicated that the water was stuck in the throats and pores. After injecting the micromodel with oil, the seawater and three nanoparticles outlined in Table 15 were inserted individually with 0.6 mL/h in the micromodel.

The micromodel saturation profiles were verified after 240 mins of insertion, as demonstrated in Figure 56. It represents the emulsions produced with oil and formation water. The previous oil generation relies on several factors: in addition to the controlling processes in the insertion method, asphaltene sedimentation, the creation of oil-in-water (O/W), and water-oil emulsions impacted the oil production rate. The oil used was sensitive to sedimentation. Thus, asphaltene sedimentation was noted in the porous medium at the throat mouths in the insertion procedure. As such, asphaltene sedimentation can change the

glass wettability and alter the movement of the replacing fluid by blocking the pores [562, 563]. In addition, the creation of O/W emulsions was observed during specific tests.

Further, the inserted phase (i.e., replacing phase) viscosity improved with the production of O/W emulsions wherein a piston-like movement occurred for the bulk liquid [554, 564]. The density of the surface charge for the cations in the water likely improved with the reduction in the atomic radius. Moreover, greater asphaltene volumes were absorbed, which caused a greater decrease in the interfacial tension [565]. Following Derjaguin–Landau–Verwey–Overbeek (DLVO) theory and the salting-in mechanism, the disjoining pressure was improved. After that, the surface charges separated, and the nanoparticles were placed into the two-liquid interface to achieve high stability for the emulsions by decreasing the interfacial tension [566].

Additionally, greater interactions between the asphaltene particles occurred with a rise in the number of free ions and anions. Given that, the steadiness improved as the asphaltene particles have several vigorous negatively charged places, including -OH, =C=O, and =N [566]. The chemical bonds tend proton adsorption, and the negatively charged asphaltene particles will likely be absorbed onto H^+ ions and become positive loads [566, 567]. Because of the variation in the pH (between high and low values), the asphaltene functional groups are charged, causing greater hydrophilicity and polarity to enhance the stability. Therefore, it is crucial to examine the methods for injections and examine the changes in the oil production rates. It has been shown that nanoparticles be able to improve the oil recovery rate via the subsequent mechanisms considerably includes: changing the injecting fluid viscosity [568], adjusting the injecting fluid density [569], lowering the IFT [542], enhancing the emulsification method [570, 571], increasing the specific heat and conductivity [153], developing different reactions between rocks and the fluids [569], modifying the wettability [569], changing the heat transfer coefficient (HTC) [547], and

lowering the formation damage by decreasing the force on the surfaces of the pore [153, 571-573].

The oil recovery results were judged based on standard deviation and one-way analysis of variance (ANOVA). The statistical analysis was done based on considering the parameters that have statistical significance on the removal efficiency. The ANOVA manipulation accepted the model terms with a P-value ≤ of 0.05, whereas values greater than 0.05 were considered insignificant.

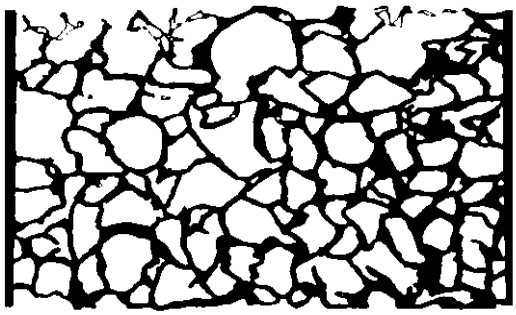

Figure 55. Micromodel after the injection of oil and formation water indicating the residual water.

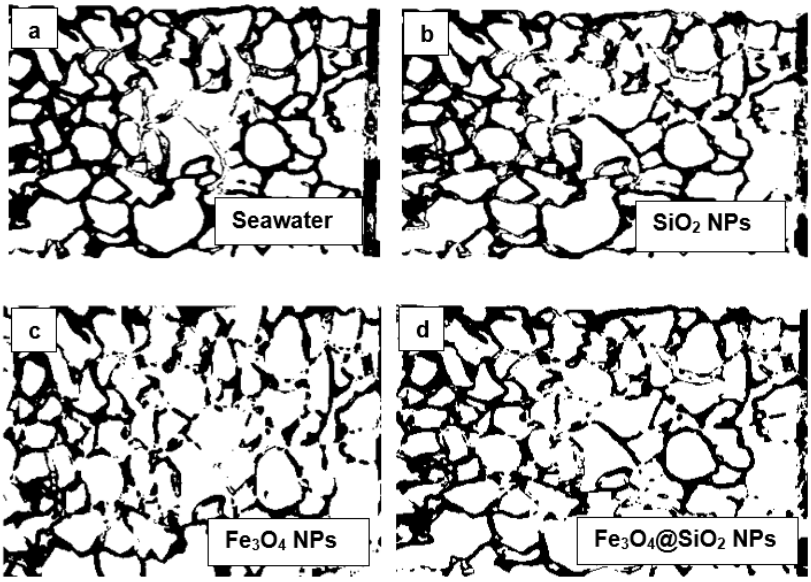

Figure 56. The micromodel images after 4 h for the four injected nanofluids.

Figure 57 outlines the separation time for each replacing sample. The image demonstrates how the modified nanoparticles (Fe_3O_4@SiO_2) exhibit the lengthiest separation time, suggesting that a comparatively longer time was necessary for this MNP before the initial water drop exiting the micromodel. The Fe_3O_4 is beneficial for absorbing the asphaltene particles onto surfaces because of their high specific surface area (SSA) [532]. Subsequently, this causes a rise in the viscosity, which influences the asphaltene particle stability and produces piston-like movements in areas with differing permeability values (i.e., high and low permeability) because of the formation of pressure resistance within the medium. Moreover, acid nanoparticles have additional energy as they produce electrostatic repulsion on the fluid surfaces. This reaction affects the disjoining pressure of the Van der Waals and capillary forces and further causes the piston-like movement to generate a greater oil production. As a result, greater spreading and piston-like movements were observed in the fluids by increasing the breakthrough (i.e., separation) time to improve the oil production efficiency. It was observed that the magnetite (Fe_3O_4) nanoparticle has the shortest separation time between the studied NPs. This can be aimed at the fact that these NPs could not overcome the disjoining pressure of the Van der Waals. Instead, they could be moved by the coming waves of pressure from the fluid, which negatively impacts the wettability, which agreed with the study reported by [574] that showed that the application of nanoparticles (including the Fe_3O_4, SiO_2) in the oil recovery process reduces the wettability alteration, reduce the oil viscosity, stabilize the formed emulsions, and reduce the IFT.

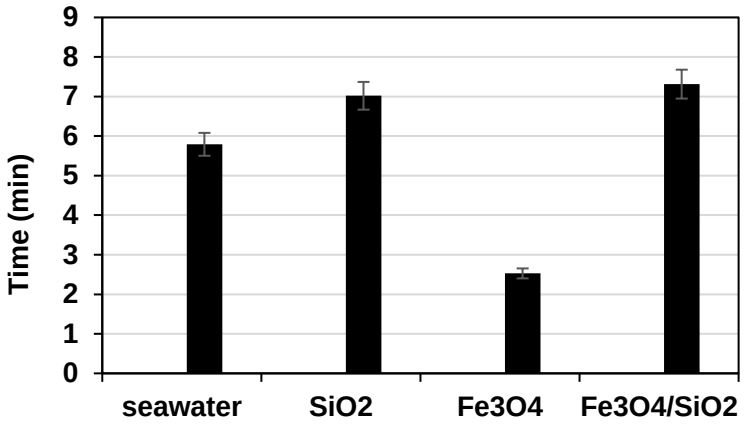

Figure 57. The breakthrough time for the four nanofluids.

The nanoparticles have a fast path to the output of the micro model rather than remaining and shifting the nanofluids near the outlet. As demonstrated in Figure 58, the Fe_3O_4@SiO_2 has the highest percentage of oil removal compared to the other nanofluid types. The nanocomposites remain in the porous medium with a sustained separation time and can create high oil generation. Additionally, specific alternations in the oil production rates correlate to the Fe_3O_4@SiO_2 NPs to change the system wettability. As observed from the oil-flooded micromodel, it is an oil-wet scheme. Moreover, Figure 58 indicates that the Fe_3O_4@SiO_2 nanoparticle injection achieved an oil production rate of 90.2%, and for the seawater injection, the oil production value was 76.5%. Further, hydrophilic nanoparticles can improve the stability and dual-layer electrostatic repulsion force, pushing the structure closer to water-wet conditions. At the same time, the electrolytes accumulate and enhance the capacity within the medium. [575] showed that iron oxide, silicon oxide, aluminium oxide, and zinc oxide (Fe_3O_4, SiO_2, Al_2O3, and ZnO) had oil recovery of 38.1%, 45.6%, 47.7%, and 35.1%, respectively. However, when the nanofluids were inserted into the formation as a displacing fluid, the oil recovery significantly increased to 50.3%, 52.0%, 53.2%, and 52.4% for (Fe_3O_4, SiO_2, Al_2O3, and ZnO). The findings obtained in this chapter, which agree with the results achieved in the present chapter, demonstrated that

nanofluid flooding has a hopeful potential to enhance oil recovery. [576] showed that the insertion of three nanofluids, alumina, iron oxide, and silica, could improve the oil recovery rate to more than 20%. The greatest oil recovery volume was noted for alumina nanoparticles and subsequently for iron oxide and silica, respectively. They are owing to the minor change in the nanofluid's viscosity compared to water and the insignificant difference in the IFT of the O/W phase for alumina and silica nanofluids.

However, as exhibited in Figure 59, the nanoparticles can change the wettability to water-wet through placement on the glass surface [577]. The wettability alteration (oil/wet-to-water/wet) leads to a discharge in the oil near the exit and increased oil production. As highlighted in Figure 59, the magnetite (Fe_3O_4) and silica (SiO_2) nanoparticles have high oil generation rates of 70.8% and 55.3%, respectively. These rates are due to the characteristics of the NP in the asphaltene absorption that helps to enhance the oil recovery process. Additionally, the SiO_2 NP can react further with water to free their surface from silanol bands (Si-O-H) which improves the stability of the asphaltene particles as the aqueous phase (i.e., water) salinity reduces in the scheme.

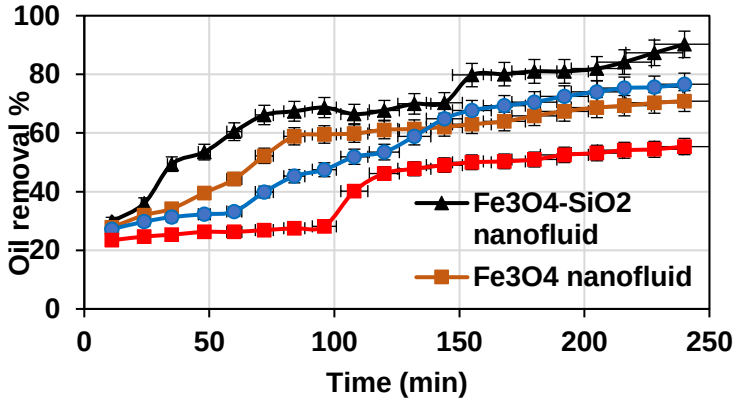

Figure 58. Oil recovery using the four nanofluids at differing injection times.

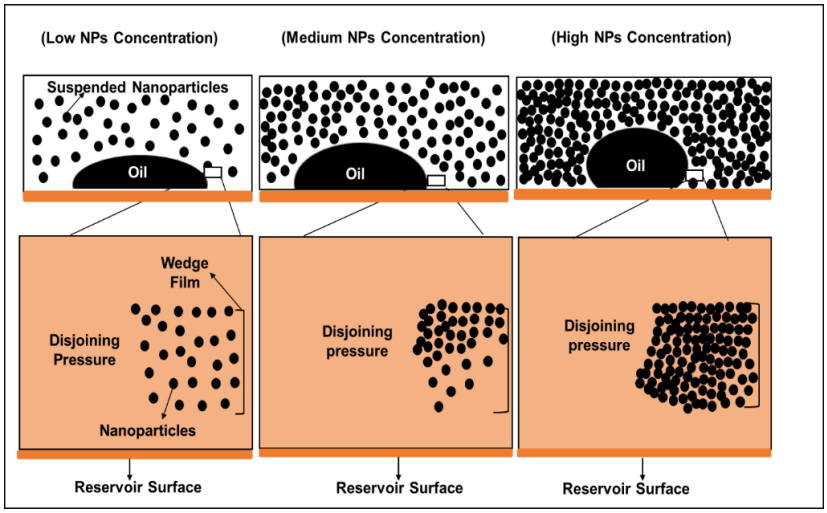

Figure 59. Representation of the wettability alteration by the nanoparticles [556].

As previously examined in the literature review [562, 578], the nanoparticles reduce the asphaltene precipitation on the glass through the adsorption of asphaltene molecules on their surface. Thus, the adsorption causes less throat blockage due to the asphaltene precipitation. As a result, a decrease in asphaltene sedimentation was observed via the injection of water (Figure 60). In addition, the SiO_2 NP can generate oil by lowering the IFT and altering the wettability. However, the SiO_2 NP alone is not effective for reducing the IFT because of the absence of surface movement. However, additional electrolytes containing polar composites in oil resin and asphaltene can improve the nanoparticle surface activity and decrease the IFT. Additionally, an alteration in the wettability can occur for several reasons, including the presence of polar composites in oil, crude oil components with polar functionality methods, surface sedimentation, and mechanisms of cations ion-bonding. The final oil production rate with the application of SiO_2 nanofluid was 55.37%, which is lower than the other nanofluid types.

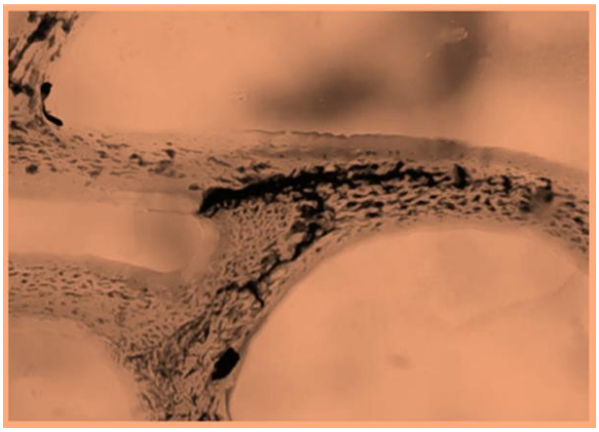

Figure 60. The view of asphaltene sedimentation without the injection of nanoparticles [556].

The glass wettability was assessed with the replacing fluids and the oil sample through contact angle measurements for approximately 240 min (i.e., 4 hours) of aging. Figure 61 illustrates the glass wettability for all nanofluids initially and again after 4 h of aging. By injecting the Fe_3O_4@SiO_2 nanoparticles into the micromodel, the oil sedimentation decreased the wettability and changed to neutral. Additionally, Figure 61 highlights the contact angle values for the Fe_3O_4, SiO_2, and Fe_3O_4@SiO_2 nanoparticles, 139°, 121°, and 106°, respectively. Thus, the glass changed from oil-wet to neutral. Following the relation of pc = 2σ cos θ/r, with the proximate of θ near 90°, the pc moves toward zero. The equilibrium interfacial tension was evaluated, and the values for the Fe_3O_4, SiO_2, and Fe_3O_4@SiO_2 NP were 26, 24, and 21 mN/m, respectively. As such, the interfacial tension decreased when the nanoparticles were injected into the scheme. Due to the presence of nanoparticles on the surface, the adsorption of oil increases, and the interfacial viscosity becomes greater because of the oil (i.e., a real surfactant) thus, causing a decline in the interfacial tension [550, 579].

Moreover, it was observed that the modified Fe_3O_4 (Fe_3O_4@SiO_2) NP effectively produces stable emulsions in the porous medium. The steady emulsions can improve the replacing

fluid viscosity to greater than the remaining oil due to the nanoparticles, which grab onto additional oil trapped in the pores to push oil to the outlet of the micromodel. Furthermore, emulsions can coagulate on the film layer over the oil particles via the method expressed by the theory of pseudo-emulsion film to enhance the emulsion stability due to a reduction in the IFT and an increase in the viscosity. Further, viscous fingering is reduced by improving the viscosity of the replacing fluid, decreasing the viscosity variation between the oil, and replacing the fluid in the medium. This leads to a piston-like movement of replacing nanofluids and an improvement in oil production.

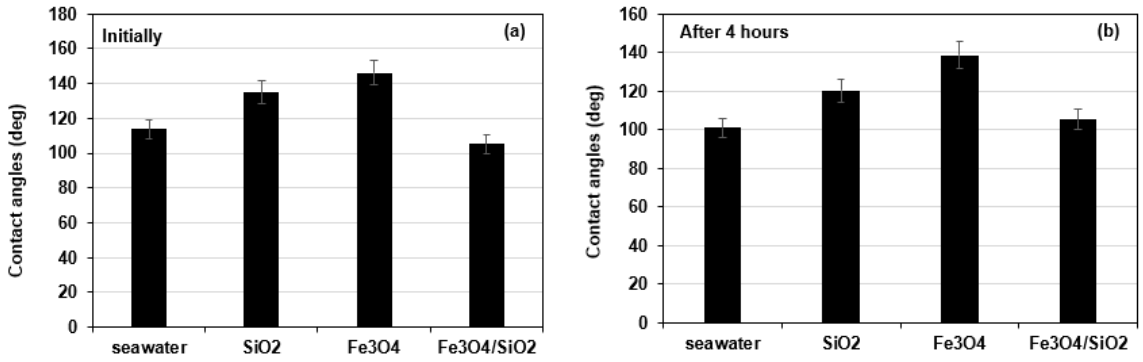

Figure 61. The glass contact angle between the four nanofluids and the produced oil. (a) initially, (b) after 4 hours.

Figure 62 demonstrates part of the micromodel during the individual insertion of the nanofluids at similar periods after the nanofluid has been injected. The grey color indicates the production of O/W emulsions. With seawater injection into the micromodel as an additional fluid, the result is the generation of W/O emulsion in front of the inserted fluid. Due to the production of emulsions, the oil droplets gather and become larger, increasing the movement of oil droplets. Because of the emulsion generation, the large porosity areas become clogged, and the oil production rate and oil recovery efficiency were enhanced [550, 570]. Figure 62 exemplifies the emulsion production of all of the nanofluids at various times. However, the emulsion production for the Fe_3O_4@SiO_2 remained stable throughout

the process. While the emulsion production is considerably enhanced because of the presence of ions (as outlined in Table 18), the steadiness of production is restricted to a specific time and eventually degrades. Primarily, this reaction occurs as not all of the ions in the water behave favourably towards emulsion creation and steadying. However, disconcerting ions can deactivate the other ions and impact which have interacted with oil and eliminate the emulsion shortly after its creation. Nevertheless, the Fe_3O_4@SiO_2 NP behaves preferably towards emulsion production, and the consequences of the promoting parameters control the opposite parameters.

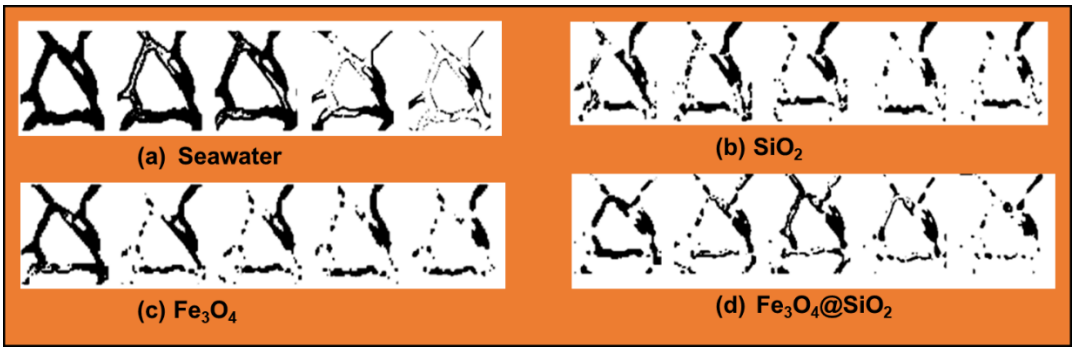

Figure 62. A section of the micromodel that contains the replacing fluid throats and pores after the injection of nanofluids.

8.5 Summary

This chapter illustrated the production of Fe_3O_4@SiO_2 nanoparticles at room temperature using a modified Stöber method. Various analysis was performed to verify the coating of the magnetite nanoparticles (Fe_3O_4) on the silica shell which provides suitable Fe_3O_4@SiO_2 nanoparticle sizes applied for the demulsification process. The produced Fe_3O_4@SiO_2 NP and other nanofluids (seawater, Fe_3O_4, and SiO_2) were examined for their ability to enhance the oil recovery in the reservoir. The Fe_3O_4@SiO_2 NP showed the greatest wettability alteration in the porous medium, and a small dosage of the Fe_3O_4@SiO_2 NP (10 mg/L) had the greatest oil recovery, 90.2%. In contrast, 76.5%, 70.8%, and 55.37% recorded oil

recovery rates for the seawater, Fe_3O_4, and SiO_2, respectively. The Fe_3O_4 NP regenerated oil by managing oil sedimentation. The SiO_2 NP enhanced the wettability and decreased the IFT. The water fluid changed the wettability, decreased the IFT, managed the oil sedimentation, and increased stable emulsions due to the effective ions. Thus, the four nanofluids were classified according to their final oil recovery rates: Fe_3O_4@SiO_2, seawater, Fe_3O_4, and SiO_2, respectively. It is recommended for future research works to consider the following:

1) Perform additional research work to understand the stability of the nanofluid, understand the dispersion conditions of nanofluids, identify the mechanisms of the EOR by NPs, and study the new uses of nanofluid emulsions.
2) Research the theoretical examination and mathematical modelling of different nanoparticles applied to EOR and identify the basic mechanisms of the EOR process. This also will assist the research in choosing suitable nano-methods and lessen their hazards in the field.
3) There is an urgent need to identify cost-effective and environmentally friendly NPs that can be used in oil recovery applications.

CHAPTER 9: EVALUATION OF THE EFFICIENCY OF IONIC LIQUIDS IN THE DEMULSIFICATION OF OIL-IN-WATER EMULSIONS

9.1 Introduction

The techniques of enhanced oil recovery (EOR) are utilized for oil recovery after initial and secondary methods of oil generation. In oil recovery procedures, polymers, surfactants, alkaline, or their integrations are added to raise the viscosity of water and achieve very low interfacial tension (IFT) among O/W-EMUL [528, 580]. Nevertheless, a portion of the formed oils is in the shape of steady emulsions, which require separation to attain proper concentrations of oil (< 200 mg/L) and water concentrations in the range < 0.3-0.5 vol% for oil movement in the pipeline to the refineries [96, 581]. Chemical demulsification is an efficient technique to speed up oil and water separation [582, 583]. Several demulsifiers, for example, polymeric flocculants, ethoxylated phenolic resins, and alkylphenol formaldehyde resins have been utilized for W/O EMULs separation from natural production processes steadied with crude oil resins and asphaltenes contents (natural surfactants). However, these materials are not operative for oil separation from generated O/W EMULs, which vary from the natural emulsions (oil field emulsions) [584]. The presence of surfactants, alkali, and polymers is strongly attached to both the oil and water [585].

In the previous chapters, magnetite magnetic nanoparticles (Fe_3O_4-MNPs), (Fe_3O_4-SiO_2-MNPs), and Fe_3O_4-SiO_2-MNPs grafted with hyperbranched polyglycerol polymers (HPG) were applied as demulsifiers for the demulsification process of O/W-EMUL [39]. The results indicated that as-synthesized Fe_3O_4-MNP could achieve a D% ≥ 90% for oil concentrations in the range of 200-660 mg/L using a demulsifier volume of 10 mg/L [39]. Similarly, the functionalized MNPs (Fe_3O_4-SiO_2-MNPs) obtained a D% ≥ 98% with a demulsifier dose of 10 mg/L [40]. The application of MNPs-HPG demulsifiers also

exhibited a significant oil recovery efficiency. For example, a demulsifier of 100 mg/L was sufficient to achieve a D% of 93% for a high oil concentration of 4000 mg/L [38]. The magnetic demulsifiers were recycled up to 15 times with a steady D% in the range of 89.1% to 88.6% for oil concentrations between 100-4000 mg/L [38].

As reported before by [586, 587], in oil recovery methods, anionic surfactants such as the mixtures of dodecyl alkyl sulphate are generally added as demulsifiers to the O/W EMULs and achieved high separation rates. Cationic surfactants can efficiently separate O/W EMULs by decreasing the electrostatic repulsion between the droplets and, hence, decreasing emulsion stability [96, 584]. ILs which could be modified to produce cationic surface-active composites via changing the integrations of cation and anion have been used for O/W EMULs or W/O EMULs separation as demulsifiers [588, 589]. Various halogenide ILs with ammonium or imidazolium cations and non-halogenide ILs with fluorinated anions such as PF6 and BF4 have been applied for W/O EMULs breaking [588, 590, 591]. All the previous ILs presented great behaviour, specifically in combination with the microwave radiation method (MR), which was used to speed up the heating and decrease the viscosity.

Nonetheless, the higher cost and the negative environmental impacts of the fluorinated anions make them undesired for applying demulsification processes. Ammonium ILs with various anions such as $[HSO_4]^-$, $[Cl]^-$ or $[H_2PO_4]^-$ were also used to remove the water from W/O EMULs, and the effectiveness of the demulsification process differs when utilizing various ILs [591]. For produced O/W EMULs, octyl trimethylammonium bromide was applied by Hirasaki and co-workers [96] as a demulsifier in addition to an industrial cationic surfactant, and both were found to be effective in oil and water separation. In every study, the effectiveness of separation using ILs has been associated with the ILs structure; however, various findings were described in the literature. Flores showed that additional

hydrophilic anions ILs were further effective demulsifiers [591], while Fortuny exhibited that hydrophobic anion ILs showed great removal rates [589]. Flores determined that the cations with longer alkyl chain length in the ILs help achieve better demulsification than the ILs with shorter ones; however, Guzman-Lucero remarked the reverse fact [588].

Nevertheless, it is not reasonable to evaluate these studies since several other considerations can impact the efficiency of the separation, for example, the properties of oil such as the water content, density, viscosity, and the conditions of the demulsification process (temperature, demulsifier concentration, mixing time and surfactant concentration) [96, 591]. It is crucial to study the mechanism of the demulsification process using these ILs and to know where the IL remains since non-regeneration of the ILs is not a sustainable method owing to the high cost. If Possible, both the ILs and the surfactant must be reused again in the process, and this can be attained if the ILs can then remove the surfactant thru the ion-exchange mechanism [592]. To guide the choice and strategy of ILs for demulsification processes and improve the knowledge about the IL's roles in the demulsification methods, the work was conducted on gasoline/water emulsions that were synthesized using polysorbate 80 surfactants (tween-80). This chapter aims to guide the choices and strategies of ILs for the demulsification process and to strengthen knowledge about the role of ILs in demulsification methods. Three types of ILs with differing hydrophobicity, sequence of phosphonium, and lengths of hydrocarbon chains were examined for oil recovery from O/W-EMUL. In addition, the D% of the ILs for oil recovery from O/W-EMUL with an oil concentration of 500 mg/L were investigated at room temperature using tube and bottle tests. Further, the mechanism of the demulsification process for all the studied ILs was determined and correlated to the change in zeta potential and Gibbs energy. The findings showed promising results for the application of ILs in the EOR process.

9.2 Material and Methods

9.2.1 Materials

Gasoline oil (95%) and Polysorbate surfactant (Tween-80, technical grade) were obtained from Sigma Aldrich. The ionic liquids were provided by Power2 Group LLC Qatar with a purity > 95% and were used as delivered. Their terms, acronyms, and forms are introduced in Table 21 and Figure 63.

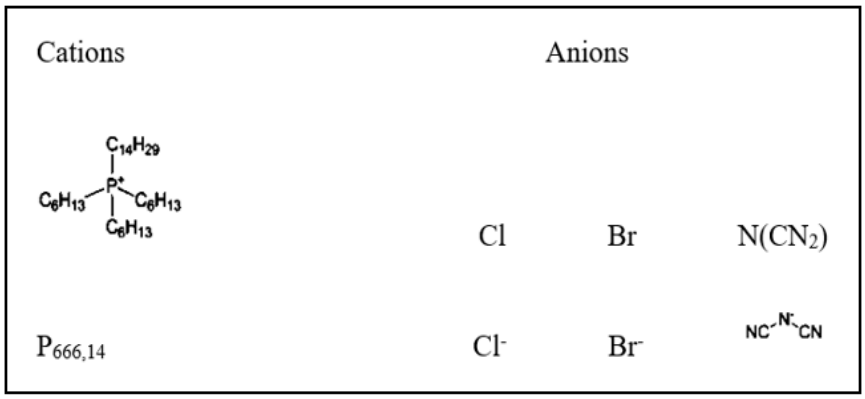

Figure 63. Studied ILs cations and anions structure.

Table 21. Studied ILs cations and anions structures.

Name of ILs	Short Forms	Abbreviation
Trihexyltetradecylphosphonium chloride	$P_{666,14}Cl$	HIL-1
Trihexyltetradecylphosphonium bromide	$P_{666,14}Br$	HIL-2
Trihexyltetradecylphosphonium dicyanamide	$P_{666,14}[N(CN)_2]$	Non-HIL

9.2.2 Synthesis of O/W-EMULs

In this chapter, gasoline was also utilized as oil and a tween-80 surfactant as an emulsifier to formulate the O/W-EMUL. First, 0.05 g/L of tween-80 surfactant and water solutions (50 mL) were added to the gasoline oil (2 mL) in a 5L glass bottle using a shear emulsifying homogenizer (model BRH1-100, USA). Then, the solution was initially mixed for 2 min at

a rate of 600 rpm, and after that, for an addition10 min at 1800 rpm to attain stable and homogenous emulsions, it was noted that no phase separation was remarked after 24 h.

9.2.3 Emulsion Characterization

An optical microscope with 10× magnification (Olympus BH-2) was used to verify the nature of the O/W-EMUL. The tests were performed by taking one drop from the O/W-EMUL and placing it onto a clean and smooth microscopic slide. The drop was allowed to seep out onto the plate with no external control. No cover glass was positioned on the emulsion sample, which helps to prevent movement of the emulsion. Images were taken for the boundary zones of oil-water droplets and were examined with specified software. A Lasentec® S400A focused beam reflectance measurement (FBRM) supplied with a PI 14/206 probe (Mettler Toledo, 8 mm) was used to measure oil's actual droplet size distributions in oil the O/W-EMUL. The FBRM measurements were carried out at a temperature of 20°C and an angle of 45°. The probe tip was placed under the emulsion surface in bottles mixed at the rate of 800 rpm to reduce the possibility of particles sticking on the probe. The FBRM uses a rotating laser beam that is reflected by the drops. The reflection times are converted into chord size distributions which are altered to actual droplet size distributions using a modification factor.

9.2.4 Demulsification Experiments

The bottle experiments were consistent with the approach outlined by Guzman-Lucero [588] and Flores [591]. First, 50 ml of synthesized O/W-EMUL was added to graduated glass bottles. Second, 10 mg/L of each IL was added. All the bottles were mixed at a rate of 800 rpm and room temperature using a four-blade impeller for 1 min. Then, the bottles were permitted to stabilize and settle while registering the removed amounts of gasoline versus the time immediately after stopping the impeller. To examine the D%, the 50 mL of the synthesized emulsion was initially moved to the tubes. After that, 10 mg/L of the IL

was added without stirring. The ratio of IL to surfactant (Tween-80) was set at 10 mg/L_{ILs}:0.05 g/L_{sur}. A tube including 50 mL emulsion and no ILs were used as a blank sample. The D% versus time was verified immediately after the addition of the ILs. The D% was calculated using Equation 27 (see section 9.2.6). All tests were carried out in triplicate, and the average value and standard deviation (St.Dev.) at a 95% confidence level were used in reporting the data.

9.2.5 Characterization Analysis

The presence of surfactant and $N(CN)_2$ in the mixture and the IL phases after the demulsification was analyzed utilizing Agilent 1200 High-Pressure Liquid Chromatography (HPLC) operated at 40°C and equipped with a ZORBAX Eclipse XDBC18 column and detector. The detection wavelength was set at 220 nm (UV, accurateness < 0.2%), and the mobile phase was a mixture of (35 vol% Na_2HPO_4 aqueous solution and 65 vol% acetonitrile) supplied at a flow rate of 0.2 mL/min. For standardization of tween-80 and $N(CN)_2$, the standard samples were formed from $P_{666,14}[N(CN)_2]$ and tween-80. In addition, the existence of the anions (Cl^-, and Br^-) in the water phase after the demulsification process was examined by applying Ion chromatography (IC-850 Professional I, Metrohm®), using anion and cation columns as well as a conductivity detector. The cation column eluent was an acidic mixture (1.7 mM 2,6-Pyridinedicarboxylic acid and 1.7 mM nitric acid) flow at a rate of 1.25 mL/min, while the anion column eluent was a basic solution (7.5 mM Na_2CO_3 and 0.75 mM KOH) flow at a rate of 1.0 mL/min. The Cl^-, and Br^- anions standard samples were made for standardization (calibration). Zeta potential measurements were conducted utilizing the electrophoretic light scattering instrument ZEN3600 (Malvern Instruments Ltd., UK). The experiments were carried out for samples diluted 100× in deionized water at room temperature, the device programmed to repeat as a minimum 5 times.

9.2.6 Definition of the Demulsification Efficiency Using ILs

The percentage demulsification efficiency (D%) is the amount of the oil removed from emulsion divided by the initial amount of oil that was dissolved obtained from equation 27 below:

$$\text{demulsification efficiency (D\%)} = \frac{V_{t0,oil} - V_{t,oil}}{V_{t0,oil}} \text{ x } 100\% \qquad (27)$$

$V_{t,\,oil}$ is the initial volume of oil introduced in the emulsions at t = 0, and $V_{t,\,oil}$ is the removed amount of gasoline at t = t. All the experiments were replicated, and the error bars are shown in the corresponding figures.

9.2.7 Statistical Analysis

The statistical analysis and student t-test were conducted using the Prism GraphPad statistics software package. All the assessments were performed in triplicate, and the outcomes were presented as mean ± standard deviation (St.Dev.). The oil recovery findings were evaluated based on the St.Dev. and one-way analysis of variance (ANOVA). The ANOVA was conducted to confirm statistical variations in the reported oil recovery rates at a significance level of 5%. The one-way analysis of variance was implemented to compare the data. A value of $p < 0.05$ was noted as statistically significant.

9.3 Results and Discussion

9.3.1 Emulsion Analysis

The stability of the emulsion is associated with the type of emulsion, droplet size distribution, and the ratio between the two-phase volumes. Before examining the demulsification of the O/W-EMUL using the ILs, the synthesized emulsion samples were analyzed. The microscopy images of the O/W-EMUL (Figure 64) indicate that oil particles fill most of the area, suggesting that the solution disperses the oil phase. As per the synthesis process, the volume of water added is greater than the gasoline oil. Thus, it can be

concluded that the O/W-EMUL were generated. This was substantiated during the analysis as a pink color was observed in the water (i.e., continuous phase) produced by the potassium permanganate ($KMnO_4$). The $KMNO_4$ is an indicator used to identify the volume of the water phase during the microscopic analysis.

The Tween-80 surfactant is soluble in water, in congruence with Bancroft's principle, which states that the continuous phase occurs when the surfactant (i.e., emulsifying agent) is highly soluble [46]. The emulsion droplet size distribution was evaluated at 800 rpm in a stirred vessel mixed using an FBRM device. After the addition of the surfactant, the electrostatic forces among the oil droplets are negligible. Consequently, the size distribution becomes smaller. Moreover, due to the coalescence of larger oil drops, the size distribution is altered to a lesser size over time because tiny droplets will remain in the emulsion. Similarly, reducing the numeric concentration of oil drops produces a secondary O/W mixture (formation of O/W-EMUL) [593].

Figure 65 highlights how the droplet's diameter was generally <100 microns, with the most frequently observed particles between 1 to 15 microns. The microscopic analysis in Figure 64 supports this. Additionally, the reported droplet size range is compatible with the values reported by other demulsification research [589, 590]. The peak near 250 microns is assumed to be produced by air bubbles, and the noise is due to the formation of microbubbles due to high mixing speed. These microbubbles contribute to the separation of O/W by creating an airlifting or stripping action of oil droplets. Thereafter, the isolated air droplets are attached to the IL and removed from the emulsion. Excluding the air bubble effect, the adjusted droplets' mean diameter is 130 microns, consistent with research by Schuur et al. [594].

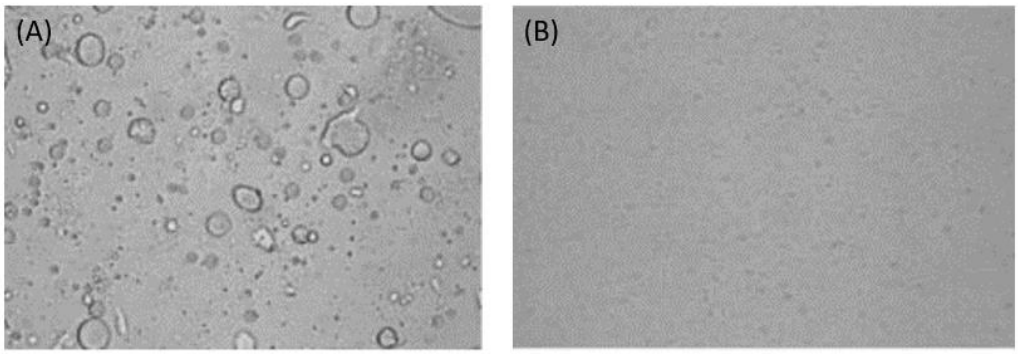

Figure 64. (A) Microscopy image of the prepared emulsions (B) Microscopy image (×10 magnification).

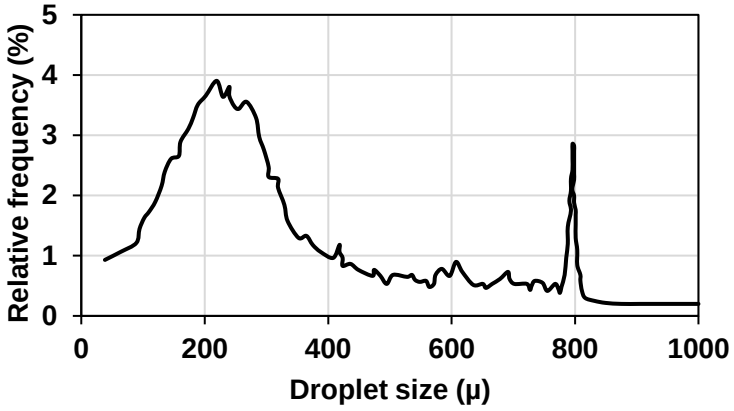

Figure 65. The droplet size distribution of the synthesized gasoline O/W-EMULs (oil phase = gasoline oil; emulsifier agent = Tween-80 surfactant).

9.4 The Efficiency of ILs as Demulsifiers

To evaluate the D% using ILs with different ion characteristics (hydrophilic and hydrophobic), bottle experiments were conducted with IL and tween-80 with a concentration ratio of 10 mg/L_{ILs} to 0.05 g/L_{sur} (Figure 66). Figure 67 illustrates the D% achieved by HIL-1, HIL-2, and the Non-HIL for the bottle test at different separation times between 0-100 min, conducted at an IL ratio to surfactant of mg/L_{ILs} to 0.05 g/L_{sur}. The D% for the two halogenide ILs (HILs-1, HILs-2) after 20 min were 97.7 %, 88.1%, respectively, which is significantly higher and faster than the D% reported for the Non-HILs.

Conversely, the D% achieved by the Non-HIL after 20 min was 85.2% and 89.5%, respectively. As highlighted by previous research, the nature of the cation (i.e., molecular weight and length of side chains) and anion (i.e., size and water solubility) ILs significantly impact the interfacial activity of the emulsion [590, 595]. Given that, the larger molecular weight of the HILs-1 and HILs-2 is a significant parameter for understanding its higher demulsification efficiency. It is thought that a larger molecular weight plays an integral role in increasing the capability of the HILs to behave as a flocculant to assemble the oil droplets. Further, the greater hydrophobic nature of the HIL cations may indicate their superior demulsification efficiency, as proposed by [596]. Compared to the Non-HIL, the high content alkyl chains in the HILs contribute to a high demulsification efficiency. As suggested by (Li, Kersten, et al. 2016), to evaluate the D% using ILs and correlate the trends to IL characteristics (hydrophilic and hydrophobic), the conductor-like screening model for natural solvents (COSMO-RS) technique was used to determine the partition coefficient (C_p) denoted as $\log_{10}(P_o/w)$.

An emulsion with C_p values from -8.3 to -10.7 is considered hydrophilic, producing significant separation efficiency by the hydrophobic HIL. It was assumed that the reported efficiency achieved in the present study was directly connected to this parameter. The higher and faster D% performed by the HILs is dependent on the halogenide anions ratio, which is 100 times greater than the Non-HIL. It is likely that halogen anion's hydration is an essential component of the demulsification process and contributes to the higher D%. However, this supposition is inconsistent with the results reported by Li et al. [597]. The researchers observed a lower D% efficiency for the HILs compared to the Non-HIL [597]. As such, further investigative research is needed to establish this correlation.

The low ionic charge on the HIL and the higher cationic portion generates hydrophobic properties with a high attachment to oil. Li et al. [598] suggested that the integration between the anion and cation on the ILs is essential for determining the hydrophobicity and hydrophilicity of the interfacial surface. Further, Li et al. [598] exemplified how high surface activity was detected because of the integration of the hydrophobic cation ($P_{666,14}$) and the hydrophilic anionic portion [$N(CN)_2$]. This consequently lowers the D% for the Non-HIL. Further, Li et al. [598] found that Non-HIL has no impact on the demulsification process as the total influence of anions with hydrophilic properties is small due to high hydrophilicity.

Figure 66. Bottle test for the Non-HIL (IL-3) after (1) 48 hours (2) 24 hours.

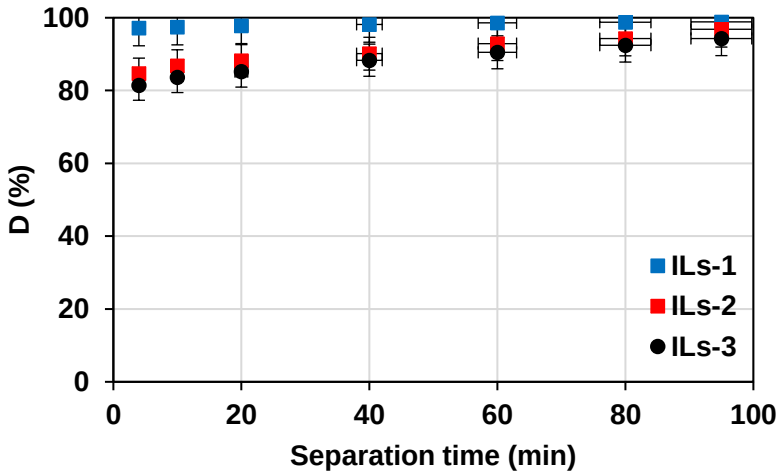

Figure 67. D% of HIL-1, HIL-2, and the Non-HIL in bottle test at different separation times between 0-100 min with surfactant volume (V_{sur}) = 0.05 g/L and ILs volume (V_{ILs}) = 10 mg/L.

9.5 The Efficiency of the Demulsification Process in Tube Tests Using ILs

As the demulsification rate of the HILs is fast, it was difficult to examine the impact of the cation alkyl chain length on the reported D% using the bottle test. Given that, the demulsification tests were repeated using tube tests without mixing. This step was taken to control the D% at a measurable scale and carefully observe the amount of oil removed. The tube tests were conducted using the HIL-1, HIL-2, and the Non-HIL at a fixed IL to surfactant ratio. The concentration of ILs was twice-diluted using isopropanol (C_3H_8O) to reduce the viscosity (for greater control). Finally, the blank tests were performed by adding an equivalent volume of C_3H_8O to the emulsion.

The findings indicated that the handled emulsions achieved high stability after 24 h. It was also determined that the impact of the C_3H_8O on the demulsification process was insignificant. The D% of the three ILs is outlined in Figure 68. Among all the examined ILs, the HIL-1 exhibited the greatest D%, followed by HIL-2 and then Non-HIL. The cation portion ($P_{666,14}$) in the Non-HIL exhibited shorter cation and better diffusivity. However, the surface action was reduced, which negatively affected the dispersity and D%.

In contrast, the significant removal rate by the HIL-1 and HIL-2 in a short time indicates that the overall amount of alkyl carbon in the cation plays an essential role in the removal process. (Though, the amount of alkyl carbon in every chain associated with phosphorus does not significantly affect the removal process.) Additionally, although the HIL-1 and HIL-2 have the same cation, the D% using HIL-1 is slightly faster than HIL-2. This difference occurred because of the small size of the Cl^- that slightly reduces Gibbs energy

of hydration to -340 kJ/mol, which is lower than Gibbs energy of hydration for Br^- (-315 kJ/mol).

The observed trends suggest that the IL diffusion controls the D% in the tube tests rather than the emulsion near the interface between the bulk phase and particles. To explain the interaction between the surfactant and the ILs, the oil removal process in tubes was conducted with V_{ILs} of 10 mg/L from HILs-1 and HILs-2 and varying volumes of surfactant ranging between 0.05-0.5 g/L. As observed in Figure 69, the highest D% was achieved after 50-90 min. The final D% corresponds to the volume of added ILs. All the tests with higher ILs and low surfactant concentrations achieved D% >95%. The oil recovery findings were evaluated depending on the St.Dev. and ANOVA. The statistical analysis relied on the factors that have statistical consequences on the oil separation efficiency. The ANOVA manipulation was consistent with the model terms with a P-value $\leq$ of 0.05, while the values more than 0.05 were judged as insignificant.

Table 22 presents a comparison between the demulsification process efficiency of both tube and bottle tests using the three IL types. As highlighted in Table 22, the highest demulsification efficiency was achieved using the two HIL in both bottle and tube tests. In addition, the D% for HIL-1 is marginally higher than HIL-2 and the Non-HIL. These results were observed because of the normal size of the Cl^- that slightly decreased Gibbs energy of Cl^-, which is lower than Gibbs energy of hydration for the two anions Br^- and $N(CN)_2$.

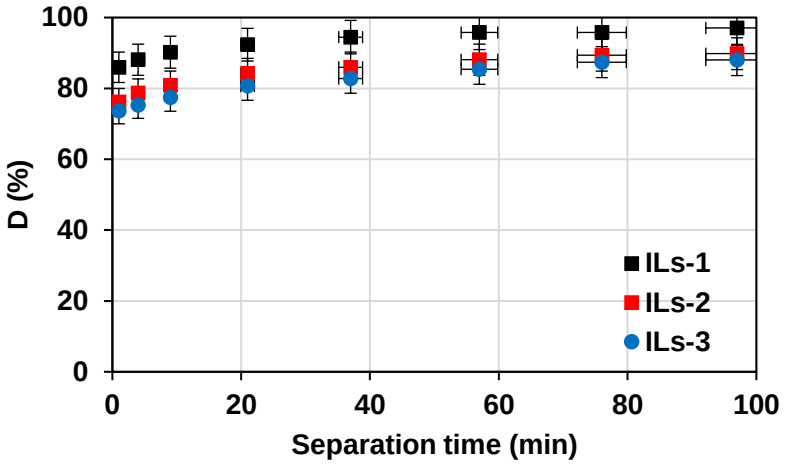

Figure 68. The D% of the three types of ILs in tube tests without mixing; surfactant volume (V_{sur}) = 0.05 g/L, ILs volume = (V_{ILs}) 10 mg/L).

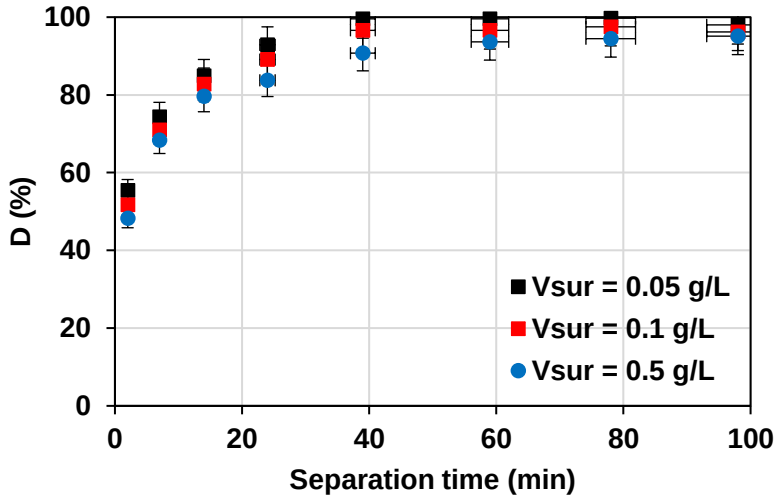

Figure 69. Demulsification efficiency of HIL-1 in tube tests with surfactant volumes (V_{sur}) ranging from 0.05 g/L to 0.5 g/L and an IL volume (V_{ILs}) of 10 mg/L.

Table 22. A comparison between the efficiency of the demulsification process of tube and bottle tests using the three IL types.

Type of ionic liquid (ILs)	D% Time (min) 20	50	90
Bottle test			
HILs-1	97.7%	>98%	>98.7%
HILs-2	88.1%	>90%	>94.2%
Non-HIL	85.2%	>88%	>92.4%
Tube tests			
HILs-1	92.3%	>94.4%	>85.7%
HILs-2	84.2%	>85.9%	>89.3%
Non-HIL	80.67%	>82.7%	>87.4%

9.6 Zeta Potential Measurements

Zeta potential (ξ) of oil droplets was examined with varying IL concentrations of (C_{IL}) 10 mg/L, 30 mg/L, and 50 mg/L. The oil droplets ξ became less negative as the C_{IL} increased, indicating that IL cations and surfactants could be adsorbed at the O/W interface. Further, the surfactant present on the oil droplets surface can be replaced because of the anion exchange mechanism. The ξ achieved a high value of ~ -49 mV without adding ILs. However, after adding 10 mg/L of HILs-1, HILs-2, and Non-HIL, the ξ value decreased to -23 mV, -25.2 mV, and -29.3 mV, respectively. The reduction in the ξ of the oil droplets suggests a decrease in the electrostatic repulsion forces, subsequently encouraging their coalescence. The ILs and the emulsion surfactants are adsorbable on the oil particle's surface, altering the zeta potential. Although ILs contain both ionic and cationic parts, the adsorption increases the negative electric charge density on the surface of the oil particles. Thus, the stabilization of oil droplets occurs through the mechanism of electrostatic stabilization.

Additionally, the ILs lowered the charge on the surface of the oil particles, reduced the film's elasticity, and decreased the interfacial tension reduction rate, which led to faster phase separation. Therefore, depending on the zeta potential measurements during different phases, the presence of ILs can have a powerful impact on the value of the zeta potential on the O/W-EMUL system. Moreover, in this study, the addition of the ILs effectively reduced the value of the zeta potential. Similarly, the efficiency of the ILs in reducing the zeta potential values was evident in all IL-O/W systems, as reported by [599]. Thus, the ILs can "neutralize" the charge of the studied O/W-EMUL systems, which can cause wettability alteration and improve the oil recovery rates [202].

9.7 Mechanism of the Demulsification Process

During the continuous and rapid separation of the oil and water phases through the HILs, some obscurity in both (oil and water) phases was noted. The lack of clarity is due to the precipitation of some solids in the samples (IL cations and the surfactant anions) rather than partial oil removal (i.e., demulsification). However, lack of clarity as partial oil removal was shown with the remaining amount of water in the gasoline phase (Figure 70). The water concentrations, estimated with Karl-Fisher titration, were 2.89%, 10.3%, and 11.99% for HILs-1, HILs-2, and the Non-HIL, respectively, suggesting an effective demulsification. Furthermore, the flocculated compounds (resulting from the IL cation and the surfactant anion) indicated that the ion exchange between the surfactant and the ILs occurred. A further indication of the ion exchange mechanism was achieved with the analysis of the water phase using ion chromatography (IC) after the oil recovery process and the addition of the ILs. The IC findings exemplify how Na^+ remained in the water phase, with > 86% of Cl^- or Br^- anions. Therefore, a faster demulsification process occurred with the use of HILs-1, HILs-2, and Non-HIL. Because of the densities, the ILs allowed us to see three

phases: the oil phase on top, the water phase on the bottom, and the IL droplets as the mid-phase.

To identify the demulsification process mechanism using HILs-1, HILs-2, and Non-HIL, the volume of surfactant and the three ILs in the water phase (after the oil removal process) were examined using an HPLC device. The analysis exemplified oil removal percentages of 89.3%, 88.5%, and 87% for three ILs, respectively, in the water phase. The IC findings also demonstrated that all the Na^+ remained in the water phase. This exemplifies how the demulsification mechanism with the three IL types was an anion exchange. Figure 71 highlights that during the demulsification process, a chemical reaction based on an ion exchange occurs between ions and the hydrophilic part of the ILs. This reaction exhibited excellent driving force and rapid demulsification when HILs were confirmed by a high value of Gibbs energy for Cl^- and Br^- hydration compared with sodium. The ion hydration Gibbs energy values at 298.15°K were -315 kJ/mol, -340 kJ/mol, and -365 kJ/mol for the bromide (Br^-), chloride (Cl^-), and sodium (Na^+), respectively. It was observed that the interaction between cations from IL s and the surfactant created an additional phase that provided an extra driving force for higher demulsification efficiency. The cation-surfactant integrations were determined to be hydrophobic with high dispersion in water, the conditions that improve the separation efficiency. As such, the ionic strength of ILs contributes to the dispersion of phases and the overall efficiency.

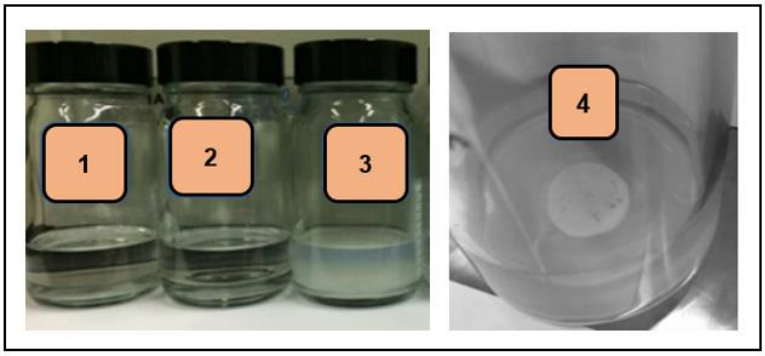

Figure 70. D% of (1) (HIL-1), (2) (HIL-2), and (3) (HIL-3) in bottle tests after settling for 24 hours using V_{sur} of 0.05 and IL volumes (V_{ILs}) 10 mg/L. (4) Top picture of sample 3 (Non-HIL).

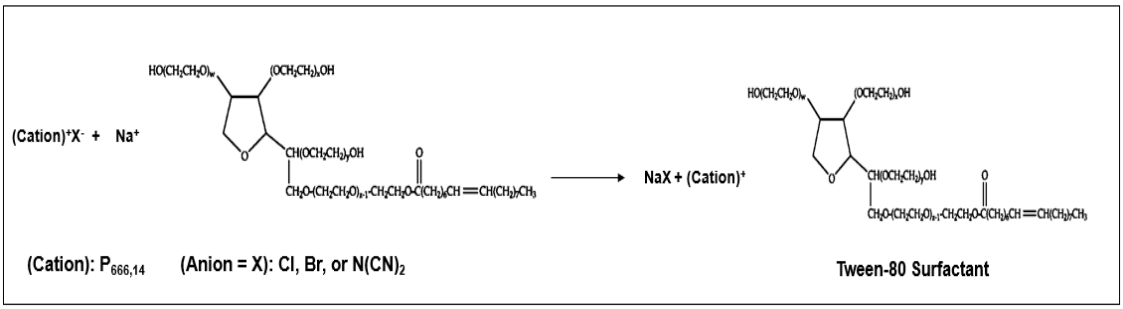

Figure 71. Anion exchange reaction between tween-80 surfactant and the ILs (HILs-1, HILs-2, and the Non-HIL).

The demulsification mechanism of the O/W-EMUL using ionic liquids contains two essential stages: diffusion and adsorption. The diffusion method disperses the IL particles in the continuous phase before reaching the O/W interface. On the other hand, the adsorption method suggests that the dispersed IL molecules move across the continuous phase (water) to the O/W interface [10, 205]. Then, the IL particles replace the natural emulsifying agents (i.e., surfactants) at the interface and alter the viscoelastic properties of the interfacial films. This results in a separation of the intense film over the O/W drop and improves the coalescence of the distributed drops [49, 200].

The oil particles present in the emulsion are steadied using the surfactant, which remains at the O/W interface with the hydrophilic polyoxyethylene group (marked in red in Figure 72) [600, 601]. This group faces the water and hydrophobic chains that connect with the oil [600, 601]. The sodium cations (marked in green in Figure 72) are distributed in water and produce an electric dual-layer, preventing droplet interaction and increasing the droplets. After adding efficient IL demulsifiers (cations marked in black including Cl^-, Br^-, $N(CN)_2$, and anions in blue) to the emulsions, the interface is damaged because of the IL and surfactant ion exchange. The damage decreases the oil droplets electrostatic repulsion and affects the stability of the emulsion. Thereafter, the oil is removed from the water phase (Figure 72a). The recently produced flocculate substances accumulate to create the third phase, as exemplified in Figure 72b. This substantiates the high efficiency of the ILs as demulsifiers for O/W-EMULs applying an ion exchange mechanism. Because of the ion exchange mechanism in the demulsification process, the anions escape into the water phase and the cations integrate with the surfactant. For the IL and surfactant regeneration, an inversed ion exchange procedure is required. However, such a procedure may restrict the industrial ability of the ILs as demulsifiers for the treatment of O/W-EMUL. As such, future research is required on the regeneration of ILs that apply ion exchange methods. Further, to make the IL demulsification process more economic, appropriate recycling methods should be used.

The IL properties and characteristics play a significant role in the demulsification process [18]. Most researchers favour creating and producing room temperature ionic liquids (RTIL). The RTIL can be obtained by producing nitrogen or phosphorous organic cations with various organic anions, inorganic anions, dicyanamide, chloride, bromide, acetate, trifluoromethyl sulfate, or hexafluorophosphate [197]. ILs are an appealing O/W interface because of their amphiphilic nature. Further, they interact with the polar parts of crude oil

because of their dielectric properties [590, 595]. ILs also have an amphiphilic structure, which attracts them to the oil and water phases, as they prefer the movement of the surfactants, consequently leading to an effective removal [27, 200]. The amphiphilic character may be in the cation or anion portion of the IL structure. Recent research has shown that hydrophobic surface-active ILs can be effectively used to demulsify O/W-EMUL in the oil and gas industries [207, 208]. The study conducted by Hazrati et al. [209] noted that hydrophobic ILs (e.g., HIL-1 and HIL-2) are better than hydrophilic ILs for the demulsification process (e.g., Non-HIL). Moreover, [209] obtained a total petroleum hydrocarbon recovery of 95%.

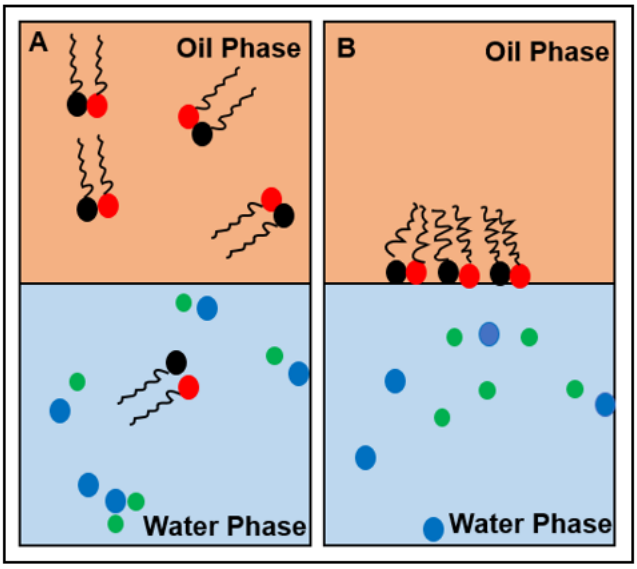

Figure 72. Demulsification mechanism of O/W EMULs using ILs. (A) Formation of ILs as flocculates after the addition of the ILs cations in both phases and the formation of two liquid phases (gasoline oil and water) after the demulsification process (B) The produced ILs precipitation and formation of a third phase between the oil and water phases (the place relied on these three phases densities).

9.8 Conclusion

- Halogenide ionic liquids with hydrophobic cations and non-halogenide ionic liquids efficiently separated oil from O/W-EMUL. An excellent demulsification efficiency was also demonstrated when similar volumes of ILs and surfactant were used (D% >95%).
- Bottle tests showed that the demulsification process using HILs has a higher oil removal rate than Non-HIL (D% of 97.7%, 88.2%, and 85.3% for HIL-1, HIL-2, and Non-HIL, respectively).
- The mechanism of the demulsification process is an ion exchange between the surfactant and the anions of the ILs, which is controlled by the discharge of sodium salt into the water phase. Moving forward, inversed ion-exchange methods are required to regenerate these ILs, which will likely reduce their industrial application as demulsifiers.
- The demulsification efficiency can be improved by choosing appropriate ILs, IL amounts for certain emulsion types and determining the optimum treatment conditions.
- ILs are green solvents, making them suitable for several potentially dangerous and volatile organic solvents currently used for oil removal.
- Although there are many advantages of ILs, their disadvantages need further investigation to determine their appropriateness for widespread usage. Further research should focus on the recycling and regeneration of ILs. A greater examination is also required to enhance the application of ILs, including verifying the best-operation conditions to reduce the necessary concentration of ILs to achieve the higher D%.

CHAPTER 10: CONCLUSION AND FUTURE WORK

The present study investigated the effect of different demulsifiers types, including (HPG polymer, magnetite MNPs, Si nanoparticles, Fe-Si MNPs, PSiMNPs, and ionic liquids, on the demulsification efficiency. The performance of the HPG demulsifier was managed by the two reactant ratios, which were below the conditions for the demulsification process. The outcomes ($\%R_{oil}$ of 48.72% and 49.5%) revealed that low removal was achieved through a small dose of both low and high molecular weight HPG, and high ($\%R_{oil}$ = 90.30%) can be achieved at optimized conditions of demulsifier dosage and time. However, the application of the Fe-MNP demonstrated a significant improvement in the efficiency of the demulsification process, although only a small amount of the MNP was used. The results showed that $\%\eta_{dem}$ declined when there was an increase in the pH and the concentration of tween-80 surfactant. Additionally, the prepared Fe-MNP were still effective after being recycled for 7 cycles and had a high removal rate ($\%R_{oil}$) ~ 90%. Also, applying a high Fe-MNP dose (100 mg/L) achieved the highest adsorption capacity and exhibited the fastest adsorption kinetics. Later the Fe_3O_4-SiO_2 nanoparticles were developed, the $\%\eta_{dem}$ an MD_{dose} as low as 10 mg/L attained a $\%\eta_{dem}$ in the range of 93% to 94.3% for O/W mixtures with C_{oil} < 2000 mg/L, which decreased to ~ 90% for higher concentrations. The $\%R_{oil}$ was > 90 ± 0.1, which declined by increasing the pH to 7 and the concentration of C_{sur} to 0.1 g/L, achieved high recyclability at an effective, stable $\%R_{oil}$ ~ 90% after 9 cycles and high adsorption capacity values reached 186 ± 5 to 35 ± 5 mg_{oil}/mg_{MD} and 86 ± 5 to 23 ± 5 mg_{oil}/mg_{MD} for the Fe_3O_4-SiO_2 and Fe_3O_4 MNPs, respectively. After that, a novel and efficient approach was developed to synthesize the Fe-MNP covered with a silica layer at varying thicknesses. Results indicated that the demulsification efficiency is low using high nanoparticle concentrations and high pH values because aggregation decreases the active surface area and absorption capacity.

Moreover, small-sized Fe-Si MNP significantly improved the oil recovery process due to the high dispersion rate. Also, increasing the thickness of the silica layer simultaneously decreased the oil adsorption capacity, reduced the saturation magnetization (M_s), and ultimately decreased the demulsification efficiency. The first demulsifier (Fe-Si-1) prepared with a TEOS amount of 0.5 ml effectively removed oil and achieved high $\%S_{oil}$>95% after 9 cycles. Then, Fe-Si MNP was produced by performing surface functionalization of the Fe-Si-MNPs to the HPG polymer to enhance the efficiency of the demulsification process. The results indicated that the prepared PSiMNPs demulsifier with essential oxygen functionalities was effectively coated with the Fe-Si-MNPs and exhibited high superparamagnetic performance. The demulsification experiments exemplified how adding small dosages of PSiMNPs to the O/W emulsion achieved a high demulsification efficiency of ≥ 90% in 5 min for emulsion samples with an oil concentration of oil 500 mg/L. Moreover, the demulsification behaviour of the PSiMNPs was excellent compared to the Fe-Si-MNPs as the suspended small oil droplets that were grafted onto the PSiMNPs were able to be easily removed from the water phase by applying magnetic separation. The results indicated that the proposed demulsifier could decrease the cost of the demulsification process within the petroleum industry. The characteristics of PSiMNPs can lessen the hazard of contaminating the environment due to the demulsifier's ability to be recycled and reused up to 15 times. After grafting the HPG, the Fe-Si-MNPs exhibited an excellent adsorption capacity for the oil in the O/W emulsion of 192.8 mg/g at a high C_{oil} of 900 mg/L using the Langmuir and Freundlich models, respectively, which was related to the solubilization of the HPG. Moreover, the demulsifier kinetic studies of oil removal were examined using the pseudo-second-order model with an R^2 value of 0.99, which was more efficient than the pseudo-first-order model, which exhibited a K_2 of 0.0169 g/mg. min. Then, The produced Fe_3O_4@SiO_2 NP and other nanofluids (seawater, Fe_3O_4, and

SiO_2) were examined for their ability to enhance the oil recovery in the reservoir. The Fe_3O_4@SiO_2 NP showed the greatest wettability alteration in the porous medium, and a small dosage of the Fe_3O_4@SiO_2 NP (10 mg/L) had the greatest oil recovery, 90.2%. In contrast, 76.5%, 70.8%, and 55.37% recorded oil recovery rates for the seawater, Fe_3O_4, and SiO_2, respectively. The Fe_3O_4 NP regenerated oil by managing oil sedimentation. The SiO2 NP enhanced the wettability and decreased the IFT. The water fluid changed the wettability, decreased the IFT, managed the oil sedimentation, and increased stable emulsions due to the effective ions. Finally, the demulsification efficiency of three ionic liquids (two halogenide and one Non-halogenide ILs) in oil/water emulsions was tested using bottle and tube tests. Results showed that HILs with hydrophobic cations and the Non-HIL were observed to separate the oil from O/W EMULs efficiently, and great demulsification efficiency was detected when similar volumes of ILs and surfactant were employed. Bottle tests revealed that the halogenide ionic liquid's demulsification process has higher oil removal rates than the Non-HIL. Moreover, the mechanism of the demulsification process was found to be anion exchange among the tween-80 surfactant and the anions of the ILs led by the discharge of sodium salt to the water phase. Also, inversed ion-exchange methods are required to regenerate these ILs, possibly reducing their applications in the industry as demulsifiers.

In the light of the development so far, the following points are suggested for further enhancing the demulsification process performance:

1. Future studies on oil recovery processes using NPs should concentrate on the following different parts:

- The production of stable emulsions in larger amounts requires to be achieved concerning commercial sides.

- Numerous NPs have demonstrated various properties and methods for the oil recovery process. Nevertheless, limited studies have been recommended on the use of NPs in emulsion mixtures. Moreover, additional uses and superior behaviour can be feasible by nanoparticle surface functionalization.
- More experimental schemes of O/W emulsions for oil recovery need to be conducted using MNPs. These schemes will enhance the knowledge in the NPs in oil recovery process nano-EOR processes in experimental conditions. Also, optimization research on the factors that affect the application of NPs in oil recovery is suggested to develop the oil recovery rates and cost-efficiency.
- The investigational study must be performed to verify the adsorption and desorption performance through NP dispersion inside the emulsion mixture since they will impact the NP's deliverability to the O/W interface.
- Combined studies on the NP's safety and health should be accomplished to avoid the hazard to humans and the environment.

2. From the published literature, it can be noticed that the HPG polymers have not been extensively studied in the field of oil removal due to their multistep preparation, which needs much knowledge, and it also requires assessing the potential of polymers structures for the application of oil removal. Furthermore, HPGs polymers are commonly used in biomedical applications; thus, the possibility of applying HPGs demulsifiers in the oil recovery process from oil in water emulsions should be further investigated.
3. The efficiency of the demulsification process was improved by using the ILs as demulsifiers; however, there are even some constraints that need more studies to make them fit for general use, such as the suitable ionic liquids type and the suitable

volume for certain emulsion types with detecting the optimum conditions of treatment.

REFERENCES

1. Jiménez, S., et al., State of the art of produced water treatment. Chemosphere, 2018. 192: p. 186-208.
2. Matijasevic, B. and J. Banhart, Improvement of aluminium foam technology by tailoring of blowing agent. Scripta Materialia, 2006. 54(4): p. 503-508.
3. Goodarzi, F. and S. Zendehboudi, A comprehensive review on emulsions and emulsion stability in chemical and energy industries. The Canadian Journal of Chemical Engineering, 2019. 97(1): p. 281-309.
4. Mohyaldinn, M.E., A.M. Hassan, and M.A. Ayoub, Application of emulsions and microemulsions in enhanced oil recovery and well stimulation, in Microemulsion-a Chemical Nanoreactor. 2019, IntechOpen.
5. Sjöblom, J., et al., Demulsifiers in the oil industry. Encyclopedic handbook of emulsion technology, 2001. 1: p. 595-619.
6. Bera, A. and T. Babadagli, Status of electromagnetic heating for enhanced heavy oil/bitumen recovery and future prospects: A review. Applied energy, 2015. 151: p. 206-226.
7. Aris, N.I.A., Demulsification of water-in-oil (W/O) emulsion by microwave heating technology. 2011, UMP.
8. Adewunmi, A.A., M.S. Kamal, and T.I. Solling, Application of magnetic nanoparticles in demulsification: A review on synthesis, performance, recyclability, and challenges. Journal of Petroleum Science and Engineering, 2020: p. 107680.
9. Teng, H., et al., Modified Hyperbranched Polyethylenimine as a Novel Demulsifier for Oil-in-Water Emulsions. Energy & Fuels, 2019. 33(10): p. 10108-10114.
10. Hassanshahi, N., G. Hu, and J. Li, Application of Ionic Liquids for Chemical Demulsification: A Review. Molecules, 2020. 25(21): p. 4915.

11. Kumar, N., A. Verma, and A. Mandal, Formation, characteristics and oil industry applications of nanoemulsions: A review. Journal of Petroleum Science and Engineering, 2021: p. 109042.
12. Liang, H. and H. Esmaeili, Application of nanomaterials for demulsification of oily wastewater: A review study. Environmental Technology & Innovation, 2021: p. 101498.
13. Ogolo, N., O. Olafuyi, and M. Onyekonwu. Enhanced oil recovery using nanoparticles. in SPE Saudi Arabia section technical symposium and exhibition. 2012. Society of Petroleum Engineers.
14. Zheng, Y., et al., Hyperbranched polymers: advances from synthesis to applications. Chemical Society Reviews, 2015. 44(12): p. 4091-4130.
15. Abidin, A., T. Puspasari, and W. Nugroho, Polymers for enhanced oil recovery technology. Procedia Chemistry, 2012. 4: p. 11-16.
16. Zhu, C.Y., et al., Detrital zircon U–Pb and Hf isotopic data for meta-sedimentary rocks from the Heilongjiang Complex, northeastern China and tectonic implications. Lithos, 2017. 282: p. 23-32.
17. Fard, A.K., et al., Enhancing oil removal from water using ferric oxide nanoparticles doped carbon nanotubes adsorbents. Chemical Engineering Journal, 2016. 293: p. 90-101.
18. Patel, D.D. and J.M. Lee, Applications of ionic liquids. The Chemical Record, 2012. 12(3): p. 329-355.
19. Zolfaghari, R., et al., Demulsification techniques of water-in-oil and oil-in-water emulsions in petroleum industry. Separation and Purification Technology, 2016. 170: p. 377-407.

20. Thompson, D., A. Taylor, and D. Graham, Emulsification and demulsification related to crude oil production. Colloids and Surfaces, 1985. 15: p. 175-189.
21. Hou, B., et al., Mechanism of wettability alteration of an oil-wet sandstone surface by a novel cationic gemini surfactant. Energy & Fuels, 2019. 33(5): p. 4062-4069.
22. Peng, K., et al., Emulsion microstructural evolution with the action of environmentally friendly demulsifying bacteria. Colloids and Surfaces A: Physicochemical and Engineering Aspects, 2018. 553: p. 528-538.
23. Wang, D., et al., Techniques for treating slop oil in oil and gas industry: A short review. Fuel, 2020. 279: p. 118482.
24. Hou, J., et al., Understanding interfacial behavior of ethylcellulose at the water–diluted bitumen interface. Energy & fuels, 2012. 26(3): p. 1740-1745.
25. Zargar, G., et al., Evaluation of a sulfanilic acid based surfactant in crude oil demulsification: an experimental study. Oil & Gas Sciences and Technology–Revue d'IFP Energies nouvelles, 2018. 73: p. 20.
26. Fan, Y., S. Simon, and J. Sjöblom, Interfacial shear rheology of asphaltenes at oil–water interface and its relation to emulsion stability: Influence of concentration, solvent aromaticity and nonionic surfactant. Colloids and Surfaces A: Physicochemical and Engineering Aspects, 2010. 366(1-3): p. 120-128.
27. Shehzad, F., et al., Polymeric surfactants and emerging alternatives used in the demulsification of produced water: A review. Polymer Reviews, 2018. 58(1): p. 63-101.
28. Zhai, M., et al., A novel silica-supported polyether polysiloxane quaternary ammonium demulsifier for highly efficient fine-sized oil droplet removal of oil-in-water emulsions. RSC Advances, 2020. 10(32): p. 18918-18926.

29. Niu, Z., et al., Changing the interface between an asphaltene model compound and water by addition of an EO–PO demulsifier through adsorption competition or adsorption replacement. Energy & Fuels, 2019. 33(6): p. 5035-5042.
30. Feng, X., et al., Mechanistic study on demulsification of water-in-diluted bitumen emulsions by ethylcellulose. Langmuir, 2010. 26(5): p. 3050-3057.
31. Adewunmi, A.A. and M.S. Kamal, Demulsification of water-in-oil emulsions using ionic liquids: Effects of counterion and water type. Journal of Molecular Liquids, 2019. 279: p. 411-419.
32. Biniaz, P., M. Farsi, and M. Rahimpour, Demulsification of water in oil emulsion using ionic liquids: Statistical modeling and optimization. Fuel, 2016. 184: p. 325-333.
33. Chen, Y., et al., Synthesis of magnetically responsive hyperbranched polyamidoamine based on the graphene oxide: application as demulsifier for oil-in-water emulsions. International Journal of Energy Research, 2019. 43(9): p. 4756-4765.
34. Hassan, S.A., B.K. Abdalla, and M.A. Mustafa, Addition of silica nano-particles for the enhancement of crude oil demulsification process. Petroleum Science and Technology, 2019. 37(13): p. 1603-1611.
35. Ye, F., et al., Preparation of reduced graphene oxide/titanium dioxide composite materials and its application in the treatment of oily wastewater. Colloids and Surfaces A: Physicochemical and Engineering Aspects, 2020. 586: p. 124251.
36. Xu, H., et al., Magnetically responsive multi-wall carbon nanotubes as recyclable demulsifier for oil removal from crude oil-in-water emulsion with different pH levels. Carbon, 2019. 145: p. 229-239.

37. Elmobarak, W.F., F. Almomani, and M.A.H.S. Saad, Utilizing environmentally friendly hyperbranched polyglycerol polymers to separate gasoline from deionized water. Greenhouse Gases: Science and Technology, 2020. 10(4): p. 759-770.

38. Elmobarak, W.F. and F. Almomani, Enhanced oil recovery using hyperbranched polyglycerol polymer-coated silica nanoparticles. Chemosphere, 2021: p. 131295.

39. Elmobarak, W.F. and F. Almomani, Application of magnetic nanoparticles for the removal of oil from oil-in-water emulsion: Regeneration/reuse of spent particles. Journal of Petroleum Science and Engineering, 2021. 203: p. 108591.

40. Elmobarak, W.F. and F. Almomani, Application of Fe3O4 magnetite nanoparticles grafted in silica (SiO2) for oil recovery from oil in water emulsions. Chemosphere, 2021. 265: p. 129054.

41. Elmobarak, W.F. and F. Almomani, A new insight into the separation of oil from oil/water emulsion by Fe3O4–SiO2 nanoparticles. Environmental Research, 2021. 202: p. 111645.

42. Kokal, S.L., Crude oil emulsions: A state-of-the-art review. SPE Production & facilities, 2005. 20(01): p. 5-13.

43. Al-Sabagh, A.M., N.G. Kandile, and M.R. Noor El-Din, Functions of demulsifiers in the petroleum industry. Separation Science and Technology, 2011. 46(7): p. 1144-1163.

44. Saad, M., et al., An overview of recent advances in state-of-the-art techniques in the demulsification of crude oil emulsions. Processes, 2019. 7(7): p. 470.

45. Raya, S.A., et al., A critical review of development and demulsification mechanisms of crude oil emulsion in the petroleum industry. Journal of Petroleum Exploration and Production Technology, 2020. 10(4): p. 1711-1728.

46. Bancroft, W.D., The theory of emulsification, V. The Journal of Physical Chemistry, 2002. 17(6): p. 501-519.

47. Wong, S., J. Lim, and S. Dol, Crude oil emulsion: A review on formation, classification and stability of water-in-oil emulsions. Journal of Petroleum Science and Engineering, 2015. 135: p. 498-504.

48. Abdulredha, M.M., H.S. Aslina, and C.A. Luqman, Overview on petroleum emulsions, formation, influence and demulsification treatment techniques. Arabian Journal of Chemistry, 2020. 13(1): p. 3403-3428.

49. Grenoble, Z. and S. Trabelsi, Mechanisms, performance optimization and new developments in demulsification processes for oil and gas applications. Advances in colloid and interface science, 2018. 260: p. 32-45.

50. Kumar, N. and A. Mandal, Surfactant stabilized oil-in-water nanoemulsion: stability, interfacial tension, and rheology study for enhanced oil recovery application. Energy & Fuels, 2018. 32(6): p. 6452-6466.

51. Abullah, M.M., H.A. Al-Lohedan, and A.M. Attah, Synthesis and application of amphiphilic ionic liquid based on acrylate copolymers as demulsifier and oil spill dispersant. Journal of Molecular Liquids, 2016. 219: p. 54-62.

52. Kovács, A., I. Erős, and I. Csóka, Optimization and development of stable w/o/w cosmetic multiple emulsions by means of the Quality by Design approach. International journal of cosmetic science, 2016. 38(2): p. 128-138.

53. Fingas, M. and B. Fieldhouse, Formation of water-in-oil emulsions and application to oil spill modelling. Journal of hazardous materials, 2004. 107(1-2): p. 37-50.

54. de Folter, J.W., M.W. van Ruijven, and K.P. Velikov, Oil-in-water Pickering emulsions stabilized by colloidal particles from the water-insoluble protein zein. Soft Matter, 2012. 8(25): p. 6807-6815.

55. Wu, J., et al., Development of a method for measurement of relative solubility of nonionic surfactants. Colloids and Surfaces A: Physicochemical and Engineering Aspects, 2004. 232(2-3): p. 229-237.

56. Wu, J., et al., Effect of demulsifier properties on destabilization of water-in-oil emulsion. Energy & fuels, 2003. 17(6): p. 1554-1559.

57. Borges, B., et al., Breaking of water-in-crude-oil emulsions. 3. Influence of salinity and water− oil ratio on demulsifier action. Energy & Fuels, 2009. 23(3): p. 1568-1574.

58. Sun, P. and D.W. Armstrong, Ionic liquids in analytical chemistry. Analytica Chimica Acta, 2010. 661(1): p. 1-16.

59. Kunz, W. and K. Häckl, The hype with ionic liquids as solvents. Chemical Physics Letters, 2016. 661: p. 6-12.

60. Langevin, D., et al., Crude oil emulsion properties and their application to heavy oil transportation. Oil & gas science and technology, 2004. 59(5): p. 511-521.

61. Saththasivam, J., K. Loganathan, and S. Sarp, An overview of oil–water separation using gas flotation systems. Chemosphere, 2016. 144: p. 671-680.

62. Luo, X., et al., Enhanced separation of water-in-oil emulsions using ultrasonic standing waves. Chemical Engineering Science, 2019. 203: p. 285-292.

63. Raffa, P., et al., Polymeric surfactants: synthesis, properties, and links to applications. Chemical reviews, 2015. 115(16): p. 8504-8563.

64. Borreani, J., et al., How do different types of emulsifiers/stabilizers affect the in vitro intestinal digestion of O/W emulsions? Food Biophysics, 2019. 14(3): p. 313-325.

65. Ojinnaka, C., et al., Formulation of best-fit hydrophile/lipophile balance-dielectric permittivity demulsifiers for treatment of crude oil emulsions. Egyptian Journal of Petroleum, 2016. 25(4): p. 565-574.

66. Kume, G., M. Gallotti, and G. Nunes, Review on anionic/cationic surfactant mixtures. Journal of Surfactants and Detergents, 2008. 11(1): p. 1-11.

67. Kamal, M.S., I.A. Hussein, and A.S. Sultan, Review on surfactant flooding: phase behavior, retention, IFT, and field applications. Energy & Fuels, 2017. 31(8): p. 7701-7720.

68. Shahi, N. and A. Bhattarai, A Survey on Applications of Surfactants and Their Investigation for Commercial Utilization.

69. Shamsuri, A.A., Functional Properties of Biopolymer-Based Films Modified with Surfactants: A Brief Review. Processes, 2020. 8(9): p. 1039.

70. Hodges, G., et al., A comparison of log K ow (n-octanol–water partition coefficient) values for non-ionic, anionic, cationic and amphoteric surfactants determined using predictions and experimental methods. Environmental Sciences Europe, 2019. 31(1): p. 1-18.

71. Zivar, D., S. Kumar, and J. Foroozesh, Underground hydrogen storage: A comprehensive review. International Journal of Hydrogen Energy, 2021. 46(45): p. 23436-23462.

72. Al-Yaseri, A. and N.K. Jha, On hydrogen wettability of basaltic rock. Journal of Petroleum Science and Engineering, 2021. 200: p. 108387.

73. Lazghab, M., et al., Wettability assessment of finely divided solids. Powder technology, 2005. 157(1-3): p. 79-91.

74. Sam, E.K., et al., Recent development in the fabrication of self-healing superhydrophobic surfaces. Chemical Engineering Journal, 2019. 373: p. 531-546.

75. Zhang, N., et al., A review on oil/water mixture separation material. Industrial & Engineering Chemistry Research, 2020. 59(33): p. 14546-14568.

76. Afekare, D.A. and M. Radonjic, From mineral surfaces and coreflood experiments to reservoir implementations: Comprehensive review of low-salinity water flooding (LSWF). Energy & fuels, 2017. 31(12): p. 13043-13062.

77. Wang, Y., et al., Surfactant induced reservoir wettability alteration: Recent theoretical and experimental advances in enhanced oil recovery. Petroleum Science, 2011. 8(4): p. 463-476.

78. De Oliveira, T., et al., Use of a clay mineral and its nonionic and cationic organoclay derivatives for the removal of pharmaceuticals from rural wastewater effluents. Chemosphere, 2020. 259: p. 127480.

79. Shi, H., et al., A modified mussel-inspired method to fabricate TiO2 decorated superhydrophilic PVDF membrane for oil/water separation. Journal of Membrane Science, 2016. 506: p. 60-70.

80. Jarrahian, K., et al., Wettability alteration of carbonate rocks by surfactants: a mechanistic study. Colloids and Surfaces A: Physicochemical and Engineering Aspects, 2012. 410: p. 1-10.

81. da Costa, A.A., et al., An experimental evaluation of low salinity water mechanisms in a typical Brazilian sandstone and light crude oil with low acid/basic number. Fuel, 2020. 273: p. 117694.

82. Mahmoudi, S., A. Jafari, and S. Javadian, Temperature effect on performance of nanoparticle/surfactant flooding in enhanced heavy oil recovery. Petroleum Science, 2019. 16(6): p. 1387-1402.

83. Purswani, P. and Z.T. Karpyn, Laboratory investigation of chemical mechanisms driving oil recovery from oil-wet carbonate rocks. Fuel, 2019. 235: p. 406-415.

84. Deljooei, M., et al., Novel green surfactant made from L-aspartic acid as enhancer of oil production from sandstone reservoirs: Wettability, IFT, microfluidic, and core flooding assessments. Journal of Molecular Liquids, 2021. 323: p. 115037.

85. Gao, M., Z. Gu, and Z. Luo, One-layer-only molecular deposition filming flooding: A review. Colloids and Surfaces A: Physicochemical and Engineering Aspects, 2019. 572: p. 182-196.

86. Issaoui, O., et al., Adsorption of Bisphenol A from Aqueous Solution by HDTMA-Tunisian Clay Synthesized Under Microwave Irradiation: A Parametric and Thermodynamic Study. Clays and Clay Minerals, 2020. 68(4): p. 361-372.

87. Wang, C., et al., The preparation of organo-bentonite by a new gemini and its monomer surfactants and the application in MO removal: A comparative study. Chemical engineering journal, 2013. 219: p. 469-477.

88. Nguemtchouin, M.G.M., et al., Characterization of inorganic and organic clay modified materials: An approach for adsorption of an insecticidal terpenic compound. Applied Clay Science, 2015. 104: p. 110-118.

89. Ghaleh, S.P., E. Khodapanah, and S.A. Tabatabaei-Nezhad, Comprehensive monolayer two-parameter isotherm and kinetic studies of thiamine adsorption on clay minerals: Experimental and modeling approaches. Journal of Molecular Liquids, 2020. 306: p. 112942.

90. Han, H., et al., A critical review of clay-based composites with enhanced adsorption performance for metal and organic pollutants. Journal of hazardous materials, 2019. 369: p. 780-796.

91. Shen, T., et al., Architecting organo silica nanosheets for regenerable cost-effective organics adsorbents. Chemical Engineering Journal, 2018. 331: p. 211-220.

92. Beshkar, F., M. Salavati-Niasari, and O. Amiri, A reliable hydrophobic/superoleophilic fabric filter for oil–water separation: hierarchical bismuth/purified terephthalic acid nanocomposite. Cellulose, 2020. 27(16): p. 9559-9575.

93. Guan, D., et al., Mesoscale simulation for heavy petroleum system using structural unit and dissipative particle dynamics (SU–DPD) frameworks. Energy & Fuels, 2019. 33(2): p. 1049-1060.

94. Hjartnes, T.N., et al., Demulsification of crude oil emulsions tracked by pulsed field gradient (PFG) nuclear magnetic resonance (NMR). Part I: chemical demulsification. Industrial & Engineering Chemistry Research, 2019. 58(6): p. 2310-2323.

95. Elmobarak, W.F. and F. Almomani, Functionalization of silica-coated magnetic nanoparticles as powerful demulsifier to recover oil from oil-in-water emulsion. Chemosphere, 2021. 279: p. 130360.

96. Hirasaki, G.J., et al., Separation of produced emulsions from surfactant enhanced oil recovery processes. Energy & fuels, 2011. 25(2): p. 555-561.

97. Agista, M.N., K. Guo, and Z. Yu, A state-of-the-art review of nanoparticles application in petroleum with a focus on enhanced oil recovery. Applied Sciences, 2018. 8(6): p. 871.

98. Esmaeilnezhad, E., et al., An experimental study on enhanced oil recovery utilizing nanoparticle ferrofluid through the application of a magnetic field. Journal of industrial and engineering chemistry, 2018. 58: p. 319-327.

99. He, L., et al., Interfacial sciences in unconventional petroleum production: from fundamentals to applications. Chemical Society Reviews, 2015. 44(15): p. 5446-5494.

100. Liang, J., et al., Magnetic demulsification of diluted crude oil-in-water nanoemulsions using oleic acid-coated magnetite nanoparticles. Colloids and Surfaces A: Physicochemical and Engineering Aspects, 2015. 466: p. 197-202.

101. Yakasai, F., et al., Current Developments and Future Outlook in Nanofluid Flooding: A Comprehensive Review of Various Parameters Influencing Oil Recovery Mechanisms. Journal of Industrial and Engineering Chemistry, 2020.

102. Ju, B., T. Fan, and M. Ma, Enhanced oil recovery by flooding with hydrophilic nanoparticles. China Particuology, 2006. 4(1): p. 41-46.

103. Bera, A. and H. Belhaj, Application of nanotechnology by means of nanoparticles and nanodispersions in oil recovery-A comprehensive review. Journal of Natural Gas Science and Engineering, 2016. 34: p. 1284-1309.

104. Munshi, A., et al., Effect of nanoparticle size on sessile droplet contact angle. Journal of Applied Physics, 2008. 103(8): p. 084315.

105. Angle, C.W., Chemical demulsification of stable crude oil and bitumen emulsions in petroleum recovery—a review. 2001, Marcel Dekker: New York. p. 541-594.

106. Maghzi, A., et al., An experimental investigation of silica nanoparticles effect on the rheological behavior of polyacrylamide solution to enhance heavy oil recovery. Petroleum science and technology, 2013. 31(5): p. 500-508.

107. Wasan, D., A. Nikolov, and K. Kondiparty, The wetting and spreading of nanofluids on solids: Role of the structural disjoining pressure. Current Opinion in Colloid & Interface Science, 2011. 16(4): p. 344-349.

108. Kong, X. and M. Ohadi. Applications of micro and nano technologies in the oil and gas industry-overview of the recent progress. in Abu Dhabi international petroleum exhibition and conference. 2010. Society of Petroleum Engineers.

109. Viebahn, P., D. Vallentin, and S. Höller, Integrated assessment of carbon capture and storage (CCS) in South Africa's power sector. Energies, 2015. 8(12): p. 14380-14406.

110. Li, Y., et al., Equilibrium and dynamic surface properties of cationic/anionic surfactant mixtures based on carboxylate Gemini surfactant. Journal of Surfactants and Detergents, 2018. 21(6): p. 845-858.

111. Deng, S., et al., Destabilization of oil droplets in produced water from ASP flooding. Colloids and Surfaces A: Physicochemical and Engineering Aspects, 2005. 252(2-3): p. 113-119.

112. Umar, A.A., et al., A review of petroleum emulsions and recent progress on water-in-crude oil emulsions stabilized by natural surfactants and solids. Journal of Petroleum Science and Engineering, 2018. 165: p. 673-690.

113. Martínez-Palou, R., et al., Demulsification of heavy crude oil-in-water emulsions: A comparative study between microwave and thermal heating. Fuel, 2013. 113: p. 407-414.

114. Ali, N., et al., Interfacially active and magnetically responsive composite nanoparticles with raspberry like structure; synthesis and its applications for heavy crude oil/water separation. Colloids and Surfaces A: Physicochemical and Engineering Aspects, 2015. 472: p. 38-49.

115. Fan, Y., S. Simon, and J. Sjöblom, Chemical destabilization of crude oil emulsions: effect of nonionic surfactants as emulsion inhibitors. Energy & Fuels, 2009. 23(9): p. 4575-4583.

116. Li, S., An experimental investigation of enhanced oil recovery mechanisms in nanofluid injection process. 2016.

117. Miranda, C.R., L.S.d. Lara, and B.C. Tonetto. Stability and mobility of functionalized silica nanoparticles for enhanced oil recovery applications. in SPE international oilfield nanotechnology conference and exhibition. 2012. Society of Petroleum Engineers.

118. Cassidy, M., et al., In vivo magnetic resonance imaging of hyperpolarized silicon particles. Nature nanotechnology, 2013. 8(5): p. 363-368.

119. Nazari Moghaddam, R., et al., Comparative study of using nanoparticles for enhanced oil recovery: wettability alteration of carbonate rocks. Energy & Fuels, 2015. 29(4): p. 2111-2119.

120. Guo, K., et al., The effect of carbon-supported nickel nanoparticles in the reduction of carboxylic acids for in situ upgrading of heavy crude oil. Energy & Fuels, 2017. 31(6): p. 6045-6055.

121. Guo, K., et al., Monodispersed nickel and cobalt nanoparticles in desulfurization of thiophene for in-situ upgrading of heavy crude oil. Fuel, 2018. 211: p. 697-703.

122. He, L., et al., A fast and remote magnetonanothermometry for a liquid environment. Measurement Science and Technology, 2015. 27(2): p. 025901.

123. Zhong, J., M. Schilling, and F. Ludwig, Magnetic nanoparticle thermometry independent of Brownian relaxation. Journal of Physics D: Applied Physics, 2017. 51(1): p. 015001.

124. Baig, R.N. and R.S. Varma, Organic synthesis via magnetic attraction: benign and sustainable protocols using magnetic nanoferrites. Green chemistry, 2013. 15(2): p. 398-417.

125. Zhang, H.-w., Y. Liu, and S.-h. Sun, Synthesis and assembly of magnetic nanoparticles for information and energy storage applications. Frontiers of Physics in China, 2010. 5(4): p. 347-356.

126. Mohammed, L., et al., Magnetic nanoparticles for environmental and biomedical applications: A review. Particuology, 2017. 30: p. 1-14.

127. Kovalenko, A., et al., Towards improved efficiency of bulk-heterojunction solar cells using various spinel ferrite magnetic nanoparticles. Organic Electronics, 2016. 39: p. 118-126.

128. Negin, C., S. Ali, and Q. Xie, Application of nanotechnology for enhancing oil recovery–A review. Petroleum, 2016. 2(4): p. 324-333.

129. Haroun, M.R., et al. Smart nano-EOR process for Abu Dhabi carbonate reservoirs. in Abu Dhabi international petroleum conference and exhibition. 2012. Society of Petroleum Engineers.

130. Joonaki, E. and S. Ghanaatian, The application of nanofluids for enhanced oil recovery: effects on interfacial tension and coreflooding process. Petroleum Science and Technology, 2014. 32(21): p. 2599-2607.

131. Shekhawat, D.S., et al. Magnetic recovery-injecting newly designed magnetic fracturing fluid with applied magnetic field for EOR. in SPE Asia pacific hydraulic fracturing conference. 2016. Society of Petroleum Engineers.

132. Hendraningrat, L., Unlocking the Potential of Hydrophilic Nanoparticles as Novel Enhanced Oil Recovery Method: An Experimental Investigation. 2015.

133. Metin, C.O., J.R. Baran, and Q.P. Nguyen, Adsorption of surface functionalized silica nanoparticles onto mineral surfaces and decane/water interface. Journal of Nanoparticle Research, 2012. 14(11): p. 1-16.

134. Kamal, M.S., et al., Recent advances in nanoparticles enhanced oil recovery: rheology, interfacial tension, oil recovery, and wettability alteration. Journal of Nanomaterials, 2017. 2017.

135. Ju, B., et al. A study of wettability and permeability change caused by adsorption of nanometer structured polysilicon on the surface of porous media. in SPE Asia Pacific oil and gas conference and exhibition. 2002. Society of Petroleum Engineers.

136. Keykhosravi, A. and M. Simjoo, Insights into stability of silica nanofluids in brine solution coupled with rock wettability alteration: An enhanced oil recovery study in oil-wet carbonates. Colloids and Surfaces A: Physicochemical and Engineering Aspects, 2019. 583: p. 124008.

137. Onyekonwu, M.O. and N.A. Ogolo. Investigating the use of nanoparticles in enhancing oil recovery. in Nigeria Annual international conference and exhibition. 2010. Society of Petroleum Engineers.

138. Hendraningrat, L., S. Li, and O. Torsaeter. Enhancing oil recovery of low-permeability berea sandstone through optimised nanofluids concentration. in SPE enhanced oil recovery conference. 2013. Society of Petroleum Engineers.

139. Shahrabadi, A., et al. Experimental investigation of HLP nanofluid potential to enhance oil recovery: A mechanistic approach. in SPE International Oilfield Nanotechnology Conference and Exhibition. 2012. Society of Petroleum Engineers.

140. Jafarnezhad, M., M.S. Giri, and M. Alizadeh, Impact of SnO2 nanoparticles on enhanced oil recovery from carbonate media. Energy Sources, Part A: Recovery, Utilization, and Environmental Effects, 2017. 39(1): p. 121-128.

141. Maghzi, A., et al., Pore-scale monitoring of wettability alteration by silica nanoparticles during polymer flooding to heavy oil in a five-spot glass micromodel. Transport in porous media, 2011. 87(3): p. 653-664.

142. Sharma, T., G.S. Kumar, and J.S. Sangwai, Comparative effectiveness of production performance of Pickering emulsion stabilized by nanoparticle–

surfactant–polymerover surfactant–polymer (SP) flooding for enhanced oil recoveryfor Brownfield reservoir. Journal of Petroleum Science and Engineering, 2015. 129: p. 221-232.

143. Corredor Rojas, L.M., The Impact of Surface Modified Nanoparticles on the Performance of Polymer Solutions for Heavy Oil Recovery. 2019.

144. Sharma, T. and J.S. Sangwai, Silica nanofluids in polyacrylamide with and without surfactant: Viscosity, surface tension, and interfacial tension with liquid paraffin. Journal of Petroleum Science and Engineering, 2017. 152: p. 575-585.

145. Sharma, T., S. Iglauer, and J.S. Sangwai, Silica nanofluids in an oilfield polymer polyacrylamide: interfacial properties, wettability alteration, and applications for chemical enhanced oil recovery. Industrial & Engineering Chemistry Research, 2016. 55(48): p. 12387-12397.

146. Kim, I., et al., Size-dependent properties of silica nanoparticles for Pickering stabilization of emulsions and foams. Journal of Nanoparticle Research, 2016. 18(4): p. 82.

147. Zhong, X., Surfactant-Nanoparticle Augmented Systems for Enhanced Oil Recovery: Formula Development and Evaluation. 2020, The University of North Dakota.

148. Corredor, L.M., M.M. Husein, and B.B. Maini, Effect of hydrophobic and hydrophilic metal oxide nanoparticles on the performance of xanthan gum solutions for heavy oil recovery. Nanomaterials, 2019. 9(1): p. 94.

149. Singh, M., et al., Effect of molecular weight of polyethylene glycol on the rheological properties of fumed silica-polyethylene glycol shear thickening fluid. Materials Research Express, 2018. 5(5): p. 055704.

150. Kondiparty, K., et al., Wetting and spreading of nanofluids on solid surfaces driven by the structural disjoining pressure: statics analysis and experiments. Langmuir, 2011. 27(7): p. 3324-3335.

151. McElfresh, P.M., D.L. Holcomb, and D. Ector. Application of nanofluid technology to improve recovery in oil and gas wells. in SPE international oilfield nanotechnology conference and exhibition. 2012. Society of Petroleum Engineers.

152. Hendraningrat, L., S. Li, and O. Torsater. Effect of some parameters influencing enhanced oil recovery process using silica nanoparticles: an experimental investigation. in SPE Reservoir Characterization and Simulation Conference and Exhibition. 2013. Society of Petroleum Engineers.

153. El-Diasty, A.I. and A.M. Aly. Understanding the mechanism of nanoparticles applications in enhanced oil recovery. in SPE North Africa technical conference and exhibition. 2015. Society of Petroleum Engineers.

154. Chengara, A., et al., Spreading of nanofluids driven by the structural disjoining pressure gradient. Journal of colloid and interface science, 2004. 280(1): p. 192-201.

155. Hendraningrat, L., S. Li, and O. Torsæter, A coreflood investigation of nanofluid enhanced oil recovery. Journal of Petroleum Science and Engineering, 2013. 111: p. 128-138.

156. Urian, Y., et al., Study of the surface properties and particle-particle interactions in oleic acid-coated Fe3O4 nanoparticles. Journal of Magnetism and Magnetic Materials, 2021. 525: p. 167686.

157. Worthen, A.J., et al., Steric stabilization of nanoparticles with grafted low molecular weight ligands in highly concentrated brines including divalent ions. Soft Matter, 2016. 12(7): p. 2025-2039.

158. Zhang, T., et al., Investigation of nanoparticle adsorption during transport in porous media. SPE Journal, 2015. 20(04): p. 667-677.

159. Kanj, M.Y., J.J. Funk, and Z. Al-Yousif. Nanofluid coreflood experiments in the ARAB-D. in SPE Saudi Arabia section technical symposium. 2009. Society of Petroleum Engineers.

160. Garcia-Olvera, G. and V. Alvarado. The potential of sulfate as optimizer of crude oil-water interfacial rheology to increase oil recovery during smart water injection in carbonates. in SPE Improved Oil Recovery Conference. 2016. Society of Petroleum Engineers.

161. Agbalaka, C.C., et al. The effect of wettability on oil recovery: A review. in SPE Asia Pacific Oil and Gas Conference and Exhibition. 2008. Society of Petroleum Engineers.

162. Saha, R., R.V. Uppaluri, and P. Tiwari, Influence of emulsification, interfacial tension, wettability alteration and saponification on residual oil recovery by alkali flooding. Journal of industrial and engineering chemistry, 2018. 59: p. 286-296.

163. Fletcher, A. and J. Davis. How EOR can be transformed by nanotechnology. in SPE improved oil recovery symposium. 2010. Society of Petroleum Engineers.

164. Xin, X., et al., Highly efficient removal of heavy metal ions by amine-functionalized mesoporous Fe3O4 nanoparticles. Chemical Engineering Journal, 2012. 184: p. 132-140.

165. Sodipo, B.K. and A.A. Aziz, Recent advances in synthesis and surface modification of superparamagnetic iron oxide nanoparticles with silica. Journal of Magnetism and Magnetic Materials, 2016. 416: p. 275-291.

166. Gnanaprakash, G., et al., Effect of digestion time and alkali addition rate on physical properties of magnetite nanoparticles. The Journal of Physical Chemistry B, 2007. 111(28): p. 7978-7986.

167. Niederberger, M., Nonaqueous sol–gel routes to metal oxide nanoparticles. Accounts of chemical research, 2007. 40(9): p. 793-800.

168. Li, H., et al., HEPES-involved hydrothermal synthesis of Fe_3O_4 nanoparticles and their biological application. 2014.

169. Ramimoghadam, D., S. Bagheri, and S.B. Abd Hamid, Progress in electrochemical synthesis of magnetic iron oxide nanoparticles. Journal of Magnetism and Magnetic Materials, 2014. 368: p. 207-229.

170. Wang, J., et al., Chemical vapor deposition prepared bi-morphological carbon-coated Fe3O4 composites as anode materials for lithium-ion batteries. Journal of Power Sources, 2015. 282: p. 257-264.

171. Sharma, G. and P. Jeevanandam, Synthesis of self-assembled prismatic iron oxide nanoparticles by a novel thermal decomposition route. RSC advances, 2013. 3(1): p. 189-200.

172. Zhu, N., et al., Surface modification of magnetic iron oxide nanoparticles. Nanomaterials, 2018. 8(10): p. 810.

173. Yu, H., et al., Transport and retention of aqueous dispersions of superparamagnetic nanoparticles in sandstone. Journal of Petroleum Science and Engineering, 2014. 116: p. 115-123.

174. Khan, S., D.K. Potter, and E. Kuru, Quantifying the transport of superparamagnetic nanoparticles in porous media using an acrylic flow cell and integrated magnetic susceptibility sensor technique. Transport in Porous Media, 2015. 106(3): p. 691-705.

175. Yusoff, A.H., M.N. Salimi, and M.F. Jamlos, A review: Synthetic strategy control of magnetite nanoparticles production. Advances in nano research, 2018. 6(1): p. 1.

176. Akbarzadeh, A., M. Samiei, and S. Davaran, Magnetic nanoparticles: preparation, physical properties, and applications in biomedicine. Nanoscale research letters, 2012. 7(1): p. 1-13.

177. Prodanovic, M., et al. Effects of magnetic field on the motion of multiphase fluids containing paramagnetic nanoparticles in porous media. in SPE Improved Oil Recovery Symposium. 2010. Society of Petroleum Engineers.

178. Pisane, K.L., E.C. Despeaux, and M.S. Seehra, Magnetic relaxation and correlating effective magnetic moment with particle size distribution in maghemite nanoparticles. Journal of Magnetism and Magnetic Materials, 2015. 384: p. 148-154.

179. Macnae, J., Superparamagnetism in ground and airborne electromagnetics: Geometrical and physical controls. Geophysics, 2017. 82(6): p. E347-E356.

180. Le Follotec, A., et al., Triblock copolymers as destabilizers of water-in-crude oil emulsions. Colloids and Surfaces A: Physicochemical and Engineering Aspects, 2010. 365(1-3): p. 162-170.

181. Wang, C., et al., Synthesis and evaluation of demulsifiers with polyethyleneimine as accepter for treating crude oil emulsions. Polymers for Advanced Technologies, 2015. 26(5): p. 442-448.

182. Pensini, E., et al., Demulsification mechanism of asphaltene-stabilized water-in-oil emulsions by a polymeric ethylene oxide–propylene oxide demulsifier. Energy & fuels, 2014. 28(11): p. 6760-6771.

183. Li, M., et al., The effect of HPAM on crude oil/water interfacial properties and the stability of crude oil emulsions. Journal of dispersion science and technology, 2007. 28(1): p. 189-192.

184. Li, M., et al., The influence of NaOH on the stability of paraffinic crude oil emulsion. Fuel, 2005. 84(2-3): p. 183-187.

185. Wang, J., et al., Demulsification of crude oil emulsion using polyamidoamine dendrimers. Separation science and technology, 2007. 42(9): p. 2111-2120.

186. Wang, J., et al., Synthesis and characterization of lower generation broom molecules. Chinese chemical letters, 2008. 19(1): p. 43-46.

187. El-Sharaky, E.S.A., A.E. El-Tabey, and M.R. Mishrif, Novel star polymeric nonionic surfactants as crude oil emulsion breakers. Journal of Surfactants and Detergents, 2019. 22(4): p. 779-793.

188. Bi, Y., et al., Dendrimer-based demulsifiers for polymer flooding oil-in-water emulsions. Energy & Fuels, 2017. 31(5): p. 5395-5401.

189. Hao, L., et al., Efficient demulsification of diesel-in-water emulsions by different structural dendrimer-based demulsifiers. Industrial & Engineering Chemistry Research, 2016. 55(6): p. 1748-1759.

190. Yao, X., et al., Synthesis of a novel dendrimer-based demulsifier and its application in the treatment of typical diesel-in-water emulsions with ultrafine oil droplets. Energy & fuels, 2014. 28(9): p. 5998-6005.

191. Zhang, L., et al., Hyperbranched poly (amido amine) as an effective demulsifier for oil-in-water emulsions of microdroplets. Fuel, 2018. 211: p. 197-205.

192. You, Z., et al., Effective treatment of emulsified oil wastewater by the coagulation–flotation process. RSC advances, 2018. 8(71): p. 40639-40646.

193. Kuang, J., et al., Demulsification of oil-in-water emulsions using hyperbranched poly (amido amine) demulsifiers with 4, 4-diaminodiphenyl methane as initial cores. Journal of Applied Polymer Science, 2020. 137(26): p. 48846.

194. Chen, K., et al., OH-and NH2-Terminated Hyperbranched Polysiloxanes: Controlled Synthesis, Characterization, Toughening, and Reinforcing Epoxy Resin. Macromolecular Chemistry and Physics, 2018. 219(18): p. 1800200.

195. Kailey, I., C. Blackwell, and J. Behles, Collaborative interactions between EO-PO copolymers upon mixing. Industrial & Engineering Chemistry Research, 2013. 52(50): p. 17913-17919.

196. Zhang, Z., et al., Demulsification by amphiphilic dendrimer copolymers. Journal of colloid and interface science, 2005. 282(1): p. 1-4.

197. Berthod, A., M. Ruiz-Angel, and S. Carda-Broch, Ionic liquids in separation techniques. Journal of Chromatography A, 2008. 1184(1-2): p. 6-18.

198. Ren, F., et al., Applications of ionic liquids in starch chemistry: a review. Green Chemistry, 2020. 22(7): p. 2162-2183.

199. Bin Dahbag, M.S., M.E. Hossain, and A.A. AlQuraishi, Efficiency of ionic liquids as an enhanced oil recovery chemical: simulation approach. Energy & Fuels, 2016. 30(11): p. 9260-9265.

200. Martínez-Palou, R. and J. Aburto, Ionic liquids as surfactants–applications as demulsifiers of petroleum emulsions. Ionic liquidscurrent state of the art, 2015: p. 305-326.

201. Alves, D., et al., Influence of ionic liquids on the viscoelastic properties of crude oil emulsions. Energy & Fuels, 2017. 31(9): p. 9132-9139.

202. Pillai, P., A. Kumar, and A. Mandal, Mechanistic studies of enhanced oil recovery by imidazolium-based ionic liquids as novel surfactants. Journal of industrial and engineering chemistry, 2018. 63: p. 262-274.

203. Sastry, N.V., N.M. Vaghela, and V.K. Aswal, Effect of alkyl chain length and head group on surface active and aggregation behavior of ionic liquids in water. Fluid Phase Equilibria, 2012. 327: p. 22-29.

204. Moradi, M., V. Alvarado, and S. Huzurbazar, Effect of salinity on water-in-crude oil emulsion: evaluation through drop-size distribution proxy. Energy & fuels, 2011. 25(1): p. 260-268.

205. Hezave, A.Z., et al., Investigating the effect of ionic liquid (1-dodecyl-3-methylimidazolium chloride ([C12mim][Cl])) on the water/oil interfacial tension as a novel surfactant. Colloids and Surfaces A: Physicochemical and Engineering Aspects, 2013. 421: p. 63-71.

206. Hezave, A.Z., et al., Dynamic interfacial tension behavior between heavy crude oil and ionic liquid solution (1-dodecyl-3-methylimidazolium chloride ([C12mim][Cl]+ distilled or saline water/heavy crude oil)) as a new surfactant. Journal of Molecular Liquids, 2013. 187: p. 83-89.

207. Atta, A.M., et al., Application of new amphiphilic ionic liquid based on ethoxylated octadecylammonium tosylate as demulsifier and petroleum crude oil spill dispersant. Journal of Industrial and Engineering Chemistry, 2016. 33: p. 122-130.

208. Forsyth, S.A., J.M. Pringle, and D.R. MacFarlane, Ionic liquids—an overview. Australian Journal of Chemistry, 2004. 57(2): p. 113-119.

209. Hazrati, N., A.A.M. Beigi, and M. Abdouss, Demulsification of water in crude oil emulsion using long chain imidazolium ionic liquids and optimization of parameters. Fuel, 2018. 229: p. 126-134.

210. Oropeza, E.A.F., et al., Dehydrating and desalting median, heavy and extra-heavy oils using ionic liquids and their formulations. 2016, Google Patents.

211. Tian, Y., et al., Ionic liquid-enhanced solvent extraction for oil recovery from oily sludge. Energy & Fuels, 2019. 33(4): p. 3429-3438.

212. Peng, J., et al., Novel magnetic demulsifier for water removal from diluted bitumen emulsion. Energy & fuels, 2012. 26(5): p. 2705-2710.

213. Nie, H., et al., Biological treatment of high salinity and low pH produced water in oilfield with immobilized cells of P. aeruginosa NY3 in a pilot-scale. Journal of Hazardous Materials, 2020. 381: p. 121232.

214. Victor-Oji, C., U. Chukwu, and O. Akaranta, Comparative Study of Cashew Nut Shell Liquid and a Commercial Demulsifier for Treating Crude Oil Emulsions. Chemical Science International Journal, 2019: p. 1-17.

215. Feng, X., et al., Effect of hydroxyl content and molecular weight of biodegradable ethylcellulose on demulsification of water-in-diluted bitumen emulsions. Industrial & Engineering Chemistry Research, 2011. 50(10): p. 6347-6354.

216. Chen, Z., et al., Demulsifying water-in-oil emulsions by ethyl cellulose demulsifiers studied using focused beam reflectance measurement. Chemical Engineering Science, 2015. 130: p. 254-263.

217. Chang, C.-C., Aging Oil-Water Interfaces with Asphaltene and Demulsifier Adsorption: Interface Rheology and Heterogeneity. 2019, University of California, Santa Barbara.

218. Feng, X., et al., Mechanistic study on demulsification of water-in-diluted bitumen emulsions by ethylcellulose. Langmuir, 2009. 26(5): p. 3050-3057.

219. Satoh, T., et al., Synthesis, structure, and characteristics of hyperbranched polyterpene alcohols. Macromolecules, 2008. 41(14): p. 5265-5271.

220. Rosly, M.B., et al., Stability of emulsion liquid membrane using bifunctional diluent and blended nonionic surfactant for phenol removal. Chemical Engineering and Processing-Process Intensification, 2020. 148: p. 107790.

221. Roodbari, N.H., et al., Tweens demulsification effects on heavy crude oil/water emulsion. Arabian Journal of Chemistry, 2016. 9: p. S806-S811.

222. Roshan, N., S. Ghader, and M.R. Rahimpour, Application of the response surface methodology for modeling demulsification of crude oil emulsion using a demulsifier. Journal of Dispersion Science and Technology, 2018. 39(5): p. 700-710.

223. Bo, Z., et al., Synthesis of aryl/alkyl building blocks for dendrimer and hyperbranched polymer synthesis. Organic letters, 2004. 6(5): p. 667-669.

224. Pochan, D.J., et al., Architectural Disparity Effects in the Morphology of Dendrimer− Linear Coil Diblock Copolymers. Macromolecules, 2002. 35(24): p. 9239-9242.

225. Sikwal, D.R., R.S. Kalhapure, and T. Govender, An emerging class of amphiphilic dendrimers for pharmaceutical and biomedical applications: Janus amphiphilic dendrimers. European Journal of Pharmaceutical Sciences, 2017. 97: p. 113-134.

226. Wang, J., et al., Synthesis of dendritic polyether surfactants for demulsification. Separation and purification technology, 2010. 73(3): p. 349-354.

227. Pradilla, D., S. Simon, and J. Sjöblom, Mixed interfaces of asphaltenes and model demulsifiers part I: Adsorption and desorption of single components. Colloids and Surfaces A: Physicochemical and Engineering Aspects, 2015. 466: p. 45-56.

228. Caminade, A.-M., et al., Dendrimers and hyper-branched polymers interacting with clays: fruitful associations for functional materials. Journal of Materials Chemistry A, 2019. 7(34): p. 19634-19650.

229. Xu, T., et al., The role of supercritical water in pyrolysis of carbonaceous compounds. Energy & Fuels, 2013. 27(6): p. 3148-3153.

230. Liu, G., X. Xu, and J. Gao, Study on the compatibility of high-paraffin crude oil with electric desalting demulsifiers. Energy & fuels, 2003. 17(3): p. 625-630.

231. Kadhim, A., et al., Synthesis and Aggregation of a Porphyrin-Cored Hyperbranched Polyglycidol and Its Application as a Macromolecular Photosensitizer for Photodynamic Therapy. Molecular pharmaceutics, 2019. 16(3): p. 1132-1139.

232. Al-Momani, F., et al., Biodegradability enhancement of textile dyes and textile wastewater by VUV photolysis. Journal of Photochemistry and Photobiology A: Chemistry, 2002. 153(1): p. 191-197.

233. Gamal El-Din, M., et al., Oxidation of resin and fatty acids by ozone: Kinetics and toxicity study. Water Research, 2006. 40(2): p. 392-400.

234. Al Momani, F., Impact of photo-oxidation technology on the aqueous solutions of nitrobenzene: Degradation efficiency and biodegradability enhancement. Journal of Photochemistry and Photobiology A: Chemistry, 2006. 179(1): p. 184-192.

235. Figiel, F.J., Azeotrope-like compositions of trichlorotrifluoroethane, methanol, ethanol, isopropanol and nitromethane. 1977, Google Patents.

236. Kainthan, R.K., et al., Synthesis, characterization, and viscoelastic properties of high molecular weight hyperbranched polyglycerols. Macromolecules, 2006. 39(22): p. 7708-7717.

237. Whelton, A.J., et al., Impact of infrastructure coating materials on storm-water quality: Review and experimental study. Journal of Environmental Engineering, 2012. 139(5): p. 746-756.

238. Hiemenz, P.C. and T.P. Lodge, Polymer chemistry. 2007: CRC press.

239. Dadkhah, M., et al., Synthesis of hyperbranched polyglycerols using ascorbic acid as an activator. RSC advances, 2018. 8(1): p. 217-221.

240. Giri, A., et al., Synthesis and characterization of biopolymer based hybrid hydrogel nanocomposite and study of their electrochemical efficacy. International journal of biological macromolecules, 2019. 123: p. 228-238.

241. Nayak, B. and R. Singh, Synthesis and characterization of grafted hydroxypropyl guar gum by ceric ion induced initiation. European Polymer Journal, 2001. 37(8): p. 1655-1666.

242. Mańko, D., A. Zdziennicka, and B. Jańczuk, Surface tension of polytetrafluoroethylene and its wetting by aqueous solution of some surfactants and their mixtures. Applied Surface Science, 2017. 392: p. 117-125.

243. Alther, G., Organoclay cost effectively removes oil from produced water. Oil and Gas Journal, 1997. 95(15).

244. Sekhon, B.S., Surfactants: pharmaceutical and medicinal aspects. 2014.

245. Tchobanoglous, G. and F.L. Burton, Wastewater engineering: treatment, disposal, and reuse. 1991: Metcalf & Eddy.

246. Al Momani, F.A., A.T. Shawaqfeh, and M.a.S. Shawaqfeh, Solar wastewater treatment plant for aqueous solution of pesticide. Solar Energy, 2007. 81(10): p. 1213-1218.

247. Al Momani, F., D.W. Smith, and M. Gamal El-Din, Degradation of cyanobacteria toxin by advanced oxidation processes. Journal of Hazardous Materials, 2008. 150(2): p. 238-249.

248. Kolhe, P., et al., Drug complexation, in vitro release and cellular entry of dendrimers and hyperbranched polymers. International journal of pharmaceutics, 2003. 259(1-2): p. 143-160.

249. Aryal, S., et al., Biodegradable and biocompatible multi-arm star amphiphilic block copolymer as a carrier for hydrophobic drug delivery. International journal of biological macromolecules, 2009. 44(4): p. 346-352.

250. Jha, P.K., V. Mahto, and V. Saxena, Study the effects of xanthan gum and aluminium stearate on the properties of oil-in-water emulsion drilling fluids. Arabian Journal for Science and Engineering, 2016. 41(1): p. 143-153.

251. Abdalla, M., et al., Impact of combined oil-in-water emulsions and particulate suspensions on ceramic membrane fouling and permeability recovery. Separation and Purification Technology, 2019. 212: p. 215-222.

252. Pal, R., Rheological behaviour of surfactant-flocculated water-in-oil emulsions. Colloids and Surfaces A: Physicochemical and Engineering Aspects, 1993. 71(2): p. 173-185.

253. Zhang, L., et al., Methacrylated hyperbranched polyglycerol as a high-efficiency demulsifier for oil-in-water emulsions. Energy & Fuels, 2016. 30(11): p. 9939-9946.

254. Muller, G., Thermal stability of high-molecular-weight polyacrylamide aqueous solutions. Polymer Bulletin, 1981. 5(1): p. 31-37.

255. Peng, S. and C. Wu, Light scattering study of the formation and structure of partially hydrolyzed poly (acrylamide)/calcium (II) complexes. Macromolecules, 1999. 32(3): p. 585-589.

256. Zhang, Y., et al., Synthesis of fluorinated silicon-containing amphiphilic copolymer and its demulsification performance. Colloids and Surfaces A: Physicochemical and Engineering Aspects, 2018. 558: p. 479-487.

257. Mandal, A., et al., Characterization of oil− water emulsion and its use in enhanced oil recovery. Industrial & engineering chemistry research, 2010. 49(24): p. 12756-12761.

258. Duan, M., et al., Treatment of wastewater produced from polymer flooding using polyoxyalkylated polyethyleneimine. Separation and Purification Technology, 2014. 133: p. 160-167.

259. Oudshoorn, M.H., et al., Synthesis and characterization of hyperbranched polyglycerol hydrogels. Biomaterials, 2006. 27(32): p. 5471-5479.

260. Igunnu, E.T. and G.Z. Chen, Produced water treatment technologies. International Journal of Low-Carbon Technologies, 2014. 9(3): p. 157-177.

261. Albatrni, H., et al., Polymeric adsorbents for oil removal from water. Chemosphere, 2019. 233: p. 809-817.

262. Farrington, J.W., Oil pollution in the marine environment i: inputs, big spills, small spills, and dribbles. Environment: Science and Policy for Sustainable Development, 2013. 55(6): p. 3-13.

263. Lahann, J., Environmental nanotechnology: Nanomaterials clean up. Nature nanotechnology, 2008. 3(6): p. 320.

264. Zang, D., et al., Novel superhydrophobic and superoleophilic sawdust as a selective oil sorbent for oil spill cleanup. Chemical Engineering Research and Design, 2015. 102: p. 34-41.

265. Wang, S., M. Li, and Q. Lu, Filter paper with selective absorption and separation of liquids that differ in surface tension. ACS Applied Materials & Interfaces, 2010. 2(3): p. 677-683.

266. Chen, P.-C. and Z.-K. Xu, Mineral-coated polymer membranes with superhydrophilicity and underwater superoleophobicity for effective oil/water separation. Scientific reports, 2013. 3: p. 2776.

267. Dunderdale, G.J., et al., Continuous, high-speed, and efficient oil/water separation using meshes with antagonistic wetting properties. ACS applied materials & interfaces, 2015. 7(34): p. 18915-18919.

268. Li, B., et al., Superwetting double-layer polyester materials for effective removal of both insoluble oils and soluble dyes in water. ACS applied materials & interfaces, 2014. 6(14): p. 11581-11588.

269. Coca, J., G. Gutiérrez, and J. Benito, Treatment of oily wastewater, in Water Purification and Management. 2011, Springer. p. 1-55.

270. Martínez-González, G., et al., Approximate method for designing a primary settling tank for wastewater treatment. Industrial & engineering chemistry research, 2009. 48(16): p. 7842-7846.

271. Bellino, P.W., M.R. Flynn, and A.S. Rangwala, A study of spreading of crude oil in an ice channel. Journal of Loss Prevention in the Process Industries, 2013. 26(3): p. 558-561.

272. Minhalma, M. and M.N. De Pinho, Flocculation/flotation/ultrafiltration integrated process for the treatment of cork processing wastewaters. Environmental science & technology, 2001. 35(24): p. 4916-4921.

273. Guix, M., et al., Superhydrophobic alkanethiol-coated microsubmarines for effective removal of oil. Acs Nano, 2012. 6(5): p. 4445-4451.

274. Lipp, P., et al., A fundamental study of the ultrafiltration of oil-water emulsions. Journal of Membrane Science, 1988. 36: p. 161-177.

275. Xu, C., Y. Xu, and J. Zhu, Photocatalytic antifouling graphene oxide-mediated hierarchical filtration membranes with potential applications on water purification. ACS applied materials & interfaces, 2014. 6(18): p. 16117-16123.

276. Zhang, W., et al., Superhydrophobic and superoleophilic PVDF membranes for effective separation of water-in-oil emulsions with high flux. Advanced Materials, 2013. 25(14): p. 2071-2076.

277. Zhang, H., et al., Preparation of a novel flocculant and its performance for treating acidic oily wastewater. RSC Advances, 2016. 6(108): p. 106102-106108.

278. Lü, T., et al., Efficient treatment of emulsified oily wastewater by using amphipathic chitosan-based flocculant. Reactive and Functional Polymers, 2019. 139: p. 133-141.

279. Rajak, V., et al., Mechanism and kinetics of separation of oil from oil-in-water emulsion by air flotation. Petroleum Science and Technology, 2015. 33(23-24): p. 1861-1868.

280. Wang, Z., Y. Wang, and G. Liu, Rapid and efficient separation of oil from oil-in-water emulsions using a Janus cotton fabric. Angewandte Chemie International Edition, 2016. 55(4): p. 1291-1294.

281. Lv, W., et al., 3D multiscale superhydrophilic sponges with delicately designed pore size for ultrafast oil/water separation. Advanced Functional Materials, 2017. 27(48): p. 1704293.

282. Crini, G. and E. Lichtfouse, Advantages and disadvantages of techniques used for wastewater treatment. Environmental Chemistry Letters, 2019. 17(1): p. 145-155.

283. Kang, W., et al., Flocculation, coalescence and migration of dispersed phase droplets and oil–water separation in heavy oil emulsion. Journal of Petroleum Science and Engineering, 2012. 81: p. 177-181.

284. Mostefa, N.M. and M. Tir, Coupling flocculation with electroflotation for waste oil/water emulsion treatment. Optimization of the operating conditions. Desalination, 2004. 161(2): p. 115-121.

285. Rubio, J., M. Souza, and R. Smith, Overview of flotation as a wastewater treatment technique. Minerals engineering, 2002. 15(3): p. 139-155.

286. Almomani, F., et al., Heavy metal ions removal from industrial wastewater using magnetic nanoparticles (MNP). Applied Surface Science, 2020. 506: p. 144924.

287. Urbanova, V., et al., Nanocrystalline iron oxides, composites, and related materials as a platform for electrochemical, magnetic, and chemical biosensors. Chemistry of Materials, 2014. 26(23): p. 6653-6673.

288. Liang, J., et al., Demulsification of oleic-acid-coated magnetite nanoparticles for cyclohexane-in-water nanoemulsions. Energy & fuels, 2014. 28(9): p. 6172-6178.

289. Li, S., et al., The synthesis of a novel magnetic demulsifier and its application for the demulsification of oil-charged industrial wastewaters. Journal of Materials Chemistry A, 2014. 2(1): p. 94-99.

290. Bagheri, S. and N.M. Julkapli, Modified iron oxide nanomaterials: Functionalization and application. Journal of Magnetism and Magnetic Materials, 2016. 416: p. 117-133.

291. Lü, T., et al., A facile method for emulsified oil-water separation by using polyethylenimine-coated magnetic nanoparticles. Journal of Nanoparticle Research, 2018. 20(4): p. 88.

292. Mirshahghassemi, S., et al., Application of high gradient magnetic separation for oil remediation using polymer-coated magnetic nanoparticles. Separation and Purification Technology, 2017. 179: p. 328-334.

293. Liang, C., et al., Adsorption-Based Synthesis of Magnetically Responsive and Interfacially Active Composite Nanoparticles for Dewatering of Water-in-Diluted Bitumen Emulsions. Energy & fuels, 2018. 32(8): p. 8078-8089.

294. Zhang, J., et al., Facile fabrication of cyclodextrin-modified magnetic particles for effective demulsification from various types of emulsions. Environmental science & technology, 2016. 50(16): p. 8809-8816.

295. Lü, T., et al., Synthesis of pH-sensitive and recyclable magnetic nanoparticles for efficient separation of emulsified oil from aqueous environments. Applied Surface Science, 2017. 396: p. 1604-1612.

296. Wang, X.L., et al., Synthesis and characterization of magnetic and luminescent Fe3O4/CdTe nanocomposites using aspartic acid as linker. Chinese Chemical Letters, 2011. 22(2): p. 233-236.

297. Li, B., et al., Synthesis of Fe3O4/polypyrrole/polyaniline nanocomposites by in-situ method and their electromagnetic absorbing properties. Journal of Saudi Chemical Society, 2017. 21(4): p. 466-472.

298. Yusoff, A., M.N. Salimi, and M.F. Jamlos. Synthesis and characterization of biocompatible Fe3O4 nanoparticles at different pH. in AIP Conference Proceedings. 2017. AIP Publishing.

299. Mukasyan, A. and P. Dinka, Novel approaches to solution-combustion synthesis of nanomaterials. International Journal of Self-Propagating High-Temperature Synthesis, 2007. 16(1): p. 23-35.

300. Rahmawati, R., et al., Synthesis of magnetite (Fe3O4) nanoparticles from iron sands by coprecipitation-ultrasonic irradiation methods. J. Mater. Environ. Sci, 2018. 9(3): p. 155-160.

301. Li, X.-M., et al., Magnetic Fe3O4 nanoparticles: Synthesis and application in water treatment. Nanoscience & Nanotechnology-Asia, 2011. 1(1): p. 14-24.

302. Daou, T., et al., Hydrothermal synthesis of monodisperse magnetite nanoparticles. Chemistry of Materials, 2006. 18(18): p. 4399-4404.

303. Wang, J., et al., One-step hydrothermal process to prepare highly crystalline Fe3O4 nanoparticles with improved magnetic properties. Materials research bulletin, 2003. 38(7): p. 1113-1118.

304. Chen, D. and R. Xu, Hydrothermal synthesis and characterization of nanocrystalline Fe3O4 powders. Materials Research Bulletin, 1998. 33(7): p. 1015-1021.

305. Darvishi, M., G. Mohseni-Asgerani, and J. Seyed-Yazdi, Simple microwave irradiation procedure for the synthesis of CuO/Graphene hybrid composite with significant photocatalytic enhancement. Surfaces and Interfaces, 2017. 7: p. 69-73.

306. Moore, J.J. and H. Feng, Combustion synthesis of advanced materials: Part I. Reaction parameters. Progress in materials science, 1995. 39(4-5): p. 243-273.

307. Mukasyan, A. and K. Manukyan, One-and Two-Dimensional Nanostructures Prepared by Combustion Synthesis, in Nanomaterials Synthesis. 2019, Elsevier. p. 85-120.

308. Aruna, S.T. and A.S. Mukasyan, Combustion synthesis and nanomaterials. Current opinion in solid state and materials science, 2008. 12(3-4): p. 44-50.

309. Rao, C.N.R. and C.N.R. Rao, Chemical approaches to the synthesis of inorganic materials. 1994: John Wiley & Sons Inc.

310. Lu, A.H., E.e.L. Salabas, and F. Schüth, Magnetic nanoparticles: synthesis, protection, functionalization, and application. Angewandte Chemie International Edition, 2007. 46(8): p. 1222-1244.

311. Varma, A., et al., Solution combustion synthesis of nanoscale materials. Chemical reviews, 2016. 116(23): p. 14493-14586.

312. Yao, Y., et al., Synthesis of Fe3O4/polyaniline nanocomposite in reversed micelle systems and its performance characteristics. Procedia Engineering, 2012. 27: p. 664-670.

313. Tang, N., et al., Nanostructured magnetite (Fe3O4) thin films prepared by sol–gel method. Journal of magnetism and magnetic materials, 2004. 282: p. 92-95.

314. Schwertmann, U. and R.M. Cornell, Iron oxides in the laboratory: preparation and characterization. 2008: John Wiley & Sons.

315. Wu, W., Q. He, and C. Jiang, Magnetic iron oxide nanoparticles: synthesis and surface functionalization strategies. Nanoscale research letters, 2008. 3(11): p. 397.

316. Ashok, A., et al., Study of ethanol dehydrogenation reaction mechanism for hydrogen production on combustion synthesized cobalt catalyst. International Journal of Hydrogen Energy, 2017. 42(37): p. 23464-23473.

317. Abinaya, R., et al., Comparative study on the Mg doped Hydroxyapatite through Sol-gel and Hydrothermal Techniques. Int J Innov Res Sci Eng, 2014. 1: p. 1-6.

318. Jin, Z., et al., Enhanced magnetic and electrochemical properties of one-step synthesized PANI-Fe3O4 composite nanomaterial by a novel green solvothermal method. Journal of Alloys and Compounds, 2017. 695: p. 1807-1812.

319. Jamal, M., et al., Mechanical Properties of the Concrete Containing Porcelain Waste as Sand. vol, 2018. 7: p. 180-184.

320. Aghazadeh, M. and F. Aghazadeh, Improve Synthesis of Iron Oxide Nanorode with Hydrothermal Method. 2013.

321. Lemine, O., et al., Sol–gel synthesis of 8 nm magnetite (Fe3O4) nanoparticles and their magnetic properties. Superlattices and Microstructures, 2012. 52(4): p. 793-799.

322. Azlina, H., et al., Synthesis of SiO2 nanostructures using sol-gel method. Acta Phys. Pol. A, 2016. 129(4): p. 842-844.

323. Taka, Z.I., et al., Preparation of Aniline Dimer-COOH Modified Magnetite (Fe3O4) Nanoparticles by Ultrasonic Dispersion Method. vol, 2018. 7: p. 185-188.

324. Shafiee, S., et al., Sol-gel synthesis of thermoluminescent Cd-doped ZnTe nanoparticles. 2015.

325. Matthew, B., M. Steven J, and B. Andrew P, Comparison of hydrothermal and sol-gel synthesis of nano-particulate hydroxyapatite by characterisation at the bulk and particle level. Open Journal of Inorganic Non-metallic Materials, 2012. 2012.

326. Mimani, T. and K. Patil, Solution combustion synthesis of nanoscale oxides and their composites. Materials Physics and Mechanics(Russia), 2001. 4(2): p. 134-137.

327. Chaki, S., et al., Magnetite Fe3O4 nanoparticles synthesis by wet chemical reduction and their characterization. Advances in Natural Sciences: Nanoscience and Nanotechnology, 2015. 6(3): p. 035009.

328. I Takai, Z., et al., Preparation and characterization of magnetite (Fe3O4) nanoparticles by sol-gel method. Journal of Human Development and Communication, 2019. 12(1): p. 37-46.

329. Zhang, L., et al., Origin of visible photoluminescence of ZnO quantum dots: defect-dependent and size-dependent. The Journal of Physical Chemistry C, 2010. 114(21): p. 9651-9658.

330. Takai, Z., M. Mustafa, and S. Asman, Preparation of high performance conductive polyaniline magnetite (PANI/Fe3O4) Nanocomposites by Sol-Gel Method. Asian J. Chem, 2018. 30(12): p. 2625-2630.

331. Kalia, S., et al., Magnetic polymer nanocomposites for environmental and biomedical applications. Colloid and Polymer Science, 2014. 292(9): p. 2025-2052.

332. Jamshidiyan, M., A. Shirani, and G. Alahyarizadeh, Solvothermal synthesis and characterization of magnetic Fe3O4 nanoparticle by different sodium salt sources. Materials Science-Poland, 2017. 35(1): p. 50-57.

333. Xu, J., et al., Preparation and magnetic properties of magnetite nanoparticles by sol–gel method. Journal of Magnetism and magnetic Materials, 2007. 309(2): p. 307-311.

334. Unni, M., et al., Thermal decomposition synthesis of iron oxide nanoparticles with diminished magnetic dead layer by controlled addition of oxygen. ACS nano, 2017. 11(2): p. 2284-2303.

335. Mamani, J.B., L.F. Gamarra, and G.E.d.S. Brito, Synthesis and characterization of Fe3O4 nanoparticles with perspectives in biomedical applications. Materials Research, 2014. 17(3): p. 542-549.

336. Mahdavi, M., et al., Optimized conditions for graft copolymerization of poly (acrylamide) onto rubberwood fibre. BioResources, 2011. 6(4): p. 5110-5120.

337. Mahdavi, M., et al., Synthesis, surface modification and characterisation of biocompatible magnetic iron oxide nanoparticles for biomedical applications. Molecules, 2013. 18(7): p. 7533-7548.

338. Rajput, S., C.U. Pittman Jr, and D. Mohan, Magnetic magnetite (Fe3O4) nanoparticle synthesis and applications for lead (Pb2+) and chromium (Cr6+)

removal from water. Journal of colloid and interface science, 2016. 468: p. 334-346.

339. Chicea, D., E. Indrea, and C. Cretu, Assesing Fe3O4 nanoparticle size by DLS, XRD and AFM. Journal of optoelectronics and advanced materials, 2012. 14(5): p. 460.

340. Pati, S., et al., High temperature phase transformation studies in magnetite nanoparticles doped with Co2+ ion. Journal of Applied Physics, 2012. 112(5): p. 054320.

341. Fock, J., et al., On the 'centre of gravity'method for measuring the composition of magnetite/maghemite mixtures, or the stoichiometry of magnetite-maghemite solid solutions, via 57Fe Mössbauer spectroscopy. Journal of Physics D: Applied Physics, 2017. 50(26): p. 265005.

342. Lehlooh, A.-F. and S.H. Mahmood, Mössbauer spectroscopy of Fe3O4 ultrafine particles. Journal of magnetism and magnetic materials, 1995. 151(1-2): p. 163-166.

343. Vijayakumar, R., et al., Sonochemical synthesis and characterization of pure nanometer-sized Fe3O4 particles. Materials Science and Engineering: A, 2000. 286(1): p. 101-105.

344. Panda, R., N. Gajbhiye, and G. Balaji, Magnetic properties of interacting single domain Fe3O4 particles. Journal of Alloys and Compounds, 2001. 326(1-2): p. 50-53.

345. Handke, B., et al., Magnesium interdiffusion and surface oxidation in magnetite epitaxial films grown on MgO (1 0 0). Vacuum, 2001. 63(1-2): p. 331-336.

346. Korecki, J., et al., Size effects in epitaxial films of magnetite. Thin Solid Films, 2002. 412(1-2): p. 14-23.

347. Li, L.-J., et al., Comparative study of photoluminescence of single-walled carbon nanotubes wrapped with sodium dodecyl sulfate, surfactin and polyvinylpyrrolidone. Nanotechnology, 2005. 16(5): p. S202.

348. Palchoudhury, S. and J.R. Lead, A facile and cost-effective method for separation of oil–water mixtures using polymer-coated iron oxide nanoparticles. Environmental science & technology, 2014. 48(24): p. 14558-14563.

349. Chen, C.-M., et al., Influence of pH on the stability of oil-in-water emulsions stabilized by a splittable surfactant. Colloids and Surfaces A: Physicochemical and Engineering Aspects, 2000. 170(2-3): p. 173-179.

350. Fang, Y. and D.G. Dalgleish, Conformation of β-lactoglobulin studied by FTIR: effect of pH, temperature, and adsorption to the oil–water interface. Journal of Colloid and Interface Science, 1997. 196(2): p. 292-298.

351. Stachurski, J. and M. MichaŁek, The effect of the ζ potential on the stability of a non-polar oil-in-water emulsion. Journal of colloid and interface science, 1996. 184(2): p. 433-436.

352. Mirshahghassemi, S., B. Cai, and J.R. Lead, Evaluation of polymer-coated magnetic nanoparticles for oil separation under environmentally relevant conditions: effect of ionic strength and natural organic macromolecules. Environmental Science: Nano, 2016. 3(4): p. 780-787.

353. Shen, Q., et al., Crystallization and aggregation behaviors of calcium carbonate in the presence of poly (vinylpyrrolidone) and sodium dodecyl sulfate. The Journal of Physical Chemistry B, 2005. 109(39): p. 18342-18347.

354. Hiemenz, P.C. and P.C. Hiemenz, Principles of colloid and surface chemistry. Vol. 188. 1986: M. Dekker New York.

355. Deng, S., et al., Effects of alkaline/surfactant/polymer on stability of oil droplets in produced water from ASP flooding. Colloids and Surfaces A: Physicochemical and Engineering Aspects, 2002. 211(2-3): p. 275-284.

356. Paixão, M.V.G. and R. de Carvalho Balaban, Application of guar gum in brine clarification and oily water treatment. International journal of biological macromolecules, 2018. 108: p. 119-126.

357. Tang, J., et al., The investigation on Fe3O4 magnetic flocculation for high efficiency treatment of oily micro-polluted water. Journal of environmental management, 2019. 244: p. 399-407.

358. Yu, L., et al., Fe3O4/PS magnetic nanoparticles: Synthesis, characterization and their application as sorbents of oil from waste water. Journal of Magnetism and Magnetic Materials, 2015. 394: p. 14-21.

359. Hameed, B. and M. El-Khaiary, Malachite green adsorption by rattan sawdust: Isotherm, kinetic and mechanism modeling. Journal of Hazardous Materials, 2008. 159(2-3): p. 574-579.

360. Peng, M., et al., A critical review of the model fitting quality and parameter stability of equilibrium adsorption models. Advances in colloid and interface science, 2018. 262: p. 50-68.

361. Ashrafi, M., et al., Application of linear and non-linear methods for modeling removal efficiency of textile dyes from aqueous solutions using magnetic Fe3O4 impregnated onto walnut shell. Spectrochimica Acta Part A: Molecular and Biomolecular Spectroscopy, 2017. 171: p. 268-279.

362. El-Dib, F.I., et al., Study the adsorption properties of magnetite nanoparticles in the presence of different synthesized surfactants for heavy metal ions removal. Egyptian Journal of Petroleum, 2020. 29(1): p. 1-7.

363. Qiu, H., et al., Critical review in adsorption kinetic models. Journal of Zhejiang University-Science A, 2009. 10(5): p. 716-724.

364. Yuh-Shan, H., Citation review of Lagergren kinetic rate equation on adsorption reactions. Scientometrics, 2004. 59(1): p. 171-177.

365. Ho, Y.-S., Review of second-order models for adsorption systems. Journal of hazardous materials, 2006. 136(3): p. 681-689.

366. Yu, L., et al., Facile preparation and characterization of modified magnetic silica nanocomposite particles for oil absorption. Applied Surface Science, 2015. 357: p. 2297-2305.

367. Ahmad, A., S. Sumathi, and B. Hameed, Adsorption of residue oil from palm oil mill effluent using powder and flake chitosan: equilibrium and kinetic studies. Water research, 2005. 39(12): p. 2483-2494.

368. Jain, P., et al., Bioelectrochemical approaches for removal of sulfate, hydrocarbon and salinity from produced water. Chemosphere, 2017. 166: p. 96-108.

369. Zhang, Y., et al., Chemical characterization of non-volatile dissolved organic matter from oilfield-produced brines in the Nanyishan area of the western Qaidam Basin, China. Chemosphere, 2020: p. 128804.

370. Jiménez, S., et al., State of the art of produced water treatment. Chemosphere, 2018. 192: p. 186-208.

371. Krebsz, M., et al., Multiple applications of bio-graphene foam for efficient chromate ion removal and oil-water separation. Chemosphere, 2021. 263: p. 127790.

372. Karhu, M., et al., Bench scale electrocoagulation studies of bio oil-in-water and synthetic oil-in-water emulsions. Separation and Purification Technology, 2012. 96: p. 296-305.

373. Li, Y., et al., Novel dual superlyophobic cellulose membrane for multiple oil/water separation. Chemosphere, 2020. 241: p. 125067.

374. Qi, W.-K., et al., Removal of emulsion oil from oilfield ASP wastewater by internal circulation flotation and kinetic models. Chemical Engineering Science, 2013. 91: p. 122-129.

375. Kong, W., et al., Superhydrophilic Al2O3 Particle Layer for Efficient Separation of Oil-in-Water (O/W) and Water-in-Oil (W/O) Emulsions. Langmuir, 2020.

376. Tawalbeh, M., et al., Microbial desalination cells for water purification and power generation: A critical review. Energy, 2020. 209: p. 118493.

377. Maruyama, H., H. Seki, and Y. Satoh, Removal kinetic model of oil droplet from o/w emulsion by adding methylated milk casein in flotation. Water research, 2012. 46(9): p. 3094-3100.

378. Santo, C.E., et al., Optimization of coagulation–flocculation and flotation parameters for the treatment of a petroleum refinery effluent from a Portuguese plant. Chemical Engineering Journal, 2012. 183: p. 117-123.

379. Kong, W., et al., Electrochemical treatment of anionic surfactants in synthetic wastewater with three-dimensional electrodes. Journal of hazardous materials, 2006. 137(3): p. 1532-1537.

380. Hafiz, A., H. El-Din, and A. Badawi, Chemical destabilization of oil-in-water emulsion by novel polymerized diethanolamines. Journal of colloid and interface science, 2005. 284(1): p. 167-175.

381. Tripathi, B.P., et al., Antifouling and tunable amino functionalized porous membranes for filtration applications. Journal of Materials Chemistry, 2012. 22(37): p. 19981-19992.

382. Tawalbeh, M., et al., Membrane separation as a pre-treatment process for oily saline water. Desalination, 2018. 447: p. 182-202.

383. Al Bsoul, A., et al., Treatment of olive mill effluent by adsorption on titanium oxide nanoparticles. Science of The Total Environment, 2019. 688: p. 1327-1334.

384. Huang, X.-F., et al., Evaluation of screening methods for demulsifying bacteria and characterization of lipopeptide bio-demulsifier produced by Alcaligenes sp. Bioresource technology, 2009. 100(3): p. 1358-1365.

385. Wang, J., et al., Properties of magnetic carbon nanomaterials and application in removal organic dyes. Chemosphere, 2018. 207: p. 377-384.

386. Kokate, M., K. Garadkar, and A. Gole, One pot synthesis of magnetite–silica nanocomposites: applications as tags, entrapment matrix and in water purification. Journal of Materials Chemistry A, 2013. 1(6): p. 2022-2029.

387. Zhang, H., et al., Facile assembly of a hierarchical core@ shell Fe 3 O 4@ CuMgAl-LDH (layered double hydroxide) magnetic nanocatalyst for the hydroxylation of phenol. Journal of Materials Chemistry A, 2013. 1(19): p. 5934-5942.

388. Almomani, F., et al., Electrochemical oxidation of ammonia on nickel oxide nanoparticles. International Journal of Hydrogen Energy, 2020. 45(17): p. 10398-10408.

389. Almomani, F., et al., Heavy metal ions removal from industrial wastewater using magnetic nanoparticles (MNP). Applied Surface Science, 2020. 506: p. 144924.

390. Al-Qodah, Z., et al., Impact of surface modification of green algal biomass by phosphorylation on the removal of copper (II) ions from water. Turkish Journal of Chemistry, 2017. 41(2): p. 190-208.

391. Al-Shannag, M., et al., On the performance of Ballota Undulata biomass for the removal of cadmium (II) ions from water. Desalination and water treatment, 2017. 67: p. 223-230.

392. Fakhru'l-Razi, A., et al., Review of technologies for oil and gas produced water treatment. Journal of hazardous materials, 2009. 170(2-3): p. 530-551.

393. Wu, L., et al., Magnetic, durable, and superhydrophobic polyurethane@ Fe3O4@ SiO2@ fluoropolymer sponges for selective oil absorption and oil/water separation. ACS applied materials & interfaces, 2015. 7(8): p. 4936-4946.

394. Liu, G., et al., Core–shell–corona-structured polyelectrolyte brushes-grafting magnetic nanoparticles for water harvesting. ACS applied materials & interfaces, 2014. 6(14): p. 11625-11632.

395. Liu, J., et al., Recent developments in the chemical synthesis of inorganic porous capsules. Journal of Materials Chemistry, 2009. 19(34): p. 6073-6084.

396. Zheng, X., et al., Novel anionic polyacrylamide-modify-chitosan magnetic composite nanoparticles with excellent adsorption capacity for cationic dyes and pH-independent adsorption capability for metal ions. Chemical Engineering Journal, 2020. 392: p. 123706.

397. Ayubi, M., et al., Magnetic nanoparticles decorated with PEGylated curcumin as dual targeted drug delivery: Synthesis, toxicity and biocompatibility study. Materials Science and Engineering: C, 2019. 104: p. 109810.

398. Kozlovskiy, A., et al., Study of phase transformations, structural, corrosion properties and cytotoxicity of magnetite-based nanoparticles. Vacuum, 2019. 163: p. 236-247.

399. Yavuz, C.T., et al., Magnetic separations: from steel plants to biotechnology. Chemical Engineering Science, 2009. 64(10): p. 2510-2521.

400. Shen, Y., et al., Preparation and application of magnetic Fe3O4 nanoparticles for wastewater purification. Separation and Purification Technology, 2009. 68(3): p. 312-319.

401. Lu, A., E. e. L. Salabas and F. Schüth. Angew. Chem., Int. Ed, 2007. 46(8): p. 1222-1244.

402. Wang, X.-D., et al., Preparation of spherical silica particles by Stöber process with high concentration of tetra-ethyl-orthosilicate. Journal of colloid and interface science, 2010. 341(1): p. 23-29.

403. Pham, X.-H., et al., Silica-coated magnetic iron oxide nanoparticles grafted onto graphene oxide for protein isolation. Nanomaterials, 2020. 10(1): p. 117.

404. Fathy, M.M., et al., Silica-coated iron oxide nanoparticles as a novel nano-radiosensitizer for electron therapy. Life sciences, 2019. 234: p. 116756.

405. Ullah, S., et al., Macrophage entrapped silica coated superparamagnetic iron oxide particles for controlled drug release in a 3D cancer model. Journal of Controlled Release, 2019. 294: p. 327-336.

406. Radwan, M., et al., SYNTHESIS, CHARACTERIZATION AND SELECTED APPLICATION OF CHITOSAN-COATED MAGNETIC IRON OXIDE NANOPARTICLES. Journal of Chemical Technology & Metallurgy, 2019. 54(2).

407. Liu, Z., et al., Oil-field wastewater purification by magnetic separation technique using a novel magnetic nanoparticle. Cryogenics, 2012. 52(12): p. 699-703.

408. Calcagnile, P., et al., Magnetically driven floating foams for the removal of oil contaminants from water. ACS nano, 2012. 6(6): p. 5413-5419.

409. Singh, H., A. Ye, and D. Horne, Structuring food emulsions in the gastrointestinal tract to modify lipid digestion. Progress in lipid research, 2009. 48(2): p. 92-100.

410. Anushree, C., D.N.G. Krishna, and J. Philip, Oil-absorbent MnOx capped iron oxide nanoparticles: Synthesis, characterization and applications in oil recovery. Journal of Molecular Liquids, 2020. 320: p. 114324.

411. Mirshahghassemi, S., B. Cai, and J.R. Lead, A Comparison between the Oil Removal Capacity of Polymer-Coated Magnetic Nanoparticles in Natural and Synthetic Environmental Samples. Environmental Science & Technology, 2019. 53(8): p. 4426-4432.

412. Deng, Y., et al., Multifunctional mesoporous composite microspheres with well-designed nanostructure: a highly integrated catalyst system. Journal of the American Chemical Society, 2010. 132(24): p. 8466-8473.

413. Reddy, P.M., et al., Functionalized magnetic iron oxide (Fe3O4) nanoparticles for capturing gram-positive and gram-negative bacteria. Journal of biomedical nanotechnology, 2014. 10(8): p. 1429-1439.

414. Ennas, G., et al., Characterization of iron oxide nanoparticles in an Fe2O3− SiO2 composite prepared by a sol− gel method. Chemistry of Materials, 1998. 10(2): p. 495-502.

415. Meng, Q., et al., One-pot synthesis of Fe2O3 loaded SiO2 hollow particles as effective visible light photo-Fenton catalyst. Journal of Alloys and Compounds, 2017. 722: p. 8-16.

416. Azarifar, D., O. Badalkhani, and Y. Abbasi, Silica-modified magnetite Fe3O4 nanoparticles grafted with sulfamic acid functional groups: an efficient heterogeneous catalyst for the synthesis of 3, 4-dihydropyrimidin-2 (1 H)-one and tetrahydrobenzo [b] pyran derivatives. Journal of Sulfur Chemistry, 2016. 37(6): p. 656-673.

417. Feyzi, M. and L. Norouzi, Preparation and kinetic study of magnetic Ca/Fe3O4@ SiO2 nanocatalysts for biodiesel production. Renewable Energy, 2016. 94: p. 579-586.

418. Mirshahghassemi, S. and J.R. Lead, Oil recovery from water under environmentally relevant conditions using magnetic nanoparticles. Environmental science & technology, 2015. 49(19): p. 11729-11736.

419. Lü, T., et al., Fabrication of recyclable multi-responsive magnetic nanoparticles for emulsified oil-water separation. Journal of Cleaner Production, 2020. 255: p. 120293.

420. Wai, M.M., et al., Optimization and characterization of magnetite–reduced graphene oxide nanocomposites for demulsification of crude oil in water emulsion. RSC advances, 2019. 9(41): p. 24003-24014.

421. Suleimanov, B.A., F. Ismailov, and E. Veliyev, Nanofluid for enhanced oil recovery. Journal of Petroleum Science and Engineering, 2011. 78(2): p. 431-437.

422. Zhang, L., et al., Magnetic colloidosomes fabricated by Fe3O4–SiO2 hetero-nanorods. Soft Matter, 2011. 7(16): p. 7375-7381.

423. Kumar, G., et al., Stability of nanoparticle stabilized oil-in-water Pickering emulsion under high pressure and high temperature conditions: comparison with surfactant stabilized oil-in-water emulsion. Journal of Dispersion Science and Technology, 2020: p. 1-14.

424. Shao, S., et al., Removal of emulsified oil from aqueous environment by using polyvinylpyrrolidone-coated magnetic nanoparticles. Water, 2019. 11(10): p. 1993.

425. Arthur, J.D., B.G. Langhus, and C. Patel, Technical summary of oil & gas produced water treatment technologies. All Consulting, LLC, Tulsa, OK, 2005.

426. Soares, S.F., et al., Recent advances on magnetic biosorbents and their applications for water treatment. Environmental Chemistry Letters, 2019: p. 1-14.

427. Liu, J., et al., Recyclable magnetic graphene oxide for rapid and efficient demulsification of crude oil-in-water emulsion. Fuel, 2017. 189: p. 79-87.

428. Lin, K.-Y.A., Y.-C. Chen, and S. Phattarapattamawong, Efficient demulsification of oil-in-water emulsions using a zeolitic imidazolate framework: Adsorptive removal of oil droplets from water. Journal of Colloid and Interface Science, 2016. 478: p. 97-106.

429. Zhang, B., et al., Fabrication of Magnetite-Graphene Oxide/MgAl-Layered Double Hydroxide Composites for Efficient Removal of Emulsified Oils from Various Oil-in-Water Emulsions. Journal of Chemical & Engineering Data, 2018. 63(12): p. 4689-4702.

430. Franco, C.A., F.B. Cortés, and N.N. Nassar, Adsorptive removal of oil spill from oil-in-fresh water emulsions by hydrophobic alumina nanoparticles functionalized with petroleum vacuum residue. Journal of Colloid and Interface Science, 2014. 425: p. 168-177.

431. Panthi, K., U. Weerasooriya, and K.K. Mohanty, Enhanced recovery of a viscous oil with a novel surfactant. Fuel, 2020. 282: p. 118882.

432. Cui, Y., et al., Investigating the dynamical stability of heavy crude oil-water systems using stirred tank. Journal of Petroleum Science and Engineering, 2019. 183: p. 106386.

433. Yi, J., et al., The physicochemical stability and in vitro bioaccessibility of beta-carotene in oil-in-water sodium caseinate emulsions. Food Hydrocolloids, 2014. 35: p. 19-27.

434. Gu, L., et al., Catalytic oxidation of anionic surfactants by electrochemical oxidation with CuO–Co2O3–PO43− modified kaolin. Journal of hazardous materials, 2006. 137(2): p. 842-848.

435. Huang, C., et al., Microbial oil production from rice straw hydrolysate by Trichosporon fermentans. Bioresource Technology, 2009. 100(19): p. 4535-4538.

436. Ambashta, R.D. and M. Sillanpää, Water purification using magnetic assistance: a review. Journal of hazardous materials, 2010. 180(1-3): p. 38-49.

437. Shurair, M., et al., Harvesting of intact microalgae in single and sequential conditioning steps by chemical and biological based – flocculants: Effect on harvesting efficiency, water recovery and algal cell morphology. Bioresource Technology, 2019. 281: p. 250-259.

438. Casillas, P.G., C.R. Gonzalez, and C.M. Pérez, Infrared spectroscopy of functionalized magnetic nanoparticles. Infrared Spectroscopy-Materials Science, Engineering and Technology, 2012. 405.

439. Sun, S., et al., Monodisperse mfe2o4 (m= fe, co, mn) nanoparticles. Journal of the American Chemical Society, 2004. 126(1): p. 273-279.

440. Cîrcu, M., et al., Refinement of magnetite nanoparticles by coating with organic stabilizers. Nanomaterials, 2016. 6(12): p. 228.

441. Kamgar, A., S. Hassanajili, and G. Karimipourfard, Fe3O4@ SiO2@ MPS core/shell nanocomposites: The effect of the core weight on their magnetic properties and oil separation performance. Journal of Environmental Chemical Engineering, 2018. 6(2): p. 3034-3040.

442. Sonmez, M., et al., Synthesis and applications of Fe3O4/SiO2 core-shell materials. Current pharmaceutical design, 2015. 21(37): p. 5324-5335.

443. Ranjbakhsh, E., et al., Enhancement of stability and catalytic activity of immobilized lipase on silica-coated modified magnetite nanoparticles. Chemical Engineering Journal, 2012. 179: p. 272-276.

444. Xie, H., et al., Facile fabrication of acid-resistant and hydrophobic Fe3O4@ SiO2@ C magnetic particles for valid oil-water separation application. Surfaces and Interfaces, 2020. 21: p. 100651.

445. Wang, L., et al., The study of thermal stability of the SiO2 powders with high specific surface area. Materials chemistry and physics, 1999. 57(3): p. 260-263.

446. Elmobarak, W.F. and F. Almomani, Application of Fe3O4 Magnetite Nanoparticles grafted in Silica (SiO2) for Oil Recovery from Oil in Water Emulsions. Chemosphere, 2020: p. 129054.

447. Rezvani, H., et al., How ZrO2 nanoparticles improve the oil recovery by affecting the interfacial phenomena in the reservoir conditions? Journal of Molecular Liquids, 2018. 252: p. 158-168.

448. Nguyen, D., et al. Evaluation of surfactants for oil recovery potential in shale reservoirs. in SPE Improved Oil Recovery Symposium. 2014. Society of Petroleum Engineers.

449. Gupta, A.K. and M. Gupta, Synthesis and surface engineering of iron oxide nanoparticles for biomedical applications. biomaterials, 2005. 26(18): p. 3995-4021.

450. Tang, S.C. and I.M. Lo, Magnetic nanoparticles: essential factors for sustainable environmental applications. Water research, 2013. 47(8): p. 2613-2632.

451. Di Marco, M., et al., Physicochemical characterization of ultrasmall superparamagnetic iron oxide particles (USPIO) for biomedical application as MRI contrast agents. International journal of nanomedicine, 2007. 2(4): p. 609.

452. Tan, B. and S.E. Rankin, Study of the Effects of Progressive Changes in Alkoxysilane Structure on Sol− Gel Reactivity. The Journal of Physical Chemistry B, 2006. 110(45): p. 22353-22364.

453. Ge, S., et al., Facile hydrothermal synthesis of iron oxide nanoparticles with tunable magnetic properties. The Journal of Physical Chemistry C, 2009. 113(31): p. 13593-13599.

454. Du, X., et al., Ag-deposited silica-coated Fe3O4 magnetic nanoparticles catalyzed reduction of p-nitrophenol. Applied Surface Science, 2012. 258(7): p. 2717-2723.

455. Dang, F., et al., Sonochemical coating of magnetite nanoparticles with silica. Ultrasonics sonochemistry, 2010. 17(1): p. 193-199.

456. Singh, R.K., et al., Biocompatible magnetite nanoparticles with varying silica-coating layer for use in biomedicine: Physicochemical and magnetic properties, and cellular compatibility. Journal of Biomedical Materials Research Part A, 2012. 100(7): p. 1734-1742.

457. Kolhatkar, A.G., et al., Tuning the magnetic properties of nanoparticles. International journal of molecular sciences, 2013. 14(8): p. 15977-16009.

458. Ding, H., et al., Fe3O4@ SiO2 core/shell nanoparticles: the silica coating regulations with a single core for different core sizes and shell thicknesses. Chemistry of Materials, 2012. 24(23): p. 4572-4580.

459. Hui, C., et al., Core-shell Fe 3 O 4@ SiO 2 nanoparticles synthesized with well-dispersed hydrophilic Fe 3 O 4 seeds. Nanoscale, 2011. 3(2): p. 701-705.

460. Mahmoudi, M., et al., Cell toxicity of superparamagnetic iron oxide nanoparticles. Journal of colloid and interface science, 2009. 336(2): p. 510-518.

461. Gao, M., et al., Synthesis and characterization of superparamagnetic Fe3O4@ SiO2 core-shell composite nanoparticles. World Journal of Condensed Matter Physics, 2011. 1(2): p. 49-54.

462. Meng, L., et al., Hydrophobic mesoporous silicon dioxide for improving foam stability. RSC Advances, 2020. 10(32): p. 18565-18571.

463. Kakati, A., G. Kumar, and J.S. Sangwai, Oil recovery efficiency and mechanism of low salinity-enhanced oil recovery for light crude oil with a low acid number. ACS omega, 2020. 5(3): p. 1506-1518.

464. Niri, M.V., et al., Removal of natural organic matter (NOM) from an aqueous solution by NaCl and surfactant-modified clinoptilolite. Journal of water and health, 2015. 13(2): p. 394-405.

465. Theurer, J., Removal of Residual Oil From Produced Water Using Magnetic Nanoparticles. 2019.

466. Soares, S.F., et al., Recent advances on magnetic biosorbents and their applications for water treatment. Environmental Chemistry Letters, 2020: p. 1-14.

467. Liu, J., et al., Separation of emulsified oil from oily wastewater by functionalized multiwalled carbon nanotubes. Journal of Dispersion Science and Technology, 2016. 37(9): p. 1294-1302.

468. Liu, J., et al., Demulsification of crude oil-in-water emulsions driven by graphene oxide nanosheets. Energy & Fuels, 2015. 29(7): p. 4644-4653.

469. Jackson, M.D., D. Al-Mahrouqi, and J. Vinogradov, Zeta potential in oil-water-carbonate systems and its impact on oil recovery during controlled salinity water-flooding. Scientific reports, 2016. 6(1): p. 1-13.

470. Mikulcová, V., et al., Pickering oil-in-water emulsions stabilized by carboxylated cellulose nanocrystals–Effect of the pH. Food Hydrocolloids, 2018. 80: p. 60-67.

471. Acedo-Carrillo, J., et al., Zeta potential and drop growth of oil in water emulsions stabilized with mesquite gum. Carbohydrate Polymers, 2006. 65(3): p. 327-336.

472. Sadeqi-Moqadam, M., S. Riahi, and A. Bahramian, An investigation into the electrical behavior of oil/water/reservoir rock interfaces: The implication for improvement in wettability prediction. Colloids and Surfaces A: Physicochemical and Engineering Aspects, 2016. 490: p. 268-282.

473. Agista, M.N., A Literature Review and Transport Modelling of Nanoparticles for Enhanced Oil Recovery. 2017, University of Stavanger, Norway.

474. Hosseini, M.S., M.T. Sadeghi, and M. Khazaei, Wettability alteration from superhydrophobic to superhydrophilic via synthesized stable nano-coating. Surface and Coatings Technology, 2017. 326: p. 79-86.

475. Al-Anssari, S., et al., Wettability of nanofluid-modified oil-wet calcite at reservoir conditions. Fuel, 2018. 211: p. 405-414.

476. Vafaei, S. and M. Podowski, Analysis of the relationship between liquid droplet size and contact angle. Advances in Colloid and Interface Science, 2005. 113(2-3): p. 133-146.

477. Khilar, K.C. and H.S. Fogler, Migrations of fines in porous media. Vol. 12. 1998: Springer Science & Business Media.

478. Morrow, N.R., Wettability and its effect on oil recovery. Journal of petroleum technology, 1990. 42(12): p. 1,476-1,484.

479. Chatzis, I. and N.R. Morrow, Correlation of capillary number relationships for sandstone. Society of Petroleum Engineers Journal, 1984. 24(05): p. 555-562.

480. Melrose, J., Role of capillary forces in detennining microscopic displacement efficiency for oil recovery by waterflooding. Journal of Canadian Petroleum Technology, 1974. 13(04).

481. Derjaguin, B. and N. Churaev, Structural component of disjoining pressure. Journal of Colloid and Interface Science, 1974. 49(2): p. 249-255.

482. Basu, S. and M.M. Sharma, Measurement of critical disjoining pressure for dewetting of solid surfaces. Journal of colloid and interface science, 1996. 181(2): p. 443-455.

483. Bergeron, V., Forces and structure in thin liquid soap films. Journal of Physics: Condensed Matter, 1999. 11(19): p. R215.

484. El-Diasty, A.I. The potential of nanoparticles to improve oil recovery in bahariya formation, Egypt: An experimental study. in SPE Asia Pacific enhanced oil recovery conference. 2015. Society of Petroleum Engineers.

485. Sun, X., et al., Application of nanoparticles in enhanced oil recovery: a critical review of recent progress. Energies, 2017. 10(3): p. 345.

486. Melle, S., M. Lask, and G.G. Fuller, Pickering emulsions with controllable stability. Langmuir, 2005. 21(6): p. 2158-2162.

487. Yang, H., et al., Magnetic-responsive switchable emulsions based on Fe 3 O 4@ SiO 2–NH 2 nanoparticles. Chemical Communications, 2018. 54(76): p. 10679-10682.

488. Ho, Y.-S. and A.E. Ofomaja, Pseudo-second-order model for lead ion sorption from aqueous solutions onto palm kernel fiber. Journal of hazardous materials, 2006. 129(1-3): p. 137-142.

489. Ali, I., et al., An overview of heavy metal removal from wastewater using magnetotactic bacteria. Journal of Chemical Technology & Biotechnology, 2018. 93(10): p. 2817-2832.

490. Ali, I., et al., Green synthesis of the innovative super paramagnetic nanoparticles from the leaves extract of Fraxinus chinensis Roxb and their application for the

decolourisation of toxic dyes. Green Processing and Synthesis, 2019. 8(1): p. 256-271.

491. Ali, I., C. Peng, and I. Naz, Removal of lead and cadmium ions by single and binary systems using phytogenic magnetic nanoparticles functionalized by 3-marcaptopropanic acid. Chinese Journal of Chemical Engineering, 2019. 27(4): p. 949-964.

492. Ali, I., et al., Sorption of cationic malachite green dye on phytogenic magnetic nanoparticles functionalized by 3-marcaptopropanic acid. RSC advances, 2018. 8(16): p. 8878-8897.

493. Chen, L., R.M. Berry, and K.C. Tam, Synthesis of β-cyclodextrin-modified cellulose nanocrystals (CNCs)@ Fe3O4@ SiO2 superparamagnetic nanorods. ACS Sustainable Chemistry & Engineering, 2014. 2(4): p. 951-958.

494. Ma, L., et al., Intelligent composite foam with reversible tunable superwettability for efficient and sustainable oil/water separation and high-concentration organic wastewater purification. Process Safety and Environmental Protection, 2021. 149: p. 144-157.

495. Matin, A., U. Baig, and M.A. Gondal, Facile preparation of superwetting surfaces by dip-coating of silane for efficient separation of different types of oils from water. Process Safety and Environmental Protection, 2020. 134: p. 226-238.

496. Pekdemir, T., M. Çopur, and K. Urum, Emulsification of Crude Oil–Water Systems Using Biosurfactants. Process Safety and Environmental Protection, 2005. 83(1): p. 38-46.

497. Al-Ghouti, M.A., et al., Produced water characteristics, treatment and reuse: A review. Journal of Water Process Engineering, 2019. 28: p. 222-239.

498. Kallem, P., et al., Polyethersulfone hybrid ultrafiltration membranes fabricated with polydopamine modified ZnFe2O4 nanocomposites: Applications in humic acid removal and oil/water emulsion separation. Process Safety and Environmental Protection, 2021. 148: p. 813-824.

499. Kumar, S., A. Mandal, and C. Guria, Synthesis, characterization and performance studies of polysulfone and polysulfone/polymer-grafted bentonite based ultrafiltration membranes for the efficient separation of oil field oily wastewater. Process Safety and Environmental Protection, 2016. 102: p. 214-228.

500. Mohammed, R.R., et al., Waste lubricating oil treatment by extraction and adsorption. Chemical Engineering Journal, 2013. 220: p. 343-351.

501. Ali, I., et al., Phytogenic magnetic nanoparticles for wastewater treatment: a review. RSC Adv 7: 40158–40178. 2017.

502. Ali, I., et al., Overview of microbes based fabricated biogenic nanoparticles for water and wastewater treatment. Journal of environmental management, 2019. 230: p. 128-150.

503. Barani, M., et al., Eco-facile application of electrospun nanofibers to the oil-water emulsion separation via coalescing filtration in pilot- scale and beyond. Process Safety and Environmental Protection, 2021. 148: p. 342-357.

504. Ali, I., et al., Development and application of novel bio-magnetic membrane capsules for the removal of the cationic dye malachite green in wastewater treatment. RSC advances, 2019. 9(7): p. 3625-3646.

505. Ali, I., et al., Yield cultivation of magnetotactic bacteria and magnetosomes: a review. Journal of basic microbiology, 2017. 57(8): p. 643-652.

506. Schwarz, S., et al., Cationic flocculants carrying hydrophobic functionalities: applications for solid/liquid separation. The Journal of Physical Chemistry B, 2007. 111(29): p. 8649-8654.

507. Rostami, A., B. Atashkar, and H. Gholami, Novel magnetic nanoparticles Fe3O4-immobilized domino Knoevenagel condensation, Michael addition, and cyclization catalyst. Catalysis Communications, 2013. 37: p. 69-74.

508. Kumar, V., et al., Immobilization of Rhizopus oryzae lipase on magnetic Fe 3 O 4-chitosan beads and its potential in phenolic acids ester synthesis. Biotechnology and bioprocess engineering, 2013. 18(4): p. 787-795.

509. Chalasani, R. and S. Vasudevan, Cyclodextrin-functionalized Fe3O4@ TiO2: reusable, magnetic nanoparticles for photocatalytic degradation of endocrine-disrupting chemicals in water supplies. ACS nano, 2013. 7(5): p. 4093-4104.

510. Vieira, M., M. da Silva, and L. O, L. O, dos Santos and MM Beppu. Eur. Polym. J, 2011. 47(3): p. 254-263.

511. Zhang, T., et al., In situ remediation of subsurface contamination: Opportunities and challenges for nanotechnology and advanced materials. Environmental Science: Nano, 2019. 6(5): p. 1283-1302.

512. Zulfikar, M.A., et al., Preparation of Fe3O4-chitosan hybrid nano-particles used for humic acid adsorption. Environmental Nanotechnology, Monitoring & Management, 2016. 6: p. 64-75.

513. Song, W., et al., Water-soluble polyacrylamide coated-Fe3O4 magnetic composites for high-efficient enrichment of U (VI) from radioactive wastewater. Chemical engineering journal, 2014. 246: p. 268-276.

514. Reid, J.M., M.S. Cresser, and D.A. MacLeod, Observations on the estimation of total organic carbon from u.v. absorbance for an unpolluted stream. Water Research, 1980. 14(5): p. 525-529.

515. Briggs, R. and K. Grattan, Instrumentation control and automation in the control of biological effluent treatment. ISA transactions, 1992. 31(1): p. 111-123.

516. TAKAHASHI, T., T. MIYAHARA, and Y. NISHIZAKI, Separation of oily water by bubble column. journal of chemical engineering of Japan, 1979. 12(5): p. 394-399.

517. Li, W., et al., Fabrication of a Fe 3 O 4@ SiO 2@ mSiO 2-HPG-COOH-Pd (0) supported catalyst and its performance in catalyzing the Suzuki cross-coupling reaction. New Journal of Chemistry, 2015. 39(4): p. 2767-2777.

518. He, Y., et al., Facile synthesis and functionalization of hyperbranched polyglycerol capped magnetic Fe3O4 nanoparticles for efficient dye removal. Materials Letters, 2015. 151: p. 100-103.

519. Zhou, L., C. Gao, and W. Xu, Robust Fe3O4/SiO2-Pt/Au/Pd magnetic nanocatalysts with multifunctional hyperbranched polyglycerol amplifiers. Langmuir, 2010. 26(13): p. 11217-11225.

520. Sadeghzadeh, S.M. and M.A. Nasseri, Methylene dipyridine nanoparticles stabilized on Fe3O4 as catalysts for efficient, green, and one-pot synthesis of pyrazolophthalazinyl spirooxindoles. Catalysis today, 2013. 217: p. 80-85.

521. Laurent, S., et al., Magnetic iron oxide nanoparticles: synthesis, stabilization, vectorization, physicochemical characterizations, and biological applications. Chemical reviews, 2008. 108(6): p. 2064-2110.

522. Shaabani, A., et al., Design, preparation and characterization of Cu/GA/Fe3O4@ SiO2 nanoparticles as a catalyst for the synthesis of benzodiazepines and imidazoles. Applied Organometallic Chemistry, 2016. 30(6): p. 414-421.

523. Kazemi, A., et al., Synthesis and sustainable assessment of thiol-functionalization of magnetic graphene oxide and superparamagnetic Fe3O4@ SiO2 for Hg (II) removal from aqueous solution and petrochemical wastewater. Journal of the Taiwan Institute of Chemical Engineers, 2019. 95: p. 78-93.

524. Tang, J., P.J. Quinlan, and K.C. Tam, Stimuli-responsive Pickering emulsions: recent advances and potential applications. Soft Matter, 2015. 11(18): p. 3512-3529.

525. Rajak, V., et al., Optimization of separation of oil from oil-in-water emulsion by demulsification using different demulsifiers. Petroleum Science and Technology, 2016. 34(11-12): p. 1026-1032.

526. Sun, Z., T. Feng, and T.P. Russell, Assembly of graphene oxide at water/oil interfaces: tessellated nanotiles. Langmuir, 2013. 29(44): p. 13407-13413.

527. Johnson, D.W., B.P. Dobson, and K.S. Coleman, A manufacturing perspective on graphene dispersions. Current Opinion in Colloid & Interface Science, 2015. 20(5-6): p. 367-382.

528. Bera, A., A. Mandal, and B. Guha, Synergistic effect of surfactant and salt mixture on interfacial tension reduction between crude oil and water in enhanced oil recovery. Journal of Chemical & Engineering Data, 2014. 59(1): p. 89-96.

529. Shih, C.-J., et al., Understanding the pH-dependent behavior of graphene oxide aqueous solutions: a comparative experimental and molecular dynamics simulation study. Langmuir, 2012. 28(1): p. 235-241.

530. Silva, I., et al., Breaking of water-in-crude oil emulsions. 5. Effect of acid-alkaline additives on the performance of chemical demulsifiers. Energy & fuels, 2014. 28(6): p. 3587-3593.

531. Yi, L., et al., Synthesis and self-assembly of Cu 1.94 S–ZnS heterostructured nanorods. CrystEngComm, 2010. 12(12): p. 4124-4130.

532. Rezvani, H., et al., A new insight into Fe3O4-based nanocomposites for adsorption of asphaltene at the oil/water interface: an experimental interfacial study. Journal of Petroleum Science and Engineering, 2019. 177: p. 786-797.

533. Nallamilli, T., E. Mani, and M.G. Basavaraj, A model for the prediction of droplet size in Pickering emulsions stabilized by oppositely charged particles. Langmuir, 2014. 30(31): p. 9336-9345.

534. Liu, J., C. Dai, and Y. Hu, Aqueous aggregation behavior of citric acid coated magnetite nanoparticles: Effects of pH, cations, anions, and humic acid. Environmental research, 2018. 161: p. 49-60.

535. Zhou, J., et al., Magnetic Pickering emulsions stabilized by Fe3O4 nanoparticles. Langmuir, 2011. 27(7): p. 3308-3316.

536. Pérez-Calderón, J., M.V. Santos, and N. Zaritzky, Optimal clarification of emulsified oily wastewater using a surfactant/chitosan biopolymer. Journal of Environmental Chemical Engineering, 2018. 6(4): p. 3808-3818.

537. Elmobarak, W.F. and F. Almomani, Application of Magnetic nanoparticles for the removal of oil from oil-in-water emulsion: regeneration/reuse of spent particles. Journal of Petroleum Science and Engineering, 2021: p. 108591.

538. Kumar, A. and A. Mandal, Characterization of rock-fluid and fluid-fluid interactions in presence of a family of synthesized zwitterionic surfactants for

application in enhanced oil recovery. Colloids and Surfaces A: Physicochemical and Engineering Aspects, 2018. 549: p. 1-12.

539. Aminzadeh, B., et al. Influence of surface-treated nanoparticles on displacement patterns during CO 2 injection. in SPE annual technical conference and exhibition. 2013. Society of Petroleum Engineers.

540. Kazemzadeh, Y., et al., Behavior of asphaltene adsorption onto the metal oxide nanoparticle surface and its effect on heavy oil recovery. Industrial & Engineering Chemistry Research, 2015. 54(1): p. 233-239.

541. Krevor, S., et al., Capillary trapping for geologic carbon dioxide storage–From pore scale physics to field scale implications. International Journal of Greenhouse Gas Control, 2015. 40: p. 221-237.

542. Cheraghian, G. and L. Hendraningrat, A review on applications of nanotechnology in the enhanced oil recovery part A: effects of nanoparticles on interfacial tension. International Nano Letters, 2016. 6(2): p. 129-138.

543. Steeb, H., et al., Phase velocity dispersion and attenuation of seismic waves due to trapped fluids in residual saturated porous media. Vadose Zone Journal, 2012. 11(3).

544. Zhang, C., et al., Influence of viscous and capillary forces on immiscible fluid displacement: Pore-scale experimental study in a water-wet micromodel demonstrating viscous and capillary fingering. Energy & Fuels, 2011. 25(8): p. 3493-3505.

545. Al-Anssari, S., et al., Wettability alteration of oil-wet carbonate by silica nanofluid. Journal of colloid and interface science, 2016. 461: p. 435-442.

546. Kazemzadeh, Y., et al., Potential effects of metal oxide/SiO2 nanocomposites in EOR processes at different pressures. Colloids and Surfaces A: Physicochemical and Engineering Aspects, 2018. 559: p. 372-384.

547. Nassar, N.N., A. Hassan, and P. Pereira-Almao, Application of nanotechnology for heavy oil upgrading: Catalytic steam gasification/cracking of asphaltenes. Energy & Fuels, 2011. 25(4): p. 1566-1570.

548. Kazemzadeh, Y., M. Sharifi, and M. Riazi, Mutual effects of Fe3O4/chitosan nanocomposite and different ions in water for stability of water-in-oil (W/O) emulsions at low–high salinities. Energy & Fuels, 2018. 32(12): p. 12101-12117.

549. Li, Q., et al., Investigation of physical properties and displacement mechanisms of surface-grafted nano-cellulose fluids for enhanced oil recovery. Fuel, 2017. 207: p. 352-364.

550. Maurya, N.K. and A. Mandal, Investigation of synergistic effect of nanoparticle and surfactant in macro emulsion based EOR application in oil reservoirs. Chemical Engineering Research and Design, 2018. 132: p. 370-384.

551. Pourabdollah, K., et al., An experimental feasibility study of in-situ nano-particles in enhanced oil recovery and heavy oil production. Energy Sources, Part A: Recovery, Utilization, and Environmental Effects, 2013. 35(23): p. 2198-2208.

552. Roustaei, A., et al. An experimental investigation of polysilicon nanoparticles' recovery efficiencies through changes in interfacial tension and wettability alteration. in SPE international oilfield nanotechnology conference and exhibition. 2012. Society of Petroleum Engineers.

553. Wei, B., et al., The potential of a novel nanofluid in enhancing oil recovery. Energy & Fuels, 2016. 30(4): p. 2882-2891.

554. Pei, H., et al. Investigation of nanoparticle and surfactant stabilized emulsion to enhance oil recovery in waterflooded heavy oil reservoirs. in SPE Canada heavy oil technical conference. 2015. Society of Petroleum Engineers.

555. Elmobarak, W.F. and F. Almomani, Application of Fe3O4 magnetite nanoparticles grafted in silica (SiO2) for oil recovery from oil in water emulsions. Chemosphere, 2020. 265: p. 129054.

556. Kazemzadeh, Y., et al., Experimental investigation into Fe 3 O 4/SiO 2 nanoparticle performance and comparison with other nanofluids in enhanced oil recovery. Petroleum Science, 2019. 16(3): p. 578-590.

557. Khalilnezhad, A., et al., A Complete experimental study of oil/water interfacial properties in the presence of TiO2 nanoparticles and different ions. Oil & Gas Science and Technology–Revue d'IFP Energies nouvelles, 2019. 74: p. 39.

558. Ma, C., et al., Preparation and characterization of monodisperse core–shell Fe3O4@ SiO2 microspheres and its application for magnetic separation of nucleic acids from E. coli BL21. Journal of biomedical nanotechnology, 2012. 8(6): p. 1000-1005.

559. Wang, L., et al., Preparation of surface plasmon resonance biosensor based on magnetic core/shell Fe3O4/SiO2 and Fe3O4/Ag/SiO2 nanoparticles. Colloids and Surfaces B: Biointerfaces, 2011. 84(2): p. 484-490.

560. Farimani, M.H.R., et al., Study of structural and magnetic properties of superparamagnetic Fe3O4/SiO2 core–shell nanocomposites synthesized with hydrophilic citrate-modified Fe3O4 seeds via a sol–gel approach. Physica E: Low-dimensional Systems and Nanostructures, 2013. 53: p. 207-216.

561. Maleki, A., Z. Alrezvani, and S. Maleki, Design, preparation and characterization of urea-functionalized Fe3O4/SiO2 magnetic nanocatalyst and application for the

one-pot multicomponent synthesis of substituted imidazole derivatives. Catalysis Communications, 2015. 69: p. 29-33.

562. Doryani, H., M. Malayeri, and M. Riazi, Visualization of asphaltene precipitation and deposition in a uniformly patterned glass micromodel. Fuel, 2016. 182: p. 613-622.

563. Doryani, H., M. Malayeri, and M. Riazi, Precipitation and deposition of asphaltene in porous media: Impact of various connate water types. Journal of Molecular Liquids, 2018. 258: p. 124-132.

564. Zhang, T., et al. Nanoparticle-stabilized emulsions for applications in enhanced oil recovery. in SPE improved oil recovery symposium. 2010. Society of Petroleum Engineers.

565. Maaref, S., et al., The effect of dispersed phase salinity on water-in-oil emulsion flow performance: a micromodel study. Industrial & Engineering Chemistry Research, 2017. 56(15): p. 4549-4561.

566. Lashkarbolooki, M., et al., Synergy effects of ions, resin, and asphaltene on interfacial tension of acidic crude oil and low–high salinity brines. Fuel, 2016. 165: p. 75-85.

567. Shojaati, F., et al., Investigating the effect of salinity on the behavior of asphaltene precipitation in the presence of emulsified water. Industrial & Engineering Chemistry Research, 2017. 56(48): p. 14362-14368.

568. Sharma, T., et al., Thermal stability of oil-in-water Pickering emulsion in the presence of nanoparticle, surfactant, and polymer. Journal of Industrial and Engineering Chemistry, 2015. 22: p. 324-334.

569. Rezvani, H., et al., Experimental investigation of interfacial properties in the EOR mechanisms by the novel synthesized Fe3O4@ Chitosan nanocomposites. Colloids and Surfaces A: Physicochemical and Engineering Aspects, 2018. 544: p. 15-27.

570. Kumar, N., T. Gaur, and A. Mandal, Characterization of SPN Pickering emulsions for application in enhanced oil recovery. Journal of industrial and engineering chemistry, 2017. 54: p. 304-315.

571. Patel, A., et al. Evaluating feasibility of hydrophilic silica nanoparticles for in-situ emulsion formation in presence of co-surfactant: An experimental study. in SPE Kingdom of Saudi Arabia annual technical symposium and exhibition. 2017. Society of Petroleum Engineers.

572. Cheraghian, G. and L. Hendraningrat, A review on applications of nanotechnology in the enhanced oil recovery part B: effects of nanoparticles on flooding. International Nano Letters, 2016. 6(1): p. 1-10.

573. Skauge, T., K. Spildo, and A. Skauge. Nano-sized particles for EOR. in SPE improved oil recovery symposium. 2010. Society of Petroleum Engineers.

574. Bennetzen, M.V. and K. Mogensen. Novel applications of nanoparticles for future enhanced oil recovery. in International petroleum technology conference. 2014. International Petroleum Technology Conference.

575. Onyemachi, J., et al., Enhancing oil recovery through nanofluids flooding with Irvingia gabonensis in the Niger Delta. Journal of Petroleum Exploration and Production Technology, 2020. 10(7): p. 2885-2894.

576. Izadi, N., et al., An Experimental Investigation of Nanofluid Flooding and Mechanisms Affecting Enhanced Oil Recovery through Glass Micromodels. 2018.

577. Ehtesabi, H., M.M. Ahadian, and V. Taghikhani, Enhanced heavy oil recovery using TiO2 nanoparticles: investigation of deposition during transport in core plug. Energy & Fuels, 2015. 29(1): p. 1-8.

578. Doryani, H., et al., Impact of asphaltene and normal paraffins on methane-synthetic oil interfacial tension: An experimental study. Journal of Natural Gas Science and Engineering, 2015. 26: p. 538-548.

579. Maurya, N.K., P. Kushwaha, and A. Mandal, Studies on interfacial and rheological properties of water soluble polymer grafted nanoparticle for application in enhanced oil recovery. Journal of the Taiwan Institute of Chemical Engineers, 2017. 70: p. 319-330.

580. Hou, J., et al., The role of viscoelasticity of alkali/surfactant/polymer solutions in enhanced oil recovery. Journal of Petroleum Science and Engineering, 2005. 47(3-4): p. 219-235.

581. Salam, K., et al., Improving the demulsification process of heavy crude oil emulsion through blending with diluent. Journal of Petroleum Engineering, 2013. 2013.

582. Razi, M., et al., Effect of a different formulation of demulsifiers on the efficiency of chemical demulsification of heavy crude oil. Journal of Chemical & Engineering Data, 2011. 56(6): p. 2936-2945.

583. Nikkhah, M., et al., Efficient demulsification of water-in-oil emulsion by a novel nano-titania modified chemical demulsifier. Chemical Engineering Research and Design, 2015. 94: p. 164-172.

584. Nguyen, D., N. Sadeghi, and C. Houston, Chemical interactions and demulsifier characteristics for enhanced oil recovery applications. Energy & fuels, 2012. 26(5): p. 2742-2750.

585. Dalmazzone, C., C. Noïk, and J.-F.o. Argillier, Impact of chemical enhanced oil recovery on the separation of diluted heavy oil emulsions. Energy & fuels, 2012. 26(6): p. 3462-3469.

586. Ko, K.M., et al., Surfactant flooding characteristics of dodecyl alkyl sulfate for enhanced oil recovery. Journal of Industrial and Engineering Chemistry, 2014. 20(1): p. 228-233.

587. Arjmand, O. and A. Roostaei, Experimental investigation of viscous surfactant based enhanced oil recovery. Petroleum science and technology, 2014. 32(13): p. 1607-1616.

588. Guzman-Lucero, D., et al., Ionic liquids as demulsifiers of water-in-crude oil emulsions: study of the microwave effect. Energy & Fuels, 2010. 24(6): p. 3610-3615.

589. Silva, E.n.B., et al., Demulsification of heavy crude oil emulsions using ionic liquids. Energy & fuels, 2013. 27(10): p. 6311-6315.

590. Lemos, R.C., et al., Demulsification of water-in-crude oil emulsions using ionic liquids and microwave irradiation. Energy & Fuels, 2010. 24(8): p. 4439-4444.

591. Flores, C.A., et al., Anion and cation effects of ionic liquids and ammonium salts evaluated as dehydrating agents for super-heavy crude oil: Experimental and theoretical points of view. Journal of Molecular Liquids, 2014. 196: p. 249-257.

592. Janssen, C.H., et al., A novel mechanism for the extraction of metals from water to ionic liquids. ChemPhysChem, 2013. 14(16): p. 3806-3813.

593. Benito, J.M., et al., Droplet size distribution of oil-water emulsions by confocal laser scanning microscopy. 2004, ACS Publications.

594. Schuur, B., et al., Hydrodynamic features of centrifugal contactor separators: Experimental studies on liquid hold-up, residence time distribution, phase behavior

and drop size distributions. Chemical engineering and processing: process intensification, 2012. 55: p. 8-19.

595. Guzmán-Lucero, D., et al., Ionic liquids as demulsifiers of water-in-crude oil emulsions: study of the microwave effect. Energy & Fuels, 2010. 24(6): p. 3610-3615.

596. Silva, E.B., et al., Demulsification of heavy crude oil emulsions using ionic liquids. Energy & Fuels, 2013. 27(10): p. 6311-6315.

597. Li, X., Ionic liquids in separations: applications for pyrolysis oil and emulsion systems. 2017.

598. Li, X., S.R. Kersten, and B. Schuur, Efficiency and mechanism of demulsification of oil-in-water emulsions using ionic liquids. Energy & fuels, 2016. 30(9): p. 7622-7628.

599. Ezzat, A.O., et al., New amphiphilic pyridinium ionic liquids for demulsification of water Arabic heavy crude oil emulsions. Journal of Molecular Liquids, 2020. 312: p. 113407.

600. Zolghadr, A.R., M.H. Ghatee, and A. Zolghadr, Adsorption and orientation of ionic liquids and ionic surfactants at heptane/water interface. The Journal of Physical Chemistry C, 2014. 118(34): p. 19889-19903.

601. Shi, W.-X. and H.-X. Guo, Structure, interfacial properties, and dynamics of the sodium alkyl sulfate type surfactant monolayer at the water/trichloroethylene interface: a molecular dynamics simulation study. The Journal of Physical Chemistry B, 2010. 114(19): p. 6365-6376.

APPENDICES

Appendix A: List of Abbreviation

Abbreviation	Stands For
EOR	Enhanced Oil Recovery
O/W	Oil in Water
NPs	NanoParticles
HPs	Hyperbranched Polymers
HPG	Hyperbranched PolyGlycerol
W/O/W	Water in Oil in Water
O/W/O	Oil in Water in Oil
RSN	Relative Solubility Number
HPAM	Hydrolyzed Polyacrylamide
HLD	Hydrophilic-Lipophilic Deviation
HLB	Hydrophilic-lipophilic balance
$\%R_{oil}$	Oil recovery rate
Conc	Concentration
HPAM	Hydrolyzed Polyacrylamide
LHP	Lipophilic and Hydrophilic polysilicon
NWP	Neutral-Wet Polysilicon
TMAOH	TetraMethylAmmonium Hydroxide
MD	Molecule deposition
LSWF	Low Salinity Water Flooding
FF	Filming Flooding
NFF	Nanoparticle Fluid Flooding
SF	Steam Flooding
CSS	Cyclic Steam Stimulation
SAGD	Steam-Assisted Gravity Drainage
MNPs	Magnetic NanoParticles
WAG	Water Alternating Gas
MMP	Minimum Miscible Pressure
CNTs	Carbon Nanotubes

Abbreviation	Stands For
PEO-PPO	Poly(Ethylene Oxide)-Poly(Propylene Oxide)
ILs	ionic liquids
Wt%	Weight%
RTILs	Room-temperature Ionic Liquids
CROP	Cationic Ring-Opening Polymerization
D_2O	Deuterium Oxide
AM	Activated Monomer
NMR	Nuclear Magnetic Resonance
FTIR	Fourier Transform Infrared
TEM	Transmission Electron Microscopy
HRTEM	High-Resolution Transmission Electron Microscopy
AFM	Atomic Force Microscope
CHN	Carbon Hydrogen Nitrogen
VSMC	Vibrating Sample Magnetization Curve
TGA	Thermal Gravimetric Analysis
XRD	X-Ray diffraction
DLS	Dynamic Light Scattering
EDX	Energy Dispersive X-ray spectrometer
SEM	Scanning Electron Microscope
VSM	Vibrating Sample Magnetometer
GPC	Gel Permeation Chromatography
UV-Vis	Ultraviolet-Visible
DSC	Differential Scanning Calorimetry
MWCO	Molecular Weight cut-off
Da	Dalton
DSA	Drop Shape Analyzer
COD	Chemical Oxygen Demand
BOD	Biological Oxygen Demand
SEC	Size Exclusion Chromatography
PBS	Phosphate Buffered Saline
PW	Produced Water
CSM	Combustion Synthesis Method

Abbreviation	Stands For
Fe-MNP	Fe_3O_4 Magnetic NanoParticle
H_{ext}	external magnetic field
g	gram
h	hour
DI	Deionized water
O-in-W-emu	Oil in Water emulsion
Co-PM	Co-Precipitation Method
HTM	Hydrothermal Method
MIRM	Microwave Irradiation Method
CSM	Combustion Synthesis Method
M^v	v-valent metal
mg/L	milligram/Liter
g/L	gram/Liter
mg/g	milligram/gram
L	Liter
min	minute
St. Dev	Standard Deviation
rpm	revolution per minute
nm	nanometer
Fe-Si MNP	Fe_3O_4-SiO_2 Magnetic NanoParticle
TEOS	Tetra Ethyl Ortho Silicate
O/W	Oil/Water
O/W-emul	Oil in Water emulsion
mg/L	milligram/Liter
PPM	Part Per Million
MNPs	Magnetic NanoParticles
PSiMNPs	HPG-Fe_3O_4-SiO_2 demulsifier
Fe-Si-MNPs	Fe_3O_4-SiO_2
PFO	Pseudo-First-Order
PSO	Pseudo-Second-Order
O/W emulsion	Oil in Water emulsion
mV	millivolts

Abbreviation	Stands For
eV	electron Volt
MD	Magnetic Demulsifier
Fe_3O_4	magnetite nanoparticle
SiO_2	Silica nanoparticles
mN/m	millinewton/meter
HTC	Heat Transfer Coefficient
SSA	Specific Surface Area
DW	Distilled Water
W/O	Water in Oil
PV	Pore Volume
Hc	Coercivity
Dia	Diameter
Cp	centipoise
M	Mole/L
cm	centimeter
µm	micrometer
mL/h	milliliter/hour
D	darcy
KV	kilovolt
ml	milliliter
API	American Petroleum Institute
O/W EMULs	Oil in Water Emulsions
W/O EMULs	Water in Oil Emulsions
HILs	Halogenide Ionic Liquids
Non-HILs	Non-Halogenide Ionic Liquid
vol%	volume%
CII	Colloidal Instability Index

Appendix B: List of Nomenclature

Symbol	Definition & Unit
T_g	glass transition temperature [Celsius degree ℃]
T_m	melting point temperature [Celsius degree ℃]
C_{oil}	oil concentration [mg/L]
C_{sur}	surfactant concentration [g/L]
$\%\eta_{dem}$	demulsification efficiency (%)
Qe	adsorption capacity [mg/g]
Q_{max}	maximum adsorption capacity [mg/g]
K_L	The energy needed for the adsorption process [L/mg]
K_f	recovery capacity
n	recovery intensity [adsorption favourability coefficient]
K_1 and K_2	adsorption rate constants [1/min]
q_t	amount of oil recovered by the MD at any specific time [mg_{oil}/mg_{MD}]
$C_{i,\,oil}$ and $C_{t,\,oil}$	The initial and final concentration of oil in O/W emulsion [mg/L]
b	Langmuir constant [mg/L]
S	slurry dosage [L]
D_{MNP}	Fe_3O_4 Magnetic NanoParticle Dose [mg/L]
$C_{i,sur}$	The initial concentration of the surfactant [g/L]
M_s	saturation magnetization [emu/g]
M^v	v-valent metal
D_{oil}	oil Dose [mg/L]
D_{sur}	surfactant Dose [g/L]
$\%S_{oil}$	oil separation rate
t_{sep}	separation time [min]
D_{MNP}	Fe-Si Magnetic Nanoparticles Dose [mg/L]
$D_{PSiMNPs}$	HPG-Fe_3O_4-SiO_2 demulsifier dose [mg/L]
C_{oil}	oil concentration [mg/L]
C_{sur}	surfactant concentration [g/L]
K_2	second-order kinetic constant [1/min]
D%	Demulsification efficiency (%)

Symbol	Definition & Unit
V_{sur}	surfactant volume [g/L]
V_{IL}	Ionic Liquid Volume [mg/L]
$V_{t,\ oil}$	The initial and final volume of oil [mg/L]
IFT	Interfacial Tension [mN/m]